Vacuum Polarisation on Higher Dimensional Black Hole Spacetimes

by

Matthew Hewitt

A thesis in partial fulfillment of the requirements for a Doctorate of Philosophy

in the School of Mathematics and Statistics

The University of Sheffield

Supervisor: Prof. E. Winstanley

September 2014

Acknowledgments

Firstly I must thank my parents for their unconditional support and love, without whom I would not have been able to reach this achievement.

I thank my supervisor, Elizabeth Winstanley, for too many things to count but above all encouragement, patience and guidance.

I thank Adrian Ottewill and Cormac Breen of University College Dublin for their collaboration on work in this thesis.

This research was financially supported by the Engineering and Physical Sciences Research Council (EPSRC) and the School of Mathematics and Statistics, The University of Sheffield.

Abstract

We consider the vacuum polarisation, $\langle \phi^2 \rangle$, of a quantum scalar field on a black hole background. We introduce additional space-like dimensions and study the vacuum polarisation outside the event horizon. We consider a massless, quantum scalar field on the static, hyperspherically symmetric Schwarzschild-Tangherlini metric with zero cosmological constant. We calculate all results for a Hartle-Hawking vacuum state. The brane and bulk cases are considered separately; the metric on the brane is the four dimensional projection resulting from a bisection of the general black hole metric. On the brane we extend previous work on the Schwarzschild metric, for a conformally coupled field, such that we choose to include up to seven extra dimensions in the bulk. To conclude the work on the brane we present numerical results for the vacuum polarisation and outside the event horizon. For the bulk with five dimensions we present a complete methodology from initial set up to test results that demonstrates a way in which such a calculation can be completed for the first time. This is achieved by the introduction of non-physical Minkowski terms into the renormalisation scheme. Finally we discuss the prospects for extending our methodology to calculating the vacuum polarisation in the bulk for more than five dimensions.

Preface

Chapters 1 and 2 contain reviews of previous work. Chapter 3 shows new work and results for on the brane. Chapters 4 and 5 are original work covering the bulk with five and six dimensions.

In Ch. 1 we give a qualitative introduction to quantum field theory in curved space and the brane/bulk universe with a review of previous work. Chapter 2 reviews the mathematics required in this research that has been been published by other authors.

In Ch. 3 we present our new work on the brane, this is complete, beginning at the initial construction of the vacuum polarisation and ending with the results we aimed to achieve.

Chapter 4 contains the main body of this research and is original work. We demonstrate a methodology allowing the, previously incalculable, renormalised vacuum polarisation outside the event horizon in the five dimensional bulk to be found. We present work extending four dimensional objects into five dimensions and investigate the repercussions. We then discuss the higher dimensional renormalisation. Then we introduce the original idea of equating renormalisation components to their equivalents in the more easily calculable Minkowski spacetime case. We then demonstrate a complete method (with test results) to find the renormalised vacuum polarisation. We follow this in Ch. 5 with original work comprising of a brief review of how the calculation would be set up in a bulk of six dimensions and a discussion of which renormalisation methods may prove advantageous for future research.

We end in Ch. 6 with conclusions drawn from the original results on brane and our unique approach to handling higher dimensional renormalisation in the bulk. This is followed by a review of future work based on this research.

Contents

List of Figures

Chapter 1

Introduction

In this chapter we shall introduce the main topic of this work before detailing its physical set up. We shall further discuss the motivation for this set up as well as reviewing relevant past work and contemporary investigations into similar topics.

We have purposefully kept this introduction mathematically light except for a few key equations. This is so we can present the background mathematics in more detail in the following chapter, Ch. 2.

1.1 Notation

Throughout this work we use the MTW [54] metric signature $(-,+,+,+)$ and units such that $8\pi G = \hbar = c = k_B = 1$. All other notation and uses of symbols are described as they are introduced.

1.2 Quantum Field Theory in Curved Space

One ongoing goal of mathematics and science goal is the achievement of a theory of quantum gravity, a theory that would unify the laws of quantum behaviour with gravity. The major obstacle in achieving such a theory is the incompatibility of quantum field theory and general relativity, regarded as highly successful in their respective areas. One explanation of this failed connection is that gravity is perturbatively unrenormalisable and hence cannot be easily expressed as a quantum field. With this in mind a first approximation to quantum gravity can be constructed by considering quantum fields but allowing the spacetime to remain classical. This approach is termed quantum field theory (QFT) in curved space [9, 56].

As this approach has a classical spacetime, i.e. its metric is treated classically, QFT in curved space is considered a semi-classical approach. We then allow any quantum fields to propagate through this spacetime. This approximation serves two purposes; firstly to provide new predictions of physical phenomena and secondly to provide a check on any proposed theory of quantum gravity. Finding phenomena predicted from this approximation validates its use but also any theory of quantum gravity must produce the same phenomena under certain limits as a check on its validity.

Quantum field theory in curved space has already produced important predictions, the most publicly famous being black hole evaporation through Hawking radiation [38]. It has also obtained results pertaining to the Casimir effect [42] and the Unruh effect [70]. The Unruh effect states that an inertial observer detects a particular vacuum state but an accelerating observer will see black body radiation at a temperature proportional to the relative acceleration. This means observers with relative acceleration will see differing vacuum states.

An object of fundamental importance in general relativity is the stress-energy tensor

[54], T_{ab} , which describes the density and flux of energy and momenta of matter, radiation and force fields. As these classical objects have now been subsumed into quantum fields the stress-energy tensor itself can no longer be classical. As it is now a quantum object we must treat it as an operator and look at its expectation value. Given a normalised state $|s\rangle$ we write the expectation value of the stress-energy tensor operator as $\langle s|T_{ab}|s\rangle$. An added advantage of this object is it allows us to bypass the concept of particles, which in a curved spacetime with a quantum field become observer dependent as discussed in §1.8. We can now express the connection between the quantum field and the background geometry through the semi-classical Einstein equations [9, 72] (with no cosmological constant)

$$G_{ab} = R_{ab} - \frac{1}{2}Rg_{ab} = \langle s|T_{ab}|s\rangle \tag{1.2.1}$$

containing Einstein's tensor G_{ab}, the Ricci tensor R_{ab}, Ricci scalar R and the spacetime metric g_{ab}. A failure of this expectation value of a quantum operator is that it is divergent when naively calculated at a point (see §2.5 and Appendix A) and hence the expectation value is formally infinite [73]. As such the expectation value must in some way be renormalised to produce $\langle s|T_{ab}|s\rangle_{\text{ren}}$, the renormalised stress-energy tensor (RSET).

Quantum field theory in curved space has been developing now for over forty years but its application is restricted to systems that have a metric solution to equation (1.2.1). As such investigations into black hole spacetimes can be greatly rewarding as they have simple descriptions but also have large enough gravitational curvature to produce effects in any quantum field not apparent at lower energies.

1.3 Brane World Theory

Brane world theory is a higher dimensional model based on the concept that our universe can be treated as a four dimensional manifold (termed the brane) embedded in a higher

dimensional spacetime (the bulk). The brane contains our four usual dimensions and is described by parameters such that it models our perceived universe [60]. While the brane is strongly proscribed in advance by needing to match our observations of the universe we are free to some extent in how we characterise the bulk. The size, nature and warping of the extra dimensions can be modeled in many ways. However certain freedoms of choice have been constrained by work demonstrating unphysical interferences on the brane, such as disproportionate gravitational strength [52].

In a brane world model it is usual to assume that non-scalar, non-gravitational particles are trapped on the brane resulting in scalar particles and gravitons escaping into the bulk, such as in the ADD model [4, 5] discussed further in §1.6. The Randall-Sundrum model [59] places the same restriction on particle propagation but introduces only a single, warped, extra dimension to account for modifications of gravity.

Such a brane world set up can be used as a solution to the hierarchy problem. In general a hierarchy problem is an issue encountered when theoretical values are vastly out of scale to those seen in experiment. In the standard model the issue termed the hierarchy problem can be briefly summarised as one of two equivalent questions; why is the weak force 10^{32} times stronger than the gravitational force or why is the Higgs boson (c. 120GeV) so much lighter than the Planck mass (c. 10^{19}GeV). Calculations for the quantum corrections to the Fermi constant in weak force studies show that it should result in a scale similar to the gravitational constant but this is not true in experiment. A similar discrepancy is seen in the theoretical versus experimental results for the Higgs mass (as demonstrated in the mass values above). In essence the problem is that current models expect the four fundamental forces to be equivalent in such a way that they can be unified for certain energies scales. This is true for the the strong nuclear, weak nuclear and the electromagnetic forces but not for gravity.

The brane world solution to the hierarchy problem makes use of the fact that the model

allows gravitational particles to escape the brane into the bulk. This would mean that the gravitational force witnessed on the brane does not represent the true scale of gravity. Now consider that stating the gravitational force is too weak (on the brane compared to the weak force) is equivalent to stating that the 4d Planck mass, $M_{p,4} = 2.2 \times 10^{-8}$kg, is too massive (the associated value for the weak force is of the order 10^{-25}kg). The brane solution states that the true Planck mass in the d dimensional bulk, $M_{p,d}$, is of the correct scale to other forces by the following relation

$$M_{p,4}^2 = (2\pi R)^{d-4} M_{p,d}^{d-2}. \tag{1.3.1}$$

where the $2\pi R$ is a scale factor relating to higher dimensional volume. This relation provides some guidance on the construction of a physically allowable model for the bulk as the ratio of the extra dimensional radius to the number of dimensions must allow for a Planck mass that results in the observed gravity on the brane [46].

Additional to this bulk Planck mass we can calculate the bulk Planck length, informing us of the true scale at which quantum gravity dominates over other interactions. The derivation is performed with non-natural units based on the bulk gravitational constant and allows us to express the bulk Planck length, $l_{p,d}$, as

$$l_{p,d} = \left(l_{p,4}^2\right)^{\frac{1}{d-2}}. \tag{1.3.2}$$

Beyond the hierarchy problem allowing for extra dimensions is physically motivated. Both string theory [63] and the Kaluza-Klein [45, 50] model show the possibility of some unification in higher dimensions however Kaluza-Klein theory is heavily constrained and string theory has yet make enough testable predictions. Researching quantum field theory in curved space with higher dimensions allows for the investigation of extra dimensions through microscopic black hole evaporation. The signature of such evaporation will be

detectable at colliders (if black holes are produced there) and such signatures will contain traces of any extra dimensions, for reviews see [18, 34].

1.4 Objectives and Setup

As stated in §1.2 the fundamental object we want for any system is $\langle s|T_{ab}|s\rangle_{\text{ren}}$ however it has no generalised method of calculation. As we will be performing research in an area of little previous investigation we initially choose factors that will allow progress to be achieved. We restrict ourselves to a scalar field and only investigate the vacuum state (to be determined, see 1.8) exterior to a black hole, $\langle 0|T_{ab}|0\rangle = \langle T_{ab}\rangle$. With these criteria the RSET depends on the renormalised object $\langle\phi^2\rangle_{\text{ren}}$ and its derivatives [3, 41]. The object $\langle\phi^2\rangle$ is the auto-correlation of the field, termed the vacuum polarisation, and gives a measure of the screening effect caused by polarised pseudoparticle pair production. The concept is more familiar for an electromagnetic field in QED where its equivalent is polarisation resulting in charge screening and from where it derives its name [31]. The renormalised vacuum polarisation's direct usefulness is that its behaviour is similar to the RSET, notably both will tend to diverge at the same places, and that it is much easier to calculate.

Our work will be to investigate the vacuum polarisation however unlike in other work we have both a brane and a bulk to consider. We can anticipate that to some extent the methodology for the vacuum polarisation on the brane will mimic that for the calculation on the Schwarzschild metric so we consider this the first of our objectives. However it is still of relevance to see how $\langle\phi^2\rangle_{\text{ren}}$ changes as the number of extra dimensions increases from zero. There has been no known previous attempt to calculate the vacuum polarisation within the bulk and so we identify this as our primary investigation target. It is prudent to state that our goal in the bulk is to find methodology that will allow calculation and accurate results in future work.

In sections 1.6 , 1.7 and 1.8 we will detail the specific choices for our physical setup (metric, brane model and vacuum state) after a review of previous work.

1.5 Previous Research

We review here some previous research that leads into our investigation, all these papers listed assume a zero cosmological constant unless stated otherwise. In 1976 Christensen [19] demonstrated a methodology from which calculations of the RSET and the vacuum polarisation (see §1.4) could be performed. The first calculations were performed by Candelas [16] who derived values for the vacuum polarisation on the horizon of a Schwarzschild black hole for a massless, conformally coupled scalar field. Candelas had previously produced in his thesis [15] necessary geometrical derivations concerning the lengths of geodesics and the expression of the vacuum polarisation. These results were followed up by Candelas and Howard [17] who extended the calculation away from the horizon. Howard [41] then was able to numerically calculate values of the stress-energy tensor for the same parameters.

Still for a Schwarzschild black hole Jensen and Ottewill [44] successfully calculated components of the stress-energy tensor for an electromagnetic (hence vector) field keeping other assumptions as before. This was followed up by Jensen, McLaughlin and Ottewill [43] who now produced the same derivation but for a field of gravitons extending previous methodology to different particle fields.

Importantly Anderson [2] collected and generalised the previous methodologies to calculate the renormalised vacuum polarisation for fields neither with general mass and coupling on a Reissner-Nordström black hole. From this work came the standardised base method from which much work in this area is derived. Anderson, Hiscock and Samuel [3] then advanced Anderson's work by developing a general method for the renormalised stress-energy tensor of a scalar field on any spherically symmetric spacetime. For a general field [21] present a methodology to achieve a qualitative picture of the RSET and lay the

groundwork for explicit calculation for four dimensions. This general method is extended to higher dimensions by [55].

Concerning spacetimes with non-zero cosmological constant, Winstanley and Young [75] first calculated the vacuum polarisation for a de Sitter, Reissner-Nordström black hole. A method was then developed by Breen and Ottewill [12] which improved upon the approach in [75] near the event horizon for more accurate results in this region. Breen and Ottewill then progressed their research to develop a method to calculate RSET on the horizon [13]. Calculations of the vacuum polarisation for an asymptotically Anti de Sitter black hole were produced by Flachi and Tanaka [29] but only for the massless, conformally coupled case.

Of note at this point is a problem encountered in more than one of these works [3, 75]. Calculation of the vacuum polarisation, and hence the RSET, became problematic near the horizon due zero frequency modes. This problem was overcome in [12] and is an issue that will be returned to at several points later in this thesis.

For black holes in more than four dimensions Frolov, Mazzitelli and Paz [32] calculated the value of the vacuum polarisation on the horizon of a Schwarzschild-Tangherlini black hole in five dimensions. In six dimensions Lemos and Thompson [69] solved the same problem in the context of a Reissner-Nordström black hole and presented a method for incorporating the renormalisation terms for any even dimension. These two studies represent all the research performed in higher dimensions that have produced results. Further both of these studies use a deWitt-Schwinger expansion to handle divergent terms. It has been recently shown in the d dimensional case [23] that using the Hadamard form is much more rigorous. The results of using the Hadamard form make calculations easier [23] and may be the way to design a general method for calculating divergent terms.

1.6 The Brane Model

For this investigation we will use the ADD brane world model [4, 5] wherein our extra dimensions are flat and sufficiently large in comparison to our black hole. If the extra dimensions were small then additional effects would be generated by the gravitational force propagating along side the brane through the thin bulk, this should be avoided as no such effects are evident [52]. Also the scales generated would not adequately account for the loss of gravitational strength on the brane in regards to the hierarchy problem. In addition if the extra dimensions were small we would not be able to use our metric, §1.7, as it would no longer be an accurate measurement of the spacetime. We note that for both these issues there is not a difficulty for small, compact dimensions. The fact the extra dimensions are flat means the cosmological constant in the bulk is zero.

We must then consider our extra dimensions to be compact but large enough compared to the black hole so that compactness can be ignored. If not compact then we encounter additional dimensions of infinite extent. We disallow such an occurrence by application of Gauss's law shown in the low mass and separation limit. This application demonstrates that the gravitational acceleration, $g(r)$, at radial coordinate r in n spatial dimensions depends on the total mass M contained within the surface area of a $(n-1)$-sphere, S_{n-1}, by

$$g(r) = \frac{-4\pi GM}{S_{n-1}} = -4\pi M \frac{G\Gamma(\frac{n}{2})}{2\pi^{\frac{n}{2}} r^{n-1}}. \tag{1.6.1}$$

From this relation and tests performed at the nanometer scale [24] we see that infinite extent dimensions must be disallowed to be physically relevant. A constraint is still in place on the size of compact dimensions to prevent gravity on the brane being too weak so their size must be kept below the millimeter scale. Note that the existence of extra dimensions of infinite extent is not an issue for the Randall-Sundrum model [59].

As is evident in equation (1.2.1) we are also taking the cosmological constant on the

brane to be zero, this is equivalent to stating that the brane is tensionless or flat. We are also assuming that our brane is four dimensional, three spatial and one temporal, and that all extra dimensions are spatial. We will denote the total number of dimensions in the bulk by d such that if we let $d = 4$ there are no extra dimensions. The black hole is then positioned so that its singularity is attached to the brane giving it a d dimensional horizon through which the brane makes a flat slice [35]. This construction matches that used at the LHC to calculate potential black hole signatures [30, 47, 74].

1.7 The Metric

For our investigation we use a simple metric so we omit charge and spin to choose the Schwarzschild-Tangherlini [67] metric,

$$ds^2 = -f(r)dt^2 + f(r)^{-1}dr^2 + r^2 d\Omega_{d-2}^2. \tag{1.7.1}$$

Details concerning the metric and its properties (definitions, temperature, surface gravity etc.) can be found in §2.3 where its implementation will be developed.

This metric is appropriate for outside the body of the black hole with Hawking temperature [8, 39] of $T_H = \kappa/2\pi$ (where κ is the surface gravity) and a radiation spectrum at spatial infinity determined by T_H. In the case where $d = 4$ equation (1.7.1) is identical to the Schwarzchild metric but they share some properties for $d \neq 4$. Importantly this metric represents the most general (classical) vacuum solution for a static black hole that is hyperspherically symmetric and asymptotically flat. This means we may assume the black hole horizon is a hypersphere in the bulk and is time invariant.

Knowing our black hole horizon is a hypersphere we take the simplest flat slice to be our brane. This is a bisection and is performed by (WLOG) setting $\theta_{i>1} = \pi/2$ we obtain

(also setting $\theta_1 = \theta$)

$$ds^2 \;=\; -f(r)dt^2 + f(r)^{-1}dr^2 + r^2(d\theta^2 + \sin^2\theta\, d\phi^2) \tag{1.7.2}$$

for the metric projection on the brane.

1.8 The Vacuum State

Related to the Unruh effect mentioned in §1.2 is that it is impossible to define an absolute vacuum state for a quantum field in a general curved space. This phenomenon arises from the definition of the creation and annihilation operators (e.g. $\hat{a}^\dagger$ and $\hat{a}$ respectively) by the choice of positive frequency in the mode expansion [56]. An observer accelerating with respect to another will naturally make a different choice of positive frequency and produce a second set of particle operators (say $\hat{b}^\dagger$ and $\hat{b}$). Either can be used to create a particle basis in a Hilbert space and they are related by the Bogolyubov transformations

$$\begin{aligned} \hat{a}^\dagger_{\mathbf{k}} &= \alpha_k \hat{b}^\dagger_{\mathbf{k}} + \beta^*_k \hat{b}_{\text{-}\mathbf{k}} \\ \text{and} \quad \hat{a}_{\mathbf{k}} &= \alpha^*_k \hat{b}_{\mathbf{k}} + \beta_k \hat{b}^\dagger_{\text{-}\mathbf{k}}. \end{aligned} \tag{1.8.1}$$

Here $\mathbf{k}$ is spatial momentum and α_k and β_k are the Bogolyubov coefficients. This result allows us to define a relative vacuum such as $|0\rangle_{(a)}$, which is void of a particles but will still contain b particles if $\hat{b}_k \neq 0$. As there is no absolute vacuum we are forced to choose one with which to calculate. It is in fact relatively easy to calculate the difference in expectation value between two vacuum states [21] as this process requires no renormalisation. This fact allows us to choose the vacuum state which will make our calculation easiest.

There are three standard vacua defined on black hole spacetimes. The Unruh vacuum [70] is a time asymmetric static state that models the late time of a Hawking collapse with the expected thermal spectrum at infinity for a black hole with a Hawking temperature.

The Boulware vacuum [10] is empty of particles at infinity and is also empty as seen by an observer moving along the integral curves of the static Killing vector field. This leads to the quantities calculated from the state being divergent at the horizon and so it is used to model the region near a neutron star just before the surface collapses within the horizon. Our choice will be the Hartle-Hawking vacuum [37] (sometimes referred to as the Israel-Gibbons-Perry vacuum) which provides the most advantageous properties for our calculations. Physically this represents a state with a thermal spectrum from a particle bath at infinity that is in equilibrium with the thermal radiation from the black hole. This means the black hole remains in thermal equilibrium, will not lose mass over time and hence will not evaporate. This vacuum has several key features: it is regular on the horizon allowing calculation in the nearby region, it allows for incoming and outgoing particles, it is non-empty at spatial infinity, particles have positive energy with respect to Kruskal coordinates on the horizon and the state is time symmetric. It is the regularity and symmetry properties that make calculations on this vacuum easier than in the other states.

1.9 Outline of Remaining Chapters

Chapter 2 reviews the mathematics required in this research that has been been published by other authors. This includes a more rigorous description of our set up, the construction and behaviour of higher dimensional functions (such as harmonics and Green's functions), renormalisation through the Hadamard expansion and the WKB approximation to numerical solutions of ODEs.

In Ch. 3 we present our new work on the brane, this is complete, beginning at the initial construction of the vacuum polarisation and ending with the results we aimed to achieve. This initially extends on previous work by modifying a function in the metric so it is now dependent on dimension and then presents new approaches and calculations

based on the new behaviour of this function. We also discuss the difficulties caused by this function in numerically solving a core ODE. Finally we present original results for the vacuum polarisation on the brane outside the event horizon in a near, and more extended, region for a bulk of up to eleven dimensions. This chapter includes the vacuum polarisation on the horizon provided by Adrian Ottewill and Cormac Breen of University College Dublin.

Chapter 4 contains the main body of this research and is original work. We demonstrate a methodology allowing the, previously incalculable, renormalised vacuum polarisation outside the event horizon in the five dimensional bulk to be found. We present work extending four dimensional objects into five dimensions and investigate the repercussions. We then discuss the higher dimensional renormalisation. We demonstrate an extension to the dimensional reduction method that fails in our case but shows promise in other applications. Then we introduce the original idea of equating renormalisation components to their equivalents in the more easily calculable Minkowski spacetime case. We then review several ways in which this idea can be implemented before demonstrating a complete method (with test results) to find the renormalised vacuum polarisation. Calculations in this chapter were supported by programming assistance from Adrian Ottewill. We follow this in Ch. 5 with original work comprising of a brief review of how the calculation would be set up in a bulk of six dimensions and a discussion of which renormalisation methods may prove advantageous for future research.

We end in Ch. 6 with conclusions drawn from the original results on brane and our unique approach to handling higher dimensional renormalisation in the bulk. This is followed by a review of future work based on this research.

Chapter 2

General Methodology

This chapter contains a review of useful definitions, initial equations and general methodology applicable for both brane and bulk cases. Specialisation of these methods to either case can be found in subsequent chapters. The methodology scheme is based on [2, 3, 19, 75] and extensions to higher dimensions are based on [23, 32, 69].

2.1 Biscalars

For our purposes we define a general biscalar as operating on two spacetime points in our manifold, $\mathcal{M}$, such that, given a biscalar $A(x, x')$,

$$A : \mathcal{M} \times \mathcal{M} \to \mathbb{C}. \tag{2.1.1}$$

We define

$$\nabla_\alpha A(x, x') = \frac{\partial A(x, x')}{\partial x^\alpha} = A_{;\alpha} \tag{2.1.2}$$

as the covariant derivative of A at x such that $A_{;\alpha}$ is a dual vector at x and a scalar at x'. We define $A_{;\alpha'}$ as a dual vector at x' and a scalar at x. We similarly extend this to

second derivatives such that we have

$$\nabla_\beta A_{;\alpha} = A_{;\alpha\beta} \quad \text{and} \quad \nabla_{\beta'} A_{;\alpha'} = A_{;\alpha'\beta'}. \tag{2.1.3}$$

In (2.1.3) we have defined two objects that are scalar valued at one event and rank two tensors at the other, by the properties of the covariant derivative the rank two tensors are symmetric. We also have

$$\nabla_{\beta'} A_{;\alpha} = A_{;\alpha\beta'} = \frac{\partial^2 A}{\partial x^{\beta'} \partial x^\alpha} = A_{;\beta'\alpha} \tag{2.1.4}$$

by the properties of partial derivatives.

The definitions and notation for biscalars can be simply used for higher order derivatives. However note that the first covariant derivative at one event is actually a simple partial derivative and so may be transposed with derivatives at the other event. For example,

$$\nabla_{\delta'} A_{;\alpha\beta\gamma} = A_{;\alpha\beta\gamma\delta'} = A_{;\alpha\beta\delta'\gamma} = A_{;\alpha\delta'\beta\gamma} = A_{;\delta'\alpha\beta\gamma}. \tag{2.1.5}$$

Although we know from equation (2.1.3) that α and β may be transposed we have no such rule for exchanges with γ. The property displayed in (2.1.5) can be generalised [58] such that given $A_{...}(x, x')$ (where ... indicates any combination of primed and unprimed indices) we have

$$A_{...;\alpha\beta'...} = A_{...;\beta'\alpha...}. \tag{2.1.6}$$

As a result the ordering within the primed and unprimed indices must be preserved but primed and unprimed indices may always be transposed.

2.2 Hyperspherical Harmonics

We define hyperspherical harmonics [27, 33, 57] which represent the angular part of solutions to equations such as the higher dimensional Laplace equation. Firstly let $\mathbf{P}$ be the space of homogeneous polynomials of degree l in $d-1$ variables such that $\forall P_l \in \mathbf{P}$

$$P_l(\lambda \mathbf{x}) = \lambda^l P_l(\mathbf{x}) \quad (\lambda \text{ is any constant}). \tag{2.2.1}$$

Let $\mathbf{A}$ be the subspace of $\mathbf{P}$ such that $A_l \in \mathbf{A}$ is harmonic. The polynomial A_l is deemed harmonic if it is a solution to Laplace's equation

$$\triangle_{d-1} A_l = \sum_{i=1}^{d-1} \frac{\partial^2 A_l}{\partial x_i^2} = 0. \tag{2.2.2}$$

Now let $\mathbf{H}$ be the space of harmonic functions A_l restricted to the $(d-2)$-sphere where

$$S^{d-2} = \{\mathbf{x} \in \mathbf{R}^{d-1} : |\mathbf{x}| = 1\}. \tag{2.2.3}$$

In line with the literature [33] the elements of $\mathbf{H}$ are denoted Y_l and are named the spherical harmonics.

The Laplacian (2.2.2) is re-expressed in spherical coordinates so that

$$\triangle_{d-1} = \frac{\partial^2}{\partial r^2} + \frac{d-2}{r}\frac{\partial}{\partial r} + \frac{1}{r^2}\triangle_{S^{d-2}} \tag{2.2.4}$$

where $\triangle_{S^{d-2}}$ contains all the angular components of the Laplacian on S^{d-2}. Now from (2.2.1) A_l can be expressed as

$$A_l(\mathbf{x}) = A_l(r\zeta) = r^l A_l(\zeta) \tag{2.2.5}$$

where ζ is a unit vector. As $A_l(\zeta)$ is restricted to the unit sphere we know $A_l(\zeta)$ is $Y_l(\zeta)$ for every $\zeta \in S^{d-2}$ and so $A_l(\mathbf{x}) = r^l Y_l(\zeta)$. Hence from the definition of $\mathbf{A}$ and (2.2.4) we obtain [33]

$$\triangle_{d-1} A_l(\mathbf{x}) = l(l-1)r^{l-2}Y_l + \frac{d-2}{r} l r^{l-1} Y_l + \frac{r^l}{r^2} \triangle_{S^{d-2}} Y_l = 0 \tag{2.2.6}$$

so that

$$r^{l-2} \left(\triangle_{S^{d-2}} Y_l + l(l+d-3)Y_l \right) = 0, \tag{2.2.7}$$

resulting in

$$\triangle_{S^{d-2}} Y_l = -l(l+d-3)Y_l. \tag{2.2.8}$$

Therefore the spherical harmonics are eigenvectors of the operator $\triangle_{S^{d-2}}$.

An important quantity to be used later is the number of linearly independent spherical harmonics of degree l in $d-1$ variables, $N(d-1,l)$. First note that that every monomial (i.e., product of variables) in an l-th degree homogeneous polynomial must be of degree l. Hence there are $K(d-1,l)$ linearly independent, homogeneous lth degree polynomials in $d-1$ variables where [33]

$$K(d-1,l) = \binom{l+d-2}{l} = \binom{l+d-2}{d-2}. \tag{2.2.9}$$

Now we apply this to harmonic polynomials through equation (2.2.2) in one of two ways that must provide identical $N(d-1,l)$. Firstly consider the homogeneous condition for each value of the index i from (2.2.2) which totals to $K(d-1,l-2)$ [6] hence the difference between this number and (2.2.9) is $N(d-1,l)$ as

$$N(d-1,l) = K(d-1,l) - K(d-1,l-2). \tag{2.2.10}$$

Secondly start with $A_l \in \mathbf{A}$ expressed as [33]

$$A_l(x_1,..,x_{d-1}) = \sum_{j=0}^{l} x_{d-1}^j h_{l-j}(x_1,..,x_{d-2}) \tag{2.2.11}$$

where h_{l-j} are homogeneous polynomials of degree $l-j$ in $d-2$ variables. Using (2.2.2) gives

$$\begin{aligned}\triangle_{d-1}A_l = \left(\frac{\partial^2}{\partial x_{d-1}^2} + \triangle_{d-2}\right) A_l &= \sum_{j=2}^{l} j(j-1)x_{d-1}^{j-2}h_{l-j} + \sum_{j=0}^{l} x_{d-1}^j \triangle_{d-2}h_{l-j} \\ &= \sum_{j=0}^{l} x_{d-1}^j \left[(j+2)(j+1)h_{l-j-2} + \triangle_{d-2}h_{l-j}\right] = 0, \end{aligned} \tag{2.2.12}$$

such that $h_{i<0} = 0$, from which we obtain recursion relations for h_{l-j}. Then [33] shows that the choice of h_l and h_{l-1} determines all h_{l-j} and hence all A_l. Both h_l and h_{l-1} can be expressed as the sum of, $K(d-2,l)$ and $K(d-2,l-1)$ respectively, countable basis polynomials hence the number of linearly independent A_l is $K(d-2,l)$ plus $K(d-2,l-1)$.

Collecting the information from equation (2.2.9) onwards we have

$$N(d-1,l) = \dim \mathbf{H} = \dim \mathbf{A} = K(d-1,l) - K(d-1,l-2) \tag{2.2.13}$$

providing the final value

$$\begin{aligned} N(d-1,l) &= K(d-1,l) - K(d-1,l-2) \\ &= \frac{(l+d-2)!}{l!(d-2)!} - \frac{(l+d-4)!}{(l-2)!(d-2)!} \\ &= \frac{(2l+d-3)(l+d-4)!}{l!(d-3)!}. \end{aligned} \tag{2.2.14}$$

The next result is obtained from the A_l through application of the divergence theorem

in $d-1$ dimensions [33],

$$\int_{B^{d-1}} \nabla_{d-1} \cdot F(x) d^{d-1}x = \int_{S^{d-2}} F(\zeta) \cdot \zeta d\Omega_{d-2}, \tag{2.2.15}$$

for vector F, unit $(d-1)$-ball, B^{d-1}, and $F(\zeta) \cdot \zeta$ being the scalar product. Consider the terms $A_n \nabla A_m$ and $A_m \nabla A_n$ where $n \neq m$ then

$$\begin{aligned}\int_{B^{d-1}} \nabla_{d-1} \cdot (A_n(x)\nabla A_m(x) - A_m(x)\nabla A_n(x))\, d^{d-1}x \\ = \int_{S^{d-2}} (A_n(\zeta)\nabla A_m(\zeta) - A_m(\zeta)\nabla A_n(\zeta)) \cdot \zeta d\Omega_{d-2}\end{aligned} \tag{2.2.16}$$

from the divergence theorem. However we also know

$$\nabla_{d-2} \cdot (A_n \nabla_{d-2} A_m) = \nabla_{d-2} A_n \cdot \nabla_{d-2} A_m + A_n \triangle_{d-2} A_m \tag{2.2.17}$$

and $\triangle_{d-2} A_m = \triangle_{d-2} A_n = 0$. Thus

$$\int_{S^{d-2}} (A_n(\zeta)\nabla A_m(\zeta) - A_m(\zeta)\nabla A_n(\zeta)) \cdot \zeta d\Omega_{d-2} = 0. \tag{2.2.18}$$

From $A_l(t\zeta) = t^l A_l(\zeta)$ for $t \in \mathbb{R}$ we may write $\nabla_{d-2} A_l(\zeta) \cdot \zeta = l A_l(\zeta)$ giving

$$(m-n) \int_{S^{d-2}} A_n(\zeta) A_m(\zeta) d\Omega_{d-2} = 0 \tag{2.2.19}$$

which integrated over S^{d-2} is the same as

$$(m-n) \int_{S^{d-2}} Y_n(\zeta) Y_m(\zeta) d\Omega_{d-2} = 0 \tag{2.2.20}$$

and due to $m \neq n$

$$\int_{S^{d-2}} Y_n(\zeta) Y_m(\zeta) d\Omega_{d-2} = 0. \tag{2.2.21}$$

However there are $N(d-1,l)$ linearly independent spherical harmonics of degree l so the result (2.2.21) must be extended to include each harmonic of degree l. We also apply an orthonormalisation scheme (e.g. Gram-Schmidt [33]) to produce a new complete, orthonormal set of harmonics

$$\{Y_l^m(\zeta)\}_{m=1}^{N(d-1,l)} \tag{2.2.22}$$

such that

$$\int_{S^{d-2}} Y_l^m(\zeta) Y_l^n(\zeta) d\Omega_{d-2} = \delta_{mn}. \tag{2.2.23}$$

This can be further generalised [6, 32] to give

$$\int_{S^{d-2}} Y_k^m(\zeta) [Y_l^n(\zeta)]^* d\Omega_{d-2} = \delta_{kl}\delta_{mn}. \tag{2.2.24}$$

Finally we make use of the completeness of the spherical harmonics set [7] to find

$$\sum_{l,m} (Y_l^m(\zeta)[Y_l^m(\eta)]^*) = \delta^{d-2}(\zeta,\eta) \tag{2.2.25}$$

for η, a unit vector on S^{d-2} and the Dirac bi-scalar is defined as

$$\delta^{d-2}(\zeta,\eta) = \prod_{i=1}^{d-2} \delta(\zeta^i - \eta^i) \tag{2.2.26}$$

and is sometimes called the bi-density [53].

2.3 Classical Field Dynamics

We begin with a classical scalar field $\phi(x)$ in a d dimensional, curved spacetime $(\mathcal{M}, g^{\mu\nu})$. The field has the action

$$S = \int_{\mathcal{M}} \sqrt{-g}\mathcal{L}(\phi, x) d^d x \tag{2.3.1}$$

where g is the metric determinant and the manifold is assumed to have no boundary, $\partial\mathcal{M} = \emptyset$. The Lagragian $\mathcal{L}$ is given by

$$\mathcal{L} = -\frac{1}{2}\left(g^{\mu\nu}\phi(x)_{;\mu}\phi(x)_{;\nu} + m^2\phi(x)^2 + \xi R(x)\phi(x)^2\right) \tag{2.3.2}$$

where m is the mass associated with the field (later the mass of the individual quanta) and ξ the constant coupling the field to the scalar curvature of the spacetime, $R(x)$. Varying the action with respect to the field gives

$$\frac{\delta S}{\delta\phi} = \sqrt{-g}\left(\Box - m^2 - \xi R\right)\phi \tag{2.3.3}$$

which, once extremised, gives the Klein-Gordon equation

$$\left(\Box - m^2 - \xi R\right)\phi = 0. \tag{2.3.4}$$

The differential operator $\Box$ in equation (2.3.4) is

$$\Box\phi = g^{\mu\nu}\nabla_\mu\nabla_\nu\phi = (-g)^{-\frac{1}{2}}\partial_\mu\left(\sqrt{-g}\,g^{\mu\nu}\partial_\nu\phi\right). \tag{2.3.5}$$

Variation of the action (2.3.1) with respect to the metric yields the stress-energy tensor [23], $T_{\mu\nu}$, as follows

$$\begin{aligned} T_{\mu\nu} =& \frac{2}{\sqrt{-g}}\frac{\delta}{\delta g^{\mu\nu}}S[\phi, g_{\mu\nu}] \\ =& (1-2\xi)\phi_{;\mu}\phi_{;\nu} + \left(2\xi - \frac{1}{2}\right)g_{\mu\nu}g^{\alpha\beta}\phi_{;\alpha}\phi_{;\beta} - 2\xi\phi\,\phi_{;\mu\nu} \\ &+ 2\xi g_{\mu\nu}\phi\,\Box\phi + \xi\left(R_{\mu\nu} - \frac{1}{2}g_{\mu\nu}R\right)\phi^2 - \frac{1}{2}g_{\mu\nu}m^2\phi^2. \end{aligned} \tag{2.3.6}$$

Looking at the above shows that the object ϕ^2 only appears in the last two terms, it is this object that will become known as the vacuum polarisation after the field has been

quantised.

We now explicitly introduce our d dimensional black hole space-time, the Schwarzschild-Tangherlini metric [67],

$$ds^2 = -f(r)dt^2 + f(r)^{-1}dr^2 + r^2 d\Omega_{d-2}^2. \tag{2.3.7}$$

Here we have Schwarzschild-like coordinates, with time t, radial distance r, angular components $\theta_1, .., \theta_{d-3}, \varphi$ and with $d\Omega_{d-2}^2$ being the metric of a unit $(d-2)$-sphere such that

$$d\Omega_1^2 = d\varphi^2, \quad d\Omega_{i+1}^2 = d\theta_i^2 + \sin^2\theta_i \, d\Omega_i^2 \quad (i \geq 1). \tag{2.3.8}$$

The metric function $f(r)$ is

$$f(r) \equiv 1 - \left(\frac{r_h}{r}\right)^{d-3}, \tag{2.3.9}$$

usually written only as f, where r_h is the event horizon radius.

The Hartle-Hawking state (see §1.8) represents a black hole in thermal equilibrium with a heat bath at temperature T_H such that the black hole must have a non-zero Hawking temperature, as measured by an observer at infinity, of $T_H = \kappa/2\pi$. Here κ is the surface gravity of the black hole and with metric (2.3.7) is found to be

$$\kappa = \frac{1}{2}\left.\frac{df}{dr}\right|_{r=r_h} = \frac{d-3}{2r_h} \tag{2.3.10}$$

so that

$$T_H = \frac{d-3}{4\pi r_h}. \tag{2.3.11}$$

For a black hole in thermal equilibrium calculations are made easier by using a Euclidean approach [3, 75]. A Wick rotation is performed on our time coordinate so that we set $t_E = it_L$ where t_L is our original Lorentzian time and t_E is our new Euclidean

time coordinate (sometimes simply referred to as the imaginary time). The Wick rotation transforms metric (2.3.7) to the Euclidean metric

$$ds_E^2 = f dt_E^2 + f^{-1} dr^2 + r^2 d\Omega_{d-2}^2 \tag{2.3.12}$$

where s_E is the Euclidean invariant interval. It is important to note that the temperature (2.3.11) and the surface gravity (2.3.10) remain the same after the Wick rotation. Note also this variable change removes from our manifold, $\mathcal{M}$, the region interior to the event horizon restricting any calculation with this metric to the exterior of the black hole.

There is a secondary effect of the Wick rotation that is seen when we consider that the Euclidean metric appears to have a conical defect at the event horizon where the Lorentzian case has a coordinate singularity. We can investigate the behaviour near (but outside) the event horizon by looking at $r = r_h + \delta^2$ for small δ such that the metric function is now

$$\begin{aligned} f &= 1 - \left(\frac{r_h}{r_h + \delta^2}\right)^{d-3} \\ &= \frac{(d-3) r_h^{d-4} \delta^2}{r^{d-3}} + O(\delta^4). \end{aligned} \tag{2.3.13}$$

In this region outside the event horizon the metric (2.3.12) is approximately (ignoring terms of $O(\delta^4)$ or higher)

$$ds_E^2 = \frac{(d-3) r_h^{d-4} \delta^2}{r^{d-3}} dt_E^2 + \frac{4 r^{d-3}}{(d-3) r_h^{d-4}} d\delta^2 + r^2 d\Omega_{d-2}^2. \tag{2.3.14}$$

If we now only look at the $t_E - \delta$ plane of metric (2.3.14) (which contains the conical defect at $\delta = 0$) then we see the invariant interval in this plane, ς, is defined by

$$d\varsigma^2 = \frac{4 r^{d-3}}{(d-3) r_h^{d-4}} \left[\left(\frac{(d-3) r_h^{d-4}}{2 r^{d-3}} \right)^2 \delta^2 dt_E^2 + d\delta^2 \right]. \tag{2.3.15}$$

This plane no longer contains a conical defect if our scaled coordinate $\frac{(d-3)r_h^{d-4}}{2r^{d-3}}t_E$ has period 2π at $r = r_h$, in other words we must have (using $\sim$ for equivalence)

$$\begin{aligned} t_E &\sim t_E + \lim_{r\to r_h}\left(\frac{4\pi r^{d-3}}{(d-3)r_h^{d-4}}\right) \\ &\sim t_E + \frac{4\pi r_h}{(d-3)}. \end{aligned}$$

Comparing this to temperature (2.3.11) we see that the period is the inverse of the Hawking temperature (commonly denoted as $T_H^{-1} = \beta$).

Hence, from the above, states on metric (2.3.12) will be periodic with period β, as an example this will be useful when applying (2.5.11). This result is not surprising as we are aware from quantum statistical mechanics that states at thermal equilibrium are periodic with respect to imaginary time with period T^{-1}, see for example [9].

For this research the implementation of the Wick rotation has no impact on our results (only the calculations). As we are investigating a static system any results hold for all values of t_E including at the origin where $t_E = 0 = t_L$, hence our results still hold for the Lorentzian system.

Important Note: For the rest of this thesis, unless explicitly stated, we will work with the Euclidean time and invariant interval denoting them respectively as t and s for simplicity. Additionally the Hawking temperature will be denoted as T.

Using our new unit definitions we can express the Euclidean metric simply as

$$ds^2 = f dt^2 + f^{-1}dr^2 + r^2 d\Omega_{d-2}^2 \tag{2.3.16}$$

which will now be used instead of (2.3.7).

For the scalar field mode solutions to (2.3.4) we use the ansatz

$$\phi(x) = e^{-i\omega t}\Upsilon(r)\Theta(\theta_1, .., \theta_{d-3})e^{im\varphi} \tag{2.3.17}$$

with coordinates as used in metric (2.3.16) such that the field is the sum of these modes. Here ω and m are introduced as arbitrary constants but we associate ω with the field mode frequency and later with the quanta frequency. Passing this ansatz through equation (2.3.4) gives an ODE for $\Upsilon(r)$, which is termed the radial ODE and is metric dependent, and an ODE for the angular functions.

Looking at (2.3.4) we note that from within $\Box$ there is a Laplace type operation on the angular functions the details of which are discussed in §2.2. First let $Y_l(\theta_1, .., \theta_{d-3}, \varphi)$ be a harmonic function on the unit $(d-2)$-sphere such that

$$Y_l(\theta_1, .., \theta_{d-3}, \varphi) = \Theta(\theta_1, .., \theta_{d-3})e^{im\varphi}. \tag{2.3.18}$$

Then from equation (2.2.8) we have

$$\triangle_{S^{d-2}} Y_l = -l(l+d-3)Y_l \tag{2.3.19}$$

creating a contribution to equation (2.3.20).

Bringing together equations (2.3.4), (2.3.16) and (2.3.17) explicitly gives us the radial ODE [48],

$$\frac{1}{r^{d-4}}\frac{d}{dr}\left[r^{d-2}f\frac{d}{dr}\Upsilon(r)\right] - \left(\frac{\omega^2 r^2}{f} + (m^2 + \xi R)r^2 + l(l+d-3)\right)\Upsilon(r) = 0. \tag{2.3.20}$$

2.4 Quantisation

We return to equation (2.3.4) except we now assume the field is quantised raising $\phi(x)$ to a field operator. In accordance with the literature the symbol for $\phi(x)$ remains unchanged. This leaves (2.3.4) unchanged in form though now we note that meaningful results can only come from expectation values.

As there is now a quantum field in curved space we must define our state, for which we choose the Hartle-Hawking vacuum [37]. We will only be using the Hartle-Hawking vacuum, whose ket vector is $|0_H\rangle$, in all following calculations. We simplify our notation such that for some field operator $A(x)$ we set $\langle 0_H|A(x)|0_H\rangle = \langle A\rangle$. We then call $\langle A\rangle$ the expectation value of $A(x)$.

Also, as the field is quantised we can no longer calculate a stress-energy tensor and must instead look at its expectation value. Equation (2.3.6) can now, schematically, be thought of as

$$\begin{aligned}\langle T_{\mu\nu}\rangle = (1-2\xi)\langle\phi_{;\mu}\phi_{;\nu}\rangle + \left(2\xi - \frac{1}{2}\right) g_{\mu\nu}g^{\alpha\beta}\langle\phi_{;\alpha}\phi_{;\beta}\rangle - 2\xi\langle\phi\,\phi_{;\mu\nu}\rangle \\ + 2\xi g_{\mu\nu}\langle\phi\,\Box\phi\rangle + \xi\left(R_{\mu\nu} - \frac{1}{2}g_{\mu\nu}R\right)\langle\phi^2\rangle - \frac{1}{2}g_{\mu\nu}m^2\langle\phi^2\rangle.\end{aligned} \tag{2.4.1}$$

A more precise derivation is given in (2.5.7).

We concentrate on the object $\langle\phi^2\rangle$ in (2.4.1), which is formally the vacuum expectation value of the auto-correlation of the field, the so-called vacuum polarisation. This is the object we seek to construct as it is the simplest to calculate and the methods required to calculate the other expectation values in (2.4.1) are based on the method to solve $\langle\phi^2\rangle$.

2.5 Point-splitting

In a naive calculation $\langle\phi^2\rangle$ (and as a result $\langle T_{\mu\nu}\rangle$) diverges as the operators act on the same spacetime point (see Appendix A), hence it will need to be renormalised. Therefore the vacuum polarisation in (2.4.1) is unrenormalised, $\langle\phi^2\rangle_{\text{unren}}$, and we seek its renormalised value, $\langle\phi^2\rangle_{\text{ren}}$. So instead of concentrating on a single spacetime event we consider two nearby events x and x' such that x' is within the normal convex neighborhood of x (this condition is to guarantee that in later steps there is a unique geodesic connecting the two events). The intention is to express the behaviour of the field modes between these points in such a way that should we allow $x' \to x$ the cause of any divergences can be isolated and removed in our renormalisation step. We refer to this approach as point-splitting.

We use a biscalar, the Feynman propagator $G_F(x, x')$, defined as

$$G_F(x, x') = i\langle T(\phi(x)\phi(x'))\rangle \tag{2.5.1}$$

where the image of $T()$ is the time ordered products of its arguments. We want such a propagator to be a Green's function of a Klein-Gordon equation, previously equation (2.3.4). It has been shown [23] that $G_F(x, x')$ satisfies

$$\left[\Box - m^2 - \xi R\right] G_F(x, x') = (-g(x))^{-\frac{1}{2}}\delta^d(x - x') \tag{2.5.2}$$

where $g(x)$ is the determinant of the metric at x. However we have yet to account for the Euclideanisation of the manifold, to do so we define a Euclidean propagator, $G_E(x; x')$, as

$$G_E(x; x') = -iG_F(x, x') = \langle T(\phi(x)\phi(x'))\rangle. \tag{2.5.3}$$

This Euclidean propagator must be related to the vacuum polarisation to be useful and it

can be shown [3] that in fact,

$$\langle \phi^2 \rangle_{\text{unren}} = Re[\lim_{x' \to x} G_E(x; x')]. \tag{2.5.4}$$

Furthemore $G_E(x, x')$ is the Green's function solution of the Klein-Gordon equation on the Euclidean spacetime (2.3.16) [23]

$$\left[\nabla_{x\mu}\nabla_x^\mu - m^2 - \xi R\right] G_E(x; x') = -g^{-\frac{1}{2}}(x)\delta^d(x - x') \tag{2.5.5}$$

where ∇_x denotes the covariant derivative at x. Equation (2.5.5) is an elliptic partial differential equation (its Lorentzian form would be hyperbolic) and as such its solutions are uniquely determined by the boundary conditions. Here the lack of a compact boundary implies equation (2.5.5) is sufficient to define the unique solution.

Having now defined the Euclidean Green's function (2.5.3) the proper form of the expectation value of $T_{\mu\nu}$ (2.4.1) is given by [23],

$$\langle T_{\mu\nu} \rangle = \lim_{x \to x'} \mathfrak{T}_{\mu\nu}(x, x') \left(G_E(x, x')\right) \tag{2.5.6}$$

where the operator $\mathfrak{T}_{\mu\nu}(x, x')$ is defined as

$$\begin{aligned} \mathfrak{T}_{\mu\nu} = {} & (1 - 2\xi) g_\nu{}^{\nu'} \nabla_\mu \nabla_{\nu'} + \left(2\xi - \frac{1}{2}\right) g_{\mu\nu} g^{\alpha\beta'} \nabla_\alpha \nabla_{\beta'} - 2\xi g_\mu{}^{\mu'} g_\nu{}^{\nu'} \nabla_{\mu'} \nabla_{\nu'} \\ & + 2\xi g_{\mu\nu} \nabla_\alpha \nabla^\alpha + \xi \left(R_{\mu\nu} - \frac{1}{2} g_{\mu\nu} R\right) - \frac{1}{2} g_{\mu\nu} m^2, \end{aligned} \tag{2.5.7}$$

where $g_\mu{}^{\mu'}$ is termed the bivector of parallel transport [19] and is defined in (2.10.17). The action of $\mathfrak{T}_{\mu\nu}$ on $G_E(x, x')$ says that the calculation of the stress-energy tensor's expectation value is dependent on 0th, 1st and 2nd order derivatives of the Euclidean Green's function. Thus any attempt to calculate $\langle T_{\mu\nu} \rangle$ in such a fashion requires the methodology presented here to first derive $G_E(x, x')$. Hence calculation of the vacuum

polarisation is treated as a first step in calculating the stress-energy tensor.

Looking at the right hand side of the Klein-Gordon equation (2.5.5) we find

$$-\delta^d(x-x') = -\delta(t-t')\delta(r-r')\delta(\Omega,\Omega'). \tag{2.5.8}$$

Also for our metric (2.3.16) we have noting that $\delta(\Omega,\Omega')$ represents the $d-2$ dimensional delta function of two vectors on the unit $(d-2)$-sphere, and

$$g^{\frac{1}{2}}(x) = r^{d-2}\prod_{i=1}^{d-3}\sin(\theta_i)^i. \tag{2.5.9}$$

Now we may write the explicit form of (2.5.5) as

$$\begin{aligned}\left(r^{-(d-2)}\partial_r(r^{d-2}f\partial_r) + f^{-1}\partial_t^2 + r^{-2}\triangle_{S^{d-2}} - m^2 - \xi R\right) G_E(t,r,\Omega;t',r',\Omega') \\ = -\left(r^{d-2}\prod_{i=1}^{d-3}\sin(\theta_i)^i\right)^{-1}\delta(t-t')\delta(r-r')\delta(\Omega,\Omega')\end{aligned} \tag{2.5.10}$$

with operator $\triangle_{S^{d-2}}$ as defined in equation (2.2.4). The form of equation (2.5.10) suggests we expand the Euclidean Green's function by separation of variables allowing us to immediately separate independent equations in (t,t') and (Ω,Ω'). Using standard Green's function techniques [32] we know that the t and Ω dependence of the Green's function is related to an appropriate form of the corresponding delta function.

For a thermal state at temperature T, such as the Hartle-Hawking state, the Euclidean Green's function is periodic in $t-t'$ with period T^{-1} so a suitable representation of the delta function of time is [32, 69]

$$\delta(t-t') = T\sum_{n=-\infty}^{\infty}\exp[2\pi n i T(t-t')]. \tag{2.5.11}$$

We now let $\epsilon = t - t'$. A related integral

$$\delta(t - t') = \frac{1}{2\pi} \int_{-\infty}^{\infty} \exp[i\omega\epsilon] d\omega \tag{2.5.12}$$

would be used for a non-thermal state [3].

2.6 The Angular Delta Function

We know from §2.2 that the spherical harmonics $\{Y_l^m(\zeta)\}$ form a complete, orthonormal set and are thus an orthonormal basis of the Hilbert space of square-integrable functions on the unit sphere. This allows us to express any function on the unit sphere as sums over the spherical harmonic basis.

However first we must correctly associate angles with their spherical harmonic indices. To give each index a unique and physical meaning in association with an angular degree of freedom they are read as the angular momentum quantum number for that degree. The angle of most importance is θ_1, which can be thought of as the primary angle as it is the only angular degree of freedom that exists in all $d \geq 3$ ($d = 3$ is a case we will not investigate). Associated with θ_1 is index l which is the total angular momentum quantum number and is the reason for its prevalence as the prime index in §2.2. The association is extended to include the azimuthal angle φ and the azimuthal quantum number m such that given a function $h(\theta_1, \varphi)$, square integrable on the (2)-sphere, we may write

$$h(\theta_1, \varphi) = \sum_{l=0}^{\infty} \sum_{m=-l}^{m=l} h_l^m \, Y_l^m(\theta_1, \varphi). \tag{2.6.1}$$

Note the index m here is the equivalent to index m first encountered in equation (2.3.17).

We extend the above indexing scheme by example in $d = 5$ where there now exist indices l, m_1 and m_2. Given a function $h(\theta_1, \theta_2, \varphi)$, square integrable on the (3)-sphere,

we may now write [27, 57]

$$h(\theta_1,\theta_2,\varphi)=\sum_{l=0}^{\infty}\sum_{m_1=0}^{l}\sum_{m_2=0}^{m_1} h_l^{m_1,m_2}\,Y_l^{m_1,m_2}(\theta_1,\theta_2,\varphi)\quad\text{where } l\geq m_1\geq m_2. \tag{2.6.2}$$

It can be seen that the indices have been redefined from the $d=4$ example to remove negative values of m hence none of these indices can be considered equivalent to the index m from (2.3.17). However m_{d-3} is always held to be the azimuthal quantum number irrelevant of its scaling. For d dimensions equation (2.6.2) is generalised to contain an index for every angular degree of freedom and is expressed in common notation [32] as

$$h(\theta_1,...,\theta_{d-3},\varphi)=\sum_{l=0}^{\infty}\sum_{\{m\}} h_l^{\{m\}}\,Y_l^{\{m\}}(\theta_1,...,\theta_{d-3},\varphi)\quad\text{where } l\geq m_1\geq ...\geq m_{d-3} \tag{2.6.3}$$

where $\{m\}=\{m_1,...,m_{d-3}\}$. However, independent of the number of indices required we know from equation (2.2.14) the exact number of terms within the l sum and so we rewrite (2.6.3) in its final form

$$h(\theta_1,...,\theta_{d-3},\varphi)=\sum_{l=0}^{\infty}\sum_{m=1}^{N(d-1,l)} h_l^m\,Y_l^m(\theta_1,...,\theta_{d-3},\varphi). \tag{2.6.4}$$

Finally to express $\delta(\Omega;\Omega')$ we compare equations (2.2.25) and (2.6.4) to find [32, 69]

$$\delta(\Omega;\Omega')=\sum_{l=0}^{\infty}\sum_{m=1}^{N(d-1,l)} Y_l^m(\zeta)Y_l^m(\eta)^*. \tag{2.6.5}$$

2.7 Mode Sums

From equations (2.5.11) and (2.6.5) we may write the Green's function (2.5.5) as [32, 69]

$$G_E(x,x') = \frac{\kappa}{2\pi}\sum_{n=-\infty}^{\infty}\exp\left[i\omega\epsilon\right]\sum_{l=0}^{\infty}S_{\omega l}(r,r')\sum_{m=1}^{N(d-1,l)}Y_l^m(\zeta)Y_l^m(\eta)^* \tag{2.7.1}$$

where we have set $\epsilon = t - t'$, the constant κ is the surface gravity of the black hole and the function $S_{\omega l}(r,r')$ is a radial Green's function to be determined. This series is convergent for $x \neq x'$ as noted in Appendix A. We will only consider modes for which $\omega = 2\pi nT$ (for $n \in \mathbb{N}$) and is related to the surface gravity and metric function by

$$\omega = 2\pi nT = n\kappa = \frac{n}{2}\left.\frac{df}{dr}\right|_{r=r_h}. \tag{2.7.2}$$

Using solution (2.7.1) in the Klein-Gordon equation (2.5.10) provides a differential equation for $S_{\omega l}(r,r')$ [32], referred to as the point split radial equation,

$$\frac{1}{r^{d-4}}\frac{d}{dr}\left[r^{d-2}f\frac{d}{dr}S_{\omega l}\right] - \left(\frac{\omega^2 r^2}{f} + (m^2+\xi R)r^2 + l(l+d-3)\right)S_{\omega l} = -\frac{1}{r^{d-2}}\delta(r-r'). \tag{2.7.3}$$

In anticipation of r and r' coinciding we define the radial Green's function as [2]

$$S_{\omega l}(r,r') = C_{\omega l}p_{\omega l}(r_<)q_{\omega l}(r_>) \tag{2.7.4}$$

such that $r_<$ is the lesser of r and r' and $r_>$ is the greater. The functions $p_{\omega l}$ and $q_{\omega l}$ are solutions to the homogeneous form of (2.7.3) with appropriate boundary conditions as detailed following (2.8.1). A normalising constant, $C_{\omega l}$, is to be defined in (2.8.3) after we let $r \to r'$. As (2.7.1) is acted upon in equation (2.5.5) we note that from within $\Box_x$ there is a Laplace type operation on the harmonics $Y_l^m(\zeta)$ and $Y_l^m(\eta)$. Defining $\triangle_{S^{d-2}}$ as the

Laplace-Beltrami operator on the $(d-2)$-sphere we have [32]

$$\triangle_{S^{d-2}} Y_l^m = -l(l+d-3)Y_l^m, \tag{2.7.5}$$

as discussed for equation (2.2.8), creating a contribution to equation (2.7.3).

To tidy equation (2.7.1) for later use we apply Müller's addition theorem [27, 57] which states (using notation from sections §2.2 and §2.6)

$$\sum_{m=1}^{N(d-1,l)} Y_l^m(\zeta) Y_l^m(\eta)^* = \frac{N(d-1,l)}{S_{d-2}} G_l^\lambda(\cos\gamma) \tag{2.7.6}$$

where $\cos\gamma = \zeta.\eta$ and G_l^λ is the Gegenbauer polynomial of order l and degree $\lambda = (d-3)/2$ with

$$S_{d-2} = \frac{2\pi^{\frac{(d-1)}{2}}}{\Gamma\left(\frac{(d-1)}{2}\right)}, \tag{2.7.7}$$

the surface area of a unit $(d-2)$-sphere. Note that in the original literature [57] this surface area is denoted ω_{d-2}.

Expressing $N(d-1,l)/\omega_{d-2}$ as $\tilde{N}_{d,l}$ we can now write (2.7.1) as

$$G_E(x,x') = \frac{\kappa}{2\pi} \sum_{n=-\infty}^{\infty} \exp\left[i\omega(t-t')\right] \sum_{l=0}^{\infty} \tilde{N}_{d,l} G_l^\lambda(\cos\gamma) S_{\omega l}(r,r') \tag{2.7.8}$$

where

$$\tilde{N}_{d,l} = \frac{(2l+d-3)(l+d-4)!}{l!(d-3)!\,2\pi^{\frac{d-1}{2}}} \Gamma\left(\frac{d-1}{2}\right) \tag{2.7.9}$$

and is called the degeneracy factor.

Finally some notes on equation (2.7.8); firstly this object will be referred to as the mode sum irrespective of which (if any) independent variables have been allowed to coincide. Secondly the order of the sums it contains is not fixed, as the independent variables are allowed to coincide whichever is brought together last determines the fixed order as is

explained in the next section.

2.8 Point Coincidence

To express (2.7.8) in a useful form we must choose a point splitting scheme. This means making a choice of which variables remain separated as the other variables coincide. We can thus express the divergence in (2.7.8) as the limit of this remaining variable coinciding. We allow the point-split variables to coincide in stages. First we consider $r \to r'$.

We define two functions $p_{\omega l}(r)$ and $q_{\omega l}(r)$ which are the solutions to the homogeneous form of (2.7.3), which is equivalent to the radial ODE (2.3.20),

$$\frac{1}{r^{d-4}}\frac{d}{dr}\left[r^{d-2}f\frac{d}{dr}S_{\omega l}\right] - \left(\frac{\omega^2 r^2}{f} + (m^2+\xi R)r^2 + l(l+d-3)\right)S_{\omega l} = 0. \tag{2.8.1}$$

Equation (2.8.1) can be solved analytically in certain numbers of dimensions in combination with certain values of ω, m, l and R, these cases will be stated explicitly when they arise. In general (2.8.1) must be solved numerically creating its own difficulty in guaranteeing accurate and correct results. This will be discussed in detail when values need to be calculated such as in §3.8 onwards and §4.6 onwards. Analysis near both singular points, $r = r_h$ and $r = \infty$, shows that at each point one solution of (2.8.1) will diverge and one will be regular. The functions $p_{\omega l}$ and $q_{\omega l}$ are distinguished by letting $p_{\omega l}$ be the solution that is regular on the horizon and $q_{\omega l}$ being that which is regular as r approaches infinity. These are then the functions $p_{\omega l}$ and $q_{\omega l}$ in equation (2.7.4). Note that we are able to define the behaviour of these functions in this manner by analysis of their associated Frobenius series, see for example §3.8.

The functions $p_{\omega l}$ and $q_{\omega l}$ allow us to usefully express $S_{\omega l}(r, r')$ from equation (2.7.3) by [2, 75]

$$\lim_{r' \to r}\left(S_{\omega l}(r, r')\right) = C_{\omega l}p_{\omega l}(r)q_{\omega l}(r), \tag{2.8.2}$$

where $C_{\omega l}$ is a normalising constant satisfying the Wronskian condition from equation (2.8.1) [2]

$$C_{\omega l}\left[p_{\omega l}\frac{dq_{\omega l}}{dr}-q_{\omega l}\frac{dp_{\omega l}}{dr}\right]=-\frac{1}{r^{d-2}f}. \tag{2.8.3}$$

Inserting equation (2.8.2) into equation (2.7.8) gives

$$G_E(x,x')=\frac{\kappa}{2\pi}\sum_{n=-\infty}^{\infty}\exp\left[i\omega(t-t')\right]\sum_{l=0}^{\infty}\tilde{N}_{d,l}G_l^{\lambda}(\cos\gamma)C_{\omega l}p_{\omega l}(r)q_{\omega l}(r). \tag{2.8.4}$$

Note that the order of the sums in equation (2.8.4) is not fixed and will depend on the order in which we allow the remaining split variables to coincide. Should the angular variables coincide last then the l sum will be the outer operation and equivalently if the time variable coincides last then the n sum will be outer. We can understand this from example in the Schwarzschild case where the difference between the order of summation is a finite amount [16]. This value is equal to the difference of the regular components of the temporal and angular Hadamard expansions. We know not to expect absolute convergence in (2.8.4) due to the distributional nature of the Green's function, see Appendix A. This can be clearly seen in a comparison of [17] and [68] which demonstrates that the order of summation will give different results.

Next we demonstrate two approaches; firstly by allowing angular coincidence and leaving temporal splitting then allowing temporal coincidence and leaving angular splitting.

Angular point coincidence is performed by taking $\gamma\to 0$, this requires being able to calculate the value of the Gegenbauer polynomial in equation (2.7.6). From [66] we know that $G_l^{\lambda}(x)$ is a special case of the Jacobi polynomial with generating function

$$\frac{1}{(1-2xt+t^2)^{\lambda}}=\sum_{l=0}^{\infty}G_l^{\lambda}(x)t^l \tag{2.8.5}$$

and can be calculated from the recurrence relations

$$G_0^\lambda(x) = 1 \tag{2.8.6}$$

$$G_1^\lambda(x) = 2\lambda x \tag{2.8.7}$$

$$G_l^\lambda(x) = \frac{1}{l}[2x(l+\lambda-1)G_{l-1}^\lambda(x) - (l+2\lambda-2)G_{l-2}^\lambda(x)]. \tag{2.8.8}$$

For our calculation we will always have $d \geq 4$ ($\lambda \geq \frac{1}{2}$), thus letting $\gamma \to 0$ we obtain

$$\lim_{\gamma\to 0} G_l^\lambda(\cos\gamma) = G_l^\lambda(1) = \begin{cases} 1 & d = 4 \\ \dfrac{1}{(d-4)!}\displaystyle\prod_{i=1}^{d-4}(l+i) & d \geq 5 \end{cases} \tag{2.8.9}$$

where the product in the second line can be expressed in several ways

$$\prod_{i=1}^{d-4}(l+i) = \frac{(l+d-4)!}{l!} = \frac{\Gamma(l+d-3)}{\Gamma(l+1)} = (l+1)_{d-4} \tag{2.8.10}$$

and the last entry is written as a Pochhammer symbol.

Now we bring together the coincident Gegenbauer polynomial (2.8.9) and the degeneracy factor resulting in, for $d = 4$,

$$G_l^{\frac{1}{2}}(1)\tilde{N}_{4,l} = \frac{2l+1}{4\pi} \tag{2.8.11}$$

and, for $d \geq 4$,

$$G_l^{\lambda\geq 1}(1)\tilde{N}_{d\geq 5,l} = \frac{(2l+d-3)\Gamma(\frac{d-1}{2})}{(d-3)!(d-4)!2\pi^{\frac{d-1}{2}}}\prod_{i=1}^{d-4}(l+i)^2. \tag{2.8.12}$$

For conciseness of notation this equation will not be inserted into our expression for the Green's function.

Our Euclidean Green's function (2.8.4) now has the form

$$\begin{aligned} G_E(\mathbf{x},t;\mathbf{x},t') &= \frac{\kappa}{2\pi}\sum_{n=-\infty}^{\infty} e^{i\omega\varepsilon}\sum_{l=0}^{\infty}\tilde{N}_{d,l}G_l^{\lambda}(1)C_{\omega l}p_{\omega l}(r)q_{\omega l}(r) \\ &= \frac{\kappa}{\pi}\sum_{n=1}^{\infty}\cos(\omega\epsilon)\sum_{l=0}^{\infty}\tilde{N}_{d,l}G_l^{\lambda}(1)C_{\omega l}p_{\omega l}(r)q_{\omega l}(r) \\ &\quad + \frac{\kappa}{2\pi}\sum_{l=0}^{\infty}\tilde{N}_{d,l}G_l^{\lambda}(1)C_{0l}p_{0l}(r)q_{0l}(r), \end{aligned} \tag{2.8.13}$$

where we have set $\varepsilon = t - t'$.

Undoing the temporal point-splitting first is done by taking $\epsilon \to 0$. Applying this to (2.8.4) gives

$$G_E(r,t,\gamma;r,t,0) = \frac{\kappa}{2\pi}\sum_{l=0}^{\infty}\tilde{N}_{d,l}G_l^{\lambda}(\cos\gamma)\sum_{n=-\infty}^{\infty}C_{\omega l}p_{\omega l}(r)q_{\omega l}(r) \tag{2.8.14}$$

after the correct ordering of the sums due to the angular variables still being split.

2.9 Renormalisation

Previous work [22, 23] has shown that the most rigorous method of isolating divergences within a Green's function of the type in (2.5.5) is through the Hadamard expansion. This is due to its ability to capture short distance behaviour and that $G_E(x,x')$ is symmetric under exchange of x and x', exactly the behaviour a Hadamard expansion emulates. The Hadamard method expands a Green's function into a sum of symmetric biscalars regular as $r' \to r$ [23]. In order to derive the expansion several objects need to be defined and it must be noted the expansion depends on whether d is odd or even. The DeWitt-Schwinger expansion [20] in $d = 4$, used for example in [75], when applied to the metric (2.3.16) agrees with the Hadamard expansion up to a term dependent on the mass of the scalar field.

Firstly Synge's world function [65], $\sigma(x,x')$, is defined by

$$\sigma(x,x') = \frac{1}{2}s(x,x')^2 \tag{2.9.1}$$

where $s(x,x')$ is the length along the unique geodesic connecting x and x'. The calculation of $\sigma(x,x')$ is discussed in §2.10.

Secondly we define the biscalar form of the Van Vleck-Morette determinant [25, 71], $\Delta(x,x')$, which measures the tidal focussing (defocussing) of geodesic flows in a spacetime. It is defined as

$$\Delta(x,x') = -\sqrt{g(x)}\det\left(-\sigma_{;\mu\nu'}(x,x')\right)\sqrt{g(x')} \tag{2.9.2}$$

and satisfies the PDE

$$\Box_x\sigma = d - 2\Delta^{-1/2}(\Delta^{1/2})_{;\mu}\sigma^{;\mu} \tag{2.9.3}$$

and boundary condition

$$\lim_{x'\to x}\Delta(x,x') = 1. \tag{2.9.4}$$

Lastly we introduce a dimensionally based constant, α_d, by

$$\alpha_d = \frac{\Gamma(\frac{d}{2}-1)}{(2\pi)^{\frac{d}{2}}} \quad (d \geq 3). \tag{2.9.5}$$

For $d \neq 2$ and even we may expand our Green's function (2.5.5) [23]

$$G_E(x,x') = \frac{\alpha_d}{2}\left(\frac{U(x,x')}{\sigma(x,x')^{\frac{d}{2}-1}} + V(x,x')\ln[\sigma(x,x')] + W(x,x')\right) \tag{2.9.6}$$

where U, V and W may be expressed as

$$\begin{aligned} U(x,x') &= \sum_{n=0}^{d/2-2} U_n(x,x')\sigma^n(x,x') \\ V(x,x') &= \sum_{n=0}^{\infty} V_n(x,x')\sigma^n(x,x') \\ W(x,x') &= \sum_{n=0}^{\infty} W_n(x,x')\sigma^n(x,x'). \end{aligned} \tag{2.9.7}$$

Note that in practice we introduce a dimensionful constant inside the logarithm, for a massive field this constant is the field mass otherwise it is free but with units of mass.

The coefficients U_n and V_n are regular, symmetric biscalars governed by the recursion relations [23]

$$\begin{aligned} &(n+1)(2n+4-d)U_{n+1} + (2n+4-d)U_{n+1;\mu}\sigma^{;\mu} \\ &\qquad - (2n+4-d)U_{n+1}\Delta^{-1/2}(\Delta^{1/2})_{;\mu}\sigma^{;\mu} + (\Box_x - m^2 - \xi R)U_n = 0 \end{aligned} \tag{2.9.8}$$

for $n = 0, 1, ..., d/2-3$ with boundary condition

$$U_0 = \Delta^{1/2} \tag{2.9.9}$$

and

$$\begin{aligned} &(n+1)(2n+d)V_{n+1} + 2(n+1)V_{n+1;\mu}\sigma^{;\mu} \\ &\qquad - 2(n+1)V_{n+1}\Delta^{-1/2}(\Delta^{1/2})_{;\mu}\sigma^{;\mu} + (\Box_x - m^2 - \xi R)V_n = 0 \end{aligned} \tag{2.9.10}$$

with boundary condition

$$(d-2)V_0 + 2V_{0;\mu}\sigma^{;\mu} - 2V_0\Delta^{-1/2}(\Delta^{1/2})_{;\mu}\sigma^{;\mu} + (\Box_x - m^2 - \xi R)U_{d/2-2} = 0. \tag{2.9.11}$$

For d odd even we may expand our Green's function (2.5.5) [23]

$$G_E(x,x') = \frac{\alpha_d}{2}\left(\frac{U(x,x')}{\sigma(x,x')^{\frac{d}{2}-1}} + W(x,x')\right) \tag{2.9.12}$$

where U and W may be expressed as

$$\begin{aligned} U(x,x') &= \sum_{n=0}^{\infty} U_n(x,x')\sigma^n(x,x') \\ W(x,x') &= \sum_{n=0}^{\infty} W_n(x,x')\sigma^n(x,x'). \end{aligned} \tag{2.9.13}$$

The coefficients U_n are regular, symmetric biscalars governed by the recursion relations [23]

$$\begin{aligned} (n+1)(2n+4-d)U_{n+1} + (2n+4-d)U_{n+1;\mu}\sigma^{;\mu} \\ - (2n+4-d)U_{n+1}\Delta^{-1/2}\Delta^{1/2}_{;\mu}\sigma^{;\mu} + (\Box_x - m^2 - \xi R)U_n = 0 \end{aligned} \tag{2.9.14}$$

with boundary condition

$$U_0 = \Delta^{1/2}. \tag{2.9.15}$$

It is important to note that for any d the coefficients W_n are regular, symmetric biscalars that obey recursion relations similar to those for the U_n and V_n. For $d \neq 2$ and even we have

$$\begin{aligned} (n+1)(2n+d)W_{n+1} + 2(n+1)W_{n+1;\mu}\sigma^{;\mu} - 2(n+1)W_{n+1}\Delta^{-1/2}\Delta^{1/2}_{;\mu}\sigma^{;\mu} + (4n+2+d)V_{n+1} \\ + 2V_{n+1;\mu}\sigma^{;\mu} - 2V_{n+1}\Delta^{-1/2}\Delta^{1/2}_{;\mu}\sigma^{;\mu} + (\Box_x - m^2 - \xi R)W_n = 0 \end{aligned} \tag{2.9.16}$$

and for d odd we have

$$(n+1)(2n+d)W_{n+1} + 2(n+1)W_{n+1;\mu}\sigma^{;\mu} \\ - 2(n+1)W_{n+1}\Delta^{-1/2}\Delta^{1/2}_{;\mu}\sigma^{;\mu} + (\Box_x - m^2 - \xi R)W_n = 0. \quad (2.9.17)$$

Now note that U_n and V_n are purely geometric in construction and do not depend on the quantum state being considered. Specifically U_n and V_n are determined only by the behaviour of the recursion relations along the geodesic connecting x and x'. In comparison there is an apparent issue in that from relations (2.9.16) and (2.9.17) we see W_0 is unconstrained and hence so are all $W_{n\geq 1}$. However this lack of constraints can be used to encode the quantum state information of the system in the W_n. By specifying W_0 in accordance with a quantum state all the W_n, and hence $W(x,x')$, are determined uniquely. This means that expansions (2.9.6) and (2.9.12) contain two pieces, the first is based on the $W_n(x,x')$ which contain geometric and quantum state information. The second, based on the $U_n(x,x')$ (and in even d $V_n(x,x')$), contain purely geometric information and are state independent. This means this second part, the purely geometric terms, will contain any divergences present as $x' \to x$.

The singular terms of the Hadamard expansion are therefore [23]

$$G_{E,sing} = \frac{\alpha_d}{2}\left(\frac{U(x,x')}{\sigma(x,x')^{\frac{d}{2}-1}} + V(x,x')\ln[\sigma(x,x')]\right) \quad (d \neq 2 \text{ and even}) \qquad (2.9.18)$$

and

$$G_{E,sing} = \frac{\alpha_d}{2}\left(\frac{U(x,x')}{\sigma(x,x')^{\frac{d}{2}-1}}\right) \quad (d \text{ odd}). \qquad (2.9.19)$$

Our renormalisation scheme will be to remove the expansions (2.9.18) and (2.9.19) from mode sums (2.8.13) and (2.8.14). The appropriate terms are those which are divergent or finite as $x' \to x$ and have had the correct point-split scheme applied (i.e. letting $r' \to r$

and either $t' \to t$ or $\gamma \to 0$). Noting that

$$\lim_{x' \to x} \sigma(x, x') = 0 \tag{2.9.20}$$

all terms that will not be divergent or finite in (2.9.18) and (2.9.19) will be zero. This means the renormalised vacuum polarisation can be expressed as

$$\langle \phi^2 \rangle_{\text{ren}} = \lim_{\substack{\epsilon \to 0 \\ \text{or} \\ \gamma \to 0}} \left(G_E(x, x') - G_{E,sing} \right). \tag{2.9.21}$$

2.10 Deriving Divergent Terms

In the previous section we laid out the scheme by which we will implement renormalisation. We constructed this by reviewing the Hadamard expansion of a Green's function and finding that all singular behaviour is expressed in a finite number of terms. We also showed how these terms are constructed from a power series in σ depending on coefficients with specific recursion relations and boundary conditions shown in the last section. However this has not yet allowed us to construct these in practice for a specific spacetime. In this section we will firstly demonstrate how the coefficients can be expressed in a useful form. Then we discuss Synge's theorem that will allow us to more easily handle higher order derivatives of the world function as we allow point coincidence. Then we will demonstrate how Synge's theorem applies in practice to set up for finally calculating the world function.

2.10.1 Structure of Singular Terms

To express (2.9.18) and (2.9.19) in a usable form $U(x, x')$ and $V(x, x')$, and hence the coefficients U_n and V_n, must be calculated. Technically this can be done by integrating the recursion relations (2.9.8), (2.9.10) and (2.9.14) along the geodesic connecting x to x'

with boundary conditions (2.9.9), (2.9.11) and (2.9.15). An alternative, more practical, method [22, 23] is to apply a covariant Taylor expansion of U_n and V_n for x' near x such that

$$\begin{aligned} U_n(x,x') &= u_n(x) + \sum_{j=1}^{\infty} \frac{(-1)^j}{j!} u_{n(j)}(x,x') \\ V_n(x,x') &= v_n(x) + \sum_{j=1}^{\infty} \frac{(-1)^j}{j!} v_{n(j)}(x,x'). \end{aligned} \tag{2.10.1}$$

The $u_{n(j)}(x,x')$ and $v_{n(j)}(x,x')$ are biscalars and our new notation is (for example for $u_{n(j)}$)

$$u_{n(j)}(x,x') = u_{na_1\ldots a_j}(x)\sigma^{;a_1}\ldots\sigma^{;a_j}. \tag{2.10.2}$$

From equations (2.10.1) covariant expansions of U_0 and V_0 can be easily constructed in terms of the new functions $u_{n(j)}(x,x')$ and $v_{n(j)}(x,x')$ but we cannot yet simply state their value from the boundary conditions.

With expansions (2.10.1) and terms for U_0 and V_0 the recursion relations (2.9.8), (2.9.10) and (2.9.14) can now be used for calculation. This can be performed with knowledge of how to calculate the Van Vleck-Morette determinant, however this rapidly becomes unwieldy in a general spacetime. To simplify the calculation the Van Vleck-Morette determinant and objects like $\Delta^{-1/2}\Delta^{1/2}_{;\mu}\sigma^{;\mu}$ derived from it are expressed as series in $\sigma^{;\mu}$. Deriving these expansions (and similar) to higher orders is ongoing work [14, 20, 22, 25] as more complicated calculations are attempted. To low order these objects are [22]

$$\begin{aligned} \Delta^{1/2} &= 1 + \frac{1}{12}R_{a_1a_2}\sigma^{;a_1}\sigma^{;a_2} - \frac{1}{24}R_{a_1a_2;a_3}\sigma^{;a_1}\sigma^{;a_2}\sigma^{;a_3} + \ldots \\ \Delta^{-1/2}\Delta^{1/2}_{;\mu}\sigma^{;\mu} &= \frac{1}{6}R_{a_1a_2}\sigma^{;a_1}\sigma^{;a_2} - \frac{1}{24}R_{a_1a_2;a_3}\sigma^{;a_1}\sigma^{;a_2}\sigma^{;a_3} + \ldots. \end{aligned} \tag{2.10.3}$$

Using (2.10.3) $U(x,x)$ and $V(x,x')$ can now be expressed only in terms of curvature functions and $\sigma^{;\mu}(x,x')$.

2.10.2 Synge's Theorem and Corollary

We introduce notation for the coincidence limit of x and x' such that

$$[\sigma^{;\mu}] = \lim_{x' \to x} \sigma^{;\mu}(x, x') \tag{2.10.4}$$

and similarly for other quantities. Using this notation we can now express Synge's theorem which will be key for calculations in the next section.

Synge's theorem states [3, 58, 65] for any bitensor T

$$[T_{\alpha_1 \ldots \alpha_n \beta'_1 \ldots \beta'_n ; \mu'}] = [T_{\alpha_1 \ldots \alpha_n \beta'_1 \ldots \beta'_n}]_{;\mu} - [T_{\alpha_1 \ldots \alpha_n \beta'_1 \ldots \beta'_n ; \mu}]. \tag{2.10.5}$$

For the final calculation of the world function we will only need to consider derivatives with respect to one variable at either point. Using the variable t as an example we can simplify (2.10.5) to

$$[\sigma_{;\underbrace{t..t}_{k}\underbrace{t'..t'}_{n}}] = [\sigma_{;\underbrace{t..t}_{k}\underbrace{t'..t'}_{n-1}}]_{;t} - [\sigma_{;\underbrace{t..t}_{k+1}\underbrace{t'..t'}_{n-1}}] \tag{2.10.6}$$

which we shall express using the notation

$$[\sigma_{;t_1..t_k t'_1..t'_n}] = [\sigma_{;t_1..t_k t'_1..t'_{n-1}}]_{;t} - [\sigma_{;t_1..t_{k+1} t'_1..t'_{n-1}}]. \tag{2.10.7}$$

Now for ease of notation in the rest of this section we will rewrite equation (2.10.7) treating the coincidence limits as functions of n and k, such that

$$[\sigma_{;t_1..t_k t'_1..t'_n}] = f(n,k) = f(n-1,k)_{;t} - f(n-1,k+1). \tag{2.10.8}$$

The equation (2.10.7) is used repeatedly in the calculation of the world function to

shift all the derivatives from x' to x. During this process a pattern was observed allowing us to posit a corollary to the single variable form of Synge's theorem, namely

$$f(n,k) = \sum_{i=0}^{n} (-1)^i \binom{n}{i} f(0, i+k)_{;t_1..t_{n-i}} \tag{2.10.9}$$

which is a binomial theorem. We shall prove this by induction where the base statement is clear from (2.10.7) and then

$$f(n+1,k) = f(n,k)_{;t} - f(n,k+1) \tag{2.10.10}$$

$$\Rightarrow f(n+1,k) = \sum_{i=0}^{n+1} (-1)^i \binom{n+1}{i} f(0, i+k)_{;t_1..t_{n+1-i}}. \tag{2.10.11}$$

Hence from equation (2.10.10)

$$\begin{aligned}
f(n+1,k) &= \sum_{i=0}^{n} (-1)^i \binom{n}{i} f(0, i+k)_{;t_1..t_{n+1-i}} - \sum_{i=0}^{n} (-1)^i \binom{n}{i} f(0, i+k+1)_{;t_1..t_{n-i}} \\
&= \sum_{i=0}^{n} (-1)^i \binom{n}{i} f(0, i+k)_{;t_1..t_{n+1-i}} - \sum_{i=1}^{n+1} (-1)^{i-1} \binom{n}{i-1} f(0, i+k)_{;t_1..t_{n+1-i}} \\
&= f(0,k)_{t_1..t_{n+1}} + \sum_{i=1}^{n} (-1)^i \binom{n}{i} f(0, i+k)_{;t_1..t_{n+1-i}} \\
&\qquad - \sum_{i=1}^{n} (-1)^{i-1} \binom{n}{i-1} f(0, i+k)_{;t_1..t_{n+1-i}} - (-1)^n f(0, k+n+1) \\
&= f(0,k)_{t_1..t_{n+1}} + \sum_{i=1}^{n} (-1)^i f(0, i+k)_{;t_1..t_{n+1-i}} \left[\binom{n}{i} + \binom{n}{i-1} \right] - (-1)^n f(0, k+n+1) \\
&= \sum_{i=0}^{n+1} (-1)^i \binom{n+1}{i} f(0, i+k)_{;t_1..t_{n+1-i}} \quad \square
\end{aligned} \tag{2.10.12}$$

The final step to achieve equation (2.10.12) makes use of Pascal's identity.

Finally we simply extend our corollary (2.10.9) by the properties of covariant derivatives to

$$f(n,k)_{;t_1..t_l} = \sum_{i=0}^{n} (-1)^i \binom{n}{i} f(0, i+k)_{;t_1..t_{l+n-i}}. \tag{2.10.13}$$

2.10.3 Preparing the World Function

Next we look at how Synge's world function is to be derived, although the final calculation will depend on the number of dimensions and our choice of point-splitting scheme. Although as stated in equation (2.9.1) the world function is half the squared distance along the geodesic connecting x to x' it is calculated from the equivalent expression

$$\sigma(x,x') = \frac{1}{2}\sigma_{;\mu}\sigma^{;\mu} = \frac{1}{2}\sigma_{;\mu'}\sigma^{;\mu'}. \tag{2.10.14}$$

This expression implies $\sigma_{;\mu} \sim \sigma^{;\mu} \sim \sigma_{;\mu'} \sim \sigma^{;\mu'} \sim O(\sigma^{1/2})$ which will be useful in the calculation of equations (2.9.18) and (2.9.19) to determine the finite and singular terms in the Hadamard form.

To calculate $\sigma(x,x')$ by equation (2.10.14) we need to know $\sigma^{;\mu}$ which is a vector at x and a scalar at x' or $\sigma^{;\mu'}$, a vector at x' and a scalar at x. We shall proceed to calculate $\sigma^{;\mu}$ though results obtained from finding $\sigma^{;\mu'}$ will also be included. As $\sigma^{;\mu}$ is a scalar at x' it can be expanded as a Taylor series in the neighbourhood of that point [3] in powers of $\epsilon^\mu = x^\mu - x^{\mu'}$. This could be continued in general but for our purposes we only want $\epsilon^t = t - t'$ or $\epsilon^\gamma = \gamma$ and we shall proceed to outline the method using the former as an example.

We take $\epsilon^\mu = \epsilon\delta_t{}^\mu$ for $\epsilon = t - t'$ and expand $\sigma^{;\mu}$ in a Taylor series as

$$\sigma^{;\mu}(x,x') = \left[\sigma^{;\mu}\right] - \left[\sigma^{;\mu}{}_{,\alpha'}\right]\epsilon^\alpha + \frac{1}{2!}\left[\sigma^{;\mu}{}_{,\alpha'\beta'}\right]\epsilon^{\alpha\beta} - ... \tag{2.10.15}$$

making use of the notation introduced in equation (2.10.4). In order to make use of expansion (2.10.15) three steps must be completed [3, 19]

1. All the partial derivatives in equation (2.10.15) need to be converted to covariant derivatives.

2. These covariant derivatives at x' need to be transformed to covariant derivatives at x.

3. The coincidence limits must be calculated.

In order to employ Synge's theorem (2.10.5) in step 2 and be able to work with bitensors, whose properties are known, we cannot have partial derivatives in our terms. We convert the partial derivatives to covariant derivatives by simple use of the definition of a covariant derivative such that given a scalar function $A(x)$

$$\begin{aligned} A_{,\mu} &= A_{;\mu} \\ A_{,\mu\nu} &= A_{;\mu,\nu} = A_{;\mu\nu} + \Gamma^{\rho}{}_{\mu\nu} A_{;\rho}. \end{aligned} \tag{2.10.16}$$

The most helpful advantage of choosing to expand (2.10.15) in $t-t'$ is that the higher order derivatives will become simplified. As our metric (2.3.16) has no time dependence time derivatives of objects depending solely on this metric, such as the Christoffel connection, will be zero by definition.

The second step is not strictly necessary but does simplify further calculation [19]. As the vacuum polarisation is calculated at the point x we wish to eventually express all our terms at the point x while isolating objects that diverge as $x' \to x$. This can be done through repeated uses of $g^{\mu}{}_{\nu'}$, the bivector of parallel transport, and the calculation of mixed derivative coincidence limits, though this quickly becomes too bulky for efficient use. However the bivector will still be useful so we define it with respect to $\sigma^{;\mu'}$. We do this by noting that $\sigma^{;\mu'}$ is the tangent at x' to the geodesic connecting x and x' directed $x \to x'$. By construction $g^{\mu}{}_{\nu'}$ must parallel transport a vector defined at x' to x along the geodesic and so it must obey

$$-\sigma^{;\mu} = g^{\mu}{}_{\nu'} \sigma^{;\nu'}. \tag{2.10.17}$$

The minus sign is required as $\sigma^{;\mu}$ is directed $x' \to x$ [19].

For now we will instead apply Synge's theorem (2.10.5) to the coefficients in (2.10.15) in conjunction with (2.10.16) as follows

$$[\sigma^{;\mu}{}_{,t'}] = [\sigma^{;\mu}{}_{;t'}] = [\sigma^{;\mu}]_{;t} - [\sigma^{;\mu}{}_{;t}] \tag{2.10.18}$$

$$\begin{aligned}[\sigma^{;\mu}{}_{,t't'}] &= [\sigma^{;\mu}{}_{;t't'} + \Gamma^{\rho}{}_{t't'}\sigma^{;\mu}{}_{;\rho}] \\ &= [\sigma^{;\mu}]_{;tt} - 2[\sigma^{;\mu}{}_{;t}]_{;t} + [\sigma^{;\mu}{}_{;tt}] + [\Gamma^{\rho}{}_{t't'}\sigma^{;\mu}{}_{;\rho}].\end{aligned} \tag{2.10.19}$$

It is clear from these first two examples how rapidly these transformations will grow in size and why corollary (2.10.9) is of use. However these calculations can be simplified in conjunction with step three by seeing if any of the coincidence limits will allow the re-expression of (2.10.18) and (2.10.19) in a more compact form.

2.10.4 Calculation of Limits and the World Function

First note that by definition [19]

$$[g_{\mu\nu}] = [g_{\mu\nu'}] = [g_{\mu'\nu'}] = g_{\mu\nu} \tag{2.10.20}$$

which for the bivector of parallel transport gives

$$[g^{\mu}{}_{\nu'}] = \delta^{\mu}{}_{\nu}. \tag{2.10.21}$$

Now by way of (2.10.20) or (2.10.21) we can state

$$[\Gamma^{\alpha}_{\beta\gamma}] = [\Gamma^{\alpha}_{\beta\gamma'}] = [\Gamma^{\alpha}_{\beta'\gamma'}] = [\Gamma^{\alpha'}_{\beta'\gamma'}] = \Gamma^{\alpha}_{\beta\gamma}. \tag{2.10.22}$$

From the definition of $\sigma(x, x')$ in equation (2.9.1) we can simply read off its coincidence limit. By comparison of (2.9.1) and (2.10.14) we see that the length of $\sigma^{;\mu}$ is also the geodetic distance between x and x' so we can simply state the coincidence limits of lowest

order

$$\begin{aligned}[\sigma] &= 0 \\ [\sigma^{;\mu}] &= 0.\end{aligned} \tag{2.10.23}$$

To find the coincidence limits of higher order derivatives of $\sigma(x,x')$ we differentiate equation (2.10.14) multiple times to obtain, for the first few orders,

$$\begin{aligned}\sigma^{;\mu} &= \sigma^{;\rho}\sigma^{;\mu}{}_{;\rho} \\ \sigma^{;\mu}{}_{;\nu} &= \sigma^{;\rho}{}_{;\nu}\sigma^{;\mu}{}_{;\rho} + \sigma^{;\rho}\sigma^{;\mu}{}_{;\rho\nu} \\ \sigma^{;\mu}{}_{;\nu\tau} &= \sigma^{;\rho}{}_{;\nu\tau}\sigma^{;\mu}{}_{;\rho} + \sigma^{;\rho}{}_{;\nu}\sigma^{;\mu}{}_{;\rho\tau} + \sigma^{;\rho}{}_{;\tau}\sigma^{;\mu}{}_{;\rho\nu} + \sigma^{;\rho}\sigma^{;\mu}{}_{;\rho\nu\tau}.\end{aligned} \tag{2.10.24}$$

From these and equations (2.10.23) we find [3, 58]

$$\begin{aligned}[\sigma^{;\mu}{}_{;\nu}] &= g^{\mu}{}_{\nu} \\ [\sigma^{;\mu}{}_{;\nu\rho}] &= 0 \\ [\sigma^{;\mu}{}_{;\nu\rho\tau}] &= S^{\mu}{}_{\nu\rho\tau} \equiv -\frac{1}{3}\left(R^{\mu}{}_{\rho\nu\tau} + R^{\mu}{}_{\tau\nu\rho}\right) \\ [\sigma^{;\mu}{}_{;\nu\rho\tau\upsilon}] &= \frac{3}{4}\left(S^{\mu}{}_{\nu\rho\tau;\upsilon} + S^{\mu}{}_{\nu\tau\upsilon;\rho} + S^{\mu}{}_{\nu\upsilon\rho;\tau}\right).\end{aligned} \tag{2.10.25}$$

Now we apply the coincidence limits in (2.10.23) and (2.10.25) to (2.10.18) and (2.10.19) to obtain

$$\begin{aligned}[\sigma^{;\mu}{}_{,t'}] &= -\delta^{\mu}{}_{t} \\ [\sigma^{;\mu}{}_{,t't'}] &= -\Gamma^{\mu}{}_{tt}.\end{aligned} \tag{2.10.26}$$

Higher derivatives have been calculated but take substantial space so we include their

results in the final form of (2.10.15) by

$$\begin{aligned}\sigma^{;\mu} =& g^{\mu}{}_{t}\epsilon - \frac{1}{2}\Gamma^{\mu}{}_{tt}\epsilon^2 + \frac{1}{6}\Gamma^{\nu}{}_{tt}\Gamma^{\mu}{}_{\nu t}\epsilon^3 - \frac{1}{24}\Gamma^{\nu}{}_{tt}\left(R^{\mu}{}_{t\nu t} + \Gamma^{\tau}{}_{\nu t}\Gamma^{\mu}{}_{\tau t}\right)\epsilon^4 \\ &- \frac{1}{120}\left(-2\Gamma^{\mu}{}_{rt}\Gamma^{r}{}_{tt}R^{r}{}_{trt} + (\Gamma^{r}{}_{tt})^2 R^{\mu}{}_{rtr} - (\Gamma^{r}{}_{tt})^2\Gamma^{t}{}_{rt}\Gamma^{\mu}{}_{rt}\right)\epsilon^5 + O(\epsilon^6)\end{aligned} \tag{2.10.27}$$

in agreement with [3].

Using (2.10.27) we can now express $\sigma(x, x')$ and its derivatives in terms of the metric (2.3.16),

$$\begin{aligned}&\sigma(x,x') = \frac{1}{2}f(r)\epsilon^2 - \frac{1}{96}f(r)f'(r)^2\epsilon^4 + O(\epsilon^6) \\ &\sigma^{;t}(x,x') = \epsilon - \frac{1}{24}f'(r)^2\epsilon^3 + O(\epsilon^5) \\ &\sigma^{;r}(x,x') = \frac{1}{4}f(r)f'(r)\epsilon^2 - \frac{1}{96}\left(\frac{1}{2}f(r)f'(r)^3 + f(r)^2 f'(r)f''(r)\right)\epsilon^4 + O(\epsilon^5) \\ &\sigma^{;\gamma}(x,x') = 0\end{aligned} \tag{2.10.28}$$

where the derivative with respect to γ means with respect to any angular coordinate. The derivative results in (2.10.28) are in agreement with [3] up to certain signs explained by the fact that in their work σ was calculated on the Lorentzian manifold.

The method presented from subsection §2.10.1 to this point can now be used to explicitly find the Hadamard expansion terms. We applied this method and calculated all required steps by hand to derive U and V (where appropriate) for $d = 4, 5, 6$, the results for $d = 4$ being a check on our implementation on a simpler known case. The results in $d = 5$, §4.3, and $d = 6$, 5.3, were checked against [23], this guaranteed a better understanding of the method in case of complications and that we agreed in every detail with others' results.

Finally, as noted previously the derivatives did not need to be shifted from x' to x. Primed and mixed derivative coincidences can be found [19, 58] such as from the first

derivative of (2.10.17),

$$\sigma^{;\mu}{}_{;\nu'} = -g_{\nu'\rho}{}^{;\mu}\sigma^{;\rho} - g_{\nu'\rho}\sigma^{;\mu\rho} \tag{2.10.29}$$

which gives

$$[\sigma^{;\mu}{}_{;\nu'}] = -g_{\mu\nu}. \tag{2.10.30}$$

However this method takes longer than the steps laid out in this section so is discussed no further.

2.11 WKB Approximation

In order to take our schematic view of renormalisation in equation (2.9.21) to a concrete calculation we must overcome a complication. In that scheme the right hand side involves the difference between an infinite sum of numerical solutions of an ODE and a singularity given in closed form. Clearly, guaranteeing that the divergences cancel to the correct finite value will pose problems, not least of which is knowing how many modes need to be calculated to demonstrate convergence of the remaining terms. In order to bypass these problems and allow us more control over the calculation we will employ an analytic approximation to the modes such that we can then concentrate on renormalising an analytic expression.

We use the WKB-like approximation of Howard [41, 75] by defining a new function $\beta_{\omega l}(r)$ as

$$\beta_{\omega l}(r) = C_{\omega l} p_{\omega l}(r) q_{\omega l}(r) \tag{2.11.1}$$

which will be expanded into a series of WKB terms. The WKB approach will allow us to approximate well modes with large l or n. Thus a mode sum of WKB terms will contain the divergent behaviour and we only need numerical calculations of modes with low l or n. This allows us to re-approach our schematic renormalisation (2.9.21) and re-express it

as

$$\langle\phi^2\rangle_{\rm ren} = \sum_{finite} (modes - \text{WKB } terms) + \lim_{\substack{\epsilon\to 0 \\ \text{or} \\ \gamma\to 0}} \left(\sum \text{WKB } terms - G_{E,sing} \right). \qquad (2.11.2)$$

The only problem introduced by this approximation is that it will break down near the horizon where $q_{\omega l}$ diverges [12, 13, 75]. This will need to be monitored during calculations to discover at what value of r the approximation breaks down. A detailed look at the cause of this breakdown is presented in the following subsection §2.11.1.

Although the equations for using the WKB approximation are known, see for example [41, 75], these have only been used in the $d = 4$ case. We reproduce here the method to find the WKB terms for an unspecified number of dimensions. To apply the WKB approach we wish to have an ODE for $\beta_{\omega l}(\zeta)$, for some variable $\zeta(r)$, of the form [41]

$$\frac{d^2 S_{\omega l}}{d\zeta^2} = \left(\chi^2(\omega, l, \zeta) + \eta(\zeta)\right) S_{\omega l}. \qquad (2.11.3)$$

It is not necessary for χ in equation (2.11.3) to contain all the dependence on ω and l however the method proves easier if η is independent of these.

To begin we look at the radial ODE (2.8.1)

$$\frac{1}{r^{d-4}} \frac{d}{dr} \left[r^{d-2} f \frac{d}{dr} S_{\omega l} \right] - \left(\frac{\omega^2 r^2}{f} + (m^2 + \xi R) r^2 + l(l + d - 3) \right) S_{\omega l} = 0 \qquad (2.11.4)$$

which is obeyed by $p_{\omega l}(r)$ and $q_{\omega l}(r)$. We introduce a change of variables by

$$\frac{d}{d\zeta} = r^{d-2} f \frac{d}{dr} \qquad (2.11.5)$$

which converts the radial ODE to

$$\frac{d^2 S_{\omega l}}{d\zeta^2} = \left((\omega r^{d-2})^2 + (m^2 + \xi R) f r^{2d-4} + l(l + d - 3) f r^{2d-6} \right) S_{\omega l}. \qquad (2.11.6)$$

Comparing equations (2.11.3) and (2.11.6) we rewrite the l term by completing the square such that (2.11.6) is now

$$\frac{d^2S_{\omega l}}{d\zeta^2} = \Bigg((\omega r^{d-2})^2 + \left[\left(l + \frac{d-3}{2}\right) f^{\frac{1}{2}} r^{d-3}\right]^2 + (m^2 + \xi R) f r^{2d-4} - \left[\frac{d-3}{2} f^{\frac{1}{2}} r^{d-3}\right]^2\Bigg) S_{\omega l} \quad (2.11.7)$$

from which we can read off that

$$\chi^2(\omega, l, \zeta) = (\omega r^{d-2})^2 + \left[\left(l + \frac{d-3}{2}\right) f^{\frac{1}{2}} r^{d-3}\right]^2 \quad (2.11.8)$$

and

$$\eta(\zeta) = (m^2 + \xi R) f r^{2d-4} - \left[\frac{d-3}{2} f^{\frac{1}{2}} r^{d-3}\right]^2. \quad (2.11.9)$$

The final step in preparing the WKB approximation is to find an ODE such that $\beta_{\omega l}$ is equal to terms containing its own derivatives to facilitate solution through series expansion as displayed in (2.11.17) . This requires some pieces which will be written without indices and using prime notation ($'$) for $\frac{d}{d\zeta}$. First consider the Wronskian (2.8.3)

$$\begin{aligned} W[p,q] &= C\left[p\frac{dq}{dr} - q\frac{dp}{dr}\right] = \frac{C}{f r^{d-2}}\left[pq' - qp'\right] = -\frac{1}{f r^{d-2}} \\ &\Rightarrow C^2\left[pq' - qp'\right]^2 = 1. \end{aligned} \quad (2.11.10)$$

Now consider

$$\begin{aligned} (\beta')^2 &= C^2\left[p^2q'^2 + q^2p'^2 + 2pqp'q'\right] \\ &= 1 + 4Cp'q'\beta \quad \text{from equation (2.11.10)} \end{aligned} \quad (2.11.11)$$

and

$$\begin{aligned}\beta'' &= C\left[pq'' + p''q + 2p'q'\right] \\ &= 2\beta\left(\chi^2 + \eta\right) + 2Cp'q' \quad \text{from equations (2.11.3) and (2.11.7).}\end{aligned} \tag{2.11.12}$$

Combining equations (2.11.10) to (2.11.12) we arrive at

$$\begin{aligned}0 &= 2\beta\beta'' - 4Cp'q'\beta - 4\beta^2(\chi^2 + \eta) \\ &= 2\beta\beta'' - (\beta')^2 - 4\beta^2(\chi^2 + \eta) + 1.\end{aligned} \tag{2.11.13}$$

Then noting that

$$\frac{d^2\sqrt{\beta}}{d\zeta^2} = \frac{\beta''}{2\sqrt{\beta}} - \frac{\beta'^2}{4\beta\sqrt{\beta}} \tag{2.11.14}$$

we can rewrite (2.11.13) as follows

$$\begin{aligned}4\beta^2(\chi^2 + \eta) - 2\beta\beta'' + (\beta')^2 &= 1 \\ \Rightarrow \beta^2 - \frac{\beta^2}{\chi^2}\left(\frac{\beta''}{2\beta} - \frac{\beta'^2}{4\beta^2} - \eta\right) &= \frac{1}{4\chi^2} \\ \Rightarrow \left[1 - \frac{1}{\chi^2}\left(\frac{1}{\sqrt{\beta}}\frac{d^2\sqrt{\beta}}{d\zeta^2} - \eta\right)\right]\beta^2 &= \frac{1}{4\chi^2}\end{aligned} \tag{2.11.15}$$

and hence into the final form of our desired ODE as

$$\beta = \frac{1}{2\chi_{\omega l}}\left[1 - \frac{1}{\chi^2}\left(\frac{1}{\sqrt{\beta}}\frac{d^2\sqrt{\beta}}{d\zeta^2} - \eta\right)\right]^{-\frac{1}{2}}. \tag{2.11.16}$$

In (2.11.16) we have rewritten the arguments, ω and l, of χ as indices in line with other objects in our choice of notation.

To find the series expansion of $\beta_{\omega l}$ we introduce a small, fictitious parameter δ into

equation (2.11.16) and return the indices to obtain [75]

$$\beta_{\omega l} = \frac{1}{2\chi_{\omega l}} \left[1 - \frac{\delta^2}{\chi_{\omega l}^2} \left(\frac{1}{\sqrt{\beta_{\omega l}}} \frac{d^2\sqrt{\beta_{\omega l}}}{d\zeta^2} - \eta \right) \right]^{-\frac{1}{2}}. \tag{2.11.17}$$

Then we expand $\beta_{\omega l}$ in powers of δ multiplying the WKB terms

$$\beta_{\omega l} = \beta_{0\omega l} + \delta^2 \beta_{1\omega l} + \delta^4 \beta_{2\omega l} + ... \tag{2.11.18}$$

and finally let $\delta \to 1$. It is readily seen that the first WKB term has the form

$$\beta_{0\omega l} = \frac{1}{2\chi_{\omega l}} \tag{2.11.19}$$

which, containing f, is dependent on the number of dimensions.

All WKB terms can be expressed as sums of coefficients multiplying inverse powers of $\chi_{\omega l}$ but the presence of the dimensionally dependent η and derivatives of $\chi_{\omega l}$ with respect to r prevent a simple, predictable pattern emerging. In fact the WKB terms, though easy in to find in principle, rapidly become large and unwieldy to calculate. This makes it an important point to decide how many WKB terms to include in our calculations. Previous work such as Winstanley and Young [75] in $d = 4$ used three WKB terms but at the cost of needing modes for the first twenty values of ω and hundreds of values of l to guarantee convergence in the mode sums. In anticipation of our dimensionally dependent modes becoming harder to calculate accurately as d increases we will use four terms in $d = 4$ and extend this is for other values of d as follows

$$\beta_{\omega l}(r) = \sum_{i=0}^{d-1} \beta_{i\omega l}(r). \tag{2.11.20}$$

We have calculated all the WKB terms for $d = 4 \to 11$ though, due to computational restrictions, for $d \geq 6$ these are expressed in a simplified form as functions of r, ω and $\chi_{\omega l}$

only. The WKB terms of relevance are included in appendix C and referenced as they are needed in the work.

In conclusion we can now express our schematic idea (2.11.2) in more detail by combining the results of this section with equation (2.9.21) and Green's function (2.8.13)

$$\begin{aligned}\langle\phi^2\rangle_{\rm ren} =& \frac{\kappa}{2\pi}\sum_{n=-\infty}^{\infty}\sum_{l=0}^{\infty}\tilde{N}_{d,l}G_l^{\lambda}(1)\left[C_{\omega l}p_{\omega l}(r)q_{\omega l}(r)-\sum_{i=0}^{d-1}\beta_{i\omega l}(r)\right]\\ &+\lim_{\epsilon\to 0}\left(\frac{\kappa}{2\pi}\sum_{n=-\infty}^{\infty}e^{i\omega\epsilon}\sum_{l=0}^{\infty}\tilde{N}_{d,l}G_l^{\lambda}(1)\sum_{i=0}^{d-1}\beta_{i\omega l}(r)-G_{E,sing}(\epsilon)\right)\end{aligned} \tag{2.11.21}$$

or Green's function (2.8.14)

$$\begin{aligned}\langle\phi^2\rangle_{\rm ren} =& \frac{\kappa}{2\pi}\sum_{l=0}^{\infty}\tilde{N}_{d,l}G_l^{\lambda}(1)\sum_{n=-\infty}^{\infty}\left[C_{\omega l}p_{\omega l}(r)q_{\omega l}(r)-\sum_{i=0}^{d-1}\beta_{i\omega l}(r)\right]\\ &+\lim_{\gamma\to 0}\left(\frac{\kappa}{2\pi}\sum_{l=0}^{\infty}\tilde{N}_{d,l}G_l^{\lambda}(\cos\gamma)\sum_{n=-\infty}^{\infty}\sum_{i=0}^{d-1}\beta_{i\omega l}(r)-G_{E,sing}(\gamma)\right).\end{aligned} \tag{2.11.22}$$

Remember that the first lines of equations (2.11.21) and (2.11.22) are found numerically while the second lines require more analytic work. This means that in practice the numeric lines will only be summed to finite values large enough to guarantee convergence of the sums to within desired numerical accuracy.

2.11.1 Breakdown of the WKB Terms

The reason the WKB approximation breaks down near the horizon is due to the particular properties of the mode functions it attempts to describe. The series expansions of the mode sums are investigated in more detail in §3.8 and §4.6. We include here some detail to discuss the relation between the series expansions and the WKB breakdown.

If we express each mode as a Frobenius series then the Frobenius roots, ν, are defined

as

$$\nu = \pm\frac{\omega r_h}{d-3} = \pm\frac{n\kappa r_h}{d-3} = \pm\frac{n r_h}{2}, \tag{2.11.23}$$

hence they differ by an integer for $n > 0$ and are zero for $n = 0$. This means the corresponding Frobenius series are expressed as

$$\begin{aligned} p &= (r-r_h)^{\nu}\sum_{j=0}^{\infty} a_j (r-r_h)^j \\ q &= (r-r_h)^{-\nu}\sum_{j=0}^{\infty} b_j (r-r_h)^j + D_{\omega l} p \log(r-r_h) \end{aligned} \tag{2.11.24}$$

where $D_{\omega l}$ is a constant that cannot vanish for $n = 0$ but may go to zero for $n > 0$. The a_j, b_j and the resulting c_j in the next equation are constants.

This means the object we wish to approximate has the form

$$pq = \sum_{j=0}^{\infty} c_j (r-r_h)^j + p^2 \log(r-r_h). \tag{2.11.25}$$

For $n > 0$ we have $p^2 \log(r-r_h) \sim 0$ for $r \sim r_h$ and for $n = 0$ near $r \sim r_h$ the sum is close to zero. The issue arises in that the WKB approximation only captures the behaviour from the sum and so when used for $n = 0$ near the horizon there is a remaining logarithmic term that diverges. This is a potential problem that will be discussed as it arises, the major example is in the results of Ch. 4, as it is not possible to state in advance how close to the horizon this issue will cause any problems. A better approximation near the horizon has been presented in [12] but is more complicated to implement, we will return to this improvement if required.

2.12 Summary

In this chapter we have demonstrated and investigated the mathematical framework implemented within this project. We began by defining the object that this project was setup up to calculate (the vacuum polarisation (VP), $\langle\phi^2\rangle$) in two key situations; firstly by extending previous work in $d = 4$ without a bulk to a brane within a higher dimensional bulk (see Ch. 3) and secondly to demonstrate the first known methodology for its calculation within the bulk (Ch. 4 and 5). We have expressed the VP using a Green's function as well as constructing this Green's function using a point splitting regime. We demonstrated that the VP is initially divergent, requires renormalisation and which method of renormalisation is most appropriate. Further we established how to implement this method to produce renormalisation terms and the variable they depend on (Synge's world function). Finally we have reviewed an approximation scheme for the scalar field modes.

It is not possible to write a general calculation scheme for the following chapters but certain points of the methodology are consistent:

- Find the initial equations in the relevant case, such as the metric, Ricci tensor, radial ODE etc.
- Choose a point splitting scheme
- Given the choice of point splitting scheme a Green's function is constructed which is regular (until point coincidence)
- Determine the renormalisation terms
- Given the form of the Green's function attempt to find a way in which the renormalisation terms can be similarly expressed
- Choose the parameters, such as mass, coupling constant, that will allow final calculation (e.g. calculation domain, any masses, coupling constant etc.)

- Using this set of parameters determine the relevant WKB terms (this is done after fixing certain parameters to prevent WKB expressions growing too large)
- Numerically calculate the field modes and any other quantities which cannot be found analytically

We now proceed to looking at the calculation of $\langle \phi^2 \rangle$ on the brane.

Chapter 3

$\langle \phi^2 \rangle$ on the Brane

In this chapter we use the methodology outlined in Ch. 2 to find the vacuum polarisation on the brane. We define the parameters (projected metric, gravitational coupling etc.) on the brane on with which we will calculate. Once parameters have been set, allowing results to be calculated, we will go through the choices of calculation method relevant to the renormalised mode sum on the brane. Finally we present our results along with any interpretation, in particular we will compare our results to the Schwarzschild case [17]. The core of the methodology in this chapter follows [3, 75] though many authors contributed work leading to these papers.

3.1 The Metric on the Brane

As discussed in §1.3 and §1.6 our choices for the brane are to make it a model for our 4d universe assuming there is no cosmological constant, $\Lambda = 0$. This is the equivalent of having no tension in the brane and allows the brane to be a flat slice through our spacetime (2.3.16). For simplicity we choose this slice to be a proper bisection through the hyperspherical, d dimensional, black hole spacetime. Due to the inherent symmetries

of the hypersphere this is achieved by setting $\theta_{i>1} = \pi/2$ (we set $\theta \equiv \theta_1$ for the brane) in (2.3.16). On this bisection we retain time symmetry but any other symmetries must be found from the metric projection on the brane which from (2.3.16) is

$$\begin{aligned} ds^2 &= f dt^2 + f^{-1} dr^2 + r^2 d\Omega_2^2 \\ &= f dt^2 + f^{-1} dr^2 + r^2 d\theta^2 + r^2 \sin^2(\theta) d\varphi^2. \end{aligned} \tag{3.1.1}$$

As can be seen from (3.1.1) we now have a 4d black hole spacetime where all influence from the number of dimensions is felt only through the metric function f (2.3.9) in which we set $r_h = 1$ without loss of generality. Note that (3.1.1) is not a solution to the vacuum Einstein field equations although metric (2.3.16) is [61] but an effective metric suitable for describing the effect of gravity on fields on the brane.

From the metric (3.1.1) we can immediately calculate the Ricci tensor, R_{ab}, Ricci scalar, R, and the square root of the metric determinant, $g^{\frac{1}{2}}$, to be the following

$$\begin{aligned} R_{ab} &= \begin{pmatrix} -\frac{f(2f'+rf'')}{2r} & 0 & 0 & 0 \\ 0 & -\frac{2f'+rf''}{2rf} & 0 & 0 \\ 0 & 0 & 1-f-rf' & 0 \\ 0 & 0 & 0 & -\sin^2(\theta)\,(f+rf'-1) \end{pmatrix} \\ &= \begin{pmatrix} \frac{(d-3)(d-4)(r^d-r^3)}{2r^{2d-1}} & 0 & 0 & 0 \\ 0 & \frac{(d-3)(d-4)r}{2(r^d-r^3)} & 0 & 0 \\ 0 & 0 & \frac{(4-d)}{r^{d-3}} & 0 \\ 0 & 0 & 0 & \frac{(4-d)\sin^2(\theta)}{r^{d-3}} \end{pmatrix}, \end{aligned} \tag{3.1.2}$$

$$R = \frac{2f + 4rf' + r^2 f'' - 2}{r^2} = \frac{(d-4)(d-5)}{r^{d-1}} \tag{3.1.3}$$

and

$$g^{\frac{1}{2}} = r^2 \sin(\theta). \tag{3.1.4}$$

In (3.1.2) we see that $R_{ab} = \underline{0}$ for $d = 4$ and in (3.1.3) we see $R = 0$ for $d = 4, 5$. From this we can anticipate similar behaviour occurring for the vacuum polarisation in $d = 4$ and 5 then some shift in behaviour as d changes from 5 to 6 however the specific forms cannot be anticipated.

3.2 Brane Mode Sums

In line with previous work in four dimensions [3, 17, 75] we choose temporal point splitting so we look at a mode sum of the form in equation (2.8.13). The angular separation, γ, is such that

$$\cos(\gamma) = \cos(\theta)\cos(\theta') + \sin(\theta)\sin(\theta')\cos(\varphi - \varphi') \tag{3.2.1}$$

and the angular coincidence makes $\cos(\gamma) = \cos(0) = 1$. For our four dimensional spacetime the Gegenbauer polynomial has upper index $\lambda = \frac{1}{2}$ so that

$$G_l^{\frac{1}{2}}(\cos(0)) = P_l(1) = 1 \tag{3.2.2}$$

where P_l is the Legendre polynomial of the first kind. The degeneracy factor $\tilde{N}_{l,d}$ (2.7.9) takes the form

$$\tilde{N}_{l,4} = \frac{2l+1}{4\pi}. \tag{3.2.3}$$

Bringing together the terms on the brane allows us to express the mode sum as

$$\begin{aligned} G_E(\mathbf{x}, t; \mathbf{x}, t') &= \frac{T}{4\pi} \sum_{n=-\infty}^{\infty} e^{i\omega\varepsilon} \sum_{l=0}^{\infty} (2l+1) C_{\omega l} p_{\omega l}(r) q_{\omega l}(r) \\ &= \frac{T}{2\pi} \sum_{n=1}^{\infty} \cos(\omega\epsilon) \sum_{l=0}^{\infty} (2l+1) C_{\omega l} p_{\omega l}(r) q_{\omega l}(r) \\ &\quad + \frac{T}{4\pi} \sum_{l=0}^{\infty} (2l+1) C_{0l} p_{0l}(r) q_{0l}(r), \end{aligned} \tag{3.2.4}$$

where we have used $\kappa = 2\pi T$.

The functions $p_{\omega l}(r)$ and $q_{\omega l}(r)$ are solutions to the radial ODE (2.8.1) expressed on the brane,

$$f\frac{d^2S_{\omega l}}{dr^2} + \left(\frac{2f}{r} + \frac{df}{dr}\right)\frac{dS_{\omega l}}{dr} - \left[\frac{\omega^2}{f} + m^2 + \xi R + \frac{l(l+1)}{r^2}\right]S_{\omega l} = 0. \tag{3.2.5}$$

3.3 Unphysical Divergences

Even though the points are still split ($\epsilon \neq 0$) our expression (3.2.4) is divergent due to the sum over l. This is technically impossible by our definition of the Green's function. A Green's function solution that still has points split must be finite so we conclude that the problem has arisen from the manner in which we set up our point splitting approach. Luckily this problem has been encountered and accounted for in previous works (first in [16] with more detailed discussion in [3, 75]). A term must be subtracted from equation (3.2.4) that contains a multiple of the delta function and results in an established modification [2, 3] to the Green's function

$$\begin{aligned} G_E(\mathbf{x},t;\mathbf{x},t') &= \frac{T}{4\pi}\sum_{n=-\infty}^{\infty}\exp(i\omega\epsilon)\sum_{l=0}^{\infty}\left[(2l+1)C_{\omega l}p_{\omega l}(r)q_{\omega l}(r) - \frac{1}{rf^{\frac{1}{2}}}\right] \\ &= \frac{T}{2\pi}\sum_{n=1}^{\infty}\cos(\omega\epsilon)\sum_{l=0}^{\infty}\left[(2l+1)C_{\omega l}p_{\omega l}(r)q_{\omega l}(r) - \frac{1}{rf^{\frac{1}{2}}}\right] \\ &\quad + \frac{T}{4\pi}\sum_{l=0}^{\infty}\left[(2l+1)C_{0l}p_{0l}(r)q_{0l}(r) - \frac{1}{rf^{\frac{1}{2}}}\right]. \end{aligned} \tag{3.3.1}$$

We must now address how this modification has been introduced if equation (2.7.1) was in fact the unique solution to the Klein-Gordon equation (2.5.5). It is important to remember that solution (2.7.1) is unique however the order of summation was never determined. After equation (2.8.4) we justified that the summation order is determined

by the order of point coincidence but we also know that the order of summation cannot be simply changed as the sum is not absolutely convergent, see also Appendix A. We must accept that in the point coincidence scheme presented some rigour was lost in the consideration of the summation order. This leads to equations (2.7.1), (2.7.8) and (2.8.4) being correct, the last due to the radial point coincidence not affecting the summation order. This then means that equation (3.2.4) is in fact wrong and requires correction. This correction is what has been previously referred to as the removal of the unphysical divergence.

There have been several methods used to calculate (3.3.1), we present here a recent method [75] based on dimensional reduction which will demonstrate an idea that will be applied later in the bulk. We begin by rewriting our initial result (2.7.1) for the Euclidean Green's function (in $d = 4$) as

$$G_E(x;x') = \frac{T}{4\pi}\sum_{n=-\infty}^{\infty}\exp(i\omega\epsilon)\times\mathcal{G}_\omega(r,\theta,\phi;r',\theta',\phi') \tag{3.3.2}$$

where

$$\mathcal{G}_\omega(r,\theta,\phi;r',\theta',\phi') = \sum_{l=0}^{\infty}(2l+1)P_l(\cos(\gamma))S_{\omega l}(r,r'). \tag{3.3.3}$$

Returning to the wave equation that we used to define G_E (2.5.5) we can find a PDE satisfied by our new function $\mathcal{G}_\omega$

$$-\frac{\delta(\mathbf{x},\mathbf{x}')}{r^2\sin\theta} = \frac{1}{r^2}\frac{\partial}{\partial r}\left[fr^2\frac{\partial\mathcal{G}_\omega}{\partial r}\right] + \frac{1}{r^2\sin\theta}\frac{\partial}{\partial\theta}\left[\sin\theta\frac{\partial\mathcal{G}_\omega}{\partial\theta}\right] + \frac{1}{r^2\sin^2\theta}\frac{\partial^2\mathcal{G}_\omega}{\partial\phi^2} - \left[\frac{\omega^2}{f}+m^2+\xi R\right]\mathcal{G}_\omega. \tag{3.3.4}$$

This has a similar form to a three dimensional wave equation with a quasi-potential

$$\tilde{V} = \frac{\omega^2}{f} + m^2 + \xi R. \tag{3.3.5}$$

Dividing (3.3.4) by a factor of f gives the governing wave equation

$$\left[\tilde{\nabla}_i\tilde{\nabla}^i - V(\mathbf{x})\right]\mathcal{G}_\omega(\mathbf{x};\mathbf{x}') \;=\; -\tilde{g}^{-\frac{1}{2}}(\mathbf{x})\delta^3(\mathbf{x},\mathbf{x}') \tag{3.3.6}$$

for potential

$$V(\mathbf{x}) = \frac{\tilde{V}}{f} = f^{-1}\left(\frac{\omega^2}{f} + m^2 + \xi R\right). \tag{3.3.7}$$

on a three dimensional metric [75]

$$d\tilde{s}^2 = dr^2 + r^2 f d\theta^2 + r^2 f \sin^2\theta\, d\varphi^2. \tag{3.3.8}$$

The term $\tilde{g}(\mathbf{x})$ is the determinant of the metric (3.3.8) and the labels on the covariant derivatives also refer to this metric. It is important to note here that throughout the above expressions the Ricci scalar R is still that from our original metric on the four dimensional brane (3.1.1).

Now we repeat an important point from the source material, 'we emphasise that [this metric] has no physical significance' [75]. The metric (3.3.8) has a curvature singularity on its horizon where $f \to 0$ though it is asymptotically flat at infinity. The potential (3.3.7) is also divergent on the horizon so this system should only be seen as mathematical tool. In this artificial system we can see that $\mathcal{G}_\omega$ is a Euclidean Green's function solution for the scalar field in (3.3.6). Fortunately the strange structure of this system does not affect the singularity structure of the Green's function. This means we may still express this structure in the normal three dimensional Hadamard form (which in three dimensions has no logarithmic term [23])

$$\mathcal{G}_\omega(\mathbf{x},\mathbf{x}') = \frac{U(\mathbf{x},\mathbf{x}')}{[2\sigma(\mathbf{x},\mathbf{x}')]^{\frac{1}{2}}} + W(\mathbf{x},\mathbf{x}'). \tag{3.3.9}$$

The biscalars $U(\mathbf{x},\mathbf{x}')$ and $W(\mathbf{x},\mathbf{x}')$ can be expanded in terms of $\sigma(\mathbf{x},\mathbf{x}')$, which has

already been performed [22, 58]. Only the lowest order term of $U(\mathbf{x},\mathbf{x}')$ will be useful here,

$$U(\mathbf{x},\mathbf{x}') = 1 + O(\sigma), \tag{3.3.10}$$

where we note the important lack of dependence on the potential up to this order.

We now implement a point splitting regime for our function $\mathcal{G}_\omega$ in three dimensions, choosing $r = r'$ and $\phi = \phi'$. As our metric (3.3.8) is spherically symmetric we can choose to take $\theta' = 0$ without loss of generality, which in (3.2.1) gives us $\cos\gamma = \cos\theta$, allowing us to rewrite (3.3.3) as

$$\mathcal{G}_\omega(r,\theta,\phi;r,0,\phi) = \sum_{l=0}^{\infty}(2l+1)P_l(\cos(\theta))C_{\omega l}p_{\omega l}(r)q_{\omega l}(r). \tag{3.3.11}$$

Due to the restriction in size of the $P_l(\cos\theta)$ terms ($|P_l(x)| < 1$ for $|x| < 1$) the sum over l here is kept finite in spite of us bringing together two of the coordinates. From this point splitting we may state

$$2\sigma = r^2 f\theta^2 + O(\theta^4). \tag{3.3.12}$$

Now we may express our Hadamard form (3.3.9) as

$$\mathcal{G}_\omega(\mathbf{x},\mathbf{x}') = \frac{1}{rf^{\frac{1}{2}}\theta} + \text{ finite terms} \tag{3.3.13}$$

which for small θ gives us

$$\sum_{l=0}^{\infty}(2l+1)P_l(\cos(\theta))C_{\omega l}p_{\omega l}(r)q_{\omega l}(r) = \frac{1}{rf^{\frac{1}{2}}\theta} + O(1), \tag{3.3.14}$$

thus showing our earlier sum in (3.2.4) diverges.

Making use of a previously proven identity [41],

$$\sum_{l=0}^{\infty} P_l(\cos(\theta)) = \frac{1}{\theta} + O(\theta), \tag{3.3.15}$$

we multiply (3.3.15) through by $1/(rf^{\frac{1}{2}})$ to find an appropriate term to subtract from (3.3.14) to render it finite. This yields

$$\sum_{l=0}^{\infty} \left[(2l+1) C_{\omega l} p_{\omega l}(r) q_{\omega l}(r) - \frac{1}{r f^{\frac{1}{2}}} \right] P_l(\cos(\theta)) = O(1) \tag{3.3.16}$$

which in the limit $\theta \to 0$ demonstrates the subtraction term $(r\sqrt{f})^{-1}$ does in fact make our mode sum in (3.3.1) finite.

There is a final point on this topic that will be discussed in more detail when applied in the bulk in §4.12. Although we have guaranteed that (3.3.1) is finite for $\epsilon \neq 0$ no method in handling the divergence in the l sum guarantees that no lower order terms should not have also been taken away. The subtraction of any term of order $O(l^{-k})$ for $k > 1$ would not alter the divergence structure but would change the final solution.

3.4 Brane Renormalisation

Now we shall apply the method laid out in §2.9, to calculate the renormalisation terms on the brane, which is the 4d Hadamard expansion. In this expansion the dimensional constant (2.9.5) is

$$\alpha_4 = \frac{1}{4\pi^2} \tag{3.4.1}$$

and the singular terms (2.9.18) are

$$G^{4\mathrm{d}}_{E,sing} = \frac{1}{8\pi^2} \left(\frac{U(x,x')}{\sigma(x,x')} + V(x,x') \ln[\sigma(x,x')] \right). \tag{3.4.2}$$

The final general form of the 4d renormalisation terms has been well established [19] and has been used repeatedly [2, 3, 75]. However the version in those sources came from DeWitt-Schwinger version, as discussed in §2.9. We state here the form derived from the Hadamard method (3.4.2) which we calculated ourselves, starting with

$$G^{\rm 4d}_{E,sing} = \frac{1}{8\pi^2\sigma} + \frac{1}{96\pi^2}R_{\alpha\beta}\frac{\sigma^\alpha\sigma^\beta}{\sigma} + \frac{1}{8\pi^2}\left(m^2 + (\xi - \frac{1}{6})R\right)\left(C + \frac{1}{2}\ln\left[\frac{\mu^2|\sigma|}{2}\right]\right). \quad (3.4.3)$$

If in (3.4.3) we consider a massive scalar field then the constant μ is equal to m however, for a massless scalar field, the constant μ remains free [3]. In the massless case it corresponds to a finite renormalisation of terms in the gravitational action [75].

The restriction of (3.4.3) to temporal splitting using equations (2.10.28) is also well established in [3, 75] so again it is quoted,

$$\begin{aligned} G^{\rm 4d}_{E,sing}(\mathbf{x},\epsilon;\mathbf{x},0) =& \frac{1}{4\pi^2\epsilon^2 f} + \frac{1}{8\pi^2}\left(m^2 + \left(\xi - \frac{1}{6}\right)R\right)\left(C + \frac{1}{2}\ln\left[\frac{\mu^2 f\epsilon^2}{4}\right]\right) \\ &+ \frac{1}{192\pi^2 f}\left(\frac{df}{dr}\right)^2 - \frac{1}{96\pi^2}\frac{d^2f}{dr^2} - \frac{1}{48\pi^2 r}\frac{df}{dr}, \end{aligned} \quad (3.4.4)$$

where the limit of (3.4.4) as $\epsilon \to 0$ is called $\langle\phi^2\rangle_{\rm div}$.

In order to make use of (3.4.4) we wish to express it in terms of mode sums, this is achieved through identities derived in appendix B,

$$\begin{aligned} \frac{1}{\epsilon^2} &= -\kappa^2\sum_{n=1}^{\infty} n\cos(n\kappa\epsilon) - \frac{\kappa^2}{12} + O(\epsilon^2) \\ \text{and} \quad -\frac{1}{2}\ln(\kappa^2\epsilon^2) &= \sum_{n=1}^{\infty}\frac{\cos(n\kappa\epsilon)}{n} + O(\epsilon^2). \end{aligned} \quad (3.4.5)$$

Using these identities with $\kappa = 2\pi T$ and $\omega = n\kappa$ we can rewrite (3.4.4) in a form suitable

to be subtracted from (3.3.1) as

$$\begin{aligned} G^{4\mathrm{d}}_{E,sing}(\mathbf{x},\epsilon;\mathbf{x},0) = &-\frac{\kappa}{4\pi^2 f}\sum_{n=1}^{\infty}\omega\cos(\omega\epsilon) - \frac{\kappa}{8\pi^2}\left(m^2+\left(\xi-\frac{1}{6}\right)R\right)\sum_{n=1}^{\infty}\frac{\cos(\omega\epsilon)}{\omega} \\ &+\frac{1}{8\pi^2}\left(m^2+\left(\xi-\frac{1}{6}\right)R\right)\left(C+\frac{1}{2}\ln\left[\frac{\mu^2 f}{4\kappa^2}\right]\right) \\ &+\frac{1}{192\pi^2 f}\left(\frac{df}{dr}\right)^2 - \frac{1}{96\pi^2}\frac{d^2 f}{dr^2} - \frac{1}{48\pi^2 r}\frac{df}{dr} - \frac{\kappa^2}{48\pi^2 f} + O(\epsilon^2). \end{aligned} \tag{3.4.6}$$

Achieving the form of (3.4.6) has an added benefit in that now the ϵ limit can be taken across both (3.3.1) and (3.4.6) very simply. Once this limit has been taken, the terms within (3.4.6) subtracted from (3.3.1) and the resulting terms are then categorised into two groups such that we may write [3, 75]

$$\langle\phi^2\rangle_{\mathrm{ren}} = \langle\phi^2\rangle_{\mathrm{analytic}} + \langle\phi^2\rangle_{\mathrm{numeric}} \tag{3.4.7}$$

where

$$\begin{aligned} \langle\phi^2\rangle_{\mathrm{analytic}} = &\frac{\kappa^2}{48\pi^2 f} - \frac{1}{192\pi^2 f}\left(\frac{df}{dr}\right)^2 + \frac{1}{96\pi^2}\frac{d^2 f}{dr^2} + \frac{1}{48\pi^2 r}\frac{df}{dr} \\ &- \frac{1}{8\pi^2}\left(m^2+\left(\xi-\frac{1}{6}\right)R\right)\left(C+\frac{1}{2}\ln\left[\frac{\mu^2 f}{4\kappa^2}\right]\right), \end{aligned} \tag{3.4.8}$$

$$\begin{aligned} \langle\phi^2\rangle_{\mathrm{numeric}} = &\frac{T}{2\pi}\sum_{n=1}^{\infty}\left\{\sum_{l=0}^{\infty}\left[(2l+1)C_{\omega l}p_{\omega l}q_{\omega l} - \frac{1}{r f^{\frac{1}{2}}}\right] + \frac{\omega}{f} + \frac{1}{2\omega}\left(m^2+\left(\xi-\frac{1}{6}\right)R\right)\right\} \\ &+\frac{T}{4\pi}\sum_{l=0}^{\infty}\left[(2l+1)C_{0l}p_{0l}q_{0l} - \frac{1}{r f^{\frac{1}{2}}}\right]. \end{aligned} \tag{3.4.9}$$

It is easy to see that (3.4.8) requires no more work before calculation so we turn to implementing the WKB approximation for mode functions in (3.4.9).

3.5 WKB Terms on the Brane

In a more complicated case it may be prudent here to move to a more general analysis of our calculations in order to attempt to find any simplifications that could be made. However for the $d = 4$ case we know from previous work such as [75] that the number of relevant terms is small enough that proceeding directly to introducing the WKB terms is justified.

We quickly restate equations (2.11.8) and (2.11.9) in their on brane forms

$$\begin{aligned} \chi_{\omega l}^2 &= \omega^2 r^4 + \left(l + \frac{1}{2}\right)^2 f r^2 \\ \eta &= (m^2 + \xi R) f r^4 - \frac{1}{4} f r^2. \end{aligned} \tag{3.5.1}$$

The ODE (2.11.17) is unchanged in form for the brane and therefore so is its expansion. For $d = 4$ we have the expansion

$$\beta_{\omega l}(r) = \sum_{i=0}^{3} \beta_{i\omega l}(r) \tag{3.5.2}$$

where as mentioned in §2.11

$$\beta_{0\omega l} = \frac{1}{2\chi_{\omega l}}. \tag{3.5.3}$$

The WKB terms can then in general be expressed as

$$\beta_{i\omega l} = \sum_{k=1}^{2i+1} A_{i,k}(\omega, m, r) \chi_{\omega l}^{-(2i+2k-1)} \tag{3.5.4}$$

for some functions $A_{i,k}$ which depend on ω but not l, from which it is important to note that for large ω or l (i.e. large $\chi_{\omega l}$)

$$\beta_{i\omega l} \sim \chi_{\omega l}^{-(2i+1)}. \tag{3.5.5}$$

The full list of the $A_{i,k}$ can be found in Appendix C though note that they are explicitly listed by the associated beta term and hence the i is removed for conciseness.

3.6 WKB Implementation

We will now introduce the WKB terms into the $n > 0$ line of equation (3.4.9) as discussed in §2.11, giving

$$\sum_{n=1}^{\infty}\left[\sum_{l=0}^{\infty}(2l+1)[C_{\omega l}p_{\omega l}q_{\omega l}-\beta_{0\omega l}-\beta_{1\omega l}-\beta_{2\omega l}-\beta_{3\omega l}]\right.$$
$$\left.+\sum_{l=0}^{\infty}(2l+1)\left[\beta_{0\omega l}+\beta_{1\omega l}+\beta_{2\omega l}+\beta_{3\omega l}-\frac{1}{rf^{\frac{1}{2}}}\right]+\frac{\omega}{f}+\frac{1}{2\omega}\left(m^2+\left(\xi-\frac{1}{6}\right)R\right)\right]. \tag{3.6.1}$$

As we know all the $\beta_{\omega l}$ terms analytically this part of the approximation is complete. Some manipulation is required to complete the sum over l in a satisfactory way and this is handled in §3.7.

The calculation of the beta terms in §3.5 only holds for $\omega \neq 0$, we now look at $n = 0$. For this we implement the WKB terms into the $n = 0$ line of (3.4.9) as

$$\sum_{l=0}^{\infty}[(2l+1)[C_{0l}p_{0l}q_{0l}-\beta_{00l}-\beta_{10l}-\beta_{20l}-\beta_{30l}]$$
$$+(2l+1)[\beta_{00l}+\beta_{10l}+\beta_{20l}+\beta_{30l}]-\frac{1}{rf^{\frac{1}{2}}}\Bigg]. \tag{3.6.2}$$

For $n = 0$ we have

$$\chi_{0l}(r)=\left(l+\frac{1}{2}\right)^{-1}rf^{\frac{1}{2}} \tag{3.6.3}$$

and using this for our first beta term gives

$$\beta_{00l} = \frac{1}{2rf^{\frac{1}{2}}}\left(l+\frac{1}{2}\right)^{-1}. \tag{3.6.4}$$

So (3.6.4) will cancel within (3.6.2) giving the $n=0$ sum as

$$\begin{aligned}\sum_{l=0}^{\infty}&[(2l+1)[C_{0l}p_{0l}q_{0l} - \beta_{00l} - \beta_{10l} - \beta_{20l} - \beta_{30l}] \\ &+(2l+1)[\beta_{10l}+\beta_{20l}+\beta_{30l}]]\,.\end{aligned} \tag{3.6.5}$$

In (3.6.5) the first line requires numerical calculation while the second line can be handled analytically so we need do no more manipulation on this part. In fact β_{k0l} is equal to the leading order term of $\beta_{k\omega l}$ with $\chi_{\omega l}$ replaced with χ_{0l} as only the leading coefficient is non-vanishing for $\omega \to 0$. Thus using equations (3.5.4), noting the only l dependence is in $\chi_{\omega l}$ and that the leading terms are always $\chi_{\omega l}^{-(2k+1)}$, we know

$$\sum_{l=0}^{\infty}(2l+1)\beta_{i0l} = \frac{2A_{i,1}}{(r\sqrt{f})^{2i+1}}\sum_{l=0}^{\infty}\left(l+\frac{1}{2}\right)^{-2i}. \tag{3.6.6}$$

Calculating (3.6.6) for the three betas in line two of (3.6.5) and naming the results we obtain

$$\begin{aligned}\Delta_1 = \sum_{l=0}^{\infty}(2l+1)\beta_{10l} &= \frac{\pi^2}{r^3 f^{\frac{3}{2}}}A_{1,1} \quad \text{from} \quad \sum_{l=0}^{\infty}\left(l+\frac{1}{2}\right)^{-2} = \frac{\pi^2}{2},\\ \Delta_2 = \sum_{l=0}^{\infty}(2l+1)\beta_{20l} &= \frac{\pi^4}{3r^5 f^{\frac{5}{2}}}B_{1,1} \quad \text{from} \quad \sum_{l=0}^{\infty}\left(l+\frac{1}{2}\right)^{-4} = \frac{\pi^4}{6}\\ \text{and} \quad \Delta_3 = \sum_{l=0}^{\infty}(2l+1)\beta_{30l} &= \frac{2\pi^6}{15r^7 f^{\frac{7}{2}}}C_{1,1} \quad \text{from} \quad \sum_{l=0}^{\infty}\left(l+\frac{1}{2}\right)^{-6} = \frac{\pi^6}{15},\end{aligned} \tag{3.6.7}$$

refer to Appendix C for $A_{1,1}$, $B_{1,1}$ and $C_{1,1}$.

This gives us a new form of equation (3.4.9)

$$\begin{aligned}\langle\phi^2\rangle_{\text{numeric}} = \frac{T}{2\pi}\sum_{n=1}^{\infty}\Bigg[&\sum_{l=0}^{\infty}(2l+1)[C_{\omega l}p_{\omega l}q_{\omega l} - \beta_{0\omega l} - \beta_{1\omega l} - \beta_{2\omega l} - \beta_{3\omega l}] \\ &+ \sum_{l=0}^{\infty}(2l+1)\left[\beta_{0\omega l} + \beta_{1\omega l} + \beta_{2\omega l} + \beta_{3\omega l} - \frac{1}{rf^{\frac{1}{2}}}\right] \\ &+ \frac{\omega}{f} + \frac{1}{2\omega}\left(m^2 + \left[\xi - \frac{1}{6}\right]R\right)\Bigg] \\ &+ \frac{T}{4\pi}\sum_{l=0}^{\infty}[(2l+1)[C_{0l}p_{0l}q_{0l} - \beta_{00l} - \beta_{10l} - \beta_{20l} - \beta_{30l}]] \\ &+ \Delta_1 + \Delta_2 + \Delta_3.\end{aligned} \tag{3.6.8}$$

We note that in (3.6.8) line five has been calculated, the mode sums in lines one and four will be found numerically then summed over a finite value of n and l such that we can find these sums to some desired numerical accuracy. Lines two and three, the second line in (3.6.1), will require some manipulation in §3.7 before final calculation.

3.7 Calculating $\langle\phi^2\rangle_{\text{numeric}}$

We now look at how to calculate lines two and three of equation (3.6.8.) We begin by looking at a method to handle the l sum as proposed by [17, 44, 75]. We apply the Watson-Sommerfeld formula, in the form from [17], to transform the l sum into integrals. The Watson-Sommerfeld identity is

$$\sum_{l=0}^{\infty}\mathcal{F}(l) = \int_0^{\infty}\mathcal{F}\left(\lambda - \frac{1}{2}\right)d\lambda - Re\left[i\int_0^{\infty}\frac{2}{1+e^{2\pi\lambda}}\mathcal{F}\left(i\lambda - \frac{1}{2}\right)d\lambda\right] \tag{3.7.1}$$

and is derived in the following section.

3.7.1 Derivation of the Watson-Sommerfeld Identity

We begin with a function, $f(l)$, that is holomorphic for $Re(l) \geq -\frac{1}{2}$ and real for $l \in \mathbb{R}$. Now we construct the function

$$g(l) = \pi \cot(\pi l) f(l), \tag{3.7.2}$$

this function is holomorphic for $Re(l) \geq -\frac{1}{2}$ except at the poles $l = l_k$ such that $l_k \in \mathbb{N}$.

Now consider the contour, γ_1, which starts at $(-\frac{1}{2}, 0)$ and goes to positive, real infinity. This is except at each l_k where its path describes a semi-circle centred at l_k with radius ϵ, for small ϵ, protruding into positive, imaginary l. This is equivalent to Fig. 1 of [17]. We term the contour around any semi-circle γ_ϵ and the contour only along the real axis $\tilde{\gamma}_1$. Hence we have

$$\int_{\gamma_1} g(l)dl = \int_{\tilde{\gamma}_1} g(l)dl + \sum_k \int_{\gamma_\epsilon} g(l)dl. \tag{3.7.3}$$

Using the fact that $g(l)$ is real and holomorphic for real l except at l_k we can multiply equation (3.7.3) by i and take the real parts of both sides to find

$$Re\left[i\int_{\gamma_1} g(l)dl\right] = Re\left[i\sum_k \int_{\gamma_\epsilon} g(l)dl\right]. \tag{3.7.4}$$

Next we consider the summand in the RHS of equation (3.7.4) by looking at the integral around a generic l_k. For γ_ϵ we find $l = l_k + \epsilon e^{i\theta}$ for θ going from π to 0, which allows us to write the integral as

$$\int_{\gamma_\epsilon} g(l)dl = \pi \int_{\pi}^{0} \cot(\pi l_k + \epsilon\pi e^{i\theta}) f(l_k + \epsilon e^{i\theta}) \epsilon i e^{i\theta} d\theta. \tag{3.7.5}$$

Note that we can expand the cotangent as

$$\cot(\pi l_k + \pi\epsilon e^{i\theta}) = \cot(\epsilon\pi e^{i\theta}) = \frac{1}{\epsilon\pi e^{i\theta}} + O(1) \tag{3.7.6}$$

hence integral (3.7.5) can be written as

$$\begin{aligned}\int_{\gamma_\epsilon} g(l)dl &= i\int_{\pi}^{0} f(l_k + \epsilon e^{i\theta}) + O(\epsilon)d\theta \\ &= if(l_k)\int_{\pi}^{0} d\theta \\ &= -i\pi f(l_k)\end{aligned} \tag{3.7.7}$$

where we have taken the limit $\epsilon \to 0$. Comparing (3.7.7) with (3.7.4) we see

$$Re\left[i\sum_k \int_{\gamma_\epsilon} g(l)dl\right] = \pi\sum_{l=0}^{\infty} f(l) \tag{3.7.8}$$

where the index on the sum matches the values of l to l_k, hence we can rewrite (3.7.4) as

$$\sum_{l=0}^{\infty} f(l) = Re\left[\frac{i}{\pi}\int_{\gamma_1} g(l)dl\right]. \tag{3.7.9}$$

Next we use an alternative representation of the cotangent,

$$\cot(\pi l) = -i + \frac{2i}{1 - e^{-2\pi i l}}, \tag{3.7.10}$$

to write (3.7.9) as

$$\begin{aligned}\sum_{l=0}^{\infty} f(l) &= Re\left[\int_{\gamma_1} f(l)dl\right] - Re\left[\int_{\gamma_1} \frac{2f(l)}{1 - e^{-2\pi i l}}dl\right] \\ &= \int_{-\frac{1}{2}}^{\infty} f(l)dl - 2Re\left[\int_{\gamma_1} \frac{f(l)}{1 - e^{-2\pi i l}}dl\right]\end{aligned} \tag{3.7.11}$$

where it is understood in the first integral of the RHS we have taken the limit $\epsilon \to 0$.

To proceed we investigate the second integral on the RHS of (3.7.11) which we will call I. To do this we examine the integrand of I, $\frac{f(l)}{1-e^{-2\pi il}}$, as it is integrated along a new contour Γ. Contour Γ is constructed of three pieces:

- γ_H is identical to γ_1 except it only extends a distance R from its start point,
- γ_R is a quarter circle centred at $(-\frac{1}{2}, 0)$ starting at the end of γ_H,
- γ_V closes the contour in a vertical line from the end of γ_V to the start of γ_H,

such that

$$I = \lim_{R\to\infty} \int_{\gamma_H} \frac{f(l)}{1-e^{-2\pi il}} dl. \tag{3.7.12}$$

Note that the integrand of I has no poles in or on contour Γ so we know

$$\int_\Gamma \frac{f(l)}{1-e^{-2\pi il}} dl = \int_{\gamma_H} \frac{f(l)}{1-e^{-2\pi il}} dl + \int_{\gamma_R} \frac{f(l)}{1-e^{-2\pi il}} dl + \int_{\gamma_V} \frac{f(l)}{1-e^{-2\pi il}} dl = 0. \tag{3.7.13}$$

On γ_R we have $l = -\frac{1}{2} + Re^{i\theta}$ for $\theta \in (0, \frac{\pi}{2}]$. Note that it is important that γ_R makes a closed contour with γ_H but does not extend on to the real line, any evaluation on the real line belongs to γ_H. The integral on γ_R becomes

$$\int_{\gamma_R} \frac{f(l)}{1-e^{-2\pi il}} dl = \int_\alpha^{\pi/2} \frac{iRe^{i\theta} f\left(-\frac{1}{2} + Re^{i\theta}\right)}{1+e^{-2\pi iRe^{i\theta}}} d\theta \tag{3.7.14}$$

where α is a small positive value arbitrarily close to zero but is not equal to zero. We may then apply the Cauchy-Schwartz to evaluate the RHS of equation (3.7.14) as follows

$$\left| \int_\alpha^{\pi/2} \frac{iRe^{i\theta} f\left(-\frac{1}{2} + Re^{i\theta}\right)}{1+e^{-2\pi iRe^{i\theta}}} d\theta \right| \leq \int_\alpha^{\pi/2} \frac{R\left|f\left(-\frac{1}{2} + Re^{i\theta}\right)\right|}{\left|1+e^{-2\pi iRe^{i\theta}}\right|} d\theta. \tag{3.7.15}$$

Now we note that from the triangle inequality we obtain

$$\begin{aligned}\left|1+e^{-2\pi iRe^{i\theta}}\right| &= \left|1+e^{2\pi R\sin(\theta)}e^{-2\pi iR\cos(\theta)}\right| \\ &\geq e^{2\pi R\sin(\theta)}-1. \end{aligned} \tag{3.7.16}$$

Hence from equations (3.7.14), (3.7.15) and (3.7.16) we may state

$$\left|\int_{\gamma_R}\frac{f(l)}{1-e^{-2\pi il}}dl\right| \leq \int_{\alpha}^{\pi/2}\frac{R\left|f\left(-\frac{1}{2}+Re^{i\theta}\right)\right|}{e^{2\pi R\sin(\theta)}-1}d\theta. \tag{3.7.17}$$

Now as θ is defined on $(0,\frac{\pi}{2}]$ we have $\sin(\theta)>0$. This means that the RHS of (3.7.17) tends to zero as R tends to infinity providing $\left|f\left(-\frac{1}{2}+Re^{i\theta}\right)\right|$ remains finite as $R\to\infty$. This marks a new, and final, condition on our original function, $f(l)$.

Now we make use of equation (3.7.13) and define new contours $\tilde{\gamma}_H=\lim_{R\to\infty}\gamma_H$ and $\tilde{\gamma}_V=\lim_{R\to\infty}\gamma_V$. This allows equation (3.7.12) to be rewritten as

$$\begin{aligned} I=\int_{\tilde{\gamma}_H}\frac{f(l)}{1-e^{-2\pi il}}dl &= -\int_{\tilde{\gamma}_V}\frac{f(l)}{1-e^{-2\pi il}}dl \\ &= \int_{\hat{\gamma}_V}\frac{f(l)}{1-e^{-2\pi il}}dl \end{aligned} \tag{3.7.18}$$

where $\hat{\gamma}_V$ is the reverse contour of $\tilde{\gamma}_V$. On $\hat{\gamma}_V$ we have $l=-\frac{1}{2}+i\lambda$ for $\lambda\in(0,\infty)$ hence I becomes

$$I=\int_0^{\infty}\frac{if(-\frac{1}{2}+i\lambda)}{1+e^{2\pi\lambda}}d\lambda. \tag{3.7.19}$$

We may now re-express equation (3.7.11) as

$$\begin{aligned}\sum_{l=0}^{\infty}f(l) &= \int_{-\frac{1}{2}}^{\infty}f(l)dl - Re\left[i\int_0^{\infty}\frac{2f(-\frac{1}{2}+i\lambda)}{1+e^{2\pi\lambda}}d\lambda\right] \\ &= \int_0^{\infty}f\left(\lambda-\frac{1}{2}\right)d\lambda - Re\left[i\int_0^{\infty}\frac{2f(-\frac{1}{2}+i\lambda)}{1+e^{2\pi\lambda}}d\lambda\right] \end{aligned} \tag{3.7.20}$$

where we have set $l = \lambda - \frac{1}{2}$ in the first integral of the RHS. The second line of equation (3.7.20) is now equivalent to equation (3.7.1).

3.7.2 Verifying the Watson-Sommerfeld Conditions

We must now verify that our WKB terms obey the conditions for the Watson-Sommerfeld identity (3.7.1). The conditions for the function, $f(l)$, to be summed over are:

1. $f(l)$ must be holomorphic for $Re(l) \geq -\frac{1}{2}$

2. $f(l)$ must be real for $l \in \mathbb{R}$

3. $f(l)$ must decay to a finite value as l approaches infinity.

We can write the jth term of the ith beta function in an unspecified number of dimensions, β_{ij}, as a function of only l as

$$\beta_{ij} = F_{ij} \frac{1}{\left(\left(l + \frac{d-3}{2}\right)^2 + K^2\right)^{i+j+\frac{1}{2}}} \tag{3.7.21}$$

such that F_{ij} is a real coefficient depending on the beta term and is independent of l. The new object K is

$$K = \frac{(d-3)nr}{2\sqrt{f}} > 0 \tag{3.7.22}$$

for $d \geq 4$.

In order to discover where β_{ij} is holomorphic we make use of the Cauchy-Riemann equations. Given a function of a complex variable, $f(z)$, such that $z = x + iy$ then we can write

$$f(z) = u(x, y) + iv(x, y). \tag{3.7.23}$$

The function, $f(z)$, is then holomorphic where ever it satisfies the equations

$$\frac{\partial u}{\partial x} = \frac{\partial v}{\partial y} \tag{3.7.24}$$

$$\frac{\partial u}{\partial y} = -\frac{\partial v}{\partial x} \tag{3.7.25}$$

which can can written concisely as

$$i\frac{\partial f}{\partial x} = \frac{\partial f}{\partial y}. \tag{3.7.26}$$

For $\beta_{ij}(l)$ with $l = x + iy$ we find

$$\frac{\partial \beta_{ij}}{\partial x} = -F_{ij}\frac{(2i+2j+1)\left(x+iy+\frac{d-3}{2}\right)}{\left(\left(l+\frac{d-3}{2}\right)^2+K^2\right)^{i+j+\frac{1}{2}}} \tag{3.7.27}$$

$$\frac{\partial \beta_{ij}}{\partial y} = -iF_{ij}\frac{(2i+2j+1)\left(x+iy+\frac{d-3}{2}\right)}{\left(\left(l+\frac{d-3}{2}\right)^2+K^2\right)^{i+j+\frac{1}{2}}} \tag{3.7.28}$$

hence

$$i\frac{\partial f}{\partial x} = \frac{\partial f}{\partial y} \tag{3.7.29}$$

for all l and β_{ij} meets condition 1.

From inspection of equation (3.7.21) and its associated definitions we can see that β_{ij} is real for $l \in \mathbb{R}$ and hence meets condition 2.

We now consider β_{ij} as l approaches infinity by setting $l = c + Re^{i\theta}$, for finite real c, and then taking the limit as $R \to \infty$. So we have

$$\lim_{R\to\infty}\beta_{ij} = \lim_{R\to\infty}F_{ij}\frac{1}{\left(\left(Re^{i\theta}+\frac{2c+d-3}{2}\right)^2+K^2\right)^{i+j+\frac{1}{2}}} = 0, \tag{3.7.30}$$

hence β_{ij} satisfies condition 3.

We have now demonstrated that the the identity (3.7.1) is applicable to our WKB terms.

3.7.3 Applying the Watson-Sommerfeld Identity

Now we use (3.7.1) to write

$$\begin{aligned}\sum_{l=0}^{\infty}(2l+1)\left[\beta_{0\omega l}-\frac{1}{rf^{\frac{1}{2}}}\right] =& I_0(\omega,r)+\tilde{J}_0(\omega,r),\\ \sum_{l=0}^{\infty}(2l+1)\beta_{k\omega l} =& I_k(\omega,r)+J_k(\omega,r),\quad (k=1,2,3),\end{aligned} \tag{3.7.31}$$

where I_k refers to the integral in the left hand term of equation (3.7.1) and J_k refers to the integral in the right hand term. We denote $\tilde{J}_0$ differently as it must undergo some manipulation before it can be brought into a form we may call J_0 and calculated [75].

Firstly we look at the I_k integrals which can be calculated easily but rapidly increase in number of terms as k increases. The full expressions can be found in appendix D however we display I_0 and I_1 here due to their immediate relevance (note $l=\lambda-\frac{1}{2}$)

$$\begin{aligned}I_0(\omega,r)&=\int_0^{\infty}\left[2\lambda\beta_{0\omega l}-\frac{1}{rf^{\frac{1}{2}}}\right]d\lambda=-\frac{\omega}{f},\\ I_1(\omega,r)&=\int_0^{\infty}2\lambda\beta_{1\omega l}d\lambda=-\frac{1}{2\omega}\left[m^2+\left(\xi-\frac{1}{6}\right)R\right]-\frac{1}{24r^2\omega}.\end{aligned} \tag{3.7.32}$$

Substituting (3.7.31) and (3.7.32) into equation (3.6.8) we obtain

$$\begin{aligned}\langle\phi^2\rangle_{\text{numeric}} = \frac{T}{2\pi}\sum_{n=1}^{\infty}\Bigg[&\sum_{l=0}^{\infty}(2l+1)[C_{\omega l}p_{\omega l}q_{\omega l}-\beta_{0\omega l}-\beta_{1\omega l}-\beta_{2\omega l}-\beta_{3\omega l}]\\ &+I_2+I_3+\tilde{J}_0+J_1+J_2+J_3-\frac{1}{24r^2\omega}\Bigg]\\ +\frac{T}{4\pi}\sum_{l=0}^{\infty}&\Big\{(2l+1)[C_{0l}p_{0l}q_{0l}-\beta_{00l}-\beta_{10l}-\beta_{20l}-\beta_{30l}]\Big\}\\ &+\Delta_1+\Delta_2+\Delta_3.\end{aligned} \tag{3.7.33}$$

Now we examine the $\tilde{J}_0$ and J_k integrals, where now $l = i\lambda - \frac{1}{2}$,

$$\begin{aligned}\tilde{J}_0(\omega,r) =& -Re\left[i\int_0^{\infty}\frac{2}{1+e^{2\pi\lambda}}\left(2\lambda i\beta_{0\omega l}-\frac{1}{rf^{\frac{1}{2}}}\right)d\lambda\right]\\ \text{and}\quad J_k(\omega,r) =& Re\left[\int_0^{\infty}\frac{4\lambda}{1+e^{2\pi\lambda}}\beta_{k\omega l}d\lambda\right]\quad(k=1,2,3).\end{aligned} \tag{3.7.34}$$

Starting with $\tilde{J}_0$ we introduce a new variable [75]

$$a = \frac{\omega r}{f^{\frac{1}{2}}} \tag{3.7.35}$$

which when substituted into the first beta term gives (with $l = i\lambda - \frac{1}{2}$)

$$\beta_{0\omega\lambda} = \frac{1}{r\sqrt{f}(a^2-\lambda^2)^{\frac{1}{2}}}. \tag{3.7.36}$$

Placing this into our integral from equation (3.7.34) gives

$$\begin{aligned}\tilde{J}_0(\omega,r) = \frac{1}{rf^{\frac{1}{2}}}Re\Bigg[&\int_0^{\infty}\frac{2i}{1+e^{2\pi\lambda}}d\lambda\\ &+\int_0^{a}\frac{2\lambda}{(1+e^{2\pi\lambda})(a^2-\lambda^2)^{\frac{1}{2}}}d\lambda\\ &+\int_a^{\infty}\frac{2\lambda}{(1+e^{2\pi\lambda})(a^2-\lambda^2)^{\frac{1}{2}}}d\lambda\Bigg].\end{aligned} \tag{3.7.37}$$

Within (3.7.37) the first and third terms will be imaginary and so will not contribute to the result. The second term is integrable but the integrand is not regular at $\lambda = a$. The integral cannot be done analytically so we use numerics which is simplified by having an integrand regular throughout the interval of integration. To achieve this we apply integration by parts to (3.7.37) to obtain

$$\tilde{J}_0(\omega, r) = \frac{\omega}{f} - \frac{4\pi\omega}{f}\int_0^a \left(1 - \frac{\lambda^2}{a^2}\right)^{\frac{1}{2}} \frac{e^{2\pi\lambda}}{(1+e^{2\pi\lambda})^2} d\lambda \tag{3.7.38}$$

which for large ω behaves as [75]

$$\tilde{J}_0(\omega, r) = \frac{1}{24\omega r^2} + O(\omega^{-3}). \tag{3.7.39}$$

Next we introduce the term $-(24\omega r^2)^{-1}$ from equation (3.7.33) into $\tilde{J}_0$ allowing us to write a final form for J_0 at large ω

$$\begin{aligned} J_0(\omega, r) &= \tilde{J}_0(\omega, r) - \frac{1}{24\omega r^2} \\ &= \frac{\omega}{f} - \frac{1}{24\omega r^2} - \frac{4\pi\omega}{f}\int_0^a \left(1 - \frac{\lambda^2}{a^2}\right)^{\frac{1}{2}} \frac{e^{2\pi\lambda}}{(1+e^{2\pi\lambda})^2} d\lambda \\ &\sim O(\omega^{-3}). \end{aligned} \tag{3.7.40}$$

Hence we know that $\sum_{n=1}^{\infty} J_0$ will converge quite rapidly so it can be considered separately from the other terms within the n sum.

We will now look at the J_k integrals. Each β_k can be schematically expressed as

$$\beta_{k\omega\lambda} = \sum_y \Gamma_y \chi_{\omega\lambda}^{-(2y+1)}. \tag{3.7.41}$$

Here the index system of y depends on k but is irrelevant for this argument, where Γ_y is a generic place holder for the appropriate coefficient. Taking a single y term we apply three

changes of variable

$$\begin{aligned}\chi_{\omega l} =&(\omega^2 r^4 - \lambda^2 r^2 f)^{\frac{1}{2}} & l &= i\lambda - \frac{1}{2}\\ =&rf^{\frac{1}{2}}(a^2-\lambda^2)^{\frac{1}{2}} & a &= \frac{\omega r}{f^{\frac{1}{2}}}\\ =&raf^{\frac{1}{2}}(1-q^2)^{\frac{1}{2}} & \lambda &= aq. \end{aligned} \tag{3.7.42}$$

Now we may write an equation for the generic term $J_{y>0}$

$$\begin{aligned}J_y =&Re\left[\int_0^\infty \frac{4aq}{1+e^{2\pi aq}}(rf^{\frac{1}{2}}a)^{-(2y+1)}(1-q^2)^{-\frac{2y+1}{2}}a\,dq\right]\\ =&4a^2(rf^{\frac{1}{2}}a)^{-(2y+1)}Re\left[\int_0^\infty \frac{q}{1+e^{2\pi aq}}(1-q^2)^{-\frac{2y+1}{2}}dq\right]\end{aligned} \tag{3.7.43}$$

where we have used a single generic $\chi^{-(2y+1)}$ term and ignored, for now, any coefficient Γ_y as they are independent of q.

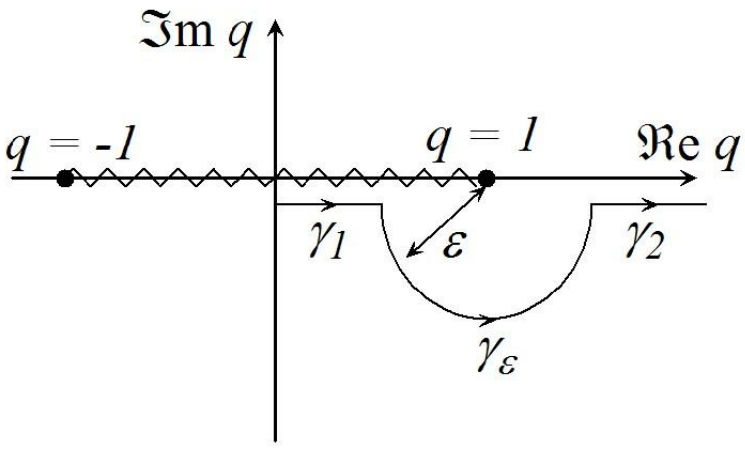

Figure 3.1: Contour used in the J_y integrals [75].

Clearly the integrands in (3.7.43) diverge at $q = \pm 1$ where they have branch points.

We cut the plane along the interval $[-1,1]$ and consider the contour γ which in Fig. 3.1 is split into three components. The contribution from γ_2 must be imaginary so we shall consider the other two sections; γ_1 takes the interval $[0,1-\varepsilon]$ and $q\in\mathbb{R}$ while on γ_ε we have $q=1-\varepsilon e^{-i\theta}$ for $\theta\in[0,\pi]$. This gives

$$\begin{aligned}J_y =&4a^2(rf^{\frac{1}{2}}a)^{-(2y+1)}Re\lim_{\varepsilon\to0}\left[\int_0^{1-\varepsilon}\frac{q}{1+e^{2\pi aq}}(1-q^2)^{-\frac{2y+1}{2}}dq\right.\\&\left.+\int_0^{\pi}\frac{1-\varepsilon e^{-i\theta}}{(1+\exp(2\pi a(1-\varepsilon e^{-i\theta})))}(2\varepsilon e^{-i\theta}-\varepsilon^2e^{-2i\theta})^{-\frac{(2y+1)}{2}}i\varepsilon e^{-i\theta}d\theta\right]\\=&4a^2(rf^{\frac{1}{2}}a)^{-(2y+1)}Re\lim_{\varepsilon\to0}\left[L_y(\omega,r)+M_y(\omega,r)\right]\end{aligned}\tag{3.7.44}$$

where L_y is the first integral on the right hand side of the first line and M_y is the remaining integral in the first line.

At this point we shall take the simplest case of $y=1$ as a sample calculation, which for L_y gives

$$\begin{aligned}L_1=&\int_0^{1-\varepsilon}\frac{q}{1+e^{2\pi aq}}(1-q^2)^{-\frac{3}{2}}dq\\=&\frac{1}{2\sqrt{\varepsilon}(1+e^{2\pi a})}-\frac{1}{2}+2\pi a\int_0^{1-\varepsilon}\frac{e^{2\pi aq}}{(1+e^{2\pi aq})^2}(1-q^2)^{-\frac{1}{2}}dq+O(\varepsilon^{\frac{1}{2}})\end{aligned}\tag{3.7.45}$$

where the second line is given through integration by parts. Considering we wish to take the limit as $\varepsilon\to0$ we have isolated two relevant terms, a divergent component and a finite integral. Applying the same approach to M_y we get

$$\begin{aligned}M_1=&\int_0^{\pi}\frac{1-\varepsilon e^{-i\theta}}{(1+\exp(2\pi a(1-\varepsilon e^{-i\theta})))}(2\varepsilon e^{-i\theta}-\varepsilon^2e^{-2i\theta})^{-\frac{3}{2}}i\varepsilon e^{-i\theta}d\theta\\=&-\frac{1}{2\sqrt{\varepsilon}(1+e^{2\pi a})}+O(\varepsilon^{\frac{1}{2}}).\end{aligned}\tag{3.7.46}$$

Expanding the integrand of M_1 in powers of ε and integrating we see this also exhibits a divergent term but one that cancels with that found in L_1. So if we perform $\lim_{\varepsilon\to0}[L_1+$

M_1] we do get a regular result that can be numerically calculated from a finite integral. Unfortunately this integral does not have a regular integrand, to fix this integration by parts can be applied again to give

$$\begin{aligned}\lim_{\varepsilon\to 0}[L_1+M_1] = &-\frac{1}{2a}+\frac{\pi^2 e^{2\pi a}}{(1+e^{2\pi a})^2}\\ &+4\pi^2\int_0^a \sin^{-1}\left(\frac{\lambda}{a}\right)\frac{e^{2\pi\lambda}(e^{2\pi\lambda}-1)}{(1+e^{2\pi\lambda})^3}d\lambda.\end{aligned} \tag{3.7.47}$$

This method can be applied for $y>1$ to demonstrate that L_y+M_y will be regular.

So far in this section we have followed the approach to these calculations as laid out in [75], performing them ourselves as a check. The problem with this approach lies in the need to apply integration by parts additional times during, and at the end of, the calculation as y increases. These steps cannot be handled by a computer leaving complicated terms to be calculated by hand. Instead we shall use a new approach, knowing that our end result will not be divergent, such that the following expressions and computer calculations are original work. We now express the J_k integrals as

$$\begin{aligned}J_k =&Re\left[\int_0^\infty \frac{4aq}{1+e^{2\pi aq}}\sum_y \Gamma_y (rf^{\frac{1}{2}}a)^{-(2y+1)}(1-q^2)^{-\frac{2y+1}{2}}a\,dq\right]\\ =&4a^2\sum_y \Gamma_y (rf^{\frac{1}{2}}a)^{-(2y+1)}Re\left[\int_0^\infty g(q)(1-q^2)^{-\frac{2y+1}{2}}dq\right]\end{aligned} \tag{3.7.48}$$

where we have set

$$g(q)=\frac{q}{1+e^{2\pi aq}}. \tag{3.7.49}$$

Next we rewrite our new function as

$$g(q)=g(q)+\tilde{g}(q)-\tilde{g}(q) \tag{3.7.50}$$

where $\tilde{g}(q)$ is the series expansion of $g(q)$ around $q=1$ up to order $y+1$ calculated for

each value of y. This gives us

$$J_y = 4a^2 \sum_y \Gamma_y (r f^{\frac{1}{2}} a)^{-(2y+1)} \Big\{ Re \left[\int_0^\infty (g(q) - \tilde{g}(q))(1-q^2)^{-\frac{2y+1}{2}} dq \right] + Re \left[\int_0^\infty \tilde{g}(q)(1-q^2)^{-\frac{2y+1}{2}} dq \right] \Big\}. \tag{3.7.51}$$

The first term of equation (3.7.51) no longer contains a pole at $q = 1$. The pole is still present in the second term but we know that this term will not be divergent as the total was shown to be regular with the previous method. The second term is taken over the same γ contour as before (with divergent terms cancelling between γ_1 and γ_ε) but the problem of multiple steps of integration by parts has been removed allowing practical calculation of these integrals by computer methods. This leaves our integrals, J_y, as

$$J_y = 4a^2 \sum_y \Gamma_y (r f^{\frac{1}{2}} a)^{-(2y+1)} \Big\{ \int_0^1 \big[g(q) - \tilde{g}(q) \big] (1-q^2)^{-\frac{2y+1}{2}} dq + Re \left[\int_0^\infty \tilde{g}(q)(1-q^2)^{-\frac{2y+1}{2}} dq \right] \Big\}. \tag{3.7.52}$$

We have now reached a final form of the numeric component (3.7.33)

$$\begin{aligned} \langle\phi^2\rangle_{\text{numeric}} = \frac{T}{2\pi} \sum_{n=1}^{\infty} \Bigg[& \sum_{l=0}^{\infty} (2l+1)[C_{\omega l} p_{\omega l} q_{\omega l} - \beta_{0\omega l} - \beta_{1\omega l} - \beta_{2\omega l} - \beta_{3\omega l}] \\ & + I_2 + I_3 + J_0 + J_1 + J_2 + J_3] \\ + \frac{T}{4\pi} \sum_{l=0}^{\infty} & [(2l+1)[C_{0l} p_{0l} q_{0l} - \beta_{00l} - \beta_{10l} - \beta_{20l} - \beta_{30l}]] \\ & + \Delta_1 + \Delta_2 + \Delta_3. \end{aligned} \tag{3.7.53}$$

It remains to find $p_{\omega l}$ and $q_{\omega l}$ to which we turn in the next section.

3.8 The Radial ODE on the Brane

We restate the on brane, radial equation (3.2.5) of which $p_{\omega l}$ and $q_{\omega l}$ are solutions

$$f(r)\frac{d^2}{dr^2}\mathbf{S}(r)+\left[\frac{2f(r)}{r}+\frac{d}{dr}f(r)\right]\frac{d}{dr}\mathbf{S}(r)-\left[\frac{\omega^2}{f(r)}+m^2+\xi R(r)+\frac{l(l+1)}{r^2}\right]\mathbf{S}(r)=0. \tag{3.8.1}$$

As discussed in section §2.8 the function $p_{\omega l}$ is the solution regular on the horizon and divergent at infinity and $q_{\omega l}$ is the solution regular at infinity and divergent on the horizon. As we now need to know the values of these functions we must solve (3.8.1) numerically for each combination of l and ω.

3.8.1 Solutions near the Horizon and Infinity

We will first analyse the singular point at $r = r_h$ by the standard method so we rewrite (3.8.1) as

$$\frac{d^2}{dr^2}\mathbf{S}(r)+u(r)\frac{d}{dr}\mathbf{S}(r)-v(r)\mathbf{S}(r)=0. \tag{3.8.2}$$

where

$$u(r)=\frac{2}{r}+\frac{f'}{f}\qquad\text{and}\qquad v(r)=\frac{\omega^2}{f^2}+\frac{m^2+\xi R}{f}+\frac{l(l+1)}{r^2 f}. \tag{3.8.3}$$

Since

$$\begin{aligned} u_0&=\lim_{r\to r_h}u(r)[r-r_h]=1\\ v_0&=\lim_{r\to r_h}v(r)[r-r_h]^2=\frac{r_h^2\omega^2}{(d-3)^2}\end{aligned} \tag{3.8.4}$$

are finite we may use the Frobenius method to write a power series for our function

$$p(r\sim r_h)\simeq\sum_{j=0}^{\infty}a_j(r-r_h)^{\nu+j} \tag{3.8.5}$$

or for the ease of future calculation we use $x = r - r_h$

$$p(x \sim 0) \simeq \sum_{j=0}^{\infty} a_j x^{\nu+j} \tag{3.8.6}$$

where the a_j are constants.

Using (3.8.6) we may produce initial values for $p_{\omega l}$ near the horizon and then numerically integrate (3.8.1) outwards towards infinity. We get our unknown power ν from the indicial equation

$$\nu(\nu - 1) + u_0\nu - v_0 = 0 \tag{3.8.7}$$

which gives

$$\nu = \pm\frac{\omega r_h}{d-3}. \tag{3.8.8}$$

We choose $\nu > 0$ for $p_{\omega l}$ so that this solution is regular at the horizon

For the singular point at $r = \infty$ it is useful to let $r = s^{-1}$ so that $s \in [0, r_h^{-1}]$. This transforms (3.8.1) to

$$s^4 f\frac{d^2\mathbf{S}}{ds^2} + s^4 f'\frac{d\mathbf{S}}{ds} - \left[\frac{\omega^2}{f} + m^2 + \xi R + l(l+1)s^2\right]\mathbf{S} = 0 \tag{3.8.9}$$

where it is understood $f \equiv f(s)$, $R \equiv R(s)$.

We again attempt to use the Frobenius method naming σ_0 as the equivalent to u_0 but obtained from ODE (3.8.9) and similarly τ_0 for v_0. As $s \to 0$ we see that σ_0 does not diverge but τ_0 diverges unless $m = \xi R = \omega = 0$. Therefore $s = 0$ is an irregular singularity of rank 1 and we must use an asymptotic series to approximate our function [2]:

$$q(s \sim 0) \simeq e^{-\Omega s^{-1}} \sum_{j=0}^{\infty} b_j s^{\rho+j} \tag{3.8.10}$$

where the b_j are constants.

The introduction of the exponential term ensures rapid convergence to zero as $s \to 0$. Our two unknown constants, Ω and ρ, in (3.8.10) are derived by placing our sum (3.8.10) back into (3.8.9) and take the form

$$\Omega^2 = m^2 + \omega^2, \tag{3.8.11}$$

$$\rho = 1 + \frac{r_h}{2}\Omega + \frac{r_h\omega^2}{2\Omega} \text{ for } d = 4 \tag{3.8.12}$$

$$\text{and} \quad \rho = 1 \text{ for } d \geq 5. \tag{3.8.13}$$

From (3.8.10) we find our initial values for $q_{\omega l}$ near $s = 0$. Now $q_{\omega l}$ may be calculated by numerically integrating (3.8.9) from $s = 0$ outwards.

To allow the use of the series solutions (3.8.6) and (3.8.10) in our calculations we set $a_0 = 1$ and $b_0 = 1$ without loss of generality as any inconsistency will be corrected by the normalisation constant $C_{\omega l}$ from the Wronskian (2.8.3).

The main issue left before we begin attempting the calculations of $p_{\omega l}$ and $q_{\omega l}$ is accuracy versus speed of convergence. As noted in section §2.11 the mode sums may need many hundreds of l values per n and more than 20 values of n to ensure convergence [75]. We have already taken a step to reduce the number of modes required by using four terms of the WKB approximation where other work used only two but we must be prepared to use methods that hasten convergence. Here the problem is that implementing such techniques (e.g. Shanks [41]) typically halves the number of accurate significant figures from our calculation [75]. So aiming to produce final results of at least six significant figure accuracy, and allowing for the application of two convergence hastening techniques, we want to aim for results of $p_{\omega l}$ and $q_{\omega l}$ accurate to 30+ significant figures. Demanding this level of accuracy will slow the numerical calculations and so we must now aim to balance the time taken per mode function versus how many mode functions we wish to produce.

3.8.2 Complications for $q_{\omega l}(s)$

We discuss here the complications that arise in finding $q_{\omega l}(s)$ from (3.8.9). The form of ODE (3.8.9) is inspired by [75] for whom the calculation, performed in FORTRAN, had no insurmountable difficulties. However in our calculation, performed in Mathematica, the ODE became stiff for large ω and l even for $d = 4$ with solutions for $q_{\omega l}$ growing from $O(10^{-70})$ to $O(10^{120})$ too rapidly across our domain. Mathematica has in built tools for handling stiff ODEs but due to the lack of an exact definition of stiffness (a good, but not definitive one, is provided by [51]) there is no structured approach for handling the problem. In addition we could anticipate the problem becoming worse as we increase the value of d.

As the stiffness arises from a too rapidly rising value for $q_{\omega l}$ we attempted to solve for a less steep function. We let $Q(s) = \ln(q(s))$ which transforms the radial ODE (3.8.9) to a non-linear form,

$$s^4 f \frac{d^2Q}{ds^2} + s^3 \left(fs\frac{dQ}{ds} + f's \right) \frac{dQ}{ds} - \left[\frac{\omega^2}{f} + m^2 + \xi R + l(l+1)s^2 \right] = 0. \tag{3.8.14}$$

This ODE (3.8.14) proved perfectly satisfactory for $d = 4$ but began to slow down for large ω and l in $d = 5$. Attempts to solve (3.8.14) for $d = 6$ almost immediately ran in to memory issues and so this ODE was discarded for general use.

The second attempt to handle the stiffness uses the change of variable

$$Q(s) = e^{\frac{\omega}{s}} q(s) \tag{3.8.15}$$

such that the exponential scale factor lets $Q(s) \sim q(s)$ near $s = 1$ but greatly raises its

value as $s \to 0$. This transforms the radial ODE (3.8.9) to

$$s^4 f \frac{d^2Q}{ds^2} + s^2 \left(2\omega + f' s^2\right) \frac{dQ}{ds} - \left[\frac{\omega^2}{f} + m^2 + \xi R + l(l+1)s^2 + f(2\omega s - \omega^2) - s^2 \omega f'\right] Q = 0. \quad (3.8.16)$$

This form of the radial ODE suited our needs throughout the brane calculation and so is the final form of the radial ODE for $q_{\omega l}(s)$. We note that this change of ODE does not affect our power series solution (3.8.10) near $s \sim 0$, we simply apply the same change of variable (3.8.15) to the series, solve the ODE and transform the solution back.

3.9 Calculation Parameters

To proceed to final results we must state the values to be used in our formulae. First a reminder that some simplification has already been chosen, we have set the cosmological constant / brane tension to zero, we have an uncharged and static spacetime, any extra dimensions are treated as flat (not periodic) and we have set the Schwarschild-Tangherlini horizon radius to unity ($r_h = 1$).

As this is the first calculation for a higher dimensional black outside the event horizon we choose parameters that will give baseline results from which further work will evolve. However we must not simplify our set up beyond physical relevance so the natural balance is to set the mass of the scalar field to zero and have our quantum field conformally coupled to the background. Conformal coupling occurs when the classical stress energy tensor is traceless, i.e.

$$T_\mu{}^\mu = 0, \quad (3.9.1)$$

which is equivalent to stating that the scalar field theory is conformally invariant [23].

From equations (2.3.4) and (2.3.6) we see that the conformal coupling constant, ξ_c, is

$$\xi_c(d) = \frac{1}{4}\frac{d-2}{d-1}. \tag{3.9.2}$$

Hence we set $\xi = \frac{1}{6}$ for the brane. If $\xi \neq \xi_c$ there are additional complications, primarily the WKB approach is no longer appropriate and a better approximation, such as Green-Liouville asymptotics [12], would be required.

Finally we look at the region from just outside the event horizon to a distance far enough away to see the behaviour as r tends to infinity, so we choose

$$r \in (1, 11] \quad \text{and} \quad s \in [\frac{1}{11}, 1). \tag{3.9.3}$$

Due to our choice of the WKB approximation we cannot calculate on the horizon itself (see §2.11) though if we could results would end here due to the Wick rotation removing the manifold inside the event horizon in §2.3. We extend to $r = 11r_h$ because we expect to see features in the region of strong curvature just outside the event horizon but we do not yet know how far from the horizon these features will extend.

3.10 Mode Calculation Accuracy

First we note that all numerical calculations were carried out in Mathematica 8.0. Our numerical solutions for ODEs were performed using the Extrapolation method of the NDSolve command which, as stated in the manual, "adapt order and step size using polynomial extrapolation". On top of this is a multistep process using Adams and Gear methods (depending on internally detected stiffness) adapting in response to internal error checking should performance of Extrapolation fail.

Series used during calculation were found in §3.8, both were implemented at order

80. The required order was tested over a wide range and although it appeared that the order could be reduced to less than 80 doing so produced no significant increase in calculations and so was implemented without change. Initial value points were tested for balance between effect on final results and calculation time. Noting that we set $x = r - r_h$ and $s = 1/r$ we found that $x = 10^{-4}$ and $s = 1/50$ produced results that could not be improved for our chosen number of significant figures and did not perceptibly prolong the calculation.

In order to monitor accuracy for our mode results we require test solutions for our proposed computer method. For this we note that choosing $m = 0$, $\omega = 0$ and $d = 4$ (i.e. $R = 0$) transforms the radial equation (3.8.1) into a form of the Legendre ODE so

$$\begin{aligned} p_{0l}(x) &= P_l(2x+1) \\ q_{0l}(x) &= Q_l(2x+1). \end{aligned} \tag{3.10.1}$$

Hence p_{0l} is the Legendre function of the first kind and q_{0l} is the Legendre function of the second kind. Both of these Legendre functions can be calculated to a high degree of accuracy and compared with the numerical solutions of our ODE for these parameter values. After making adjustments to the parameters in the Mathematica calculations we found an agreement of $28 \to 70$ significant figures. However during this comparison we noted that the second line in (3.10.1) requires a minor adjustment due to a scale factor and that for some function $h(l)$

$$Q_l(2x+1) = h(l) \times q_{0l}(x). \tag{3.10.2}$$

As $h(l)$ is a constant for each calculation it will simply be absorbed into our normalisation factor $C_{\omega l}$ along with any other consistent scaling factors not already taken into account.

A second feature seen during our comparisons was that the accuracy remained high near $x = 0$ and $x = 10$ but became less accurate around the midpoint. This occurred

when numerically solving across the whole of r or s and its cause could not be found. A grid solution was suggested [11] in which our region was split into a large number of sub-regions (in this case a hundred). We perform our numerical integration from a starting point to the end of the first sub-region and then use our calculated value for this end point as our initial value for the next sub-region. This is simply repeated until the entire region has been spanned. Comparison of this technique to the original showed no change in maximum accuracy but there was a significant increase in accuracy in the previously troubling middle region.

As a secondary check on our method and to test varying the value of d we note that for $m = 0$, $\omega = 0$ but with $d = 5$ (still $R = 0$)

$$\begin{aligned} p_{0l}(x) &= P_l(x) \\ q_{0l}(x) &\propto Q_l(x). \end{aligned} \tag{3.10.3}$$

Applying our comparison method again shows no difference in accuracy but gives confidence our program works well for changes in d.

In another check to verify the accuracy of our modes for any value of d we turn to the normalisation constant in the Wronskian (2.8.3). We take the produced modes and calculate $C_{\omega l}$ for every point on our integration grid to see if it remains constant. In all dimensions $C_{\omega l}$ remains constant to 26 significant figures, where the drop below 30 significant figures only occurs for $d > 6$ and large ω and l. This provides strong support for the accuracy of our results.

3.11 Results for $\langle\phi^2\rangle_{\text{analytic}}$

Using the parameters from §3.9 we can rewrite (3.4.8) as

$$\begin{aligned}\langle\phi^2\rangle_{\text{analytic}} &= \frac{\kappa^2}{48\pi^2 f} - \frac{1}{192\pi^2 f}\left(\frac{df}{dr}\right)^2 + \frac{1}{96\pi^2}\frac{d^2f}{dr^2} + \frac{1}{48\pi^2 r}\frac{df}{dr} \\ &= \frac{(d-3)}{192\pi^2 f}\left((8-2d)\left(\frac{1}{r}\right)^{d-1} + (d-5)\left(\frac{1}{r}\right)^{2d-4} + d - 3\right) \end{aligned} \tag{3.11.1}$$

where we used equation (2.7.2) to find the value of κ.

Having lost the logarithmic term in our expression (3.4.8), due to our choice of field mass and coupling, our new function (3.11.1) can be plotted immediately for the dimensional values we wish to study (see Fig. 3.2). In this figure our results have only been plotted out to $r = 4$ as it is already clear that in all cases they exhibit rapid asymptotic behaviour to finite, non-zero values as r tends to infinity. These asymptotic values are easily read off from (3.11.1) for the dimensions in which we are interested, in units for which $r_h = 1$:

$$\begin{aligned} \langle\phi^2\rangle^{(d=4)}_{\text{analytic}} &= \frac{1}{192\pi^2} & \langle\phi^2\rangle^{(d=5)}_{\text{analytic}} &= \frac{1}{48\pi^2} \\ \langle\phi^2\rangle^{(d=6)}_{\text{analytic}} &= \frac{3}{64\pi^2} & \langle\phi^2\rangle^{(d=7)}_{\text{analytic}} &= \frac{1}{12\pi^2} \\ \langle\phi^2\rangle^{(d=8)}_{\text{analytic}} &= \frac{25}{192\pi^2} & \langle\phi^2\rangle^{(d=9)}_{\text{analytic}} &= \frac{3}{16\pi^2} \\ \langle\phi^2\rangle^{(d=10)}_{\text{analytic}} &= \frac{49}{64\pi^2} & \langle\phi^2\rangle^{(d=11)}_{\text{analytic}} &= \frac{1}{3\pi^2} \end{aligned} \tag{3.11.2}$$

from the general form

$$\lim_{r\to\infty}\langle\phi^2\rangle_{\text{analytic}} = \frac{(d-3)^2}{192\pi^2}. \tag{3.11.3}$$

We see in Fig. 3.2 that the different dimensional cases do not act similarly near the horizon. A close up view of this region for the $d = 4 \to 8$ cases (see Fig. 3.3) shows the

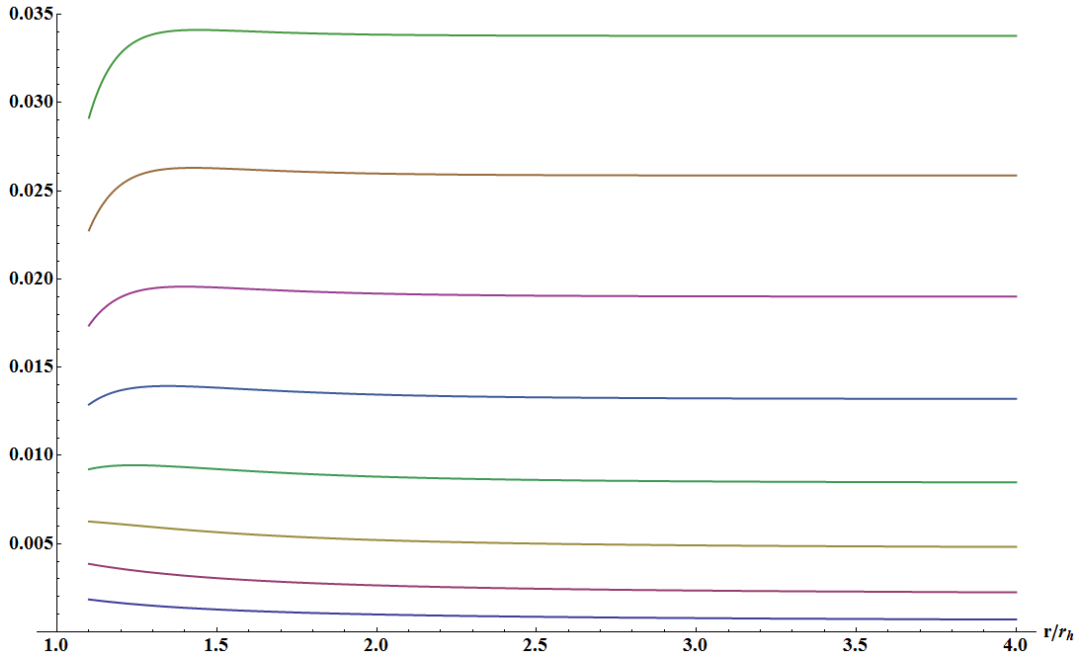

Figure 3.2: $\langle\phi^2\rangle_{\text{analytic}}$ from $r = r_h$ to $r = 4r_h$, the plots from bottom to top at $r = r_h$ run from $d = 4$ to $d = 11$ respectively.

key shift in behaviour as the number of bulk dimensions changes. As first mentioned in §2.3 the post Wick rotation manifold has no interior to the event horizon but the simple analytic form of (3.11.1) allows for a natural extension across the horizon where it is clearly regular. Although mathematically allowed we cannot draw too much from what we see in this pseudo-interior as its validity is questionable. Further, even if we accepted the form of $\langle\phi^2\rangle_{\text{analytic}}$ as valid inside the horizon we cannot state how close to the singularity this form holds due to the break down of quantum field theory in curved space as we approach the quantum gravity regime. However the behaviour of (3.11.1) just inside the horizon does inform us about its nature in this region.

For $d = 4$ and $d = 5$ we see in Fig. 3.3 that $\langle\phi^2\rangle_{\text{analytic}}$ is monotonically increasing into the black hole, seemingly tending to positive infinity at the singularity. At $d = 6$ we see a maximum occur on the horizon (verifiable from (3.11.1)), following which the function monotonically decreases tending to negative infinity at the singularity. As we increase the

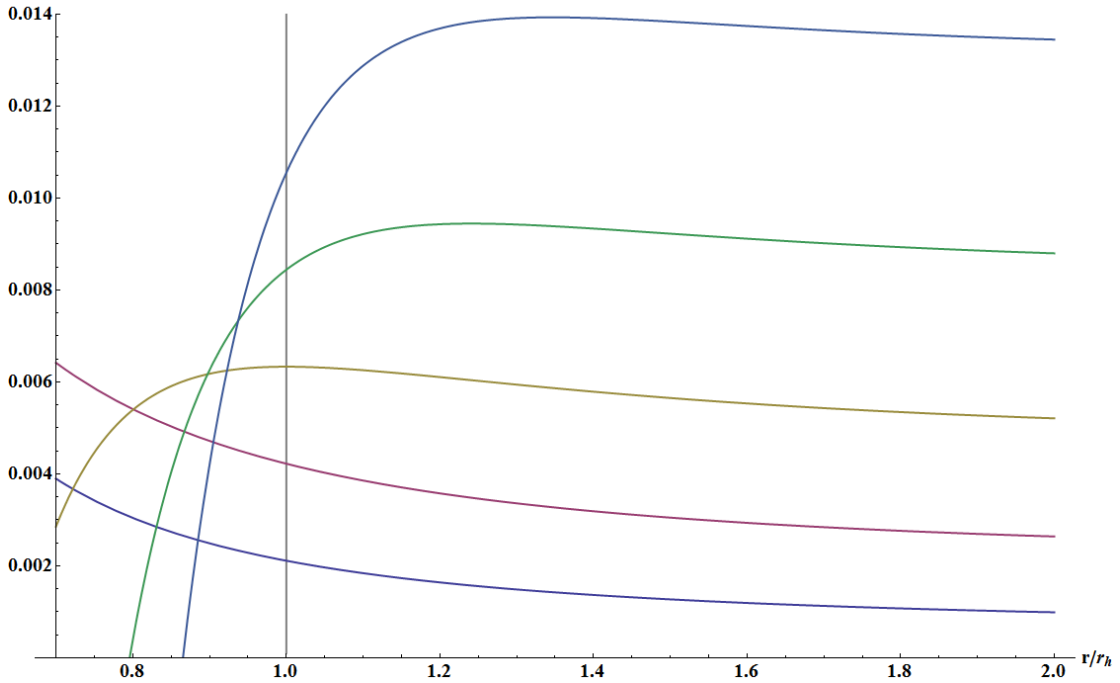

Figure 3.3: $\langle\phi^2\rangle_{\text{analytic}}$ from just inside the horizon to $r = 2r_h$, the plots from bottom to top run from $d = 4$ to $d = 8$ respectively and the vertical line marks the horizon.

number of dimensions past six $\langle\phi^2\rangle_{\text{analytic}}$ achieves a maximum that is slightly further out from the horizon for each increase in d and displays a corresponding increasingly faster descent to negative infinity. However from inspection of (3.11.1) it can be seen that its value crossing the horizon will always remain positive and increases by a constant step between each value of d:

$$\begin{aligned}
\langle\phi^2\rangle^{(d=4)}_{\text{analytic}} &= \frac{1}{48\pi^2} & \langle\phi^2\rangle^{(d=5)}_{\text{analytic}} &= \frac{1}{24\pi^2} \\
\langle\phi^2\rangle^{(d=6)}_{\text{analytic}} &= \frac{1}{16\pi^2} & \langle\phi^2\rangle^{(d=7)}_{\text{analytic}} &= \frac{1}{12\pi^2} \\
\langle\phi^2\rangle^{(d=8)}_{\text{analytic}} &= \frac{5}{48\pi^2} & \langle\phi^2\rangle^{(d=9)}_{\text{analytic}} &= \frac{1}{8\pi^2} \\
\langle\phi^2\rangle^{(d=10)}_{\text{analytic}} &= \frac{7}{48\pi^2} & \langle\phi^2\rangle^{(d=11)}_{\text{analytic}} &= \frac{1}{6\pi^2}
\end{aligned} \tag{3.11.4}$$

from the general form

$$\lim_{r\to r_h}\langle\phi^2\rangle_{\text{analytic}} = \frac{d-3}{48\pi^2}. \tag{3.11.5}$$

We note that this change in behaviour at $d = 6$ coincides with two shifts in properties in our original equations: the Ricci scalar (3.1.3) is non-zero for $d \geq 6$ and our radial equation (3.8.1) for $\omega = 0$ can no longer be modified to become the Legendre differential equation.

3.12 Results for $\langle\phi^2\rangle_{\text{numeric}}$

In Fig. 3.6 we present $\langle\phi^2\rangle_{\text{numeric}}$ obtained from equation (3.7.53) where the final mode sums were performed for $n = 0 \to 8$ and $l = 0 \to 50$. The results for $d > 4$ are original calculations. However we must first check the convergence inside these results occur as expected.

Although we know that the mode sums in (3.7.53), lines one and three, are finite by construction it is important that we check we get such a result from our calculations. Further we must be confident that we have summed over enough values of l and n to achieve our desired level of accuracy. We show in Fig. (3.4) and Fig. (3.5) a simple demonstration that we have achieved a desired level of accuracy in the mode sums. We have removed from the plots the point closest to the horizon that demonstrated numerical error due to the WKB terms. In Fig. (3.4) we show the modes, having been summed to $l = 50$, for only $n = 1$, summing over $n = 1 \to 3$ and summing over $n = 1 \to 8$. The plots are presented with thick lines for a clearer image but even with finer lines it is impossible to distinguish between the sums over $n = 1 \to 3$ and over $n = 1 \to 8$ by sight. In Fig. (3.5) we show plots of the absolute difference between successive partial sums over the modes. The plot with the largest values shows the mode sum for $n = 1 \to 5$ minus the sum over $n = 1 \to 4$, the next largest plot shows $n = 1 \to 6$ minus $n = 1 \to 5$, the

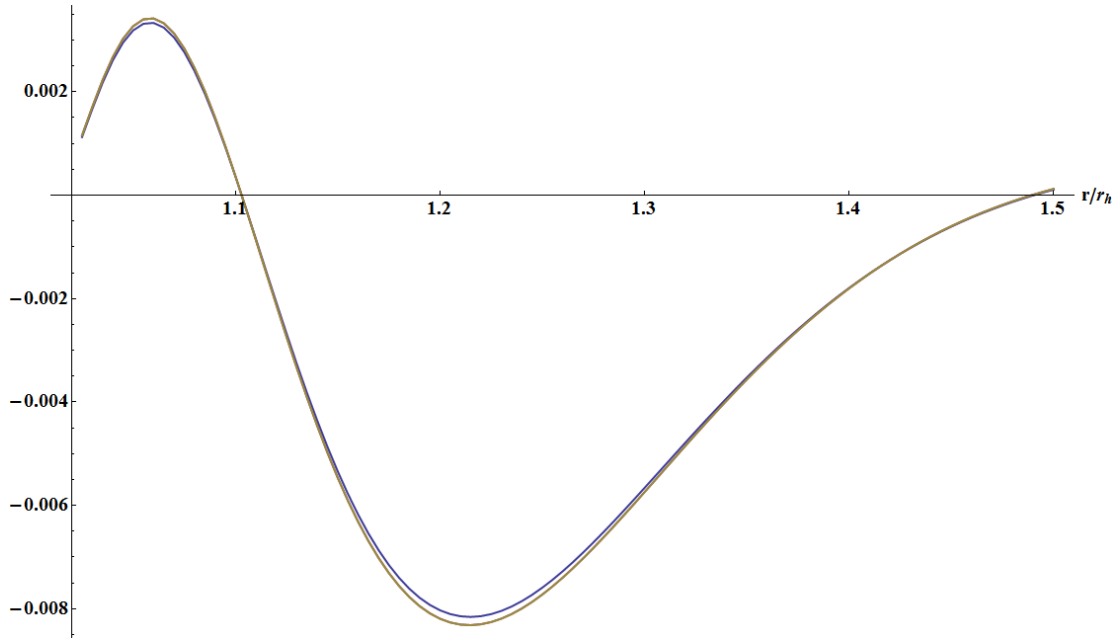

Figure 3.4: The mode sums from $\langle\phi^2\rangle_{\text{numeric}}$ with the l sum completed from $r \sim r_h$ to $r = \frac{3}{2}r_h$, the smaller plot is only $n = 1$, the larger plot is the sum over the modes from $n = 1 \to 8$, a plot summing over $n = 1 \to 3$ is obscured by the previous plot.

next $n = 1 \to 7$ minus $n = 1 \to 6$ and the smallest plot, $n = 1 \to 8$ minus $n = 1 \to 7$. Even with some numeric error near the horizon Fig. (3.5) strongly implies the absolute difference in successive partial sums goes to zero. Together Fig. (3.4) and Fig. (3.5) provide some evidence we have achieved a level of desired accuracy with our values of n and l.

A more analytic look can be taken by examining the summands within equation (3.7.53). Working from investigations into the WKB terms in §2.11, §3.5, §3.6 and [75] we

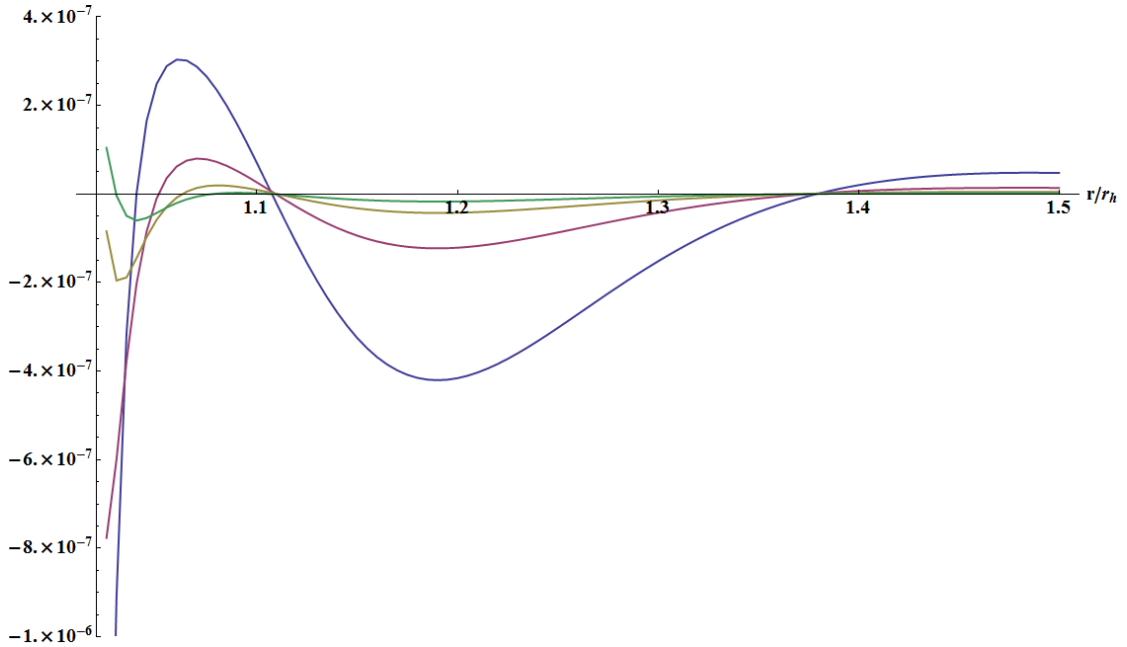

Figure 3.5: The absolute difference between partial mode sums from $\langle\phi^2\rangle_{\text{numeric}}$, the largest plot is the sum over $n = 1 \to 5$ minus the sum over $n = 1 \to 4$, the next largest plot is for $n = 1 \to 6$ minus $n = 1 \to 5$ until the smallest plot is for $n = 1 \to 8$ minus $n = 1 \to 7$.

may state

$$\begin{aligned}
\beta_{0\omega l} &\sim O(\chi^{-1}) \sim O(n^{-1}) \\
\beta_{1\omega l} &\sim O(\chi^{-3}) \sim O(n^{-3}) \\
&\vdots \\
\beta_{k\omega l} &\sim O(\chi^{-(2k+1)}) \sim O(n^{-(2k+1)})
\end{aligned} \tag{3.12.1}$$

which in turn allows us to state

$$\begin{aligned}
\sum_{l=0}^{\infty}(2l+1)\beta_{0\omega l} &\sim O(n) \\
&\vdots \\
\sum_{l=0}^{\infty}(2l+1)\beta_{k\omega l} &\sim O(n^{-2k+1}).
\end{aligned} \tag{3.12.2}$$

Using the above we schematically construct (only the orders are relevant to this investigation) a mode sum over several WKB terms as follows

$$\sum_{n=1}^{\infty}\sum_{l=0}^{\infty}(2l+1)\left[C_{\omega l}p_{\omega l}q_{\omega l}-\sum_{i=0}^{k}\beta_{i\omega l}\right]=\sum_{n=1}^{\infty}\sum_{l=0}^{\infty}(2l+1)O(\chi^{-(2k+3)})$$
$$=\sum_{n=1}^{\infty}O(n^{-(2k+1)}). \tag{3.12.3}$$

So for our work, where we have used WKB terms up to and including $\beta_{3\omega l}$, we expect the sum over n to be $O(n^{-7})$.

In Appendix E we display results for a check on the order of convergence for our data. This has been carried out for $d = 4$ where we are very confident of our data, $d = 6$ where the Ricci scalar first becomes non-zero and for $d = 11$ where our numerical results were harder to produce accurately. The check was carried out from the point closest to the event horizon out to near the end of our domain to see if any problem with the WKB terms could be seen and to confirm consistency of convergence across the domain. Each check compares our data to the expected order shown above, $O(n^{-7})$. It is clear that there is some level of deviation from the expected order in all three dimensional cases (unsurprisingly $d = 11$ has the worst results). This is especially true at either ends of the domain with much less deviation from the expected values near the centre of the domain. However all these deviations are small scale and for every instance of the order seeming to be slightly worse than expected there is one or more case where the order of summation is in fact better.

Before discussing the features of $\langle\phi^2\rangle_{\text{numeric}}$ we present in Fig. 3.7 a close up of the numeric results, as functions of both number of dimensions and radius, in order to display detail missing from Fig. 3.6.

As is readily apparent from both Figures 3.6 and 3.7 the numeric component begins in $d = 4$ as a small positive contribution to $\langle\phi^2\rangle_{\text{ren}}$ but as d increases $\langle\phi^2\rangle_{\text{numeric}}$ becomes

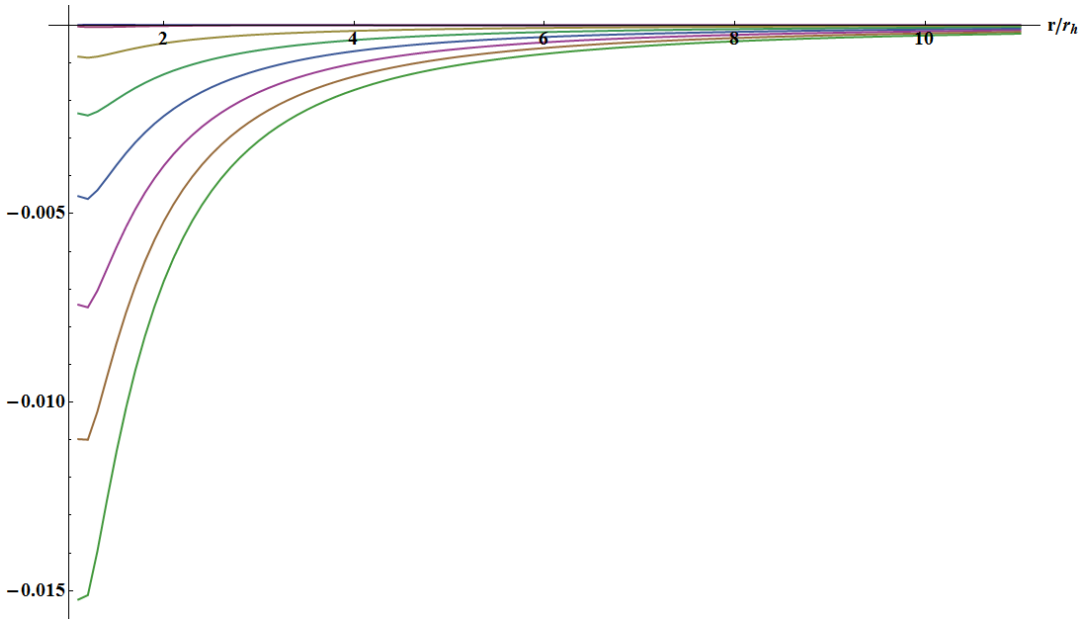

Figure 3.6: $\langle\phi^2\rangle_{\text{numeric}}$ from $r = r_h$ to $r = 11r_h$, the plots from top to bottom run from $d = 4$ to $d = 11$ respectively.

an increasingly negative contribution. However it is also clear that we lose detail in the region close to the horizon, visible flicks are evident as we do not have enough calculated points to retain smoothness. The worrisome issue is that we cannot tell if this means $\langle\phi^2\rangle_{\text{numeric}}$ diverges at the horizon for some, or all, of our values of d. We anticipate that $\langle\phi^2\rangle_{\text{numeric}}$ is finite on the horizon but we must keep in mind that the WKB approximation breaks down in this region so divergences may not be correctly cancelling. This issue will be investigated in §3.14.

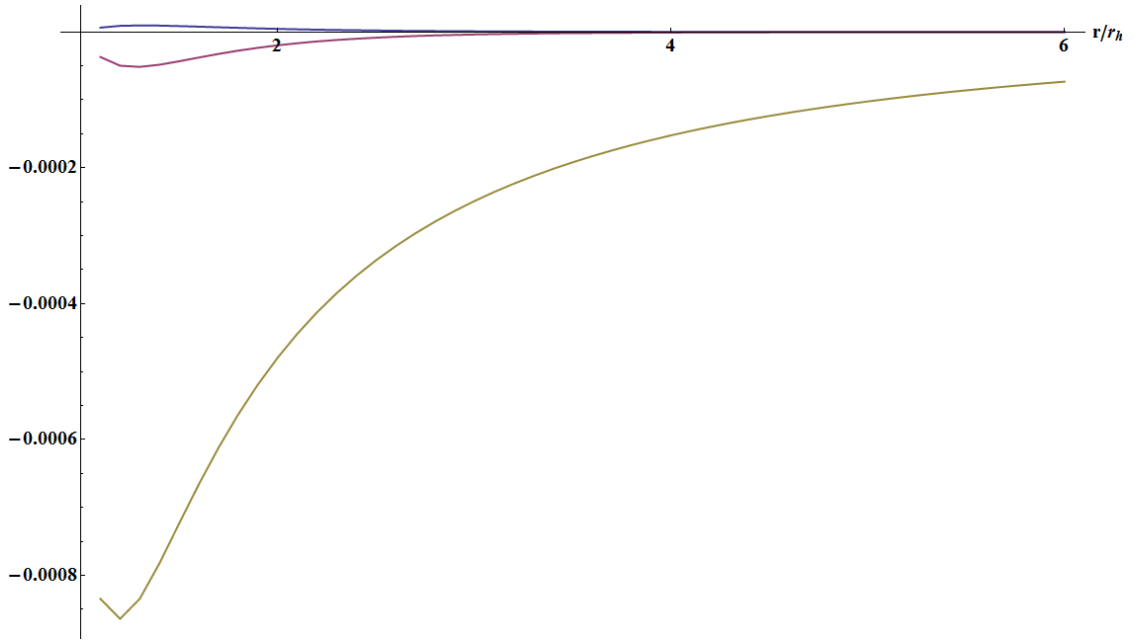

Figure 3.7: $\langle\phi^2\rangle_{\rm numeric}$ from $r = r_h$ to $r = 6r_h$ from the singularity, the plots from top to bottom run from $d = 4$ to $d = 6$ respectively.

3.13 Results for $\langle\phi^2\rangle_{\rm ren}$

It can be seen by comparing Figures 3.2 and 3.6 that $\langle\phi^2\rangle_{\rm numeric}$ makes a much smaller contribution to $\langle\phi^2\rangle_{\rm ren}$ than $\langle\phi^2\rangle_{\rm analytic}$. This is true across out whole domain for $d = 4$ and $d = 5$ and remains so for $d > 5$ away from the horizon. We show in Fig. 3.8 the values of $\langle\phi^2\rangle_{\rm analytic}$ for $r = 1.1 \to 11$ and $d = 4 \to 11$. We then, immediately following, present $\langle\phi^2\rangle_{\rm ren}$ in Fig. 3.9 over the same range of values (the full range over which numerics were calculated). This is to allow direct comparison to be made between $\langle\phi^2\rangle_{\rm analytic}$ pre- and post- adjustment by $\langle\phi^2\rangle_{\rm numeric}$.

Of interest while comparing Figures 3.8 and 3.9 is the $d = 4$ case, the Schwarschild metric. The values of $\langle\phi^2\rangle_{\rm ren}$ and $\langle\phi^2\rangle_{\rm analytic}$ for this case have been calculated previously [17] and provide a final check on our results. Our data matches [17] to a minimum of 6 significant figures for all r, an impressive accuracy when considering the difference in

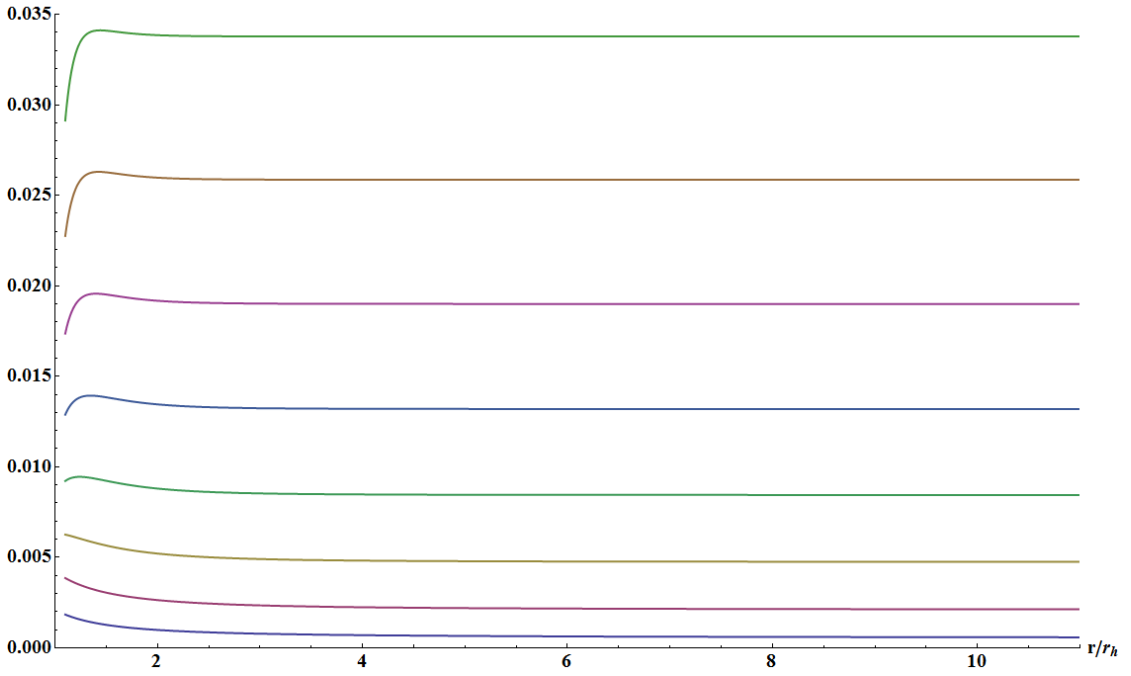

Figure 3.8: $\langle\phi^2\rangle_{\text{analytic}}$ from $r = r_h$ to $r = 11r_h$, the plots from bottom to top run from $d = 4$ to $d = 11$ respectively.

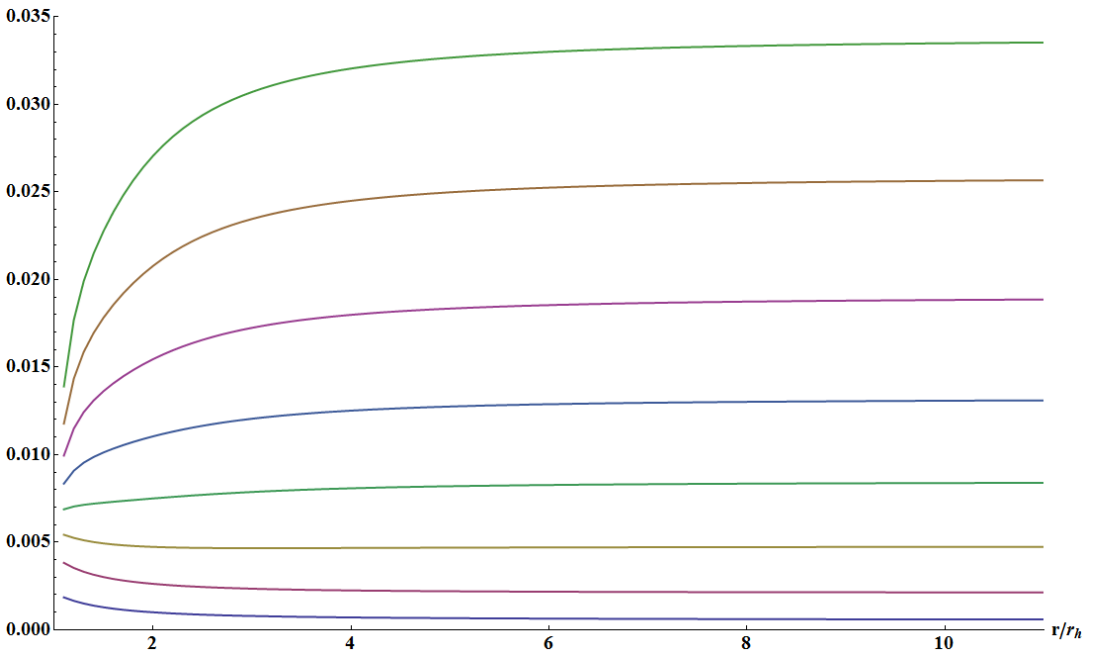

Figure 3.9: $\langle\phi^2\rangle_{\text{ren}}$ from the $r = r_h$ to $r = 11r_h$, the plots from bottom to top run from $d = 4$ to $d = 11$ respectively.

approaches and providing confidence in our original higher dimensional results.

Also of particular interest from the figures is comparing the $d = 4$ case to $d > 4$ on a particular point commented on in [17]. When $\langle\phi^2\rangle_{\rm ren}$ and $\langle\phi^2\rangle_{\rm analytic}$ were first calculated the authors noted that $\langle\phi^2\rangle_{\rm analytic} \sim \langle\phi^2\rangle_{\rm ren}$ as depicted in Fig. 3.10. The implication was that in calculations not requiring greater accuracy the much easier and faster to calculate $\langle\phi^2\rangle_{\rm analytic}$ could be used instead of $\langle\phi^2\rangle_{\rm ren}$. However as can be seen by comparing Figures 3.8 and 3.9 this approximation becomes less accurate as d increases. The table below shows the maximum relative differences (δ_{max}) between $\langle\phi^2\rangle_{\rm analytic}$ and $\langle\phi^2\rangle_{\rm ren}$ over the hundred points for which we have numerical data:

$$
\begin{aligned}
&d = 4,\ \delta_{max} \simeq 0.69\% && d = 5,\ \delta_{max} \simeq 1.5\% \\
&d = 6,\ \delta_{max} \simeq 14\% && d = 7,\ \delta_{max} \simeq 25\% \\
&d = 8,\ \delta_{max} \simeq 35\% && d = 9,\ \delta_{max} \simeq 42\% \\
&d = 10,\ \delta_{max} \simeq 48\% && d = 11,\ \delta_{max} \simeq 52\%.
\end{aligned}
\tag{3.13.1}
$$

It is clear that for $d = 4, 5$ $\langle\phi^2\rangle_{\rm analytic}$ is a good approximation to $\langle\phi^2\rangle_{\rm ren}$ but the maximum relative difference jumps for $d = 5 \to 6$. Note that this coincides with the Ricci scalar becoming non-zero and matches the changing behaviour of $\langle\phi^2\rangle_{\rm analytic}$ at $d = 6$ from §3.11.

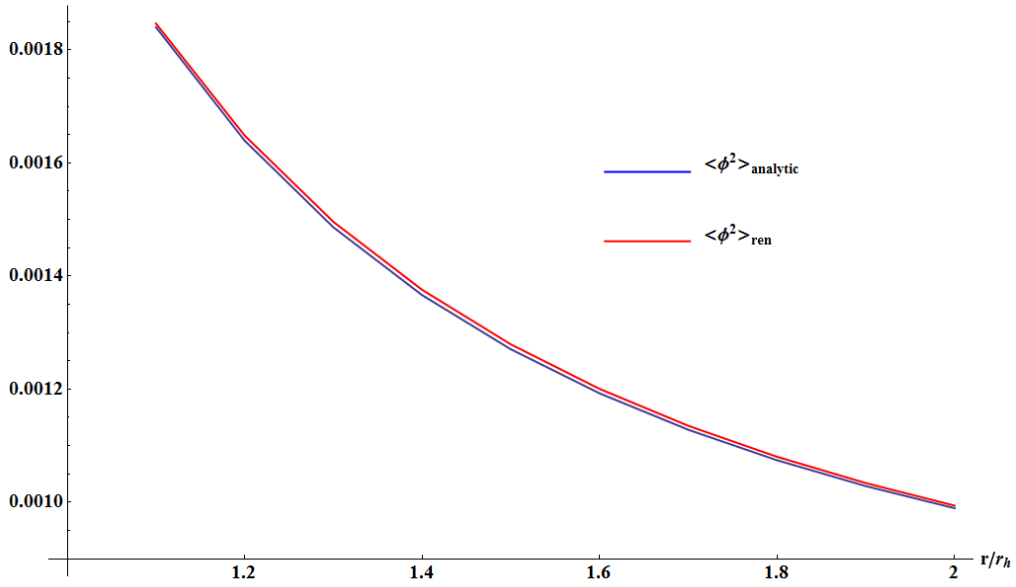

Figure 3.10: A close look at the region of greatest difference between $\langle\phi^2\rangle_{\text{analytic}}$ and $\langle\phi^2\rangle_{\text{ren}}$ for $d = 4$.

3.14 $\langle\phi^2\rangle_{\text{ren}}$ Near the Horizon

Inspecting the data presented in Fig. 3.6 to Fig. 3.9 we see that we have lost detail in the most active region of $\langle\phi^2\rangle_{\text{ren}}$, $r_h < r < 2r_h$. Secondly we are aware of the potential failure of the WKB approximation close to the horizon and so this missing detail could hide problems in our results.

It was decided that the calculation would be run again for $r = 1.05 \to 1.5$, although there is interesting activity extending beyond $r = 1.5$ the results demonstrate no loss of detail in this outer region. Such a calculation expectedly proved more challenging as in this region the terms that diverge at the horizon, like the $n = 0$ modes, provide much larger contributions that need to be cancelled. Further the numerical ODE solver used to calculate the modes required much better fine tuning to achieve reasonable accuracy versus time required. Although the data processing took longer than for the larger radial

region the experience gained calculating in that region helped keep overall computing time required down.

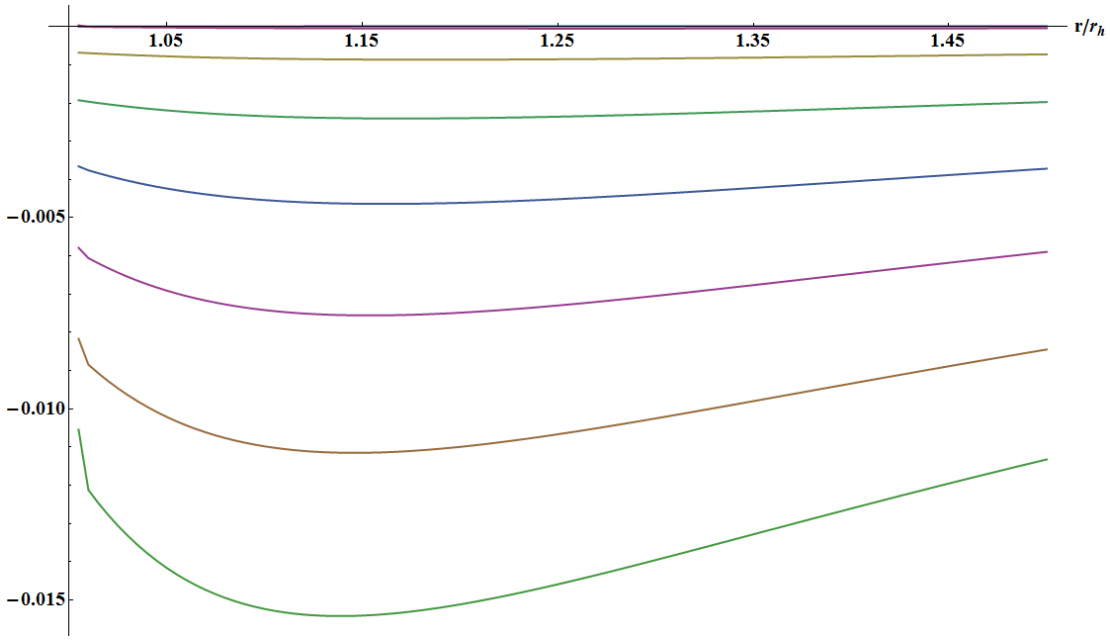

Figure 3.11: $\langle\phi^2\rangle_{\rm numeric}$ from $r = r_h$ to $r = \frac{3}{2}r_h$, the plots from top to bottom run from $d = 4$ to $d = 11$ respectively.

There is no need to show a close up of $\langle\phi^2\rangle_{\rm analytic}$ as this demonstrates no new features that cannot be seen in the exterior region of Fig. 3.3. In Fig. 3.11 we show $\langle\phi^2\rangle_{\rm numeric}$ in our new region. It is now clear that close to the horizon $\langle\phi^2\rangle_{\rm numeric}$ is finite (if not tending to zero for low values of d) for our range of dimensions. Again we see a lack of smoothness in the nearest few points but we have enough information here to not need to look at an even closer region. Further we must remember that with every step closer to the horizon the WKB terms could be distorting our result.

In Fig. 3.12 we show $\langle\phi^2\rangle_{\rm ren}$ in our close up region. Here we can see more detail but only one new feature of relevance. There is a strong indication that there is a maximum on-horizon value with respect to dimension as the higher dimensional values of $\langle\phi^2\rangle_{\rm ren}$ rapidly fall under the influence of $\langle\phi^2\rangle_{\rm numeric}$. This is in contrast to our results on the

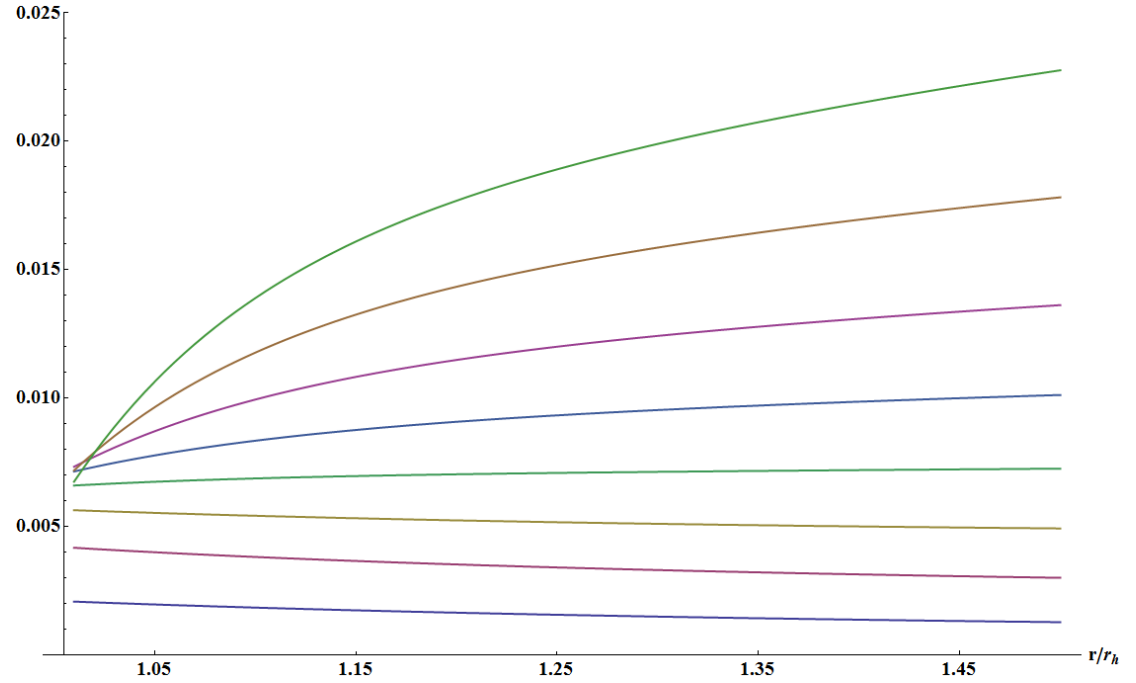

Figure 3.12: $\langle\phi^2\rangle_{\text{ren}}$ from $r = r_h$ to $r = \frac{3}{2}r_h$, the plots from bottom to top run from $d = 4$ to $d = 11$ respectively.

larger region where $\langle\phi^2\rangle_{\text{analytic}}$ on the horizon increases linearly with respect to dimension and $\langle\phi^2\rangle_{\text{numeric}}$ appeared to be a simple adjustment. The behaviour on the horizon is discussed in the next section.

3.15 $\langle\phi^2\rangle_{\text{ren}}$ on the Horizon

In order to investigate the behaviour of $\langle\phi^2\rangle_{\text{ren}}$ on the horizon we collaborated with Cormac Breen who co-authored a paper [12] calculating $\langle\phi^2\rangle_{\text{ren}}$ on the horizon of a lukewarm black hole. As stated previously our WKB approximation cannot be used on the horizon however in [12] Breen and Ottewill developed an alternative approach making use of extended Green-Liouville asymptotics that can be applied there. Making use of the same software that had been used in [12] Breen was able to give us values of $\langle\phi^2\rangle_{\text{ren}}$ on the event horizon for our range of bulk dimensions.

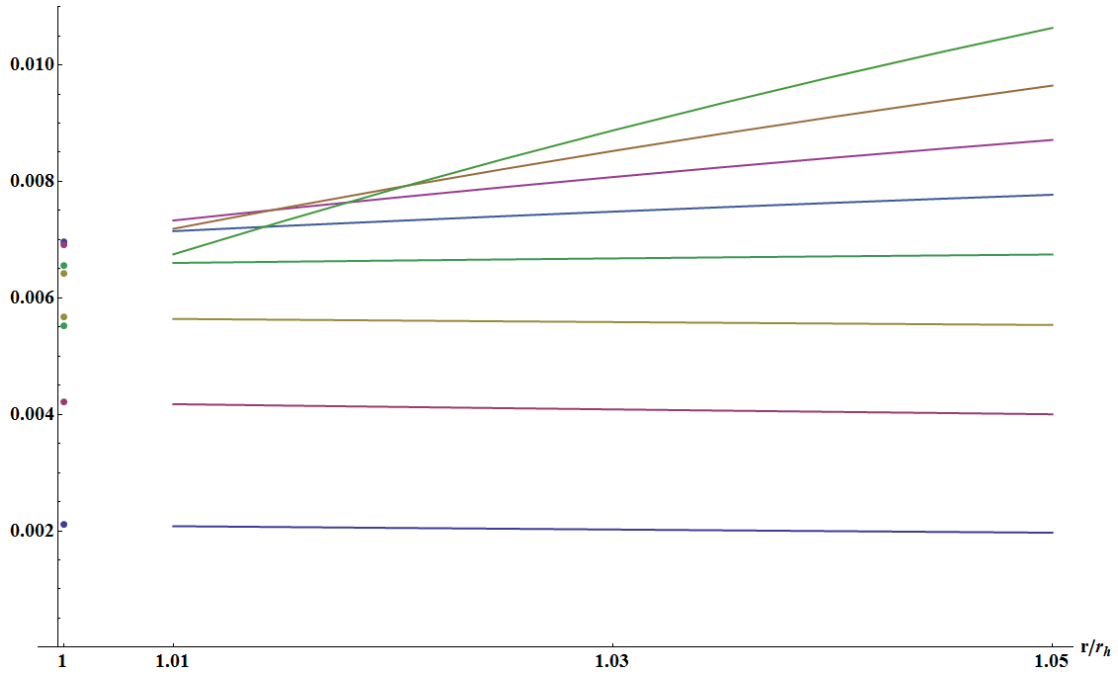

Figure 3.13: $\langle\phi^2\rangle_{\text{ren}}$ on the horizon and for $r/r_h = 1.01 \to 1.05$. Looking at the far right the plots from bottom to top run from $d = 4$ to $d = 11$ respectively and the on horizon points match the dimensionally differentiated colours.

In Fig. 3.13 we display our calculated values for $\langle\phi^2\rangle_{\rm ren}$ for the region $r = 1.01 \to 1.05$, this ignores the point we calculated closest to the horizon as these points suffer from numerical error due to the WKB terms. We also display in Fig. 3.13 the on horizon values provided by Breen, note that the vertical axis has been pulled slightly back from $r = r_h$ to allow a clearer view of the values. It can be seen that for $d = 4 \to 7$ our results match up very well with the horizon but when the value begins to fall for $d > 7$ it lowers much more rapidly on the horizon than our data would suggest. Using a quartic polynomial extrapolation to extend our results to the horizon we can see the relative difference,

$$\delta\langle\phi^2\rangle_{\rm ren} = \frac{\text{(on horizon result)} - \text{(extrapolation result)}}{\text{(on horizon result)}}, \tag{3.15.1}$$

between the accurate on-horizon and the extrapolation from our results:

d	$\delta\langle\phi^2\rangle_{\rm ren}$
4	0.015
5	0.011
6	0.005
7	-0.007
8	-0.029
9	-0.066
10	-0.133
11	-0.251

Higher order polynomials used to extend our results to the horizon only affect $\delta\langle\phi^2\rangle_{\rm ren}$ beyond three decimal places.

To investigate this trend we try a new extrapolation that best fits to the on-horizon results against dimension from our data and see what features can be found. We can see from the interaction of $\langle\phi^2\rangle_{\rm numeric}$ and $\langle\phi^2\rangle_{\rm analytic}$ that the on-horizon total must continue to fall rapidly. Also we are not interested in values for $d < 4$. We choose a quartic

polynomial as the best fit from tests ran, higher order polynomials matching our data are problematic extrapolating for $d > 11$ due to the potentially large number of turning points in the output. The best fit quartic polynomial is

$$\langle\phi^2\rangle_{\text{horizon}} = -0.01561 + 0.006871d - 0.0007473d^2 + 3.840 \times 10^{-5}d^3 - 1.035 \times 10^{-6}d^4. \tag{3.15.2}$$

This function for $d = 4 \to 11$ compared to our data has a relative error with mean $\mu = -1.5 \times 10^{-5}$ and standard deviation $\sigma = 4.8 \times 10^{-4}$. From equation (3.15.2) we see $\langle\phi^2\rangle_{\text{horizon}}$ achieves a maximum at $d = 5.38$ and equals zero at $d = 13.91$ (for $d > 3$). Comparing these results to order six and eight order polynomials, which should be accurate this close to the data, we see an agreement on the maximum at $d = 5.38$ so this result has little physical relevance as d must be an integer. Looking for the value of d that gives $\langle\phi^2\rangle_{\text{horizon}} = 0$ shows a value that lies close to $d = 14$. During testing with non-quartic polynomials $\langle\phi^2\rangle_{\text{horizon}} = 0$ occurred close and on either side $d = 14$ indicating that this may be the value for which there is no vacuum polarisation on the horizon. However we may state with confidence from the information gathered in these brane results §3.11-3.14 that $\langle\phi^2\rangle_{\text{horizon}} \to -\infty$ as $d \to \infty$.

3.16 Summary

In this chapter we have extended previously developed methods to calculate $\langle\phi^2\rangle_{\text{ren}}$ in $d = 4$ to the case of a $d = 4$ brane in a bulk of $d = 5 \to 11$ dimensions. We have then produced results for $\langle\phi^2\rangle_{\text{ren}}$ from numerical solutions accurate to over twenty significant figures (up to the validity of our approximations as in previous works) on two radial domains; $r = 1.1 \to 11$ and $r = 1.005 \to 1.5$. These results are valid for a bulk of $d = 4 \to 11$ (the $d = 4$ calculation is to check whether our results match those of previous works). We demonstrated that, unlike in the $d = 4$ form of our metric, the analytic

contributions to $\langle\phi^2\rangle_{\text{ren}}$ are no longer a good approximation to the whole value of $\langle\phi^2\rangle_{\text{ren}}$ and in fact become worse as d increases. Finally in collaboration with Cormac Breen we performed a check on our results near the horizon by comparing them to his results on the horizon and found only a small, expected discrepancy caused by the WKB approximation breaking down near the horizon.

In order to produce these results we had to find several analytic expressions and perform multiple numerical calculations. Using our choice of temporal point splitting we have derived a Green's function from which $\langle\phi^2\rangle_{\text{ren}}$ can be calculated. We have derived the WKB approximation terms for $d = 4 \rightarrow 11$. We used these WKB terms to establish the numeric contribution to $\langle\phi^2\rangle_{\text{ren}}$. We used Mathematica to twice produce over four hundred field mode values at one hundred radial points at accuracies of over twenty eight significant figures. This involved reworking the radial ODE to determine values regular at infinity, this was due to the numeric solutions of the original ODE breaking down for $d > 4$. Using these accurate mode values we were able to determine the numeric contribution to $\langle\phi^2\rangle_{\text{ren}}$ which involved applying the Watson-Sommerfeld formula and finding numerical integrals. We applied previously established methods to perform these numerical integrals and introduced a new method that became required as d increased.

In the next chapter we demonstrate how to transfer the methodology for the calculation of $\langle\phi^2\rangle$ from the brane into the bulk.

Chapter 4

$\langle\phi^2\rangle$ in the Bulk in 5d

In this chapter we will specialise our earlier general set up for the $d = 5$ bulk in which we will calculate the vacuum polarisation. Following §2.12 we will then layout equations from chapter 2 as relevant to this number of dimensions in what will hopefully be the most useful form. Once calculation parameters have been set we will go through the choices of calculation method that have been investigated in this research. This will include previous methodologies extended to $d = 5$ with discussion of why they fail in this case. We then present our new methodologies and their potential for success before describing our original approach that proved most appropriate to this calculation. Finally we present original results along with interpretation and comparison to previous works.

4.1 The Metric for the 5d Bulk

The bulk is our whole manifold and so is described simply, it is not warped, has zero cosmological constant and, as mentioned in §1, we assume our black hole to be small enough that we may ignore compactification. As there are no restrictions on the bulk it has retained full hyperspherical symmetry allowing us to immediately present some initial

geometric objects such as the metric from (2.3.16):

$$\begin{aligned} ds^2 &= f dt^2 + f^{-1} dr^2 + r^2 d\Omega_3^2 \\ &= f dt^2 + f^{-1} dr^2 + r^2 \left(d\theta_2^2 + \sin^2(\theta_2) d\theta_1^2 + \sin^2(\theta_2) \sin^2(\theta_1) d\varphi^2 \right). \end{aligned} \tag{4.1.1}$$

The Ricci tensor is given by

$$R_{ab} = \begin{pmatrix} -\frac{fA(r)}{2r} & 0 & 0 & 0 & 0 \\ 0 & -\frac{A(r)}{2rf} & 0 & 0 & 0 \\ 0 & 0 & B(r) & 0 & 0 \\ 0 & 0 & 0 & -\sin^2(\theta_2) B(r) & 0 \\ 0 & 0 & 0 & 0 & -\sin^2(\theta_2) \sin^2(\theta_1) B(r) \end{pmatrix} \tag{4.1.2}$$

where

$$\begin{aligned} A(r) &= r f'' + 3 f' \\ B(r) &= r f' + 2 f - 2 \end{aligned}$$

and the Ricci scalar is

$$R = \frac{6 - 6f - 6 r f' - r^2 f''}{r^2}. \tag{4.1.3}$$

The metric function for $d = 5$ is

$$f(r) = 1 - \left(\frac{r_h}{r} \right)^2 \tag{4.1.4}$$

such that

$$\begin{aligned} R_{ab} &= \underline{\mathbf{0}} \\ R &= 0 \end{aligned} \tag{4.1.5}$$

. The metric determinant is

$$g^{\frac{1}{2}} = r^3 \sin(\theta_1)\sin^2(\theta_2). \tag{4.1.6}$$

As expected these quantities show that the spacetime is Ricci flat which will greatly simplify later geometric work.

4.2 Mode Sums in the 5d Bulk

We choose for now to move forward using the brane methodology as an example, see §3.2, so we choose temporal point splitting and look at a mode sum of the form in equation (2.8.13). Here the term $\cos(\gamma)$ has already been set to one hence we turn to the other quantities. The Gegenbauer polynomial (2.8.9) for $d = 5$ has upper index $\lambda = 1$ so that

$$G_l^1(1) = U_l(1) = l + 1 \tag{4.2.1}$$

where U_l is the Chebyshev polynomial of the second kind. The degeneracy factor (2.7.9), $\tilde{N}_{l,d}$, takes the form

$$\tilde{N}_{l,5} = \frac{(l+1)^2}{2\pi^2}. \tag{4.2.2}$$

We could use the values of the Gegenbauer polynomial and the degeneracy factor in our mode sum but in anticipation of later work we will leave out their explicit values. To tidy our notation, unless stated explicitly otherwise, we write $G_l = G_l^1(1)$ and $N_l = \tilde{N}_{l,5}$ so that the point-split Euclidean Green's function is

$$G_E(\mathbf{x}, \epsilon; \mathbf{x}, 0) = \frac{\kappa}{2\pi} \sum_{n=-\infty}^{\infty} e^{i\omega\epsilon} \sum_{l=0}^{\infty} N_l G_l C_{\omega l} p_{\omega l}(r) q_{\omega l}(r). \tag{4.2.3}$$

The functions $p(r)$ and $q(r)$ are solutions to the radial ODE (2.8.1) for $d = 5$,

$$\frac{1}{r}\frac{d}{dr}\left[r^3 f \frac{d}{dr} S_{\omega l}\right] - \left(\frac{\omega^2 r^2}{f} + m^2 r^2 + l(l+2)\right) S_{\omega l} = 0, \tag{4.2.4}$$

where we have taken into account the fact that the spacetime is Ricci flat.

4.3 5d Bulk Renormalisation

As on the brane we follow the method laid out in §2.9 to calculate the renormalisation terms but for $d = 5$. In this expansion the dimensional constant (2.9.5) is

$$\alpha_5 = \frac{1}{8\sqrt{2}\pi^2} \tag{4.3.1}$$

and the singular terms (2.9.19) are

$$G^{5\mathrm{d}}_{E,sing} = \frac{1}{16\sqrt{2}\pi^2}\left(\frac{U(x,x')}{\sigma(x,x')^{\frac{3}{2}}}\right). \tag{4.3.2}$$

In order to calculate $U(x,x')$ we require its expansion up to $O(\sigma^{\frac{3}{2}})$ (we must include any finite terms) as discussed in sections 2.9 and 2.10. Hence the required expansion is (dropping the arguments)

$$U = U_0 + U_1\sigma + O(\sigma^2) \tag{4.3.3}$$

with

$$\begin{aligned} U_0 &= u_0 - u_{0a}\sigma^{;a} + \frac{1}{2}u_{0ab}\sigma^{;a}\sigma^{;b} - \frac{1}{6}u_{0abc}\sigma^{;a}\sigma^{;b}\sigma^{;c} + O(\sigma^2) \\ U_1 &= u_1 - u_{1a}\sigma^{;a} + O(\sigma) \end{aligned} \tag{4.3.4}$$

where the order of $\sigma^{;a}$ was determined in §2.10.3.

The next step is to employ the boundary condition given in §2.9 allowing us to imme-

diately read off some of the required terms [23]:

$$\begin{aligned} U_0 = \Delta^{\frac{1}{2}} \Rightarrow u_0 &= 1 \\ u_{0a} &= 0 \\ u_{0ab} &= \frac{1}{6} R_{ab} \\ u_{0abc} &= \frac{1}{4} R_{ab;c}. \end{aligned} \tag{4.3.5}$$

These results can then be used to solve for U_1 in the recursion relation (2.9.14)

$$-U_1 - U_{1;a}\sigma^{;a} + U_1 \Delta^{-\frac{1}{2}} \Delta^{\frac{1}{2}}{}_{;a} \sigma^{;a} + \Box U_0 - (m^2 + \xi R) U_0 = 0, \tag{4.3.6}$$

where we find that

$$\begin{aligned} U_{1;a} &= u_{1;a} - u_{1a} + O(\sigma^{\frac{1}{2}}) \\ \Box U_0 &= \frac{1}{3} R_a{}^{\mu}{}_{;\mu} \sigma^{;a} + \frac{1}{3} R_a{}^{\mu} \sigma^{;a}{}_{;\mu} - \frac{1}{4} R_{(ab;c)} \sigma^{;a} \sigma^{;b}{}_{\mu} \sigma^{;c\mu} + \frac{1}{6} R_{ab}{}^{;\mu} \sigma^{;a} \sigma^{;b}{}_{;\mu} + O(\sigma) \end{aligned} \tag{4.3.7}$$

and an expansion of $\Delta^{-\frac{1}{2}} \Delta^{\frac{1}{2}}{}_{;a} \sigma^{;a}$ in powers of σ,

$$\Delta^{-\frac{1}{2}} \Delta^{\frac{1}{2}}{}_{;a} \sigma^{;a} = \frac{1}{6} R_{ab} \sigma^{;a} \sigma^{;b} + O(\sigma^{\frac{3}{2}}), \tag{4.3.8}$$

is provided by [22].

After several lines of algebra we achieve the results

$$\begin{aligned} U_0 &= 1 + \frac{1}{12} R_{ab} \sigma^{;a} \sigma^{;b} - \frac{1}{24} R_{ab;c} \sigma^{;a} \sigma^{;b} \sigma^{;c} \\ U_1 &= -\left(m^2 + \left(\xi - \frac{1}{6} \right) R \right) + \frac{1}{2} \left(\xi - \frac{1}{6} \right) R_{;a} \sigma^{;a} \end{aligned} \tag{4.3.9}$$

which, making use of the spacetime's Ricci flatness, can be used in (4.3.2) to find the Hadamard singularity

$$G^{\mathrm{5d}}_{E,sing} = \frac{1}{16\sqrt{2}\pi^2} \left(\frac{1 - m^2 \sigma}{\sigma^{\frac{3}{2}}} \right). \tag{4.3.10}$$

Now we wish to find the form of (4.3.10) for temporal point splitting. We refer to §2.10.4 in which we calculated σ for temporal point splitting and see that equations (2.10.28) always hold, irrespective of brane or bulk (though higher orders of ϵ may be needed). In fact σ only depends on the number of dimensions through the metric function, f. This means we can write equation (4.3.10) as

$$\begin{aligned} G^{5\mathrm{d}}_{E,sing} &= \frac{1}{16\sqrt{2}\pi^2}\left[\frac{1}{\sigma^{\frac{3}{2}}} - \frac{m^2}{\sigma^{\frac{1}{2}}}\right] \\ &= \frac{1}{8f^{\frac{3}{2}}\pi^2}\left[\frac{1}{\epsilon^3} + \frac{f'^2}{32\epsilon} - \frac{m^2 f}{2\epsilon} + O(\epsilon)\right]. \end{aligned} \tag{4.3.11}$$

Finally we can bring result (4.3.11) together with equation (4.2.3) to give

$$\begin{aligned} \langle\phi^2\rangle_{\mathrm{ren}} = \lim_{\epsilon\to 0}\Bigg[&\frac{\kappa}{2\pi}\sum_{n=-\infty}^{\infty} e^{i\omega\epsilon}\sum_{l=0}^{\infty} N_l G_l C_{\omega l} p_{\omega l}(r) q_{\omega l}(r) \\ &- \frac{1}{8f^{\frac{3}{2}}\pi^2}\left(\frac{1}{\epsilon^3} + \frac{f'^2}{32\epsilon} - \frac{m^2 f}{2\epsilon}\right)\Bigg] \end{aligned} \tag{4.3.12}$$

This concludes the construction of the renormalisation terms. Dealing with these terms will form a major point of the methodology for the 5d bulk which will be discussed in later sections after we have prepared all relevant terms in the mode sums.

As on the brane the modes $p_{\omega l}$ and $q_{\omega l}$ and the normalisation constant $C_{\omega l}$ are all to be found numerically. As on the brane we will employ the WKB approximation for the modes to help hasten the convergence of the sums and provide analytic terms for analysis.

4.4 Implementation of WKB Terms in the 5d Bulk

Implementation of the WKB approximation occurs as in §3.5 except equations (2.11.8) and (2.11.9) for the 5d bulk become

$$\begin{aligned} \chi_{\omega l}^2 &= \omega^2 r^6 + (l+1)^2 f r^4 \\ \eta &= m^2 f r^6 - f r^4. \end{aligned} \tag{4.4.1}$$

For $d = 5$ we have the expansion

$$\beta_{\omega l}(r) = \sum_{i=0}^{4} \beta_{i\omega l}(r) \tag{4.4.2}$$

where as mentioned in §2.11 we always have

$$\beta_{0\omega l} = \frac{1}{2\chi_{\omega l}}. \tag{4.4.3}$$

We mentioned in §2.11 that we have calculated, using Mathematica, the WKB terms in general for $d = 5$. However their large size makes presentation problematic as even Mathematica has memory issues outputting them to screen. We can state that the $\beta_{i\omega l}$ can be written as

$$\beta_{i\omega l} = \sum_{j=0}^{2i} D_{ij}(r) \frac{n^{2j}}{[\Omega^2 + n^2]^{i+j+1/2}} \tag{4.4.4}$$

where this form of the numerator and denominator will more useful for later analysis of the behaviour of n. The object Ω represents the relevant terms gathered from $\chi_{\omega l}$ which for our curved spacetime is

$$\Omega = \frac{l+1}{r}\sqrt{f}. \tag{4.4.5}$$

The D_{ij} are functions of r but importantly are independent of n. Hence we are guaranteed that $\beta_{0\omega l}$ has no dependence on n in its numerators.

We implement the WKB terms here into equation (4.3.12) simply as

$$\begin{aligned}\langle\phi^2\rangle_{\text{ren}} = \lim_{\epsilon\to 0}\Bigg[&\frac{\kappa}{2\pi}\sum_{n=-\infty}^{\infty} e^{i\omega\epsilon}\sum_{l=0}^{\infty}\left(N_l G_l C_{\omega l} p_{\omega l}(r) q_{\omega l}(r) - \sum_{i=0}^{4}\beta_{i\omega l}(r)\right)\\ &+\frac{\kappa}{2\pi}\sum_{n=-\infty}^{\infty} e^{i\omega\epsilon}\sum_{l=0}^{\infty}\sum_{i=0}^{4}\beta_{i\omega l}(r) - \frac{1}{8f^{\frac{3}{2}}\pi^2}\left(\frac{1}{\epsilon^3}+\frac{f'^2}{32\epsilon}-\frac{m^2 f}{2\epsilon}\right)\Bigg].\end{aligned} \tag{4.4.6}$$

Unlike the calculation on the brane this is as far as we will take the general form of the temporally point-split $\langle\phi^2\rangle_{\text{ren}}$. By leaving equation (4.4.6) in this form we are left with the most possible flexibility with which to attempt final calculation (for our choice of temporal point splitting).

4.5 Calculation Parameters

We look now at the chosen calculation parameters as this will simplify our analysis of the radial ODE. Just as in §3.9 we choose parameter values that are appropriate for a first calculation in new research such that we will produce baseline results can be expanded upon later. The most important of these is that we set the mass of the scalar field to zero. Further in order to compare the results in the bulk to those on the brane we also choose to set $r_h = 1$ and to calculate over the same range of values of the radial coordinate,

$$r \in (1, 11] \quad \text{and} \quad s \in [\frac{1}{11}, 1) \tag{4.5.1}$$

where $s = r^{-1}$.

The only importance difference between the brane and bulk parameters is that we do not have to choose conformal coupling to the background as the coupling constant no longer appears in our equations. However this is only true as we are calculating the vacuum polarisation, in the case of calculating the RSET we would need to fix the coupling constant as it would appear in higher terms during renormalisation.

4.6 The Radial ODE in the 5d Bulk

We proceed as in §3.8 by restating the radial ODE (2.8.1) in the 5d bulk,

$$\frac{1}{r}\frac{d}{dr}\left[r^3 f\frac{d}{dr}S_{\omega l}\right] - \left(\frac{\omega^2 r^2}{f} + l(l+2)\right)S_{\omega l} = 0. \tag{4.6.1}$$

We keep the distinction between $p_{\omega l}$ and $q_{\omega l}$ the same as on the brane.

We investigate the radial ODE (4.6.1) using the same method of investigating the indicial equation outlined in equations (3.8.2), (3.8.4) and (3.8.7) in order to expand $p_{\omega l}$ near the event horizon with the Frobenius method as

$$p(r\sim 1) \simeq \sum_{j=0}^{\infty} a_j (r-1)^{\nu+j}. \tag{4.6.2}$$

We state here the general bulk (i.e. unspecified number of dimensions), then the 5d bulk, coefficients of the indicial referenced above;

$$\begin{aligned} u(r) =& \frac{d-2}{r} + \frac{f'}{f} \\ v(r) =& \frac{\omega^2}{f^2} + \frac{l(l+d-3)}{r^2 f} \end{aligned} \tag{4.6.3}$$

resulting in,

$$\begin{aligned} u_0 =& 1 \\ v_0 =& \frac{\omega^2}{(d-3)^2} = \frac{\omega^2}{4} \end{aligned} \tag{4.6.4}$$

which then gives,

$$\nu = \pm\frac{\omega}{d-3} = \pm\frac{n}{2} \tag{4.6.5}$$

such that we find ν is independent of the number of dimensions.

The investigation of the $q_{\omega l}$ Frobenius expansion again follows that on the brane where we now obtain, setting $s = r^{-1}$, the following ODE

$$s^4 f \frac{d^2 S_{\omega l}(s)}{ds^2} + s^3(f's + (4-d)f)\frac{dS_{\omega l}(s)}{ds} - \left[\frac{\omega^2}{f} + l(l+d-3)s^2\right] S_{\omega l}(s) = 0. \quad (4.6.6)$$

The ODE (4.6.6) also fails to provide a standard Frobenius series near $s = 0$ like its $d = 4$ counterpart so we use the ansatz as used on the brane, equation (3.8.10),

$$q(s \sim 0) \simeq e^{-\Omega s^{-1}} \sum_{j=0}^{\infty} b_j s^{\rho+j}. \quad (4.6.7)$$

As we have set the mass to zero we now have $\Omega = \omega$ and therefore this series only hold for $\omega \neq 0$.

Substituting(4.6.7) into ODE (4.6.6) allows us to derive ρ though in practice this is easier by reversing the variable change, $s = r^{-1}$, and placing it in (4.6.1). We find

$$\rho = \frac{d-2}{2} \quad (4.6.8)$$

when m and ω are not both simultaneously zero. To investigate this alternate case, as we must with our zero mass system, we turn back to ODE (4.6.6) and see that if $m = \omega = 0$ then the standard Frobenius series is allowed;

$$q(s \sim 0) \simeq \sum_{j=0}^{\infty} b_j s^{\tau+j}. \quad (4.6.9)$$

for which we find

$$\tau = l + d - 3 = l + 2. \quad (4.6.10)$$

4.6.1 Finding $q_{\omega l}(s)$ in the Bulk

We follow up on §3.8.2 by looking at what is required to calculate $q_{\omega l}(s)$ in the bulk. We have already displayed our initial ODE with $s = r^{-1}$ in equation (4.6.6). It can be seen in the coefficient of the first derivative that we pick up an additional term when $d \neq 4$ however this term does not significantly change the type of the output during numerical integration. The ODE are still stiff and so we again attempt a change of variables.

Using the first alternative, $Q(s) = \ln q(s)$, gives the ODE

$$s^4 f \frac{d^2Q}{ds^2} + s^3 \left(fs\frac{dQ}{ds} + f's + (4-d)f \right) \frac{dQ}{ds} - \left[\frac{\omega^2}{f} + l(l+d-3)s^2 \right] = 0 \qquad (4.6.11)$$

where again we gain an additional term for $d \neq 4$. This ODE (4.6.11) suffers from the same issues its equivalent had on the brane and so is of little use.

The second alternative proposed, $Q(s) = e^{\omega s^{-1}} q(s)$, results in the ODE

$$s^4 f \frac{d^2Q}{ds^2} + s^2 \left(2\omega + f's^2 + (4-d)fs\right) \frac{dQ}{ds} - \left[\frac{\omega^2}{f} + l(l+1)s^2 + f(2\omega s - \omega^2) - s^2\omega f' - (4-d)\omega f s \right] Q = 0. \qquad (4.6.12)$$

Here we have two additional terms for $d \neq 4$ which could potentially cause more problems. At first this ODE seemed to be of little use as its output was highly dependent on the level of accuracy demanded, changing not only detail but broader features as well. Eventually a balance was found in which we demanded an overly high accuracy but adjusted this demand through conditional clauses. The case for $\omega = 0$ is more complicated, as can be seen in equations (2.11.24), and as such required 200 significant figures of internal accuracy to guarantee reliable results. For $\omega > 0$ we required 100 significant figures of internal accuracy. Surprisingly after these modifications it became the solutions for $p_{\omega l}$ which became the greater drain on time as no automated conditions could be deduced in

that case to balance accuracy and calculation time.

4.6.2 Radial ODE in the 5d bulk with $\omega = 0$

Under the particular condition that we set $\omega = 0$ we may rewrite the ODE (4.6.1) as

$$\frac{1}{r}\frac{d}{dr}\left[r^3 f \frac{d}{dr} S_{0l}(r)\right] - l(l+2)S_{0l}(r) = 0. \tag{4.6.13}$$

Now using a series of transformations from [32] it is possible to express the ODE (4.6.13) in a form that can be solved analytically.

We begin by setting

$$r = \cosh\left(\frac{x}{2}\right) \quad \text{and} \quad l = 2\nu \tag{4.6.14}$$

such that

$$\frac{d}{dr} = \frac{2}{\sinh\left(\frac{x}{2}\right)}\frac{d}{dx}. \tag{4.6.15}$$

This change of variable transforms the ODE (4.6.13) to

$$\frac{1}{\sinh(x)}\frac{d}{dx}\left(\sinh(x)\frac{d}{dx}S_{0l}(x)\right) - \nu(\nu+1)S_{0l}(x) = 0. \tag{4.6.16}$$

Now set $y = \cosh(x)$ which transforms ODE (4.6.16) to

$$\begin{aligned} &\frac{d}{dy}\left(\sinh^2(x)\frac{d}{dy}S_{0l}(y)\right) - \nu(\nu+1)S_{0l}(y) = 0 \\ \Rightarrow\ &(y^2-1)\frac{d^2}{dy^2}S_{0l}(y) + 2y\frac{d}{dy}S_{0l}(y) - \nu(\nu+1)S_{0l}(y) = 0, \end{aligned} \tag{4.6.17}$$

the standard form of the Legendre ODE. Thus using

$$r^2 = \cosh^2\left(\frac{x}{2}\right) = \frac{1}{2}(1+y) \tag{4.6.18}$$

we may immediately state

$$\begin{aligned} S_{0l}(y) =& C_1 P_\nu(y) + C_2 Q_\nu(y) \\ S_{0l}(r) =& C_1 P_{\frac{l}{2}}(2r^2-1) + C_2 Q_{\frac{l}{2}}(2r^2-1) \end{aligned} \tag{4.6.19}$$

where functions P and Q are the Legendre functions of the first and second kind respectively and C_i are constants. We equate results (4.6.19) to our desired functions as follows

$$\begin{aligned} p_{\omega l} &= P_{\frac{l}{2}}(2r^2-1) \\ q_{\omega l} &= Q_{\frac{l}{2}}(2r^2-1) \end{aligned} \tag{4.6.20}$$

In order to make use of the results (4.6.19) and (4.6.20) we also require the normalising constant, C_{0l}, derived from the Wronskian. We look at a generalised Wronskian, $\mathcal{W}$, for Legendre functions given in equation (14.2.10) of [26]

$$\begin{aligned} \mathcal{W}\{P_\nu^\mu(y), Q_\nu^\mu(y)\} &= e^{\mu\pi i}\frac{\Gamma(\nu+\mu+1)}{\Gamma(\nu-\mu+1)(1-y^2)} \\ \mathcal{W}\{P_\nu(y), Q_\nu(y)\} &= \frac{1}{1-y^2} \quad (\mu=0) \\ \mathcal{W}\{P_\nu(2r^2-1), Q_\nu(2r^2-1)\} &= \frac{1}{1-(2r^2-1)^2}\frac{dy}{dr} \\ &= \frac{-1}{r^3 f}. \end{aligned} \tag{4.6.21}$$

Hence comparing (4.6.21) to the Wronskian calculated from the ODE (4.6.13) requires that $C_{0l} = 1$.

This means for $d = 5$ we may use

$$C_{0l} p_{0l}(r) q_{0l}(r) = P_{\frac{l}{2}}(2r^2-1) Q_{\frac{l}{2}}(2r^2-1). \tag{4.6.22}$$

This substitution is advantageous in two ways; firstly it lets us avoid numerical work

for $\omega = 0$ which often presents problems in accuracy and secondly it provides a new comparison by which we can test our numerical solver for the bulk radial ODE.

Note that substitution (4.6.22) is rarely shown explicitly during equation manipulation for the rest of this chapter in order to keep methodology tidier.

4.7 $\langle\phi^2\rangle_{\rm ren}$ Complications in the Bulk

In order to proceed to calculation we look at §3.4 to see how the ϵ singularities were handled on the brane. In that section we used distributional identities found in appendix B to express our renormalised vacuum polarisation, schematically, as

$$\langle\phi^2\rangle^{4d}_{\rm ren} = \lim_{\epsilon\to 0}\left[\sum_{n,l}\cos(\omega\epsilon)A_{n,l} - \sum_{n}\cos(\omega\epsilon)B_n + O(\epsilon^2)\right] + \text{finite terms.} \tag{4.7.1}$$

In (4.7.1) $A_{n,l}$ is the term derived from the modes and B_n is the term derived from the renormalisation contribution. We may label the vacuum polarisation as $4d$ because on the brane the renormalisation is calculated on the 4d projection on the brane irrespective of the total number of dimensions considered. It is clear in equation (4.7.1) that the limit $\epsilon \to 0$ can be taken simply allowing us to proceed so let us apply this approach in the bulk.

First we look at the current form of our vacuum polarisation from equation (4.4.6) implementing choices made since its statement

$$\begin{aligned}\langle\phi^2\rangle_{\rm ren} =& \frac{\kappa}{2\pi}\sum_{n=-\infty}^{\infty}\sum_{l=0}^{\infty} N_l G_l \left[C_{\omega l}p_{\omega l}(r)q_{\omega l}(r) - \beta(r)\right] \\ &+ \frac{\kappa}{2\pi}\lim_{\epsilon\to 0}\left[\sum_{n=-\infty}^{\infty} e^{i\omega\epsilon}\sum_{l=0}^{\infty}\beta(r) - \frac{1}{8f^{\frac{3}{2}}\pi^2}\left(\frac{1}{\epsilon^3} + \frac{f'^2}{32\epsilon}\right)\right].\end{aligned} \tag{4.7.2}$$

where, for a tidier expression, we have set

$$\beta(r) = \sum_{i=0}^{d-1} \beta_{i\omega l}(r) \quad \text{and for } \omega = 0 \quad \beta_0(r) = \sum_{i=0}^{d-1} \beta_{i0l}(r). \tag{4.7.3}$$

In equation (4.7.2) we see the relevant distributional identities in appendix B are

$$\begin{aligned} \frac{1}{\epsilon} &= \sum_{n=1}^{\infty} \kappa \sin(n\kappa\epsilon) + O(\epsilon) \\ \frac{1}{\epsilon^3} &= -\frac{1}{2} \sum_{n=1}^{\infty} \kappa^3 n^2 \sin(n\kappa\epsilon) + O(\epsilon). \end{aligned} \tag{4.7.4}$$

Implementing these identities using the same scheme as in the brane case above we can see the structure (with respect to epsilon) of the limit in equation (4.7.2),

$$\langle\phi^2\rangle_{\text{ren}} = \lim_{\epsilon\to 0} \left[\sum_{n,l} \cos(\omega\epsilon) A_{n,l} - \sum_{n} \sin(\omega\epsilon) B_n + O(\epsilon) \right]. \tag{4.7.5}$$

Immediately it is clear that there is a problem in that the limit $\epsilon \to 0$ can no longer be simply taken inside the sum due to $\sin(\omega\epsilon) \to 0$. If this were to happen all renormalisation terms would vanish and we would be left only with the modes sums which are by definition not regular. This demonstrates a lack of absolute convergence in the sums and no apparent method of handling said limit. Here we find our key difficulty for the $d = 5$ calculation. We have no obvious way in which to express the divergent terms of (4.7.2) as a double sum that we can take the limit of epsilon over.

This has demonstrated that the simple identity substitution approach used on the brane is no longer applicable for the $d = 5$ bulk calculation and in the next sections we review alternative methods. However first we look ahead at the bulk calculations for $d > 5$ to see where this complication leads. Using the information given in §2.9 and §2.10 we

can write in general

$$\begin{aligned} G_{E,sing} &= \sum_i \frac{a_i}{\epsilon^{2i-1}} \quad \text{for } d \text{ odd} \\ G_{E,sing} &= \sum_i \frac{b_i}{\epsilon^{2i}} + c_i \ln(\epsilon) \quad \text{for } d \text{ even} \end{aligned} \tag{4.7.6}$$

Here the a_i, b_i and c_i are functions of r whose quantity are determined by the number of dimensions such that the higher number of bulk dimensions implies more terms. Then looking at the distributional identities in appendix B we may state in general

$$\begin{aligned} \frac{1}{\epsilon^{2i+1}} &= d_i \sum_n n^{2i} \sin(\omega\epsilon) + O(\epsilon) \\ \frac{1}{\epsilon^{2i}} &= e_i \sum_n n^{2i-1} \cos(\omega\epsilon) + O(\epsilon^2) \end{aligned} \tag{4.7.7}$$

where d_i and e_i are functions of r similar to a_i, b_i and c_i above. It is obvious that the use of the distributional identities will fail to work for any odd value of d unless a method is found to handle the limit. Although we see that the distributional identities are applicable for even values of d there is the introduction of a logarithmic term that needs careful handling as it may diverge. In our brane calculations this problem never arose due to our massless, conformally coupled field however glancing at [23] shows this will not remain true for $d = 6$. Other sources, for example [75], have to deal with this logarithm in $d = 4$ and so will any extension of this work to massive or non-conformally coupled fields for any even value of d hence some care must always be taken using the presented identities.

4.8 Dimensional Reduction

Our first method of handling the divergence is based on an idea introduced in §3.3. The concept is to split our Green's function in such a way that we may reduce the number of dimensions required to proceed to further calculation. Although this approach requires

us to start back before we allowed any point coincidence it should simplify the terms we wish to renormalise. To begin with we will work in an unspecified number of dimensions to create a general method, we will choose particular values of d when required.

4.8.1 d Dimensional Methodology

We begin by looking at equation (2.8.4) without allowing radial point coincidence, hence,

$$G_E(x,x') = \frac{\kappa}{2\pi}\sum_{n=-\infty}^{\infty} e^{i\omega\epsilon}\sum_{l=0}^{\infty}\tilde{N}_{d,l}G_l^{\lambda}(\cos\gamma)S_{\omega l}(r,r'). \tag{4.8.1}$$

For our massless system the Green's function (4.8.1) satisfies the Klein-Gordon equation

$$\Box G_E(x,x') = 0 \quad \text{for } x \neq x' \tag{4.8.2}$$

with our d dimensional metric (2.3.16) for which we will express the determinant function, $\sqrt{g}$ as

$$\sqrt{g} = r^{d-2}\sqrt{h_{d-2}} \tag{4.8.3}$$

where h_{d-2} is the determinant of the metric on the unit $(d-2)$-sphere. Now we can write the Klein-Gordon equation (4.8.2) by using equation (2.3.5) as

$$f^{-1}\partial_t^2 G_E + \frac{1}{r^{d-2}}\partial_r\left(fr^{d-2}\partial_r G_E\right) + \frac{1}{r^2\sqrt{h_{d-2}}}\partial_{\theta_i}\left(h_{d-2}^{ii}\sqrt{h_{d-2}}\partial_{\theta_i}G_E\right) = 0, \tag{4.8.4}$$

where h_{d-2}^{ii} are the components of the metric on the unit $(d-2)$-sphere.

Now we introduce the dimensional reduction by expressing our Green's function in the following way

$$G_E(x;x') = \frac{\kappa}{2\pi}\sum_{n=-\infty}^{\infty} e^{i\omega\epsilon}\times\mathcal{G}_{\omega}(\widetilde{x};\widetilde{x}') \tag{4.8.5}$$

where $\widetilde{x} = (r,\theta_1,...,\theta_{d-2})$. Then our $d-1$ dimensional Green's function, $\mathcal{G}_{\omega}(\widetilde{x};\widetilde{x}')$, satisfies

the following

$$-\frac{\omega^2}{f}\mathcal{G}_\omega + \frac{1}{r^{d-2}}\partial_r\left(fr^{d-2}\partial_r\mathcal{G}_\omega\right) + \frac{1}{r^2\sqrt{h_{d-2}}}\partial_{\theta_i}\left(h^{ii}_{d-2}\sqrt{h_{d-2}}\partial_{\theta_i}\mathcal{G}_\omega\right) = 0. \tag{4.8.6}$$

Now we find a $d-1$ dimensional metric, $\widetilde{g}_{\mu\nu}$, with which the $d-1$ dimensional Klein-Gordon equation (possibly including a potential term) expands to become equation (4.8.6). For $\widetilde{g}_{\mu\nu}$ we begin with ansatz

$$\widetilde{ds}^2 = A(r)dr^2 + B(r)d\Omega^2_{d-2} \tag{4.8.7}$$

such that $A(r)$ and $B(r)$ are to be determined, then

$$\sqrt{\widetilde{g}} = \sqrt{AB^{d-2}}\sqrt{h_{d-2}}. \tag{4.8.8}$$

On the metric (4.8.7) the Klein-Gordon equation is

$$\frac{1}{\sqrt{AB^{d-2}}}\partial_r\left(A^{-1}\sqrt{AB^{d-2}}\partial_r\mathcal{G}_\omega\right) + \frac{1}{B\sqrt{h_{d-2}}}\partial_{\theta_i}\left(h^{ii}_{d-2}\sqrt{h_{d-2}}\partial_{\theta_i}\mathcal{G}_\omega\right) = 0. \tag{4.8.9}$$

Now we compare Klein-Gordon equations (4.8.6) and (4.8.9), this gives

$$\begin{aligned} A^{-1}\sqrt{AB^{d-2}} &= fr^{d-2} \\ D\sqrt{AB^{d-2}} &= r^{d-2} \\ BD &= r^2 \end{aligned} \tag{4.8.10}$$

for some $D(r)$. After some algebra we then find

$$\begin{aligned} A &= f^{\frac{d-4}{3-d}} \\ B &= f^{\frac{1}{d-3}}r^2 \\ D &= f^{-\frac{1}{d-3}} \end{aligned} \tag{4.8.11}$$

which for $d = 4$ yields

$$\begin{aligned} A &= 1 \\ B &= fr^2 \end{aligned} \tag{4.8.12}$$

in agreement with the work carried out in [75] and §3.3. For general d, $\mathcal{G}_\omega$ satisfies the following equation

$$\begin{aligned} 0 =& -\frac{\omega^2}{f}\mathcal{G}_\omega + f^{\frac{1}{d-3}}\Box_{d-1}\mathcal{G}_\omega \\ 0 =& \Box_{d-1}\mathcal{G}_\omega - \omega^2 f^{-\frac{d-2}{d-3}}\mathcal{G}_\omega, \end{aligned} \tag{4.8.13}$$

which has the form of a Klein-Gordon equation with additional potential $\widetilde{V} = \omega^2 f^{-\frac{d-2}{d-3}}$.

We may now investigate the leading order divergence structure of $\mathcal{G}_\omega$, beyond leading order will require specifying the number of dimensions. To find the leading order divergence we use the Hadamard method as discussed in §2.9 for which will need to know the form of Synge's world function, σ. We will proceed by allowing point coincidence on all variables except θ_1, setting $\gamma = \theta_1 - \theta_1'$, then we have

$$\begin{aligned} \sigma &= \frac{1}{2}\sigma_{;\mu}\sigma^{;\mu} \\ &= \frac{1}{2}\left(A\sigma_{;r}\sigma^{;r} + Bh^{ij}_{d-2}\sigma_{;i}\sigma_{;j}\right) \\ &= \frac{1}{2}B\gamma^2 + O(\gamma^4). \end{aligned} \tag{4.8.14}$$

Now we can construct the leading order singularity in the Hadamard expansion, $\mathcal{G}_{los}$, as follows

$$\mathcal{G}_{los} = \frac{\alpha_{d-1}}{2}\frac{1}{\sigma^{\frac{d-3}{2}}} = \alpha_{d-1}\frac{2^{\frac{d-5}{2}}}{r^{d-3}f^{\frac{1}{2}}\gamma^{d-3}}. \tag{4.8.15}$$

In order to proceed further with this method we now apply the results of this section to $d = 5$.

4.8.2 Application to $d = 5$

For $d = 5$ we now have the Klein-Gordon equation (4.8.13)

$$0 = \Box_4 \mathcal{G}_\omega - \omega^2 f^{-\frac{3}{2}} \mathcal{G}_\omega \tag{4.8.16}$$

for the metric

$$\widetilde{ds}^2 = f^{-\frac{1}{2}} dr^2 + f^{\frac{1}{2}} r^2 d\Omega_3^2, \tag{4.8.17}$$

where we stress that, as in §3.3, this metric is unphysical.

Using equations (4.8.16) and (4.8.17) we can find the Hadamard singularity of $\mathcal{G}_\omega$. We follow the notation used in §2.9, use the same point splitting as in the d dimensional methodology above and retain the use of a tilde to mean an object derived from our dimensionally reduced equations. This means $\widetilde{R}_{ab}$ and $\widetilde{R}$ are from the metric (4.8.17) and do not disappear as for the $d = 5$ metric. This then gives;

$$\begin{aligned}
\mathcal{G}_{sing} &= \frac{\alpha_4}{2}\left[\frac{U}{\sigma} + V \ln \sigma\right] \\
&= \frac{\alpha_4}{2}\left[\frac{1}{\sigma} + \frac{\widetilde{R}_{ab}\sigma^{;a}\sigma^{;b}}{12\sigma} + \frac{1}{2}\left(\widetilde{V} - \frac{1}{6}\widetilde{R}\right)\ln\sigma\right] \\
&= \frac{\alpha_4}{2}\left[\frac{2}{r^2 f^{\frac{1}{2}}\gamma^2} + Y(r) + \frac{1}{2}\left(\widetilde{V} - \frac{1}{6}\widetilde{R}\right)\ln\left(\frac{1}{2}r^2 f^{\frac{1}{2}}\gamma^2\right)\right] + O(\gamma^2).
\end{aligned} \tag{4.8.18}$$

In $\mathcal{G}_{sing}$ the function $Y(r)$ is the sum of all terms that do not diverge as $\gamma \to 0$, specifically

$$\begin{aligned}
Y(r) &= \frac{1}{96 r^2 f^{\frac{3}{2}}}(16 f^2 + 8 r f f' + r^2 f'^2) + \frac{\widetilde{R}_{ab}\sigma^{;a}\sigma^{;b}}{12\sigma} \\
&= \frac{(1-2r^2)^2}{24 r^6 f^{\frac{3}{2}}} + \frac{\widetilde{R}_{ab}\sigma^{;a}\sigma^{;b}}{12\sigma}
\end{aligned} \tag{4.8.19}$$

though this form will be of little use to us. The coefficient of the logarithm can equally

be shown explicitly to be

$$\begin{aligned}\frac{1}{2}\left(\widetilde{V}-\frac{1}{6}\widetilde{R}\right) &= \frac{\omega^2}{2f^{\frac{3}{2}}}-\frac{1}{48r^2f^{\frac{3}{2}}}(-48f^2+3r^2f'^2-12f(-4+5rf'+r^2f'')) \\ &= \frac{4r^6\omega^2-1}{8r^6f^{\frac{3}{2}}}.\end{aligned} \tag{4.8.20}$$

To proceed we express $\mathcal{G}_\omega$ as

$$\begin{aligned}\mathcal{G}_\omega &= \sum_{l=0}^{\infty}\tilde{N}_{5,l}G_l^1(\cos\gamma)S_{\omega l}(r) \\ &= \mathcal{G}_{reg}+\mathcal{G}_{sing}\end{aligned} \tag{4.8.21}$$

such that we aim to subtract appropriate terms from its sum form in line one so that only its regular part, $\mathcal{G}_{reg}$, remains in line two. In order to use $\mathcal{G}_{sing}$ effectively we follow the on brane methodology and seek to express the singularities as sums. The only apparent identity of relevance (excluding those listed in Appendix B) is the generating function of the Gegenbauer polynomials

$$\sum_{l=0}^{\infty}t^lG_l^\lambda(x)=\frac{1}{(1-2xt+t^2)^\lambda} \tag{4.8.22}$$

which under $t\to 1$, $x\to\cos\gamma$ and $\lambda=1$ gives

$$\sum_{l=0}^{\infty}G_l^1(\cos\gamma)=\frac{1}{2(1-\cos\gamma)}=\frac{1}{\gamma^2}+\frac{1}{12}+O(\gamma^2). \tag{4.8.23}$$

We take a multiple of (4.8.23),

$$\frac{\alpha_4}{2}\sum_{l=0}^{\infty}G_l^1(\cos\gamma)\frac{2}{r^2f^{\frac{1}{2}}}=\frac{\alpha_4}{2}\left[\frac{2}{r^2f^{\frac{1}{2}}\gamma^2}+\frac{1}{6r^2f^{\frac{1}{2}}}+O(\gamma^2)\right], \tag{4.8.24}$$

and subtract it from equation (4.8.21) to find

$$\sum_{l=0}^{\infty}\left[\tilde{N}_{5,l}S_{\omega l}(r)-\frac{\alpha_4}{r^2 f^{\frac{1}{2}}}\right]G_l^1(\cos\gamma)$$
$$=\frac{\alpha_4}{2}\left[-\frac{1}{6r^2f^{\frac{1}{2}}}+Y(r)+\frac{1}{2}\left(\widetilde{V}-\frac{1}{6}\widetilde{R}\right)\ln\sigma+O(\gamma^2)\right]+\mathcal{G}_{reg}. \quad (4.8.25)$$

Expression (4.8.25) no longer has any pole-like singularities but retains its logarithmic singularity, there are two ways to handle this remaining singularity and we present both. First consider (4.8.25) for $n=0$,

$$\sum_{l=0}^{\infty}\left[\tilde{N}_{5,l}S_{0l}(r)-\frac{\alpha_4}{r^2 f^{\frac{1}{2}}}\right]G_l^1(\cos\gamma)$$
$$=\frac{\alpha_4}{2}\left[-\frac{1}{6r^2f^{\frac{1}{2}}}+Y(r)-\frac{1}{8r^6f^{\frac{3}{2}}}\ln\sigma+O(\gamma^2)\right]+\mathcal{G}_{reg}. \quad (4.8.26)$$

Adding (4.8.25)+$(4r^6\omega^2-1)$(4.8.26) which gives

$$\sum_{l=0}^{\infty}\left[\tilde{N}_{5,l}\left[S_{\omega l}(r)+(4r^6\omega^2-1)S_{0l}(r)\right]-\frac{4\alpha_4 r^4\omega^2}{f^{\frac{1}{2}}}\right]G_l^1(\cos\gamma)$$
$$=\frac{\alpha_4}{2}\left[4r^6\omega^2\left(Y(r)-\frac{1}{6r^2f^{\frac{1}{2}}}\right)+O(\gamma^2)\right]+\mathcal{G}_{reg}. \quad (4.8.27)$$

It is clear that in the limit $\gamma\to 0$ this expression is regular and so appears to be as desired. However it is unclear if the expression is complete as the function $Y(r)$ is still present.

In standard Hadamard renormalisation finite renormalisation terms must still be removed when encountered and this has not been done here. We cannot be definite if $Y(r)$ should still be removed or if and how to do so rigorously. For the analogous method applied on the brane no such finite terms remain as in that case we reduced from $d=4$ to $d=3$ which contains neither finite nor logarithmic terms and so is simpler. We shall return to this point after we demonstrate the second method to remove the logarithm.

In the second method we take note of the issue found in the first method and isolate the logarithm by subtracting (4.8.26) from (4.8.25), giving

$$\sum_{l=0}^{\infty}\left[\tilde{N}_{5,l}\left(S_{\omega l}(r)-S_{0l}(r)\right)\right]G_l^1(\cos\gamma)=\frac{\alpha_4}{2}\left[\frac{\omega^2}{2f^{\frac{3}{2}}}\ln\left(\frac{1}{2}r^2f^{\frac{1}{2}}\gamma^2\right)+O(\gamma^2)\right]+\mathcal{G}_{reg}. \tag{4.8.28}$$

Now we implement a slightly rearranged identity (the original can be found in Appendix B)

$$\ln\left(x^2\right)=-2\sum_{l=0}^{\infty}\frac{\cos[(l+1)x]}{l+1} \tag{4.8.29}$$

which allows us to express (4.8.28) as

$$\sum_{l=0}^{\infty}\left[\tilde{N}_{5,l}\left(S(r)-S_{0l}(r)\right)G_l^1(\cos\gamma)+\frac{\alpha_4\omega^2}{2f^{\frac{3}{2}}}\frac{\cos[(l+1)\frac{1}{\sqrt{2}}rf^{\frac{1}{4}}\gamma]}{l+1}\right]=O(\gamma^2)+\mathcal{G}_{reg}. \tag{4.8.30}$$

In this expression if we let $\gamma\to 0$ what remains is a sum that should be regular as the right hand side is $\mathcal{G}_{reg}$. The problem here is that actual calculation of the left hand side to find $\mathcal{G}_{reg}$ becomes intractable. Attempting to use the numerical modes does not demonstrate convergence and using the WKB terms in their place also fails to give a convergent analytic result.

In summary the dimensional reduction method shows great potential and may be useful in other physical models (as demonstrated in [75]). However in our case, whether through lack of identity options or uncertainty in our rigour, this method failed to help solve the renormalisation problem. It did however provide some tangential inspiration as seen in the next section.

4.9 The Minkowski Bulk

While investigating the method presented in the previous section an important issue became finding new methods to express the terms in a Hadamard singularity, preferably in a double sum to match our Green's function. One such is looking at the equivalent physical system for the Euclidean Minkowski bulk [68]. The remaining methods presented to handle the divergent terms for the Schwarzschild-Tangherlini bulk will make use of this new method. In this section we will cover relevant information about the Minkowski bulk Green's function before returning to our renormalisation problem.

Most mathematical statements about the Minkowski bulk can be easily written down by letting $f \to 1$ in equations for our original bulk, such as for the metric

$$ds^2 = dt^2 + dr^2 + r^2 d\Omega_3^2 \tag{4.9.1}$$

giving $R_{ab} = 0$ and $R = 0$ as expected. However, for both the spacetime and the Minkowski Euclidean Green's function $G_E^{\mathcal{M}}$, some properties become simplified and some quantities take new values. These are covered below. In addition we will state some results for massive fields that have not been touched on previously.

Statements apply for $d \geq 4$ when possible, some statements apply only for $d = 3$ and this is made clear where relevant.

4.9.1 Minkowski Radial ODE

First we consider massive scalar field modes. The homogeneous ODE (2.8.1) now has the form

$$r^2 S''_{\omega l}(r) + (d-2) S'_{\omega l}(r) - \left[(\omega^2 + m^2) r^2 + l(l+d-3)\right] S_{\omega l}(r) = 0 \tag{4.9.2}$$

but we will use the transformion

$$S(r) = r^{\frac{3-d}{2}} Y(r) \tag{4.9.3}$$

to investigate its solutions as well as letting $\Omega^2 = \omega^2 + m^2$.

This transformation takes the ODE (4.9.2) to

$$r^2 Y''(r) + rY'(r) - \left[\Omega^2 r^2 + \left(l + \frac{d-3}{2}\right)^2\right] Y(r) = 0 \tag{4.9.4}$$

the solution to which is

$$S(r) = r^{\frac{3-d}{2}} \left(AI_\alpha(\Omega r) + BK_\alpha(\Omega r)\right) \tag{4.9.5}$$

where A and B are constants of integration, $\alpha = l + \frac{d-3}{2}$ and I_α, K_α are modified Bessel functions of the first and second kind respectively. Previously we associated the mode $p_{\omega l}$ with the result from the radial ODE that is regular on the horizon so here we make the connection $p_{\omega l} \sim I_\alpha$. Similarly we associate $q_{\omega l}$ with the result that is regular infinity so here we make the connection $q_{\omega l} \sim K_\alpha$. Hence the mode functions take the form

$$\begin{aligned} p_{\omega l} &= r^{\frac{3-d}{2}} I_\alpha(\Omega r) \\ q_{\omega l} &= r^{\frac{3-d}{2}} K_\alpha(\Omega r). \end{aligned} \tag{4.9.6}$$

From this result we find that the normalisation constant for the modes, $C_{\omega l}$, is equal to one so we can write the modes as

$$C_{\omega l} p_{\omega l} q_{\omega l} = r^{3-d} I_\alpha(\Omega r) K_\alpha(\Omega r) \qquad \Omega \neq 0. \tag{4.9.7}$$

It is obvious solution (4.9.7) cannot hold for $\Omega = 0$ as this would not give us a radial ODE of the Bessel type. We return to the ODE (4.9.2) for $m = \omega = 0$ and find in this

case

$$S(r) = Ar^l + Br^{3-d-l}, \tag{4.9.8}$$

where A and B are constants of integration. As above we associate our modes by whether they are regular on the horizon or infinity hence $p_{\omega l} \sim r^l$ (as $l \geq 0$) and $p_{\omega l} \sim r^{3-d-l}$ (as $l \geq 0$ and $d \geq 4$). Calculating the mode normalisation constant from the Wronskian now gives

$$C_{0l} = \frac{1}{2l+d-3} \tag{4.9.9}$$

and hence

$$C_{0l}p_{0l}q_{0l} = \frac{r^{3-d}}{2l+d-3}\left(= \lim_{\Omega\to 0} C_{\omega l}p_{\omega l}q_{\omega l}\right). \tag{4.9.10}$$

Note that equation (4.9.10) is constant in r for $d = 3$, depending only on l. This may pose a problem as the $n = 0$ modes being divergent at the horizon was a required feature for the brane calculation. We will return to this later.

4.9.2 Massless $\langle\phi^2\rangle^{\mathcal{M}}_{ren}$ and Renormalisation

The main difference between the vacuum polarisation calculation performed on Minkowski spacetime and non-flat spacetimes is that the calculation can be achieved via an alternative method. We see that using thermal field theory $\langle\phi^2\rangle^{\mathcal{M}}_{ren}$ can be calculated from the non-thermal state without much difficulty.

We begin with the Euclidean propagator for the non-thermal field, $G^{\mathcal{M}}_{E,vac}$, which is derived from the Feynman propagator, $G^{\mathcal{M}}_{F,vac}$, expressed using Cartesian coordinates in Minkowski spacetime,

$$\begin{aligned} G^{\mathcal{M}}_{E,vac} = -iG^{\mathcal{M}}_{F,vac} &= \frac{\alpha_d}{2}\frac{1}{\sigma^{\frac{d}{2}-1}} \\ &= \frac{\alpha_d}{2}\left[(t-t')^2 + \sum_i (x_i - x_i')^2\right]^{-\left(\frac{d}{2}-1\right)}\left(\frac{1}{2}\right)^{-\left(\frac{d}{2}-1\right)}, \end{aligned} \tag{4.9.11}$$

where the x_i are the variables for the space-like dimensions. This gives us the thermal propagator, $G_E^{\mathcal{M}}$, by taking advantage of the required temporal periodicity for a Euclidean thermal field

$$\begin{aligned} G_E^{\mathcal{M}} = -iG_F^{\mathcal{M}} &= \sum_{n=-\infty}^{\infty} -iG_{F,vac}^{\mathcal{M}}\left(t+n\beta, x_i; t', x_i'\right) \\ &= \frac{\alpha_d}{2}\sum_{n=-\infty}^{\infty}\left[(t-t'+n\beta)^2 + \sum_i (x_i - x_i')^2\right]^{-\left(\frac{d}{2}-1\right)} \left(\frac{1}{2}\right)^{-\left(\frac{d}{2}-1\right)} \end{aligned} \tag{4.9.12}$$

where $\beta = T^{-1}$ and T is the temperature of the field.

We may now proceed directly to $\langle\phi^2\rangle_{ren}^{\mathcal{M}}$ by subtracting $G_{E,vac}^{\mathcal{M}}$ from $G_E^{\mathcal{M}}$ then coinciding all the variables (i.e. $x_i' \to x_i$ and $t' \to t$), renormalising and calculating the remaining terms,

$$\begin{aligned} \langle\phi^2\rangle_{ren}^{\mathcal{M}} &= \frac{\alpha_d}{2}\sum_{\substack{n=-\infty \\ n\neq 0}}^{\infty}\left[(n\beta)^2\right]^{-\left(\frac{d}{2}-1\right)}\left(\frac{1}{2}\right)^{-\left(\frac{d}{2}-1\right)} \\ &= \alpha_d 2^{\frac{d}{2}-1}\beta^{2-d}\sum_{n=1}^{\infty} n^{2-d} \\ &= \alpha_d 2^{\frac{d}{2}-1}\beta^{2-d}\zeta(d-2) \end{aligned} \tag{4.9.13}$$

where ζ is the Riemann zeta function. The renormalisation of $G_E^{\mathcal{M}}$ was implemented in the first line by removing the $n = 0$ mode.

Note that (4.9.13) the calculation fails for $d = 3$. Some hint that this value of d may be problematic was found from the modes but now we know that $d = 3$ Minkowski spacetime cannot support massless thermal fields.

Finally for the massless Green's function we cover the renormalisation terms. Assuming

temporal point splitting we may simply state for the world function

$$\begin{aligned} \sigma &= \frac{1}{2}\epsilon^2 \\ \sigma_{;t} &= \epsilon \end{aligned} \tag{4.9.14}$$

where the other covariant derivatives are zero. For the Hadamard expansion we find

$$\Delta^{\frac{1}{2}} = 1 \Rightarrow U_0 = 1 \tag{4.9.15}$$

and

$$\left.\begin{matrix} U_{n>0} \\ V_n \end{matrix}\right\} = O(m^2) = 0. \tag{4.9.16}$$

Now we can state the Hadamard singularity of the Minkowski Green's function

$$G^{\mathcal{M}}_{E,sing} = \frac{\alpha_d}{2}\sigma^{-(\frac{d}{2}-1)} = \frac{\alpha_d}{4}2^{\frac{d}{2}}\epsilon^{2-d}. \tag{4.9.17}$$

4.9.3 Massive $\langle\phi^2\rangle^{\mathcal{M}}_{ren}$ and Renormalisation

In the case of a massive thermal field we begin with the same concept as for the massless case but must start carefully from the base definitions. We begin with a two point correlation function similar to that constructed in [42] (ours is a Wick ordered two point function while the source uses a different sign convention for a Lorentzian calculation)

$$\begin{aligned} \langle\phi(x)\phi(x')\rangle^{\mathcal{M}} &= -i\left[G^{\mathcal{M}}_F(x,x') - G^{\mathcal{M}}_{F,vac}(x,x')\right] \\ &= \int \frac{2\pi\delta(|k|^2 - m^2)}{e^{\beta|k_0|}-1}\left[\theta(k_0)e^{-ik.(x-x')} + \theta(-k_0)e^{ik.(x-x')}\right]\frac{d^{n+1}k}{(2\pi)^{n+1}} \end{aligned} \tag{4.9.18}$$

where θ is the Heaviside function, $k = (k_0, ..., k_n)$ is the momentum and $d = n + 1$ for n being the number of space-like dimensions.

To proceed we change from a two point correlation to an auto-correlation function

(the vacuum polarisation) by taking the limit $x' \to x$, by construction this will produce a renormalised result as the vacuum has been subtracted. This results in

$$\begin{aligned}\langle\phi^2\rangle^{\mathcal{M}}_{ren} &= \int \frac{\delta(|k|^2 - m^2)}{e^{\beta|k_0|} - 1} \left[\theta(k_0) + \theta(-k_0)\right] \frac{d^{n+1}k}{(2\pi)^n} \\ &= \int \frac{\delta(|k|^2 - m^2)}{e^{\beta|k_0|} - 1} \frac{dk_0 ... dk_n}{(2\pi)^n}.\end{aligned} \tag{4.9.19}$$

Next we relabel the mass-momentum relation such that $(a^2 = m^2 + k_1^2 + ... + k_n^2)$, hence we write

$$\langle\phi^2\rangle^{\mathcal{M}}_{ren} = \int \frac{\delta((k_0)^2 - a^2)}{e^{\beta|k_0|} - 1} \frac{dk_0 ... dk_n}{(2\pi)^n}. \tag{4.9.20}$$

We now make use of the following identity,

$$\delta(x^2 - y^2) = \frac{1}{2|y|}[\delta(x - y) + \delta(x + y)], \tag{4.9.21}$$

so that equation (4.9.20) can be written as

$$\langle\phi^2\rangle^{\mathcal{M}}_{ren} = \int \frac{1}{2|k_0|} \frac{1}{e^{\beta|k_0|} - 1} \left[\delta(k_0 - a) + \delta(k_0 + a)\right] \frac{dk_0 ... dk_n}{(2\pi)^n}. \tag{4.9.22}$$

Now we restrict our calculation to being on shell which allows us to define

$$a = |k_0| = \omega = \sqrt{(k_1)^2 + ... + (k_n)^2 + m^2} \tag{4.9.23}$$

where we take ω to be the field mode frequency. Using this relation for a we may perform the integral over k_0 in (4.9.22) to result in

$$\langle\phi^2\rangle^{\mathcal{M}}_{ren} = \int \frac{1}{\omega(e^{\beta\omega} - 1)} \frac{dk_1 ... dk_n}{(2\pi)^n}. \tag{4.9.24}$$

To proceed from (4.9.24) we use the characteristics of being on-shell and introduce a change of integration variables. This is done by exchanging k for r and θ_i through the

addition of the Jacobean $J(\theta_1, ..., \theta_{n-1})$, the definition $r^2 = \omega^2 - m^2$ and introducing a factor of r for each introduced θ_i. This gives

$$\langle\phi^2\rangle^{\mathcal{M}}_{ren} = \frac{1}{(2\pi)^n}\int_{r=0}^{\infty}\frac{r^{n-1}}{\omega(e^{\beta\omega}-1)}J(\theta_1,...,\theta_{n-1})d\theta_1...d\theta_{n-1}dr. \tag{4.9.25}$$

Now we can perform the integration over the angular measure and transform the remaining integration variable to achieve a final calculable form;

$$\begin{aligned}\langle\phi^2\rangle^{\mathcal{M}}_{ren} &= \frac{S_{n-1}}{(2\pi)^n}\int_m^{\infty}\frac{r^{n-2}}{e^{\beta\omega}-1}d\omega \\ &= \frac{S_{n-1}}{(2\pi)^n}\int_m^{\infty}\frac{(\omega^2-m^2)^{\frac{n-2}{2}}}{e^{\beta\omega}-1}d\omega,\end{aligned} \tag{4.9.26}$$

such that S_{n-1} is the surface area of a unit $(n-1)$-sphere.

To conclude we must check that result (4.9.26) holds for $d = 3$, inputting $n = 2$ we obtain

$$\begin{aligned}\langle\phi^2\rangle^{\mathcal{M}}_{ren,3d} &= \frac{S_1}{(2\pi)^2}\int_m^{\infty}\frac{1}{e^{\beta\omega}-1}d\omega \\ &= \frac{1}{2\pi}\lim_{\alpha\to\infty}\left[\frac{1}{\beta}\Big(\ln(e^{\beta\omega}-1)-\beta\omega\Big)\right]_m^{\alpha} \\ &= \frac{1}{2\pi\beta}\lim_{\alpha\to\infty}\Big[\ln(1-e^{-\beta\alpha})-\ln(1-e^{-\beta m})\Big] \\ &= \frac{1}{2\pi\beta}\ln\left(\frac{e^{\beta m}}{e^{\beta m}-1}\right).\end{aligned} \tag{4.9.27}$$

This gives a real value for $m > 0$ and diverges as $m \to 0$ hence confirming that $d = 3$ Minkowski spacetimes cannot support massless thermal field, only massive thermal fields.

Now we look at renormalisation for the massive case, this will be done for $d = 5$ and $d = 3$ specifically as only these numbers of dimensions will be used later and a general expression becomes complicated. For $d = 5$ we may simply state, from [23] and equation

(4.3.11), that

$$\begin{aligned} G^{\mathcal{M},m}_{E,sing} &= \frac{\alpha_5}{2}\frac{U}{\sigma^{\frac{3}{2}}} \\ &= \frac{\alpha_5}{2}\left(\frac{1}{\sigma^{\frac{3}{2}}} - \frac{m^2}{\sigma^{\frac{1}{2}}}\right) \\ &= \frac{\alpha_5}{\sqrt{2}}\left(\frac{2}{\epsilon^3} - \frac{m^2}{\epsilon}\right) \end{aligned} \tag{4.9.28}$$

where we have used temporal point splitting and the Minkowski world function (4.9.14). For the $d = 3$ case we have shown above that the field must be massive or the vacuum polarisation diverges and the system is unphysical. However looking at the renormalisation terms we see that the mass plays no role in the relevant terms [23] and so the terms are derived from equation (4.9.29) as in the massless case. This results in

$$G^{\mathcal{M},3d}_{E,sing} = \frac{\alpha_3}{\sqrt{2}\epsilon}. \tag{4.9.29}$$

4.9.4 Minkowski Summary

We briefly present how the results gathered in this section are expressed as explicit versions of the equation

$$\langle\phi^2\rangle^{\mathcal{M}}_{ren} = \lim_{\epsilon\to 0}\left(\langle\phi^2\rangle^{\mathcal{M}}_{unren} - \langle\phi^2\rangle^{\mathcal{M}}_{sing}\right). \tag{4.9.30}$$

We are able to do this as we have found $\langle\phi^2\rangle^{\mathcal{M}}_{ren}$ in two distinct ways; by direct calculation and by expression of a mode sum subtracting Hadamard terms.

Expressing $\langle\phi^2\rangle^{\mathcal{M}}_{ren}$ as the above is accomplished by setting $\langle\phi^2\rangle^{\mathcal{M}}_{unren}$ equal to the mode sum (2.8.13) expressed in the correct number of dimensions. We have further tidied the expressions [17] by use of the identity (B.0.2),

$$\sum_{n=1}^{\infty}\cos(n\kappa\epsilon) = -\frac{1}{2}, \tag{4.9.31}$$

to express $\langle\phi^2\rangle^{\mathcal{M}}_{unren}$ as a double sum over the standard mode minus the $\omega = 0$ modes (note $\omega = n$ for $d = 5$).

For a massless field we find

$$\alpha_d 2^{\frac{d}{2}-1}\beta^{2-d}\sum_{n=1}^{\infty} n^{2-d} = \lim_{\epsilon\to 0}\left[\frac{\kappa}{\pi}\sum_{n=1}^{\infty}\cos(\omega\epsilon)\sum_{l=0}^{\infty}\tilde{N}_{l,d}G_l^{\frac{d-3}{2}}r^{3-d}\left[I_\alpha(nr)K_\alpha(nr) - \frac{1}{2l+d-3}\right] - \frac{\alpha_d}{4}2^{\frac{d}{2}}\epsilon^{2-d}\right]. \tag{4.9.32}$$

For a massive field in $d = 5$ we obtain

$$\frac{1}{16\pi^3}\int_m^{\infty}\frac{\omega^2-m^2}{e^{\beta\omega}-1}d\omega = \lim_{\epsilon\to 0}\left[\frac{\kappa}{\pi}\sum_{n=1}^{\infty}\cos(\omega\epsilon)\sum_{l=0}^{\infty}\tilde{N}_{l,5}G_l^1 r^{-2}\left[I_\alpha(\Omega r)K_\alpha(\Omega r) - I_\alpha(mr)K_\alpha(mr)\right] - \frac{\alpha_5}{\sqrt{2}}\left(\frac{2}{\epsilon^{\frac{3}{2}}} - \frac{m^2}{\epsilon^{\frac{1}{2}}}\right)\right] \tag{4.9.33}$$

and in $d = 3$ we find

$$\frac{1}{2\pi\beta}\ln\left(\frac{e^{\beta m}}{e^{\beta m}-1}\right) = \lim_{\epsilon\to 0}\left[\frac{\kappa}{\pi}\sum_{n=1}^{\infty}\cos(\omega\epsilon)\sum_{l=0}^{\infty}\left[I_\alpha(\Omega r)K_\alpha(\Omega r) - I_\alpha(mr)K_\alpha(mr)\right] - \frac{\alpha_3}{\sqrt{2}\epsilon}\right]. \tag{4.9.34}$$

All of the above will be used from §4.11 onwards.

4.10 The Modified Abel-Plana Formula

In a final step before we return to our renormalisation problem we introduce the Abel-Plana formula (APF) the use of which will be analogous to that of the Watson-Sommerfeld

formula on the brane, see §3.7. The common form of the APF is the following [62]

$$\sum_{n=0}^{\infty} f(n) = \int_0^{\infty} f(x)dx + \frac{1}{2}f(0) + i\int_0^{\infty} \frac{f(ix) - f(-ix)}{e^{2\pi x} - 1}dx \tag{4.10.1}$$

which holds for $f(x)$ satisfying the following

$$\lim_{y\to\infty} e^{-2\pi y}|f(x+iy)| = 0 \tag{4.10.2}$$

uniformly on any finite interval of x. Importantly it also requires the analyticity of $f(x)$ in the right hand half-plane [28].

The APF can be extended for non-integrable branch-point singularities in the modified Abel-Plana formula (MAPF), derived in [28], resulting in

$$\begin{aligned}\sum_{n=0}^{\infty} \frac{f(n)}{(n^2+w^2)^{k+1/2}} &= \int_0^{\infty} \frac{f(x)}{(x^2+w^2)^{k+1/2}}dx \\ &- i\pi \underset{z=0}{Res}\left(\frac{f(z)}{(n^2+w^2)^{k+1/2}}\frac{1}{1-e^{-2\pi z}}\right) + 2(-1)^k\int_w^{\infty}\frac{\Delta h(x)}{(x-w)^{k+1/2}}dx\end{aligned} \tag{4.10.3}$$

where

$$\Delta h(x) = \frac{f(xe^{i\pi/2})}{(x+w)^{k+1/2}}\frac{1}{e^{2\pi x}-1}. \tag{4.10.4}$$

The form of the initial sum in this expression is similar in form to our WKB terms in §4.4 and this connection has been investigated before [68].

We may express our ith beta term as the following

$$\beta_{i\omega l} = \sum_{j=0}^{2i} C_{ij}(r)\frac{n^{2j}}{[\Omega^2+n^2]^{i+j+1/2}}, \tag{4.10.5}$$

where we note $\omega = n$ for $d = 5$. The object Ω represents the relevant terms gathered from

$\chi_{\omega l}$ which for our curved spacetime is

$$\Omega = \frac{l+1}{r}\sqrt{f} \tag{4.10.6}$$

and for a Minkowski spacetime has $f \to 1$. The C_{ij} are functions of r but importantly are independent of n

We now consider the n sum over an individual j term and apply the MAPF. A simplification is made when looking at (4.10.3) by analysing the difference of the Taylor expansion of the argument of the residue with the integrand of the final integral as detailed in [28]. This results in [68]

$$\sum_{n=0}^{\infty} \frac{n^{2j}}{[\Omega^2+n^2]^{i+j+1/2}} = -\frac{\delta_{j0}}{2\Omega^{2i+1}} + \int_0^{\infty} \frac{n^{2j}}{[\Omega^2+n^2]^{i+j+1/2}} dn + 2(-1)^{i+j} \frac{\sqrt{\pi}}{\Gamma(i+j+1/2)} \int_{\Omega}^{\infty} \frac{h^{(i+j)}(s)}{(s-\Omega)^{\frac{1}{2}}} ds \tag{4.10.7}$$

where δ_{j0} is the standard Kronecker delta and $h(s)$ is defined by

$$h(s) = \frac{(-1)^j s^{2j}}{(s+\Omega)^{i+j+1/2}} \frac{1}{e^{2\pi s}-1}, \tag{4.10.8}$$

such that $h^{(i)}(s)$ means the ith derivative of h with respect to s.

The first integral in the right hand side of (4.10.7) can be performed explicitly [68]

$$\int_0^{\infty} \frac{n^{2j}}{[\Omega^2+n^2]^{i+j+1/2}} dn = \frac{1}{\Omega^{2i}} \frac{\Gamma(i)\Gamma(j+1/2)}{2\Gamma(i+j+1/2)} \tag{4.10.9}$$

which allows us to state

$$\sum_{n=1}^{\infty}\beta_{i\omega l} = -\frac{C_{i0}(r)}{2\Omega^{2i+1}} + \sum_{j=0}^{2i}\frac{C_{ij}(r)}{2\Omega^{2i}}\frac{\Gamma(i)\Gamma(j+1/2)}{\Gamma(i+j+1/2)} + \sum_{j=0}^{2i}\frac{2C_{ij}(r)(-1)^{i+j}\sqrt{\pi}}{\Gamma(i+j+1/2)}\int_{\Omega}^{\infty}\frac{h^{(i+j)}(s)}{(s-\Omega)^{\frac{1}{2}}}ds. \quad (4.10.10)$$

An important note is that the above methodology could as easily have been applied to the internal l sum rather than the outer n sum. This would be done by re-expression of the right hand side of (4.10.5) so that the C_{ij} and Ω contain only n and r. This freedom will allow us to apply the MAPF at different stages of analysis, whether to achieve calculation or to study the behaviour of either sum. The specifics of using the MAPF in our particular problem will be discussed as they arise.

4.11 Implementing the Minkowski Bulk

We will now make use of the information gathered about the Minkowski bulk in an attempt to express $G_{E,sing}$ in a useful manner. We take $G_{E,sing}$ from equation (4.3.11) and restate it here taking into account that we wish to study a massless field on the black hole spacetime and that we will ultimately let $\epsilon \to 0$,

$$G_{E,sing} = \frac{1}{8f^{\frac{3}{2}}\pi^2}\left[\frac{1}{\epsilon^3} + \frac{f'^2}{32\epsilon}\right]. \quad (4.11.1)$$

Note that the lack of superscript notation now refers to quantities relating to our massless field on the $d = 5$ Schwarzschild-Tangherlini spacetime.

Now we use the fact that the time interval $\epsilon = t - t'$ is identical in both the Schwarzschild-Tangherlini and Minkowski spacetimes. This means we may look at sections §4.9.2 to §4.9.4 to find alternate methods of expressing powers of epsilon. First note that from (4.9.29)

we have

$$\frac{1}{\epsilon^3} = \frac{1}{\sqrt{2}\alpha_5} G^{\mathcal{M},m=0}_{E,sing,5d}, \tag{4.11.2}$$

however from (4.9.30) $G^{\mathcal{M},m=0}_{E,sing,5d}$ can be expressed as a combination of its associated renormalised vacuum polarisation and mode sum hence we can write

$$2T^3\zeta(3) = \lim_{\epsilon\to 0}\left[\frac{\tilde{\kappa}}{\sqrt{2}\pi\alpha_5}\sum_{n=1}^{\infty}\sum_{l=0}^{\infty}\tilde{N}_{5,l}G^1_l\left[\tilde{C}_{\omega l}\tilde{p}_{\omega l}\tilde{q}_{\omega l} - \tilde{C}_{0l}\tilde{p}_{0l}\tilde{q}_{0l}\right] - \frac{1}{\epsilon^3}\right]. \tag{4.11.3}$$

We have chosen to leave the modes in this form for now, we may later introduce their exact Bessel forms.

We are able to implement this combination as we have calculated $\langle\phi^2\rangle^{\mathcal{M}}_{\text{ren}}$ in two distinct ways. First we made use of §4.9.4 to calculate it directly. Secondly we have used the same approach as we have in our black hole spacetimes by setting the metric function to unity ($f \equiv 1$) and finding the exact mode solutions. By definition these different approaches give the same result.

Similarly we may look at the case of $d = 3$ Minkowski case and write

$$\frac{T}{\sqrt{2}\alpha_3\pi}\ln\left(\frac{e^{\beta m}}{e^{\beta m}-1}\right) = \lim_{\epsilon\to 0}\left[\frac{\sqrt{2}\hat{\kappa}}{\pi\alpha_3}\sum_{n=1}^{\infty}\sum_{l=0}^{\infty}\left[\hat{C}_{\omega l}\hat{p}_{\omega l}\hat{q}_{\omega l} - \hat{C}_{0l}\hat{p}_{0l}\hat{q}_{0l}\right] - \frac{1}{\epsilon}\right]. \tag{4.11.4}$$

Before proceeding further we must take into account that we are now considering three different spacetimes (one Schwarzschild-Tangherlini spacetime and two Minkowski spacetimes) for which we have derived terms with almost identical notation. Firstly we must address that we have introduced quantities $\tilde{\kappa}$ and $\hat{\kappa}$ into equations (4.11.3) and (4.11.4) without proper definition. In the black hole spacetime calculation these objects would be the specific gravities but this has no meaning in a Minkowski spacetime. To make this meaningful, and further simplify differences between the spacetimes, we choose that all three spacetimes contain fields at the same temperature T and hence, as $T = 2\pi\kappa$,

we also choose to fix $\tilde{\kappa} = \hat{\kappa} = \kappa$. Secondly we know that any separation in point split variables, whether temporal or in primary angle θ_1, can be chosen to be identical in all three. For example we choose $\epsilon = t - t'$ to be the same for all three spacetimes. However it is highly unlikely that radial measurements will match identically between the spacetimes hence we clarify our ongoing notation. We introduce two new radial variables ρ and σ such that

$$\begin{aligned} p_{\omega l} &= p_{\omega l}(r) \\ \tilde{p}_{\omega l} &= \tilde{p}_{\omega l}(\rho) \\ \hat{p}_{\omega l} &= \hat{p}_{\omega l}(\sigma) \end{aligned} \tag{4.11.5}$$

and in this example we retain characters with a tilde in association with a massless field in $d = 5$ Minkowski and those with hats for a massive field in $d = 3$ Minkowski. During the course of this approach we will look for mappings $\rho = \rho(r)$ and $\sigma = \sigma(r)$ so that final calculations are made over one radial variable.

Now we collect our terms by considering equations (4.11.3), (4.11.4) and (4.11.1) then expressing the new form of the vacuum polarisation (4.7.2), after taking the limit $\epsilon \to 0$,

$$\begin{aligned} \langle\phi^2\rangle_{\text{ren}} =& \frac{\kappa}{2\pi} \sum_{n=-\infty}^{\infty} \sum_{l=0}^{\infty} N_l G_l \left[C_{\omega l} p_{\omega l} q_{\omega l} - \beta(r) \right] \\ &+ \frac{1}{8 f^{\frac{3}{2}} \pi^2} \left(2T^3 \zeta(3) + \frac{T}{\sqrt{2}\alpha_3 \pi} \ln\left(\frac{e^{\beta m}}{e^{\beta m} - 1} \right) \right) \\ &+ \frac{\kappa}{\pi} \sum_{n=1}^{\infty} \sum_{l=0}^{\infty} N_l G_l \left(\beta(r) - \beta_0(r) \right) \\ &- \frac{\kappa}{8\sqrt{2} f^{\frac{3}{2}} \pi^3} \left(\frac{1}{\alpha_5} \sum_{n=1}^{\infty} \sum_{l=0}^{\infty} N_l G_l \left[\tilde{C}_{\omega l} \tilde{p}_{\omega l} \tilde{q}_{\omega l} - \tilde{C}_{0l} \tilde{p}_{0l} \tilde{q}_{0l} \right] \right. \\ &\qquad \left. + \frac{f'^2}{16\alpha_3} \sum_{n=1}^{\infty} \sum_{l=0}^{\infty} \left[\hat{C}_{\omega l} \hat{p}_{\omega l} \hat{q}_{\omega l} - \hat{C}_{0l} \hat{p}_{0l} \hat{q}_{0l} \right] \right), \end{aligned} \tag{4.11.6}$$

after some tidying. Note that the above onwards we remove the tilde notation from the

degeneracy factor, N_l, to avoid confusion with terms from the massless field in the $d = 5$ Minkowski spacetime. This will also help make it clear that this factor is dependent on dimension only, not the spacetime metric.

In tidying equation (4.11.6) the limit on epsilon has been carried out leaving an object that we may proceed to attempt to calculate. The order of the terms has been rearranged on purpose; lines one and two are both finite (except potentially at the horizon but that is not a renormalisation issue), lines three to five (hereafter referred to as the divergent terms) contain all the information concerning the renormalised divergence and it is these we will look at next. However note that this method has come at the cost of introducing a free parameter, the mass of the $d = 3$ Minkowski field. Although we have managed to construct an object of the type we know in principle how to calculate we must now be wary of introducing any fine tuning issues.

The analysis of the divergent terms will be qualitatively and very briefly summarised here as no matching of the radial coordinates leads to a regular result. Details of the analysis methods that proved useful will be covered in the next section where an improved implementation is attempted and a more thorough discussion of implementation is given.

We know from sources like [75] that double sums such as in line three of (4.11.6) function such that the result of the internal sum raises the order of the indexed variable of the outer sum. Hence we desire an order of the inner summand so that its sum does not raise the order of the outer summand to the point that the outer sum converges so slowly that it is not practically calculable (convergence accelerators can be used but lose accuracy). The structure of the inner and outer summands can be studied using one of, or in combinations of, techniques such as direct numerical summation, expansions in inverse order of indexed variables and applications of the Abel-Plana formula (original and modified). It is also possible to investigate the high order l and ω behaviour separately by introducing WKB approximations for the Minkowski modes. This may seems superfluous as we have analytic

results for the modes but analysis of our combinations of modified Bessel functions can be problematic; for testing radial matchings they can be highly oscillatory and have very large gradients near the horizon often smearing out numerical calculations. Numerical tests to achieve a final result for the vacuum polarisation were further complicated by the presence of the $f^{-\frac{3}{2}}$ multiplying the Minkowski terms creating a non-renormalisation related divergence at the horizon.

In this case no combination of $\rho(r)$ and $\sigma(r)$ could be found that resulted in a regular output. An inverse power expansion of the inner summand over l showed that for any combination of radial matching a term of $O(1)$ remained, not only not low enough for the outer sum but leading to a divergence on its own. This should not be possible as our setup is intended to be regular by definition implying some detail was missing. Of interest is that the next to leading order term was $O(l^{-3})$, sufficient to proceed if potentially making both sums slow to converge. This shows promise and again implies that a small change in the methodology should provide the desired result. This is potentially a result of the Minkowski spacetime Green's functions not capturing all the angular behaviour of the curved spacetime Green's functions.

In the interest of seeing if this failure in finding a regular result was due to our choice of expressing $G_{E,sing}$ in (4.11.1) in terms of a massless field in $d = 5$ and a massive field in $d = 3$ Minkowski spacetimes, other combinations of Minkowski spacetime fields were tested. A few were found that could be combined to match (4.11.1) by use of expressions such as in (4.11.2), for example

$$G_{E,sing} = \frac{1}{f^{\frac{3}{2}}}\left[\left(1+\frac{f'^2}{16m^2}\right)G^{\mathcal{M},m=0}_{E,sing,5d} - \frac{f'^2}{16m^2}G^{\mathcal{M},m\neq 0}_{E,sing,5d}\right]. \tag{4.11.7}$$

All these cases demonstrated the same outcomes as discussed above.

Comparing the work of this section to that carried out in §4.8, both methods produce terms that treat the order of l in the inner summand as having not changed from the $d = 4$

case. We know that the order has increased and hence both have failed to capture some piece of information. Interestingly the size of the terms at orders $O(1)$ and $O(l^{-3})$ that remained in the best coordinate matching attempts were quite small and simple seemingly indicating that if there was one more variable to be adjusted or if some change had been made much earlier in construction of the inner summand then they could be removed. In the next section we proceed with implementing the second of these concepts demonstrating in more detail the analysis of the summands in question.

4.12 Unphysical Divergences in the Bulk

This approach is inspired from the results of the previous section reminding us of the work carried out in §3.3. In that section an inner divergent sum was found to be unphysical from its setup and its summand was adjusted at the beginning of the calculation to make a guarantee a regular sum. The setup for the $d = 5$ bulk calculation is identical except in the number of dimensions and so we may proceed with attempting a similar approach.

First though we must follow up on comments made at the end of §3.3 concerning the rigour of this method. Two methods have been used to calculate the terms used to adjust the unphysical sum, the first in [3] used a direct method of examining an expansion of the summand in inverse powers of the sum's variable to find terms that once removed then regularise the sum. The second method, in [75] and in this work in §3.3, is more rigorous in its justification of why those specific terms must be removed. However neither method considers a potential complication namely whether there are any lower order corrections. For a relevant example consider Hadamard renormalisation in §2.9, it is clear that under many circumstances the divergent terms, $G_{E,sing}$, contain a finite contribution that has no effect on the divergence structure but is required for accurate renormalisation. Neither of the two above approaches to the unphysical divergence problem can justify that they should not contain terms of lower order than $O(l^{-1})$. An important question then is what

difference could lower order terms make. In the $d = 4$ or brane cases the additional terms cannot contain any n of order higher than $O(n^{-4})$. Any such terms would interfere with the divergence structure of the outer sum and we have a strict renormalisation scheme there that has worked in many situations. Any lower order terms would inevitably depend on r but we can claim with confidence that such terms cannot diverge at the horizon or infinity due to the required regularity of our Hartle-Hawking state at these points. Now, knowing the previous two facts and that this work is an extension of the brane case, we can say that the presence of the lower order terms is of lesser importance to our work here. Lower order terms cannot interfere with our attempt to find a method of handling renormalisation terms for the $d = 5$ bulk. Further, for purposes of interpreting final results, they cannot result in any divergences in the final calculation of the vacuum polarisation. Such divergences would be the only occurrences that could imply a breakdown of the RSET and an unphysical situation. We must accept all of the above and in fact find advantage in it, with this information we can justify using either method presented for handling unphysical divergences as we are primarily concerned with finding a method to handle renormalisation. We will choose whichever makes calculation more efficient.

We begin by introducing a function, $g_{\omega l}(r)$, which represents the terms to be subtracted within the summand and is defined by writing the Euclidean Green's function as

$$G_E(x, x') = \frac{\kappa}{2\pi} \sum_{n=-\infty}^{\infty} e^{i\omega\epsilon} \sum_{l=0}^{\infty} N_l G_l \left[C_{\omega l} p_{\omega l} q_{\omega l} - g_{\omega l} \right] \tag{4.12.1}$$

such that the inner sum is regular. Note that we set $N_l \equiv \tilde{N}_{l,5}$ and $G_l \equiv G_l^1$, this is to avoid confusion with the use of the tilde and that in this section we have $d = 5$. Also the values of the degeneracy factor, N_l, and Gegenbauer polynomial, G_l, depend only on the hyperspherical symmetries of the spacetime and its number of dimensions, as these are the same for Schwarzschild-Tangherlini and Minkowski spacetimes no additional indices are required.

We can now use the form of equation (4.12.1) and extend it to Minkowski spacetimes. We find the following expressions of the form of equation (4.3.12) for the vacuum polarisation on our curved spacetime and our massless, and massive, fields on Minkowski spacetimes. In this section we will use the expression of the renormalisation terms given in (4.11.7) so all spacetimes have five dimensions;

$$\begin{aligned}
\langle\phi^2\rangle_{\text{ren}} &= \lim_{\epsilon\to 0}\left[\frac{\kappa}{2\pi}\sum_{n=-\infty}^{\infty}e^{i\omega\epsilon}\sum_{l=0}^{\infty}N_l G_l\left[C_{\omega l}p_{\omega l}q_{\omega l}-g_{\omega l}\right]-\frac{\sqrt{2}\alpha_5}{f^{\frac{3}{2}}}\left(\frac{1}{\epsilon^3}+\frac{f'^2}{32\epsilon}\right)\right]\\
\langle\phi^2\rangle^{\mathcal{M}}_{\text{ren}} &= \lim_{\epsilon\to 0}\left[\frac{\kappa}{2\pi}\sum_{n=-\infty}^{\infty}e^{i\omega\epsilon}\sum_{l=0}^{\infty}N_l G_l\left[\tilde{C}_{\omega l}\tilde{p}_{\omega l}\tilde{q}_{\omega l}-\tilde{g}_{\omega l}\right]-\frac{\sqrt{2}\alpha_5}{\epsilon^3}\right]\\
&= 2\sqrt{2}\alpha_5 T^3\zeta(3)\\
\langle\phi^2\rangle^{\mathcal{M},m}_{\text{ren}} &= \lim_{\epsilon\to 0}\left[\frac{\kappa}{2\pi}\sum_{n=-\infty}^{\infty}e^{i\omega\epsilon}\sum_{l=0}^{\infty}N_l G_l\left[\hat{C}_{\omega l}\hat{p}_{\omega l}\hat{q}_{\omega l}-\hat{g}_{\omega l}\right]-\frac{\alpha_5}{\sqrt{2}}\left(\frac{2}{\epsilon^3}-\frac{m^2 f}{\epsilon}\right)\right]\\
&= \frac{S_3}{(2\pi)^4}\int_m^{\infty}\frac{\omega^2-m^2}{e^{\beta\omega}-1}d\omega \qquad \text{where} \qquad S_3 = 2\frac{\pi^2}{\Gamma(2)}.
\end{aligned} \tag{4.12.2}$$

We continue a similar notation scheme to that used in §4.11 such that a tilde refers to quantities referring to a massless field in a $d = 5$ Minkowski spacetime and a hat now refers to quantities relating to a massive field in a $d = 5$ Minkowski spacetime. Note that this means we have three introduced functions, $g_{\omega l}$, $\tilde{g}_{\omega l}$ and $\hat{g}_{\omega l}$ however as a group they will be referred to as the functions $g_{\omega l}$.

We now combine equations (4.12.2) and equation (4.11.7) to provide one expression

for our vacuum polarisation in which we have take the limit $\epsilon \to 0$,

$$\begin{aligned}\langle\phi^2\rangle_{\text{ren}} =&\frac{\kappa}{2\pi}\sum_{n=-\infty}^{\infty}\sum_{l=0}^{\infty}N_l G_l\left[C_{\omega l}p_{\omega l}q_{\omega l}-g_{\omega l}\right]\\&-\frac{1}{f^{\frac{3}{2}}}\left[\left(1+\frac{f'^2}{16m^2}\right)\left(\frac{\kappa}{2\pi}\sum_{n=-\infty}^{\infty}\sum_{l=0}^{\infty}N_l G_l\left[\tilde{C}_{\omega l}\tilde{p}_{\omega l}\tilde{q}_{\omega l}-\tilde{g}_{\omega l}\right]-\langle\phi^2\rangle_{\text{ren}}^{\mathcal{M}}\right)\right.\\&\left.-\frac{f'^2}{16m^2}\left(\frac{\kappa}{2\pi}\sum_{n=-\infty}^{\infty}\sum_{l=0}^{\infty}N_l G_l\left[\hat{C}_{\omega l}\hat{p}_{\omega l}\hat{q}_{\omega l}-\hat{g}_{\omega l}\right]-\langle\phi^2\rangle_{\text{ren}}^{\mathcal{M},m}\right)\right],\end{aligned} \tag{4.12.3}$$

such that now all we need do is find a way to calculate this object.

We begin by breaking equation (4.12.3) into pieces. First notice that the introduction of WKB approximation terms and splitting of the sum allows line one of this equation to be written as

$$\frac{\kappa}{\pi}\sum_{n=1}^{\infty}\sum_{l=1}^{\infty}N_l G_l\left[C_{\omega l}p_{\omega l}q_{\omega l}-\beta_{\omega l}\right]+\frac{\kappa}{\pi}\sum_{n=1}^{\infty}\sum_{l=1}^{\infty}N_l G_l\left[\beta_{\omega l}-g_{\omega l}\right]+\frac{\kappa}{2\pi}\sum_{l=1}^{\infty}N_l G_l\left[C_{0l}p_{0l}q_{0l}-g_{0l}\right]. \tag{4.12.4}$$

We then apply this expansion to the Minkowski terms as well allowing us to break equation (4.12.3) into three pieces; a finite contribution,

$$\begin{aligned}\langle\phi^2\rangle_{\text{ren,finite}} =&\frac{\kappa}{\pi}\sum_{n=1}^{\infty}\sum_{l=0}^{\infty}N_l G_l\Big(C_{\omega l}p_{\omega l}q_{\omega l}-\beta_{\omega l}\\&-\frac{1}{f^{\frac{3}{2}}}\left[\left(1+\frac{f'^2}{16m^2}\right)\left(\left[\tilde{C}_{\omega l}\tilde{p}_{\omega l}\tilde{q}_{\omega l}-\tilde{\beta}_{\omega l}\right]-\langle\phi^2\rangle_{\text{ren}}^{\mathcal{M}}\right)\right.\\&\left.-\frac{f'^2}{16m^2}\left(\left[\hat{C}_{\omega l}\hat{p}_{\omega l}\hat{q}_{\omega l}-\hat{\beta}_{\omega l}\right]-\langle\phi^2\rangle_{\text{ren}}^{\mathcal{M},m}\right)\right]\Big),\end{aligned} \tag{4.12.5}$$

a contribution with a single sum,

$$\langle\phi^2\rangle_{\text{ren,l}} = \frac{\kappa}{2\pi}\sum_{l=0}^{\infty} N_l G_l \left(C_{0l}p_{0l}q_{0l} - g_{0l} - \frac{1}{f^{\frac{3}{2}}}\left(1+\frac{f'^2}{16m^2}\right)\left[\tilde{C}_{0l}\tilde{p}_{0l}\tilde{q}_{0l} - \tilde{g}_{0l}\right] + \frac{f'^2}{16m^2 f^{\frac{3}{2}}}\left[\hat{C}_{0l}\hat{p}_{0l}\hat{q}_{0l} - \hat{g}_{0l}\right]\right) \tag{4.12.6}$$

and a contribution with a double sum,

$$\langle\phi^2\rangle_{\text{ren,n}} = \frac{\kappa}{\pi}\sum_{n=1}^{\infty}\sum_{l=0}^{\infty} N_l G_l \left(\beta_{\omega l} - g_{\omega l} - \frac{1}{f^{\frac{3}{2}}}\left(1+\frac{f'^2}{16m^2}\right)\left[\tilde{\beta}_{\omega l} - \tilde{g}_{\omega l}\right] + \frac{f'^2}{16m^2 f^{\frac{3}{2}}}\left[\hat{\beta}_{\omega l} - \hat{g}_{\omega l}\right]\right). \tag{4.12.7}$$

In order to analyse equations (4.12.5) to (4.12.7) we now require the proper form of the functions $g_{\omega l}$. We look at (4.12.2) then, as discussed at the beginning of this section, expand the inner summand in inverse powers of l and set the functions $g_{\omega l}$ be the divergent terms that we require to be removed. This results in

$$\begin{aligned} g_{\omega l} &= \frac{-16f^2 + r^2(f'^2 - 16n^2) + 4f(12 + 16l + 8l^2 - 5rf' - r^2 f'')}{64(l+1)^3 r^2 f^{\frac{3}{2}}} \\ \tilde{g}_{\omega l} &= \frac{2(l+1)^2 - n^2\rho^2}{4(l+1)^3\rho^2} \\ \hat{g}_{\omega l} &= \frac{2(l+1)^2 - (n^2+m^2)\sigma^2}{4(l+1)^3\sigma^2}. \end{aligned} \tag{4.12.8}$$

For these functions we have guaranteed all sums over l in our mode expressions (4.12.2) converge as $O(l^{-2})$. This is not ideal as we would prefer the sums over l to be $O(l^{-4})$, such an order would guarantee quick convergence of the l sum and would not substantially slow the convergence of the n sum. We may however be able to improve the order of l through radial matching.

Initial analysis of the n based summand in (4.12.7), before the l sum is performed, by expansion in inverse powers of n provides potential solutions for the radial matching. In

order to cancel leading order terms in the expansion we set

$$\rho = \sigma = \frac{r}{\sqrt{f}} \tag{4.12.9}$$

resulting in a leading order of $O(n^{-3})$. This result is not final but this radial matching produced the best results in §4.11 and also was hinted at in §4.8. This is encouraging that this radial matching provides a starting point if calculation becomes problematic.

Equation (4.12.6) is the easiest to analyse as in contains only a single sum with a summand that is analytic. The difference of the curved space modes and the function $g_{\omega l}$, multiplied by the degeneracy factor, must have a regular sum over l by construction and so these pieces can be ignored for now. Attempting to sum the remaining pieces of (4.12.6) is problematic in part because of the high frequency nature of the modified Bessel functions for large n and l and also, as in the previous attempted calculations, the presence of the metric function in the denominators. The issue of the Bessel functions can be handled by introduction of WKB approximation terms which mimic large n and l behaviour. Using the radial matching (4.12.9) the sum can then be attempted, a direct summation reveals very slow convergence behaviour and convergence accelerators must be used. We attempt both the Aitken's [1] and Shank's [64] methods as convergence accelerators. Both take a sequence of numerical partial sums and, applying their own individual algorithm, transform that sequence to a new sequence that converges to the original sum much faster but at the price of halving expected accuracy. However both methods show that this sum is not regular as repeated uses of either changes the sign of the final sum and appear to demonstrate unrestrained growth in the limit of the partial sums. The problem of repeated reflections occurring is a sign that the Aitken and Shanks approximation to the partial sums do not capture all the behaviour. This is not unexpected and means a regular overall result requires equations (4.12.7) and (4.12.6) to be calculated together as in the brane calculation (except for those pieces of (4.12.6) identified as having

a regular sum).

To consider equations (4.12.6) and (4.12.7) together we make use of identity (B.0.2) so we have one double sum to analyse. As in previous sections we neglect the details here as we immediately ran into unsurmountable difficulties. An initial attempt to roughly calculate the double sum directly showed very slow behaviour so convergence accelerators were again used. Both Shanks and Aitken's techniques were employed and displayed inconsistent results. The difference between using i and $i+1$ applications of either method showed a reflection in the r axis as before and numerical artifacts that rapidly distorted the results. This is inconclusive, either the sum is not convergent or the partial sums cannot be approximated well with either technique. The form of the summand does seem well suited to the Abel-Plana Formula so identity (4.10.1) was applied to the l sum. Within the APF is a numerical integral that must be handled carefully, this integral could not be made to give a regular result. This was problematic but not disastrous until is was discovered all other pieces of the APF gave regular results leaving nothing for the divergent numerical integral to cancel with.

We must stress that the above analysis was based upon the radial coordinate matching (4.12.9) and this was not determined to be the only radial matching that would work. Again creating a double sum and implementing the APF allows some attempt to see if another radial matching scheme would give a regular result. This analysis is extremely difficult due to the required balancing of analytic and numeric calculations and no alternate radial scheme could be identified.

We do not deny that the method in this section could be made to work but the large number of complications arising from the form of a summand including our functions $g_{\omega l}$ proved too complicated to handle. The discovery of alternate identities (for convergence acceleration, sum expansions etc.) to handle intermediate calculations may make this approach viable but the number of difficulties to be handled makes this inefficient. A

discussion of the difficulties encountered in this and previous sections is included in the beginning of the following section where we will then present our solution.

4.13 Angular Separation and a Generalised Approach

4.13.1 Motivation and Construction

In the previous sections we have outlined several methods for calculating the vacuum polarization, namely, (1) a method of dimensional reduction in §4.8, (2) an introduction of Minkowski spacetime terms only in §4.11 and (3) using Minkowski spacetime terms as well as removing unphysical divergences in §4.12. The key difficulties raised in these methods are:

- The power of l introduced by the degeneracy factor (4.2.2) increased by two between $d = 4$ and $d = 5$, this prevented the use of known identities to be used for a direct calculation as shown in §4.7
- Our assumption that the outer sum of a mode sum such as in (4.11.6) has its indexed variable raised by one order after the completion of the inner sum, as it did in the brane case, has been disproven in §4.11
- Directly matching the Minkowski Green functions, §4.11, with the curved space renormalisation terms does not provide enough flexibility to achieve canceling out all singularities
- Inverse metric functions introduced by the time split renormalisation terms complicate analysis and interfere with the cancelling of diverging terms seen in §4.11 and §4.12
- Simplifying the calculation through the removal of unphysical divergences within the l sum first introduces several problems seen in §4.12; difficulty in applying the

Abel-Plana Formula (or other such techniques) for analysis, raises the the order of the outer sum in unpredictable ways and complicates the required radial matching

A quick note on the last point is that an obvious suggestion to solve some issues is to make the terms, $g_{\omega l}$, cut off the unphysical divergence in the l based summand, including removing terms at a lower order. While this would fix the influence on the outer sum the functions $g_{\omega l}$ would become vastly more complex, hence analysis and radial matching become equally more difficult. This is true even if attempted using Mathemetica which in simpler attempts at radial matching requires guidance to find solutions without running out of memory. Hence this is not a viable solution.

In order to handle these points we introduce two changes to our approach; a switch to angular point separation and the introduction of terms we call coefficient functions. Such an approach, also using terms from Minkowski spacetimes, has been previously seen to work for a Schwarzschild spacetime threaded by a cosmic string in [68]. Angular point separation, discussed in §2.8, will affect our first point above by having the order of l in the final summand not determined until after all point coincidence has occurred. This will also make the l sum the outer sum meaning it can be more easily handled by the renormalisation terms. The angular split renormalisation terms also correct our fourth point by removing the presence of inverse metric terms. Objects we have termed coefficient functions will be used to fix the second and third points, these functions will multiply the introduced Minkowski terms and will not be fixed until radial matching is to be attempted thus rendering moot the influence of the inner sum and lack of flexibility. The fifth point is handled by a combination of the two changes, any unphysical divergences are now handled at the same time as the renormalisation so no disruptive functions need to be placed within the sums and this approach is directly tied to the radial matching therefore simplifying that step. Further as the l sum is now the outer sum we have simplified the n sum for analysis by our chosen techniques.

The structure of the curved space Green's function is that shown in equation (2.8.14) for $d = 5$ using our current notation

$$G_E(r,t,\gamma;r,t,0) = \frac{\kappa}{2\pi}\sum_{l=0}^{\infty} N_l G_l(\cos\gamma) \sum_{n=-\infty}^{\infty} C_{\omega l} p_{\omega l} q_{\omega l} \tag{4.13.1}$$

such that the vacuum polarisation is

$$\langle\phi^2\rangle_{\rm ren} = \lim_{\gamma\to 0}\left[\frac{\kappa}{2\pi}\sum_{l=0}^{\infty} N_l G_l(\cos\gamma) \sum_{n=-\infty}^{\infty} C_{\omega l} p_{\omega l} q_{\omega l} - \langle\phi^2\rangle_{\rm div}\right]. \tag{4.13.2}$$

The world function σ, calculated as in §2.10.4, for angular point splitting is

$$\sigma(\gamma) = \frac{r^2\gamma^2}{2} - \frac{r^2 f\gamma^4}{24} + O(\gamma^6) \tag{4.13.3}$$

when expressed as a series in γ. Then the general, $d = 5$ renormalisation terms for a massive field (of mass m) on a Schwarzschild-Tangherlini background are calculated from σ and (4.3.10),

$$\langle\phi^2\rangle_{\rm div} = \frac{\sqrt{2}\alpha_5}{r^3}\left[\frac{1}{\gamma^3} + \frac{f - 4m^2r^2}{8\gamma}\right]. \tag{4.13.4}$$

We now introduce fields in Minkowski space, the previous approaches used two fields so here we introduce three all in $d = 5$ spacetimes, one massless field and two of differing masses μ and ν. We now have three Minkowski spacetimes as we do not yet know if they share a radial coordinate. We retain r as the radial coordinate for our black hole spacetime and is associated with objects with no overscript. For our massless field we use radial coordinate ρ and associate it with objects with a tilde. One massive field has mass μ, radial coordinate σ and objects with a hat, the other massive field has mass ν, radial

coordinate τ and objects with a horizontal over-bar. This notation is summarised as

$$\begin{aligned} p_{\omega l} &= p_{\omega l}(r) \\ \tilde{p}_{\omega l} &= \tilde{p}_{\omega l}(\rho) \\ \hat{p}_{\omega l} &= \hat{p}_{\omega l}(\sigma) \\ \bar{p}_{\omega l} &= \bar{p}_{\omega l}(\tau). \end{aligned} \tag{4.13.5}$$

Using this notation we can implement our coefficient functions A_i by defining our renormalisation terms (4.13.4)

$$\langle\phi^2\rangle_{\rm div} = A_0\langle\phi^2\rangle^{\mathcal{M},0}_{\rm div} + A_\mu\langle\phi^2\rangle^{\mathcal{M},\mu}_{\rm div} + A_\nu\langle\phi^2\rangle^{\mathcal{M},\nu}_{\rm div} \tag{4.13.6}$$

where all $A_i = A_i(r,\rho,\sigma,\tau)$.

The Minkowski vacuum polarisations are defined as in sections §4.9.2 and §4.9.3 but with the angular separated world function (4.13.3). Hence we write the Minkowski field vacuum polarisations in terms of their mode sums for angular separation as follows, such that they have a similar structure to equation (4.13.2) with regards to the ordering of sums,

$$\begin{aligned} \langle\phi^2\rangle^{\mathcal{M},0}_{\rm ren} &= \lim_{\gamma\to 0}\left[\frac{\kappa}{2\pi}\sum_{l=0}^{\infty} N_l G_l(\cos\gamma)\sum_{n=-\infty}^{\infty}\tilde{C}_{\omega l}\tilde{p}_{\omega l}\tilde{q}_{\omega l} - \langle\phi^2\rangle^{\mathcal{M},0}_{\rm div}\right] \\ &= 2\sqrt{2}\alpha_5 T^3\zeta(3) \\ \langle\phi^2\rangle^{\mathcal{M},\mu}_{\rm ren} &= \lim_{\gamma\to 0}\left[\frac{\kappa}{2\pi}\sum_{l=0}^{\infty} N_l G_l(\cos\gamma)\sum_{n=-\infty}^{\infty}\hat{C}_{\omega l}\hat{p}_{\omega l}\hat{q}_{\omega l} - \langle\phi^2\rangle^{\mathcal{M},\mu}_{\rm div}\right] \\ &= \frac{S_3}{(2\pi)^4}\int_\mu^\infty \frac{\omega^2-\mu^2}{e^{\beta\omega}-1}d\omega \qquad \text{where} \qquad S_3 = 2\frac{\pi^2}{\Gamma(2)}. \end{aligned} \tag{4.13.7}$$

where the vacuum polarisation of the field of mass ν is the same as the field for mass μ with the masses and modes appropriately changed.

We first proceed by introducing the WKB approximation terms, we have seen in §4.12 that the modified Bessel functions are not always amenable to analysis and the WKB terms enable some tidying to be performed. The introduction to the curved space Green's function (4.13.1) appears as

$$G_E(r,t,\gamma;r,t,0) = \frac{\kappa}{2\pi}\sum_{l=0}^{\infty} N_l G_l(\cos\gamma) \sum_{n=-\infty}^{\infty} [C_{\omega l} p_{\omega l} q_{\omega l} - \beta_{\omega l}] + \frac{\kappa}{2\pi}\sum_{l=0}^{\infty} N_l G_l(\cos\gamma) \sum_{n=-\infty}^{\infty} \beta_{\omega l} \quad (4.13.8)$$

and is simply extended to the Minkowski expressions.

We now combine equations (4.13.6), (4.13.7) and (4.13.8) into equation (4.13.2). The result is large and unwieldy so we do not display it yet. The result now only contains γ within well-behaved Gegenbauer polynomials and so we may take the limit $\gamma \to 0$. After some re-arrangement the curved space vacuum polarisation can then be written

$$\begin{aligned}\langle\phi^2\rangle_{\rm ren} =& \frac{\kappa}{2\pi}\sum_{l=0}^{\infty} N_l G_l(1) \sum_{n=-\infty}^{\infty} \Big([C_{\omega l} p_{\omega l} q_{\omega l} - \beta_{\omega l}] - A_0 \left[\tilde{C}_{\omega l}\tilde{p}_{\omega l}\tilde{q}_{\omega l} - \tilde{\beta}_{\omega l}\right] \\ & - A_\mu \left[\hat{C}_{\omega l}\hat{p}_{\omega l}\hat{q}_{\omega l} - \hat{\beta}_{\omega l}\right] - A_\nu \left[\bar{C}_{\omega l}\bar{p}_{\omega l}\bar{q}_{\omega l} - \bar{\beta}_{\omega l}\right] \Big) \\ & + A_0\langle\phi^2\rangle_{\rm ren}^{\mathcal{M},0} + A_\mu\langle\phi^2\rangle_{\rm ren}^{\mathcal{M},\mu} + A_\nu\langle\phi^2\rangle_{\rm ren}^{\mathcal{M},\nu} \\ & + \frac{\kappa}{2\pi}\sum_{l=0}^{\infty} N_l G_l(1) \sum_{n=-\infty}^{\infty} \left[\beta_{\omega l} - A_0\tilde{\beta}_{\omega l} - A_\mu\hat{\beta}_{\omega l} - A_\nu\bar{\beta}_{\omega l}\right].\end{aligned} \quad (4.13.9)$$

This expression shall be treated as three pieces; line one is the mode sums minus large n and l behaviour, line two is the Minkowski vacuum polarisations and line three deals with the WKB approximation terms. Note that, excluding the potential influence of the coefficient functions A_i, lines one and two are by definition finite, line three should then also be finite (as otherwise our model would be unphysical) but contains cancelling divergences so deserves more care. The important point from this is that the fact we have introduced three unspecified functions should allow us to find a combination that leaves

all three lines finite and thus easier to calculate.

Before we analyse any particular line we present information available about the coefficient functions A_i at this time. From equation (4.13.4) we find the massless Schwarzschild-Tangherlini and Minkowski divergent terms

$$\begin{aligned}
\langle\phi^2\rangle_{\text{div}} &= \frac{\sqrt{2}\alpha_5}{r^3}\left[\frac{1}{\gamma^3}+\frac{f}{8\gamma}\right] \\
\langle\phi^2\rangle_{\text{div}}^{\mathcal{M},0} &= \frac{\sqrt{2}\alpha_5}{\rho^3}\left[\frac{1}{\gamma^3}+\frac{1}{8\gamma}\right] \\
\langle\phi^2\rangle_{\text{div}}^{\mathcal{M},\mu} &= \frac{\sqrt{2}\alpha_5}{\sigma^3}\left[\frac{1}{\gamma^3}+\frac{1-4\mu^2\sigma^2}{8\gamma}\right].
\end{aligned} \tag{4.13.10}$$

Using these divergent terms we may compare coefficients between equations (4.13.4) and (4.13.6). This comparison finds A_0 and A_μ in terms of only A_ν,

$$\begin{aligned}
A_0 &= \frac{\rho^3}{r^3\sigma^3\tau^3}\left(\sigma^3\tau^3 - A_\mu r^3\tau^3 - A_\nu r^3\sigma^3\right) \\
&= \frac{\rho^3}{4r^3\mu^2\sigma^2\tau^3}\left((4\mu^2\sigma^2-1)\tau^3 + 4A_\nu r^3(\nu^2\tau^2-\mu^2\sigma^2) + f\tau^3\right), \\
A_\mu &= \frac{\sigma}{4r^3\mu^2\tau}\left(\tau - \tau f - 4A_\nu\nu^2 r^3\right).
\end{aligned} \tag{4.13.11}$$

We now have one undetermined function, A_ν.

4.13.2 Analysis of the Sum over WKB Terms

We begin the proper analysis of (4.13.9) by looking at line three, this line is where we expect divergences to cancel and may be the key to matching the radial coordinates. We use the Modified Abel-Plana Formula as expressed in equation (4.10.10) but first we must express our terms in a similar form as required by the formula. To begin we look at the

n sum in line three of (4.13.9) and rewrite it as

$$\begin{aligned}\sum_{n=-\infty}^{\infty}\left[\beta_{\omega l}-A_0\tilde{\beta}_{\omega l}-A_\mu\hat{\beta}_{\omega l}-A_\nu\bar{\beta}_{\omega l}\right] =&2\sum_{n=1}^{\infty}\left[\beta_{\omega l}-A_0\tilde{\beta}_{\omega l}-A_\mu\hat{\beta}_{\omega l}-A_\nu\bar{\beta}_{\omega l}\right]\\ &+\beta_{0l}-A_0\tilde{\beta}_{0l}-A_\mu\hat{\beta}_{0l}-A_\nu\bar{\beta}_{0l}.\end{aligned} \tag{4.13.12}$$

Next note that we may express a curved space beta term as in 4.4.4 [68],

$$\begin{aligned}\beta_{\omega l}&=\sum_{i=0}^{4}\sum_{j=0}^{2i}C_{ij}\frac{n^{2j}}{(n^2r^6+(l+1)^2fr^4)^{i+j+\frac{1}{2}}}\\ &=\sum_{i=0}^{4}\sum_{j=0}^{2i}D_{ij}\frac{n^{2j}}{(n^2+\Omega^2)^{i+j+\frac{1}{2}}}\end{aligned} \tag{4.13.13}$$

for

$$\Omega=\frac{l+1}{r}\sqrt{f} \tag{4.13.14}$$

where D_{ij} is the appropriate coefficient depending only on r. This is simply extended for the $n=0$ case as

$$\beta_{0l}=\sum_{i=0}^{4}D_{i0}\frac{1}{\Omega^{2i+1}} \tag{4.13.15}$$

with the value of Ω unchanged from (4.13.14). These expansions of the WKB terms are applied in the Minkowski spacetimes by setting $f\to 1$ and replacing r with the appropriate radial coordinate, any mass terms exist in the coefficients D_{ij} only and do not affect the structure.

Now we can look at the first obvious source of any divergences within the sum in (4.13.12), that is the case $i=0$ (implying $j=0$)

$$\text{summand}=\frac{1}{2r^3(n^2+\Omega^2)^{\frac{1}{2}}}-\frac{A_0}{2\rho^3(n^2+\tilde{\Omega}^2)^{\frac{1}{2}}}-\frac{A_\mu}{2\sigma^3(n^2+\hat{\Omega}^2)^{\frac{1}{2}}}-\frac{A_\nu}{2\tau^3(n^2+\bar{\Omega}^2)^{\frac{1}{2}}} \tag{4.13.16}$$

which is order $O(n^{-1})$. Inputting the expressions for A_0 and A_μ from (4.13.11) produces

a large expression that we determine is simplified by setting $\tau = \sigma = \rho$ leaving

$$\text{summand} = \frac{1}{2r^3}\left(\frac{1}{(n^2+\Omega^2)^{\frac{1}{2}}} - \frac{1}{(n^2+\tilde{\Omega}^2)^{\frac{1}{2}}}\right). \tag{4.13.17}$$

It is obvious this expression vanishes if we use the radial matching that was found in (4.12.9), hence we choose

$$\rho = \sigma = \tau = \frac{r}{\sqrt{f}}. \tag{4.13.18}$$

We then apply this same matching to the WKB terms with $n = 0$ in (4.13.12) and immediately find they cancel hence for these WKB terms $i \geq 1$.

We briefly restate the form of the MAPF that we will immediately implement, (note that although we have prepared the WKB terms to match the form of the functions in the MAPF we did not need to apply the formula to find our proposed radial matching)

$$\sum_{n=0}^{\infty} \frac{n^{2j}}{[\Omega^2+n^2]^{i+j+1/2}} = -\frac{\delta_{j0}}{2\Omega^{2i+1}} + \int_0^{\infty} \frac{n^{2j}}{[\Omega^2+n^2]^{i+j+1/2}} dn + 2(-1)^{i+j}\frac{\sqrt{\pi}}{\Gamma(i+j+1/2)}\int_{\Omega}^{\infty} \frac{h^{(i+j)}(s)}{(s-\Omega)^{\frac{1}{2}}} ds, \tag{4.13.19}$$

such that $h^{(i)}(s)$ is the ith derivative and $h(s)$ is defined by

$$h(s) = \frac{(-1)^j s^{2j}}{(s+\Omega)^{i+j+1/2}} \frac{1}{e^{2\pi s}-1}. \tag{4.13.20}$$

We also previously stated

$$\int_0^{\infty} \frac{n^{2j}}{[\Omega^2+n^2]^{i+j+1/2}} dn = \frac{1}{\Omega^{2i}} \frac{\Gamma(i)\Gamma(j+1/2)}{2\Gamma(i+j+1/2)} \tag{4.13.21}$$

however note that if $i = 0$ this has a singular result so to be implemented we require $i \geq 1$ as we have just shown. We can now the above expression of the MAPF to demonstrate it applied to one of our WKB terms. We shall use the curved space version but as before

the extension to the Minkowski terms is trivial,

$$\sum_{i=1}^{4}\sum_{j=0}^{2i}\sum_{n=1}^{\infty} D_{ij}\frac{n^{2j}}{(n^2+\Omega^2)^{i+j+\frac{1}{2}}} = \sum_{i=1}^{4}\sum_{j=0}^{2i} D_{ij}\left[-\frac{\delta_{j0}}{2\Omega^{2i+1}} + \frac{1}{2\Omega^{2i}}\frac{\Gamma(i)\Gamma(j+1/2)}{\Gamma(i+j+1/2)} + \frac{2(-1)^{i+j}\sqrt{\pi}}{\Gamma(i+j+1/2)}\int_{\Omega}^{\infty}\frac{h^{(i+j)}(s)}{(s-\Omega)^{\frac{1}{2}}}ds\right]. \quad (4.13.22)$$

We now use equation (4.13.22) and consider only the $j=0$ terms which gives (for our sample WKB term)

$$\sum_{i=1}^{4}\sum_{n=1}^{\infty} D_{i0}\frac{1}{(n^2+\Omega^2)^{i+\frac{1}{2}}} = \sum_{i=1}^{4} D_{i0}\left[-\frac{1}{2\Omega^{2i+1}} + \frac{1}{2\Omega^{2i}}\frac{\sqrt{\pi}\Gamma(i)}{\Gamma(i+1/2)} + \frac{2(-1)^{i}\sqrt{\pi}}{\Gamma(i+1/2)}\int_{\Omega}^{\infty}\frac{h^{(i)}(s)}{(s-\Omega)^{\frac{1}{2}}}ds\right]. \quad (4.13.23)$$

Note that if this expression was doubled and added to the $n=0$ beta term in (4.13.12) for the same spacetime then the first term on the right hand side would cancel with that $n=0$ term. This is true for both the curved and Minkowski spacetimes. Now look again at equation (4.13.12), in this equation we now have double the MAPF expression plus the $n=0$ beta for each spacetime hence the afore mentioned cancellation occurs.

We may now state the behaviour of a generic WKB term in line three of (4.13.9)

$$\frac{\kappa}{2\pi}\sum_{l=0}^{\infty} N_l G_l \sum_{n=-\infty}^{\infty} A\beta = \frac{\kappa}{\pi}\sum_{l=0}^{\infty} N_l G_l A \sum_{i=1}^{4}\sum_{j=0}^{2i} D_{ij}\left[\frac{1}{2\Omega^{2i}}\frac{\Gamma(i)\Gamma(j+1/2)}{\Gamma(i+j+1/2)} + \frac{2(-1)^{i+j}\sqrt{\pi}}{\Gamma(i+j+1/2)}\int_{\Omega}^{\infty}\frac{h^{(i+j)}(s)}{(s-\Omega)^{\frac{1}{2}}}ds\right] \quad (4.13.24)$$

such that $A=1$ for the Schwarzschild-Tangherlini WKB approximation, $A=A_\mu$ for the massless Minkowski case etc. It is vital to remember the behaviour displayed in (4.13.24) is only true in the context of all the WKB approximations being together as structured in equation (4.13.9) under the radial matching stated in equation (4.13.18).

We now look at the final form of equation (4.13.24), considering we really have four such terms together, and examine it as a summand over l. We see in the second term of the RHS that a series expansion in inverse l of the integrand is $O(l^{-3})$ at leading order but due to the structure of the integrand we cannot simply state the order of the resulting integral. The integral is computed numerically for every value of l and r required and due to the exponential cutoff in (4.13.20) the results rapidly diminish in size. This means that the convergence of the l sum of this term can be quickly verified by direct summation.

The first term on the RHS of (4.13.24) (which we will call the gamma term) is clearly $O(l^{-2})$ at leading order and can be handled analytically. The leading order behaviour is confirmed with a series expansion in inverse l over all the gamma terms from all the WKB approximations. In this expansion the terms at $O(l^{-2})$ and $O(l^{-3})$ depend on f and r only, inputting the correct form of the metric functions shows both terms to actually be zero. The $O(l^{-4})$ term is structurally simple and contains one unknown, the yet to be fixed A_ν. As we anticipate the other lines of (4.13.9) are finite but hard to analyse due to numerical calculations we determine A_ν here by setting the $O(l^{-4})$ term to zero, this gives

$$\begin{aligned} A_\nu = \frac{1}{240r^3\nu^2(\nu^2\tau^2-\mu^2\sigma^2)}\tau\big(&2183-60\mu^2\sigma^2-2470f+60\mu^2\sigma^2f+287f^2-2240rf' \\ &+596rff'+152r^2f'^2-320r^2f''-208r^2ff''-32r^3f'f'' \\ &+8r^4f''^2-152r^3ff^{(3)}-16r^4f'f^{(3)}-16r^4ff^{(4)}\big) \\ = \frac{1}{240r^4\nu^2(\nu^2-\mu^2)\sqrt{f}}\big(&2183f-60\mu^2r^2-2470f^2+60\mu^2r^2f+287f^3-2240rff' \\ &+596rf^2f'+152r^2ff'^2-320r^2ff''-208r^2f^2f''-32r^3ff'f'' \\ &+8r^4ff''^2-152r^3f^2f^{(3)}-16r^4ff'f^{(3)}-16r^4f^2f^{(4)}\big) \end{aligned} \tag{4.13.25}$$

which we state in full for completeness.

We can now express all three general functions in (4.13.6) in terms of only r, μ and ν as follows

$$\begin{aligned}
A_0 &= \frac{29 - 42r^2 - 3r^4 + 80r^{12}\mu^2\nu^2 - 20r^8(\mu^2+\nu^2) + 4r^6(4 + 5\mu^2 + 5\nu^2)}{80r^{12}(1-r^{-2})^{\frac{3}{2}}\mu^2\nu^2} \\
A_\mu &= \frac{-29 + 13r^2 + 16r^4 - 20r^6\nu^2}{80r^{10}(1-r^{-2})^{\frac{1}{2}}\mu^2(\mu^2-\nu^2)} \\
A_\nu &= -\frac{-29 + 13r^2 + 16r^4 - 20r^6\nu^2}{80r^{10}(1-r^{-2})^{\frac{1}{2}}\nu^2(\mu^2-\nu^2)}.
\end{aligned} \tag{4.13.26}$$

When we look at these expressions of the general functions in (4.13.26) we can discern several pieces of information. Concerning the masses we cannot have $\mu = \nu$, $\mu = 0$ or $\nu = 0$ without causing a singularity. This is expected as for any of these cases, with $\rho = \sigma = \tau$, it would reduce us from three general functions to two as in previous approaches which we demonstrated did not work. Also a singularity will be approached as $r \to 1$, this is more difficult to understand as the vacuum polarisation is regular across the horizon for our vacuum state, and has been calculated before [32], so for now we must assume this effect is negated in the final calculation.

We must also mention an issue that was first encountered with the approach in §4.11. In that approach we made use of a massive field in Minkowski spacetime and how that came at the cost of introducing a free parameter into the calculation (the mass). In our current approach we now have two free parameters which have some restrictions on their value discussed in the previous paragraph but otherwise must be kept free. If this approach only works for certain values of μ and ν then we have a fine tuning problem and our methodology will be weaker.

In summary we have demonstrated that line three of equation (4.13.9), which contains the cancellation of divergences due to renormalisation, is regular up to the potential issues at the horizon discussed directly above. From this analysis we have also been able to fix the expressions for the coefficient functions, A_i. Calculation of the final value of line

three of equation (4.13.9) will be discussed in concert with the calculation of the rest of (4.13.9) but presents no problems as all the terms are analytic barring one numerical integral (repeated in four sets) which is simple to calculate and can be demonstrated to converge rapidly.

4.13.3 Analysis of the Sums over Numerical Contributions

We now look at at the other lines of equation (4.13.9) which are based around numerical calculations. Line two reads

$$A_0\langle\phi^2\rangle^{\mathcal{M},0}_{\rm ren} + A_\mu\langle\phi^2\rangle^{\mathcal{M},\mu}_{\rm ren} + A_\nu\langle\phi^2\rangle^{\mathcal{M},\nu}_{\rm ren} \tag{4.13.27}$$

where we now know the coefficient functions (4.13.26) and have previously calculated,

$$\langle\phi^2\rangle^{\mathcal{M},0}_{\rm ren} = \frac{\zeta(3)}{(2\pi)^5} \tag{4.13.28}$$

and

$$\langle\phi^2\rangle^{\mathcal{M},m}_{\rm ren} = \frac{1}{16\pi^2}\int_m^\infty \frac{n^2-m^2}{e^{\beta\omega}-1}dn \tag{4.13.29}$$

as $\omega = n$ for $d = 5$. Although result (4.13.29) needs to calculated numerically it and result (4.13.28) are simply constants and require no more work. As in the case for the WKB terms in the last section the only complication in final calculations will be cancelling out the divergences caused by the coefficient functions, A_i.

Line one of (4.13.9) reads

$$\frac{\kappa}{2\pi}\sum_{l=0}^{\infty} N_l G_l(1) \sum_{n=-\infty}^{\infty}\Big([C_{\omega l}p_{\omega l}q_{\omega l} - \beta_{\omega l}] - A_0\left[\tilde{C}_{\omega l}\tilde{p}_{\omega l}\tilde{q}_{\omega l} - \tilde{\beta}_{\omega l}\right] - A_\mu\left[\hat{C}_{\omega l}\hat{p}_{\omega l}\hat{q}_{\omega l} - \hat{\beta}_{\omega l}\right] - A_\nu\left[\bar{C}_{\omega l}\bar{p}_{\omega l}\bar{q}_{\omega l} - \bar{\beta}_{\omega l}\right]\Big). \tag{4.13.30}$$

In practice, as for the brane calculations in §3.12, these sums need not be taken to infinity as the WKB terms cancel out any large l and n behaviour. The sums can be handled directly using the same number of l terms and n terms as in the brane case, $l = 0 \to 50$ and $n = 0 \to 8$. The program used to produce the summed numerical modes was found to produce modes that match analytic modes, where available, to a minimum of twenty seven significant figures. This provides great confidence in the results of direct summation. To facilitate easy calculation we split (4.13.30) into two pieces, for $n = 0$ and $n > 0$ then restate the forms of the modes. Hence we have

$$\frac{\kappa}{2\pi}\sum_{l=0}^{\infty} N_l G_l(1)\left(\left[C_{0l}p_{0l}q_{0l}-\beta_{0l}\right]-A_0\left[\tilde{C}_{0l}\tilde{p}_{0l}\tilde{q}_{0l}-\tilde{\beta}_{0l}\right]\right.$$
$$\left.-A_\mu\left[\hat{C}_{0l}\hat{p}_{0l}\hat{q}_{0l}-\hat{\beta}_{0l}\right]-A_\nu\left[\bar{C}_{0l}\bar{p}_{0l}\bar{q}_{0l}-\bar{\beta}_{0l}\right]\right) \quad (4.13.31)$$

where

$$\begin{aligned} C_{0l}p_{0l}q_{0l} &= \text{ numerical results from §4.6} \\ \tilde{C}_{0l}\tilde{p}_{0l}\tilde{q}_{0l} &= \frac{1}{2(l+1)\rho^2} \\ \hat{C}_{0l}\hat{p}_{0l}\hat{q}_{0l} &= \sigma^{-2}\left[I_{l+1}(\mu\sigma)K_{l+1}(\mu\sigma)\right] \\ \bar{C}_{0l}\bar{p}_{0l}\bar{q}_{0l} &= \tau^{-2}\left[I_{l+1}(\nu\tau)K_{l+1}(\nu\tau)\right]. \end{aligned} \quad (4.13.32)$$

This means $\left[\tilde{C}_{0l}\tilde{p}_{0l}\tilde{q}_{0l}-\tilde{\beta}_{0l}\right]=0$.

We also have

$$\frac{\kappa}{\pi}\sum_{l=0}^{\infty} N_l G_l(1)\sum_{n=1}^{\infty}\left(\left[C_{\omega l}p_{\omega l}q_{\omega l}-\beta_{\omega l}\right]-A_0\left[\tilde{C}_{\omega l}\tilde{p}_{\omega l}\tilde{q}_{\omega l}-\tilde{\beta}_{\omega l}\right]\right.$$
$$\left.-A_\mu\left[\hat{C}_{\omega l}\hat{p}_{\omega l}\hat{q}_{\omega l}-\hat{\beta}_{\omega l}\right]-A_\nu\left[\bar{C}_{\omega l}\bar{p}_{\omega l}\bar{q}_{\omega l}-\bar{\beta}_{\omega l}\right]\right) \quad (4.13.33)$$

where

$$\begin{aligned}
C_{\omega l}p_{\omega l}q_{\omega l} &= \text{ numerical results from §4.6} \\
\tilde{C}_{\omega l}\tilde{p}_{\omega l}\tilde{q}_{\omega l} &= \rho^{-2}\left[I_{l+1}(\omega\rho)K_{l+1}(\omega\rho)\right] \\
\hat{C}_{\omega l}\hat{p}_{\omega l}\hat{q}_{\omega l} &= \sigma^{-2}\left[I_{l+1}\left(\sqrt{(\omega^2+\mu^2)}\sigma\right)K_{l+1}\left(\sqrt{(\omega^2+\mu^2)}\sigma\right)\right] \\
\bar{C}_{\omega l}\bar{p}_{\omega l}\bar{q}_{\omega l} &= \tau^{-2}\left[I_{l+1}\left(\sqrt{(\omega^2+\nu^2)}\tau\right)K_{l+1}\left(\sqrt{(\omega^2+\nu^2)}\tau\right)\right].
\end{aligned} \tag{4.13.34}$$

This section has demonstrated that lines one and two of (4.13.9) contain no divergences due to renormalisation but have the same issue as in the previous section, the need to cancel divergences caused by the coefficient functions, A_i. In the next section we will display results of these calculations and the influence the coefficient functions have.

4.14 $\langle\phi^2\rangle_{\rm ren}$ Results Using a Generalised Approach

Here we shall begin by showing total results for $\langle\phi^2\rangle_{\rm ren}$ with different masses, μ and ν, for the Minkowski fields. This will allow us to see if these masses are in fact free parameters and how much influence the coefficient functions, A_i, hold (they strongly depend on the two masses). We will then investigate further any features that become apparent. One feature we can state immediately is that if the values of μ and ν are reversed the total is unchanged which is not unexpected from our definition in (4.13.6). Calculations were made to support this but the results are not featured as the results are identical to beyond 30 significant figures.

We display in Fig. 4.1 and Fig. 4.2 the $\langle\phi^2\rangle_{\rm ren}$ for a range of masses, μ and ν, over the region $r = r_h \to 11r_h$ (as in §3.13). In Fig. 4.3 we show a selection of mass values chosen to display the emerging pattern we will discuss. It is clear that the results in Fig. 4.1 and Fig. 4.2 appear strongly mass dependent and so we must concern ourself if our methodology requires fine tuning. Also the potential problem of a divergence at the

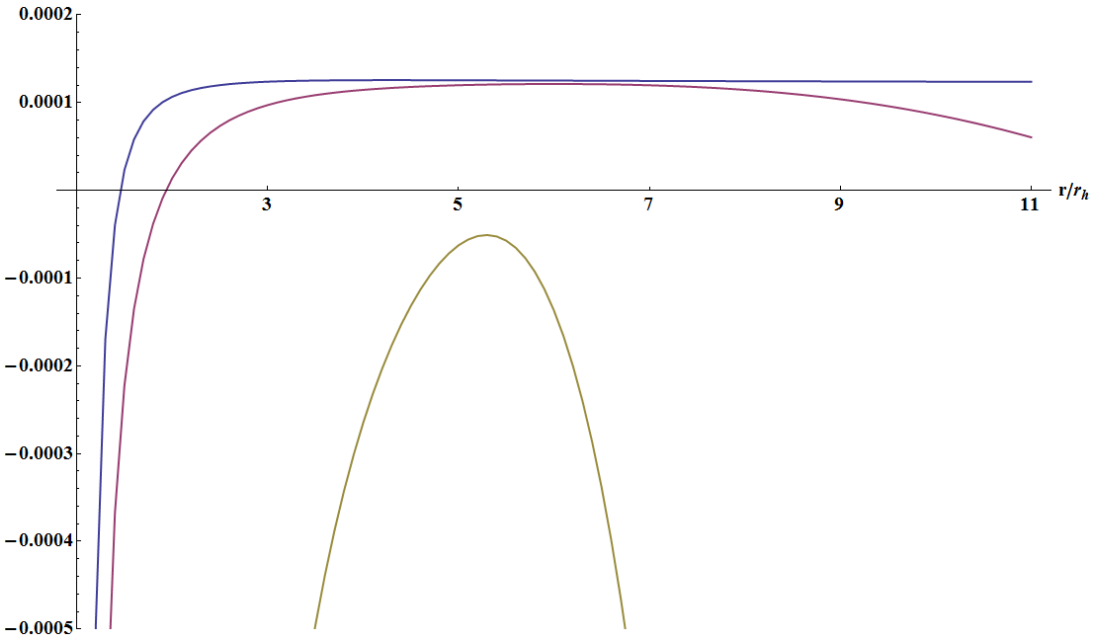

Figure 4.1: $\langle\phi^2\rangle_{\text{ren}}$ from $r = r_h$ to $r = 11r_h$, the top plot is for ($\mu = 1$, $\nu = 2$), the middle is ($\mu = 1$, $\nu = 10$) and the bottom is ($\mu = 10$, $\nu = 11$).

horizon is confirmed though interestingly whether the divergence is positive or negative seems to be mass dependent. Finally we also note that for the larger mass values the results also diverge as r tends to infinity.

Comparing all these mass values together in Fig. 4.3 shows a distinct pattern that may provide more information. As r tends to infinity the large mass values cause a negative divergence and as the mass is lowered $\langle\phi^2\rangle_{\text{ren}}$ tends to a finite value. Near the horizon large mass values again cause a negative divergence but as the mass is lowered the divergence flips sign to become a positive divergence. This poses the question of is there a specific value for the masses that provides finite values for the whole domain. Unless the masses become too high or too low we do see a finite agreement in the middle of our domain. If we increase the masses beyond those displayed here we see a curve below the r axis that diverges more strongly near the horizon and as r tends to infinity as hinted at in Fig. 4.1. Decreasing the masses simply increases the rapidity of the divergence occurring near the

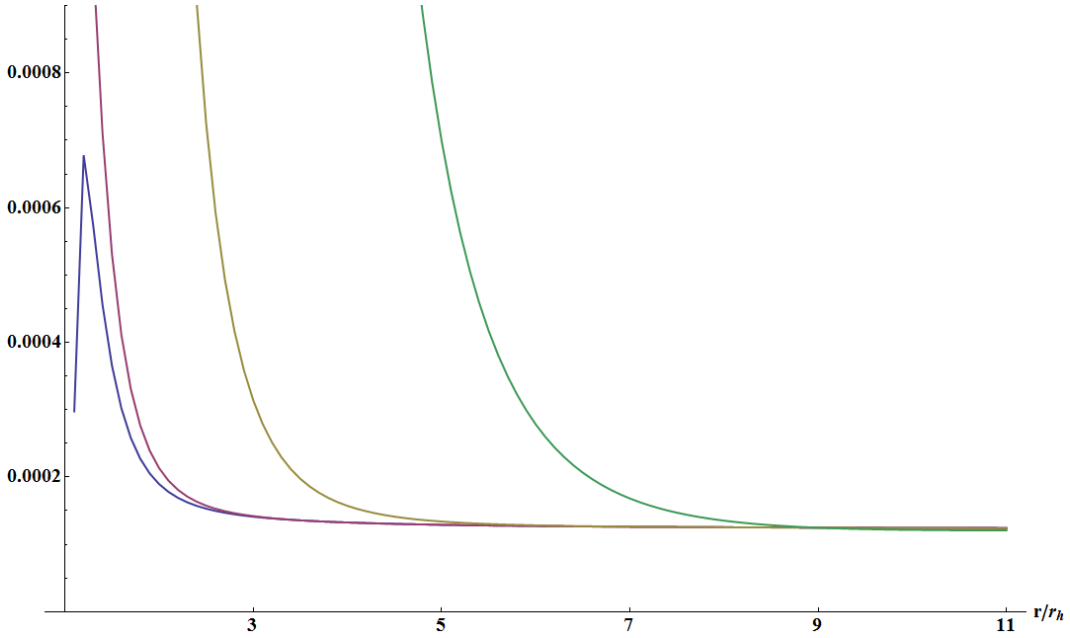

Figure 4.2: $\langle\phi^2\rangle_{\text{ren}}$ from $r = r_h$ to $r = 11r_h$ from the singularity, the plots from left to right are ($\mu = 1/4$, $\nu = 1/5$), ($\mu = 1/4$, $\nu = 1/6$), ($\mu = 1/10$, $\nu = 1/11$) and ($\mu = 1/10$ $\nu = 1/100$) respectively.

horizon as shown in Fig. 4.2.

First we look at the question of regularity across the horizon, we show a close up of this region with some relevant mass values in Fig. 4.4. We see in Fig. 4.4 that it would seem like there is an ideal set of mass values lying between ($\mu = 1/4$, $\nu = 1/6$) and ($\mu = 1/5$, $\nu = 1/6$) that would provide a regular value of $\langle\phi^2\rangle_{\text{ren}}$ across the horizon. We posit that this is not an issue of fine tuning but a relic of using the WKB approximation during our methodology which we know breaks down near the horizon, see §2.11.1. We will now display in Fig. 4.5 and Fig. 4.6 a breakdown of the components of $\langle\phi^2\rangle_{\text{ren}}$ for two of our mass choices as samples to demonstrate the behaviour.

Looking at Fig. 4.5 and Fig. 4.6, which display the components of $\langle\phi^2\rangle_{\text{ren}}$, there are many important details to keep in mind. The plots are on very different scales such that the contributions from line two of (4.13.9) (the Minkowski renormalised totals) in each are comparable. In Fig. 4.6 we see how the divergence arises as r increases with larger

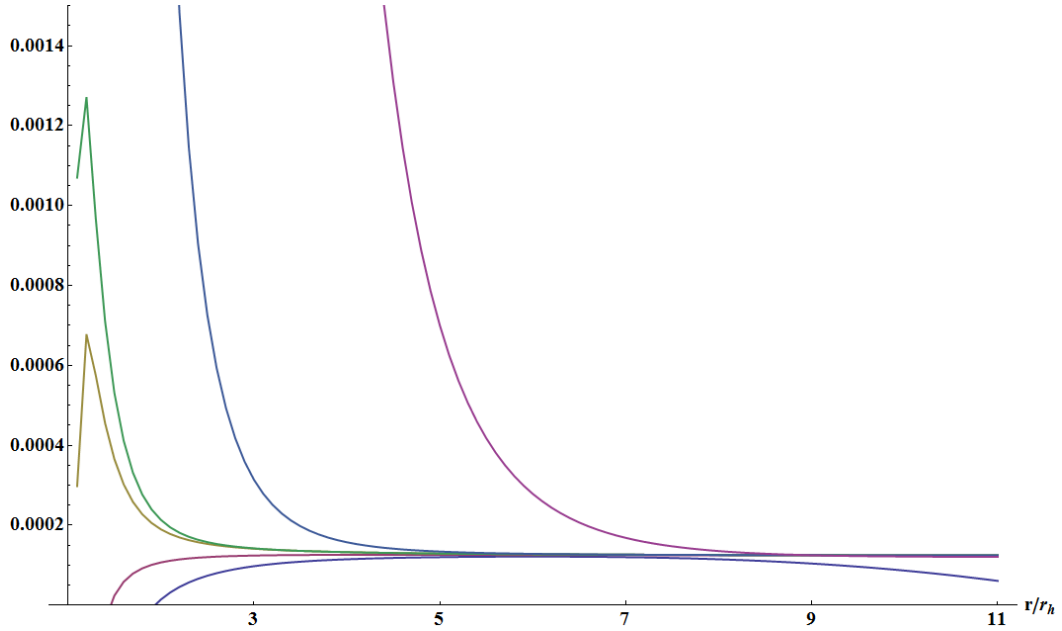

Figure 4.3: $\langle\phi^2\rangle_{\text{ren}}$ from $r = r_h$ to $r = 11r_h$ from the singularity, the plots from bottom to top show the results from Fig. 4.1 and Fig. 4.2 from masses ($\mu = 1$, $\nu = 10$) to ($\mu = 1/10$, $\nu = 1/100$).

masses. The contributions from the mode sums and the numerical part of the MAPF calculation begin to diverge with opposite signs. Then as the masses become too large these contributions no longer successfully cancel, however we must allow that this could be numeric problem caused by a lack of accuracy in our method. We also see at the horizon three strong divergences that we had hoped would cancel but the results appear to have been let down by the numerical work. A similar problem was encountered in [75] and was solved in [12] through the use of extended Green-Liouville asymptotics that guarantee all quantities are manifestly finite on the horizon.

It is strange that in comparing these results to those in Fig. 4.5 we see that the case with smaller masses has two negative divergent components and two positive (the larger mass had one and two respectively). Even with this the lower mass case still results in an overall positive divergence at the horizon indicating how closely balanced the terms are in this region. It appears that in these two cases (and in others), from the final results

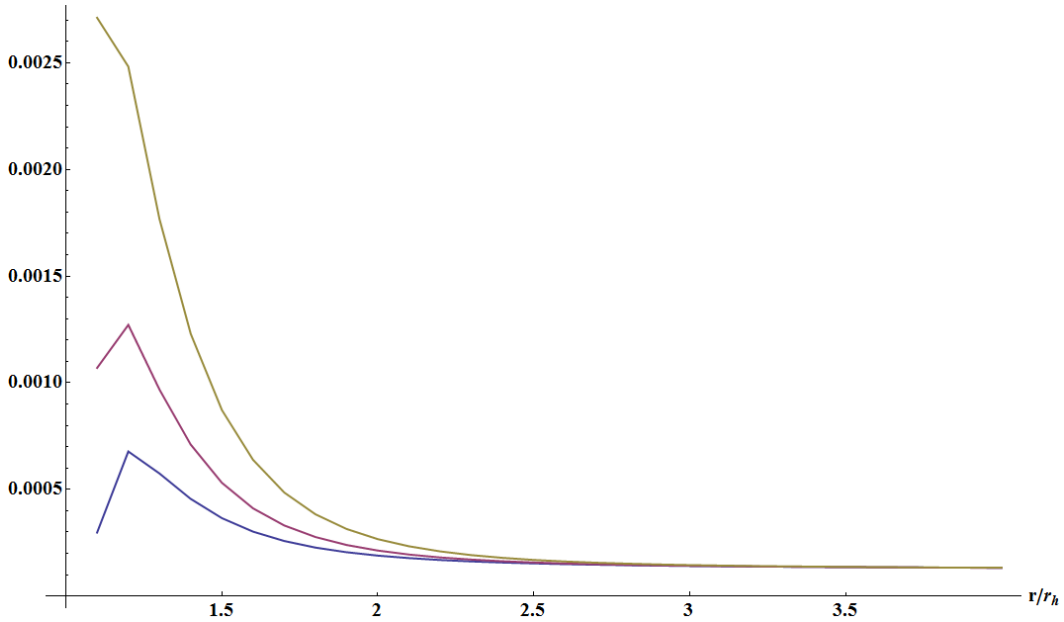

Figure 4.4: $\langle\phi^2\rangle_{\text{ren}}$ from $r = r_h$ to $r = 4r_h$, the plots from bottom to top show results for masses ($\mu = 1/4$, $\nu = 1/5$), ($\mu = 1/4$, $\nu = 1/6$) and ($\mu = 1/5$, $\nu = 1/6$).

and the analysis of the components, that these divergences should cancel. However the final calculation relies on several numerical pieces: the curved space modes from (4.6.1), the Minkowski renormalised totals (4.9.32), (4.9.33) and (4.9.34) and the integral within the MAPF (4.13.22). However none of these pieces pose difficult calculation to us after improving our numerical solving methods in this work, assuming those methods hold to be appropriate. We must turn to the role of the coefficient functions which we previously saw in (4.13.26) do diverge near the horizon. These functions were formed in section §4.13.2 based on analysis of terms containing WKB approximations which we know lose accuracy near the horizon (see §2.11). We claim the fault in final numerics lies with this approximation and that we have strongly argued that our methodology has produced a regular object to be calculated using more accurate techniques.

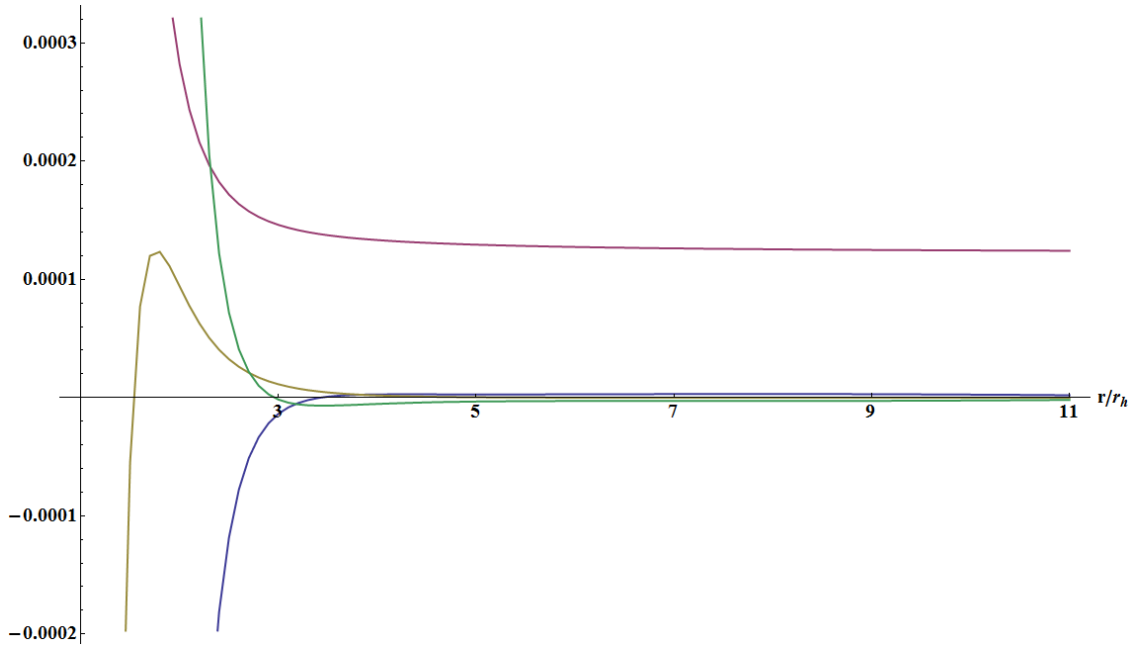

Figure 4.5: Components of $\langle\phi^2\rangle_{\text{ren}}$ from $r = r_h$ to $r = 11r_h$ with ($\mu = 1/4$, $\nu = 1/6$). The plot with negative divergence but no maximum is line one of (4.13.9), the plot that is non-zero as $r \to \infty$ is line two of (4.13.9), the plot with a maximum is the analytic calculation from the MAPF used in line three of (4.13.9) and the remaining plot is the numeric calculation from the MAPF used in line three of (4.13.9).

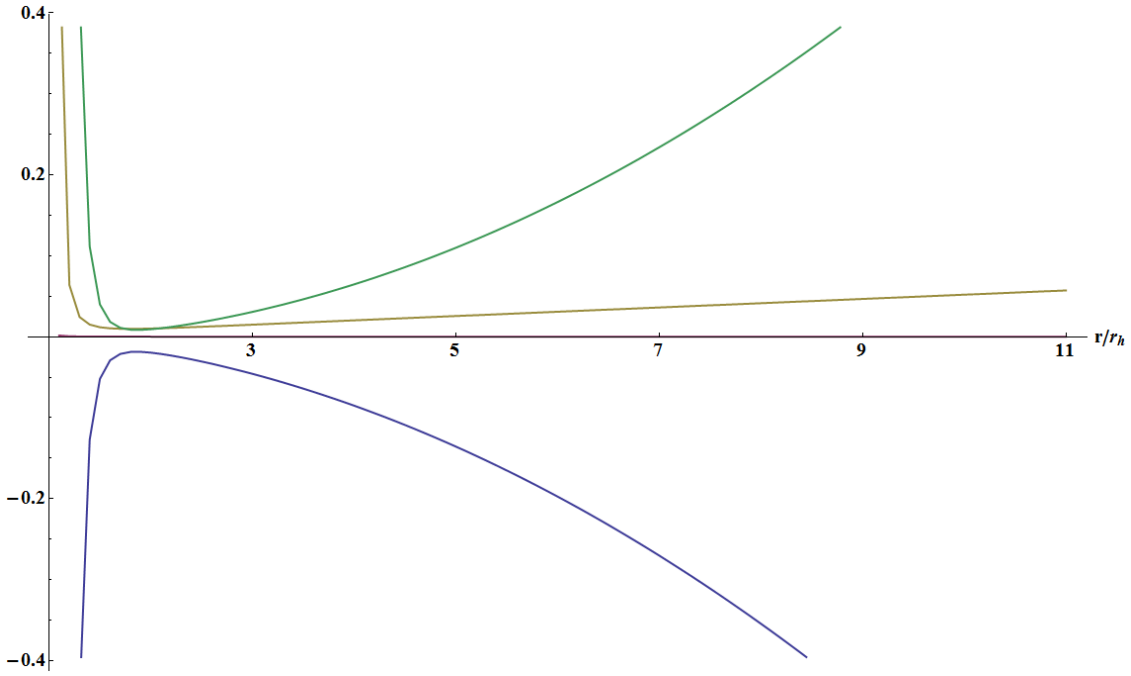

Figure 4.6: Components of $\langle\phi^2\rangle_{\text{ren}}$ from $r = r_h$ to $r = 11r_h$ with ($\mu = 1$, $\nu = 2$). The plot with negative divergence is line one of (4.13.9), the plot with smallest absolute value is line two of (4.13.9), the plot with positive divergence closest to the horizon is the analytic calculation from the MAPF used in line three of (4.13.9) and the remaining plot is the numeric calculation from the MAPF used in line three of (4.13.9).

4.15 $\langle\phi^2\rangle_{\mathbf{ren}}$ Results Near the Horizon

As in the brane calculation, §3.14, we repeated our numerics for a region close to the horizon to see if this would provide more information. This meant calculating new curved space modes and numeric integrals for the implementation of the MAPF. Even though from the last section we strongly suspect that nothing can be done near the horizon without a change of approximation scheme it would be preferable to see results that do not contain fragments due to break downs in our numeric technique near the horizon (such as the characteristic flicks in Figures 4.2 and 4.4).

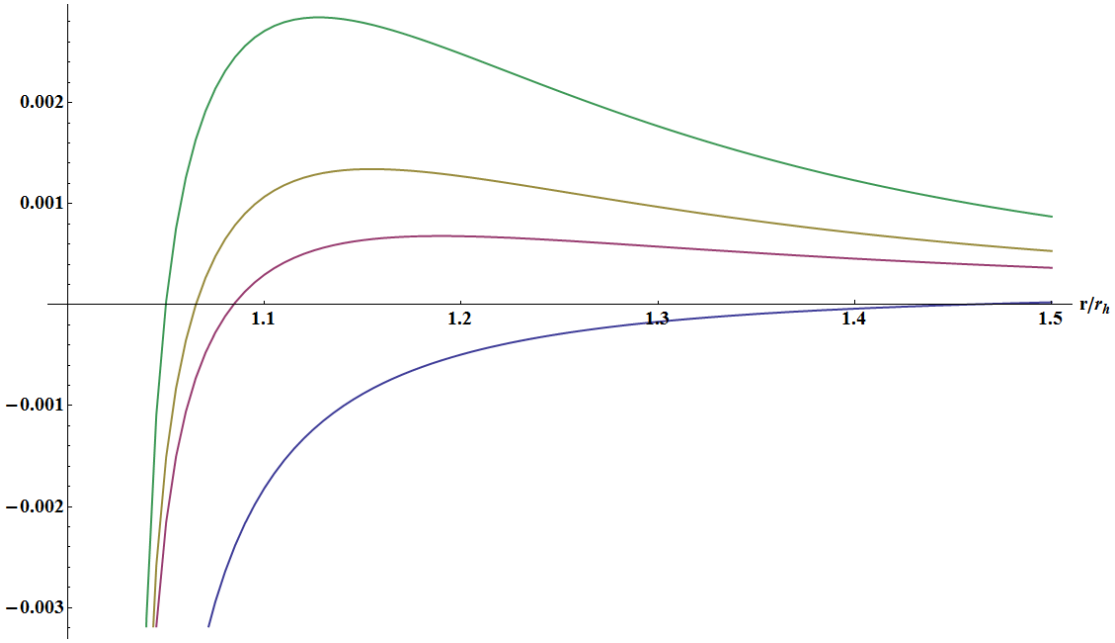

Figure 4.7: $\langle\phi^2\rangle_{\rm ren}$ from $r = r_h$ to $r = \frac{3}{2}r_h$, the plots from bottom to top show results for masses ($\mu = 1$, $\nu = 2$), ($\mu = 1/4$, $\nu = 1/5$), ($\mu = 1/4$, $\nu = 1/6$) and ($\mu = 1/5$, $\nu = 1/6$).

We show in Fig. 4.7 a selection of the previously better behaved mass values in the region $r = r_h \to \frac{3}{2}r_h$. These results were checked against the larger region results and matched beyond thirty significant figures. At first glance these plots show nothing significant except that in Fig. 4.4 the results for ($\mu = 1/5$, $\nu = 1/6$) appeared to diverge

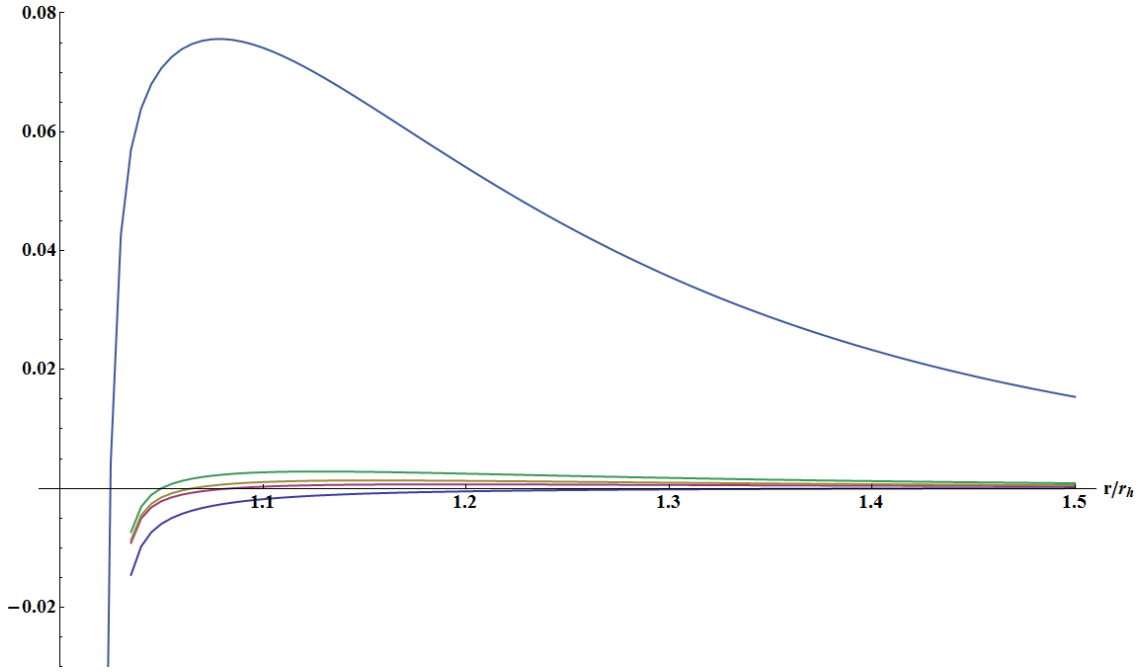

Figure 4.8: $\langle\phi^2\rangle_{\rm ren}$ from $r = r_h$ to $r = \frac{3}{2}r_h$, the plots are as in Fig. 4.7 now also including ($\mu = 1/10$, $\nu = 1/11$).

in a positive fashion as they approached the horizon. In Fig. 4.7 we clearly see that they in fact tend to negative infinity as is the case for all larger mass values. To see if this is a trend we then show in Fig. 4.8 the same plots as in Fig. 4.7 (for comparison) but also include ($\mu = 1/10$, $\nu = 1/11$), a mass case that before clearly diverged positively at the horizon in Fig. 4.4. Now we see again that in fact the result tends to negative infinity at the horizon, tests on other masses (above the ($\mu = 1/20$, $\nu = 1/21$) scale) all demonstrate the same behaviour. As we now know that the issue at the horizon is always a negatively diverging trend we present in Fig. 4.9 a breakdown of the terms composing the ($\mu = 1/5$, $\nu = 1/6$) case to complement the breakdowns displayed in Fig. 4.5 and Fig. 4.6. These original breakdowns show that in general that the negative contribution is a result of the sum over the modes while Fig. 4.9 is an example showing that within the mode sum it is the contribution from the $n = 0$ modes that cause the divergence. This behaviour can be shown in all investigated cases but we leave its discussion for our conclusions. This is

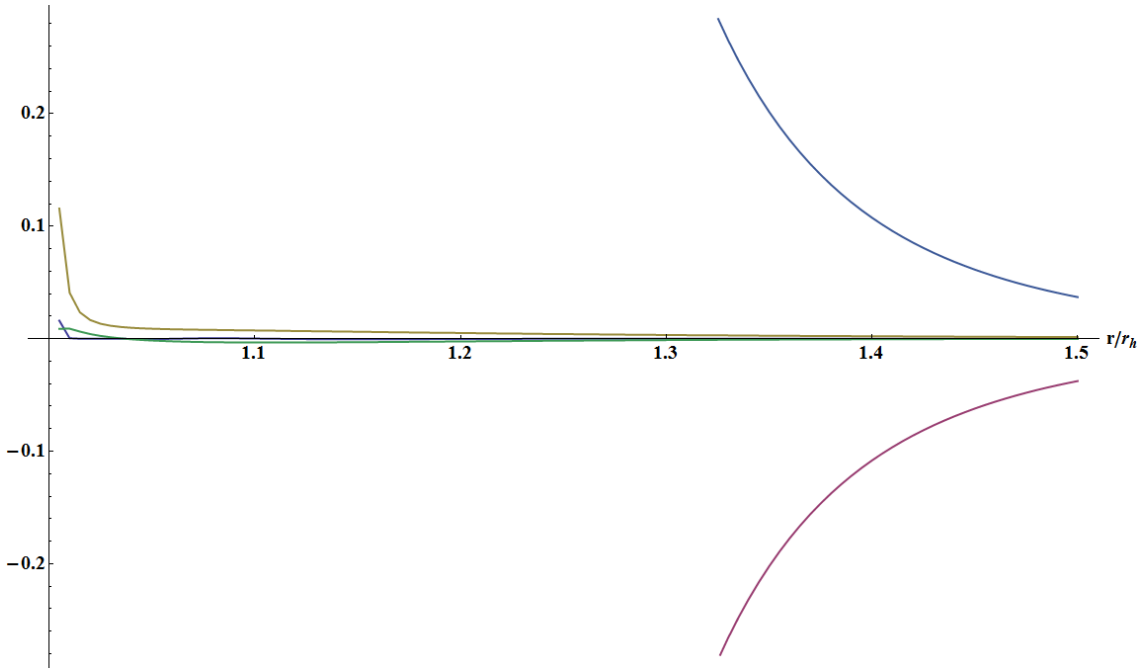

Figure 4.9: Components of $\langle\phi^2\rangle_{\text{ren}}$ from $r = r_h$ to $r = \frac{3}{2}r_h$ with ($\mu = 1/5$, $\nu = 1/6$). The plots from top to bottom are; $n \neq 0$ modes, the renormalised Minkowski total, (plot that is largest near the horizon) the numeric integrals from the MAPF used in line three of (4.13.9), (plot that is mostly negative) the analytic calculation from the MAPF used in line three of (4.13.9) and the $n = 0$ modes.

a problem that has occurred in other works on calculating the vacuum polarisation, the $n = 0$ modes were cause of most of the problems experienced in [75].

We briefly note than unlike for the brane calculation where the results are regular on the entire domain, the divergence in the $d = 5$ bulk results near the horizon prevents a comparison of our results to those on the horizon. The on-horizon value is provided by [32]

$$\langle\phi^2\rangle_{\text{ren}}|_{r=r_h} = \frac{1}{24\pi^3 r_h^3} \tag{4.15.1}$$

Although result (4.15.1) is of a similar order of magnitude to our results it is impossible to say whether our plots would cross the horizon near this value.

4.16 Summary

The main result of this chapter is that we have presented an original methodology to calculate $\langle\phi^2\rangle_{\text{ren}}$ on the $d = 5$ black hole. In order for the methodology to work we introduced the idea of using terms from the calculation of the vacuum polarisation for fields in Minkowski spacetime. In Minkowski spacetime, calculations for a quantum scalar field are much easier to perform, allowing the expression of the vacuum polarisation through both direct calculation and as a mode sum. To link the renormalisation terms associated with the black hole with the vacuum polarisation calculation from the Minkowski spacetime we introduced coefficient functions, A_i, which depend on the radial coordinates from all the spacetimes involved. The values of the Minkowski radial coordinates can be chosen to be expressed in terms of our original r in such a way that we can guarantee the double mode sum in line three of 4.13.9 does not diverge. A side effect of using massive fields in the Minkowski spacetimes was the introduction of free mass parameters.

To check our methodology we have produced test results plotted on both $r/r_h = 1.1 \to 11$ and $r/r_h = 1.005 \to 1.5$ from which we can deduce three insights. Firstly, our numerical results are highly sensitive to the values of the masses of the auxiliary scalar fields on Minkowski space. This sensitivity adds to the difficulty of cancelling divergent terms at the beginning and end of our domain which, as the masses grow larger, means that the results are not regular near the horizon nor as r tends to infinity. When we look at the final forms of our coefficient functions A_i (4.13.26) we can see how the masses have such an effect. These functions show that the two introduced masses cannot be equal and that the functions are divided by the difference of the squared masses so we cannot use masses too large or too small. Finally our test results near the horizon demonstrated that the major problem is always a negative divergence near the horizon. The calculation component breakdown (plotted in Fig. 4.9) shows that this is due to the $n = 0$ contribution from the field modes. This is not unexpected, as was discussed

in §2.11.1, where we demonstrated that the WKB approximation breaks down near the horizon. On the brane this did not become an issue, as we has a massless, conformally coupled field, but clearly in this more complicated scenario the WKB terms are no longer satisfactory. A difficulty arises in attempting to discern in general which terms should be cancelling with this mode contribution as for differing masses different contributions are positive and negative. Further we cannot state with confidence if the mode contribution is too large or is correct and the cancelling terms are too small, this is because the coefficient functions, A_i, are complicated to apply. It is also possible that the WKB terms play a role in the lack of cancellation of divergences for larger r, if the WKB was correctly capturing the mode function behaviour then the masses would not have as much effect on the values here. A further point is that unlike other methods for vacuum polarisation calculations [3, 32, 75] we chose to use angular rather temporal point splitting. This choice was made on purpose as attempts to use temporal point splitting with a generalised approach proved too difficult to work with, even with Mathematica, though this does not rule it out completely.

What the test results do show is that we can calculate results for $\langle\phi^2\rangle_{\rm ren}$ that are, for the most part, regular. We can even pin point that the central issue is the WKB approximation. Hence we have provided the first methodology to solve the problem of calculating the vacuum polarisation for $d = 5$ outside of the horizon, in that we have presented a method in §4.13 that allows the incorporation of the renormalisation terms (4.13.4) into the mode sum (4.13.2) in a calculable way 4.13.9. Further we have provided the first keys for future work to produce improved calculations by identifying problem areas and, in the case of the mode function approximation, a potential solution in the extended Green-Liouville asymptotics.

In order to produce this methodology and the test results we were required to derive many objects. We derived $d = 5$ Green's functions (4.2.3) and (4.13.1) which are equal to the two point correlation equivalent of $\langle\phi^2\rangle$ and calculated the Green's function's components. We used Mathematica to twice produce over four hundred field mode values

at one hundred radial points at accuracies of over thirty significant figures and derived their WKB approximation terms (4.4). The mode calculations required further work to strengthen accuracy and reduce calculation time as the ODE became more complicated for $d = 5$, §4.6. We investigated a method of dimensional reduction, §4.8, in an attempt to reduce our problem to one in $d = 4$. Although this showed promise (and hinted at our final radial matching) it proved to be insufficient here. In order to investigate using the VP calculation from Minkowski spacetimes we needed to derive, §4.9, all the same terms in these scenarios as we needed in our curved space problem i.e. Green's function expressions, WKB terms, numeric mode values, renormalisation terms. This was done for $d = 5$ massive and massless scalar fields and for $d = 3$ scalar fields (which must be massive) along with the direct calculations to obtain $\langle\phi^2\rangle_{\rm ren}$, summarised in §4.9.4. We investigated a method, 4.12, in which we isolated and removed the unphysical divergence within the Green's function caused by the inner summand. We calculated the terms required to be removed but ultimately were unable to proceed to a final regular result. This step is not wrong but requires careful handling once the renormalisation terms are introduced, further the number and complexity of the terms to be removed will grow quickly if d increases. Finally for our successful methodology, §4.13 , of a general approach we had to recalculate the Green's function and renormalisation terms to reflect angular separation. For both analysis and final calculation we also implemented the Abel-Plana formula in various forms, requiring both analysis of analytic terms and the calculation of numeric integrals.

We end this chapter with a side note to be considered. We show in Fig. 4.10 the value of $\langle\phi^2\rangle_{\rm ren}$ on the brane for a bulk of $d = 4$ and $d = 5$ and within the bulk for $d = 5$. We have presented several steps in our calculation that depend on whether the Green's function is in an even (as it is always for a on brane calculation) or odd number of dimensions. Hence there is no reason to expect these three results to be similar but a simple comparison of scale reveals a few details. Firstly the results are of comparable magnitude. Secondly

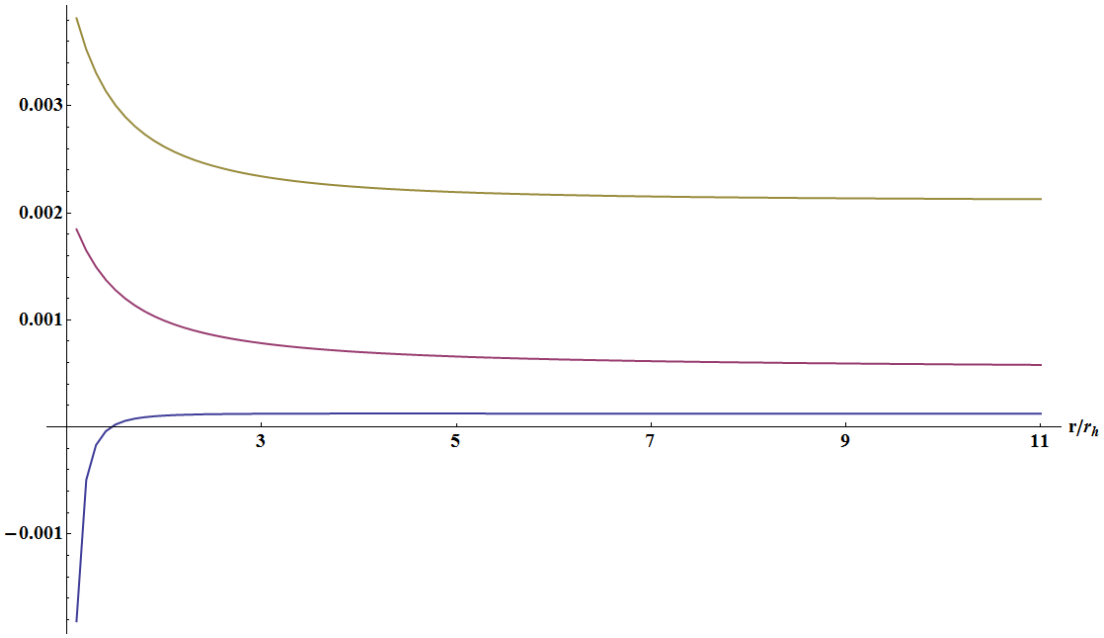

Figure 4.10: The plots from top to bottom are $\langle\phi^2\rangle_{\text{ren}}$ for $d = 5$ brane, $d = 4$ brane and $d = 5$ bulk.

we see the potential for a pattern emerging, in even numbers of dimensions it is possible to separate $\langle\phi^2\rangle_{\text{ren}}$ into an analytic and a numeric contribution (as seen in the on brane calculation, §3.4). The analytic contribution is always a finite amount and the numeric is a much smaller modification. However the numeric contribution does grow larger for higher numbers of dimensions but does so in a predictable manner, see Fig. 3.6. In an odd number of dimensions there is a finite base made from the Minkowski $\langle\phi^2\rangle_{\text{ren}}$ results but this is much smaller than the even dimensional case. The modification is also small indicating that in odd numbers of the dimensions the result will always be much smaller than in an even number. We hope to see such a trend is confirmed in further work.

This could be linked to previous work to calculate the Hawking flux from a higher dimensional black hole as summarised in [49]. A discussion of scalar flux has not been previously relevant as the calculations involved only use the off-diagonal terms of the RSET and therefore do not need renormalising. A good example of how the flux results

demonstrate the number of dimensions is in Table 6 of [36], which is calculated on a Schwarzschild-Tangherlini black hole. It shows the ratio of bulk to brane emission rates for a scalar field and demonstrates a trend that for $d = 5 \to 7$ the ratio rapidly falls. However as d increases after $d = 7$ the ratio increases again tending towards one. It is possible that results for $\langle \phi^2 \rangle_{\rm ren}$ in the bulk increase after $d = 7$ in a matching pattern and such an investigation would prove informative.

In the next chapter we briefly discuss the problem of calculating $\langle \phi^2 \rangle_{\rm ren}$ for the $d = 6$ bulk.

Chapter 5

$\langle\phi^2\rangle$ in the Bulk in 6d

In this chapter we present some objects relevant to the calculation of $\langle\phi^2\rangle_{\text{ren}}$ in the $d = 6$ bulk. Due to the difficulties in calculation of the $d = 5$ bulk we did not take this calculation further but present what we have found for later use. Unless there is a significant difference for an object between the $d = 5$ and $d = 6$ cases we will present our results briefly assuming the techniques demonstrated in previous chapters.

5.1 The Metric for the 6d Bulk

The general spacetime structure remains similar so we state from (2.3.16):

$$\begin{aligned} ds^2 &= f dt^2 + f^{-1} dr^2 + r^2 d\Omega_4^2 \\ &= f dt^2 + f^{-1} dr^2 + r^2 \left(d\theta_3^2 + \sin^2(\theta_3) d\theta_2^2 \right. \\ &\qquad \left. + \sin^2(\theta_3)\sin^2(\theta_2) d\theta_1^2 + \sin^2(\theta_3)\sin^2(\theta_2)\sin^2(\theta_1) d\varphi^2 \right). \end{aligned} \tag{5.1.1}$$

The Ricci tensor is

$$R_{ab} = \begin{pmatrix} -\frac{fA(r)}{2r} & 0 & 0 & 0 & 0 & 0 \\ 0 & -\frac{A(r)}{2rf} & 0 & 0 & 0 & 0 \\ 0 & 0 & -B(r) & 0 & 0 & 0 \\ 0 & 0 & 0 & -s_3^2 B(r) & 0 & 0 \\ 0 & 0 & 0 & 0 & -s_2^2 s_3^2 B(r) & 0 \\ 0 & 0 & 0 & 0 & 0 & -s_1^2 s_2^2 s_3^2 B(r) \end{pmatrix} \tag{5.1.2}$$

where

$$s_i = \sin(\theta_i)$$
$$A(r) = rf'' + 4f'$$
$$B(r) = rf' + 3f - 3.$$

From (5.1.1) the metric function is

$$f = 1 - \left(\frac{r_h}{r}\right)^3, \tag{5.1.3}$$

such that the Ricci tensor vanishes

$$R_{ab} = \underline{\mathbf{0}}. \tag{5.1.4}$$

and so does the Ricci scalar

$$R = \frac{12 - 12f - 8rf' - r^2 f''}{r^2} = 0. \tag{5.1.5}$$

As expected these quantities show that the spacetime is Ricci flat.

The metric determinant is

$$g^{\frac{1}{2}} = r^4 \sin(\theta_1) \sin^2(\theta_2) \sin^2(\theta_3). \tag{5.1.6}$$

5.2 Mode Sums in the 6d Bulk

Due to the similarities between the $d = 6$ and $d = 4$ cases (as discussed in §4.7) we proceed by returning to temporal point splitting. Here we present the degeneracy factor (2.7.9) and the Gegenbauer polynomial (2.8.9) for $d = 6$,

$$G_l^{3/2}(1)\tilde{N}_{l,6} = \frac{(2l+3)(l+1)^2(l+2)^2}{32\pi^2}. \tag{5.2.1}$$

The above factors then provide the mode sum expression derived from (2.8.13)

$$G_E(\mathbf{x},\varepsilon;\mathbf{x},0) = \frac{\kappa}{2\pi}\sum_{n=-\infty}^{\infty} e^{i\omega\varepsilon}\sum_{l=0}^{\infty} N_l G_l C_{\omega l} p_{\omega l}(r) q_{\omega l}(r) \tag{5.2.2}$$

where now the modes $p(r)$ and $q(r)$ are solutions to the radial ODE (2.8.1) for $d = 6$

$$\frac{1}{r^2}\frac{d}{dr}\left[r^4 f \frac{d}{dr} S_{\omega l}\right] - \left(\frac{\omega^2 r^2}{f} + m^2 r^2 + l(l+3)\right) S_{\omega l} = 0. \tag{5.2.3}$$

5.3 6d Bulk Renormalisation

The renormalisation terms are calculated as before from §2.9 producing

$$\alpha_6 = \frac{1}{(2\pi)^3} \tag{5.3.1}$$

and the total of the renormalisation terms

$$G_{E,sing} = \frac{1}{2(2\pi)^3}\left(\frac{U}{\sigma^2} + V\ln[\sigma]\right). \tag{5.3.2}$$

The relevant expansion terms are then [23] (for an expansion relating to a massless

field)

$$\begin{aligned} U &= U_0 + U_1\sigma + O(\sigma^2) \\ U_0 &= 1 + \frac{1}{360}R_{p(a|q|b}R^p{}_{c}{}^q{}_{d)}\sigma^{;a}\sigma^{;b}\sigma^{;c}\sigma^{;d} + O(\sigma^{\frac{5}{2}}) \\ U_1 &= \frac{1}{360}R^{pqr}{}_{(a}R_{|pqr|b)}\sigma^{;a}\sigma^{;b} + O(\sigma^{\frac{3}{2}}) \\ V &= -\frac{1}{720}R_{pqrs}R^{pqrs} + O(\sigma^{\frac{1}{2}}). \end{aligned} \tag{5.3.3}$$

Hence the full expression for the renormalisation terms is

$$G_{E,sing} = \frac{1}{16\pi^3}\left(\frac{1}{\sigma^2} + \frac{R_{paqb}R^p{}_{c}{}^q{}_{d}\sigma^{;a}\sigma^{;b}\sigma^{;c}\sigma^{;d}}{360\sigma^2} + \frac{R^{pqr}{}_{a}R_{pqrb}\sigma^{;a}\sigma^{;b}}{360\sigma} - \frac{1}{720}R_{pqrs}R^{pqrs}\ln[\sigma]\right). \tag{5.3.4}$$

We note that to calculate enough terms to express σ usefully in this number of dimensions goes beyond the limits of equations (2.10.25). We calculated the limit $[\sigma^{;\mu}{}_{t't't't't't'}]$ by hand before discovering the calculation had been generalised to any variable in [40]. The remaining calculations were performed using a program written in Mathematica supplied by Adrian Ottewill of University College Dublin.

We use equation (2.10.28) and the material from [40] to find the renormalisation terms (5.3.4) explicitly. We split $G_{E,sing}$ into two pieces, one that will contain only pole like divergences $G_{E,pole}$ and one that will contain the logarithmic divergence $G_{E,log}$. We are now required to address a feature that first occurred in equation (3.4.3) but was not needed to be discussed at that time as the coefficient of that logarithm was taken to zero. In order for the argument of the logarithm to be dimensionless we introduce a parameter μ that must have dimensions of mass, if we worked with a massive field then μ would be the mass of the field. However as we are working with a massless field the parameter μ remains

free. Hence our renormalisation terms are

$$\begin{aligned} G_{E,pole} &= \frac{1}{4\pi^3 f^2}\left[\frac{1}{\epsilon^4}+\frac{f'^2}{24\epsilon^2}+\frac{11r^2f'^4-24r^2ff'^2f''+16f^2(4f'^2+r^2f''^2)}{11520r^2}\right] \\ &= \frac{1}{4\pi^3 f^2}\left[\frac{1}{\epsilon^4}+\frac{f'^2}{24\epsilon^2}+\frac{P(r)}{11520r^2}\right] \\ G_{E,log} &= \frac{-(24-48f+24f^2+8r^2f'^2+r^4f''^2)}{11520\pi^3 r^4}\ln\left[\frac{f\mu^2\epsilon^2}{2}\right] \\ &= \frac{-L(r)}{11520\pi^3 r^4}\ln\left[\frac{f\mu^2\epsilon^2}{2}\right] \end{aligned} \tag{5.3.5}$$

where we introduce the terms $P(r)$ and $L(r)$ to keep the expressions succinct.

As mentioned in §5.2 our renormalisation terms are, in important ways, similar to those in $d=4$, particularly the fact that the only powers of epsilon are even and we have a logarithmic term. This means we can proceed with the method implemented on the brane by using distributional identities from appendix B, specifically

$$\begin{aligned} \ln(\kappa\epsilon) &= -\sum_{n=1}^{\infty}\frac{1}{n}\cos(n\kappa\epsilon)+O(\epsilon^2) \\ \frac{1}{\epsilon^2} &\sim -\sum_{n=1}^{\infty}\kappa^2 n\cos(n\kappa\epsilon)-\frac{\kappa^2}{12}+O(\epsilon^2) \\ \frac{1}{\epsilon^4} &\sim \frac{1}{6}\sum_{n=1}^{\infty}\kappa^4 n^3\cos(n\kappa\epsilon)-\frac{\kappa^4}{720}+O(\epsilon^2). \end{aligned} \tag{5.3.6}$$

Using these identities allows us to write the renormalisation terms (5.3.5) as

$$\begin{aligned} G_{E,pole} &= \frac{1}{4\pi^3 f^2}\left[\frac{1}{6}\sum_{n=1}^{\infty}n^3\kappa^4\cos(n\kappa\epsilon)-\frac{\kappa^4}{720}-\frac{f'^2}{24}\sum_{n=1}^{\infty}n\kappa^2\cos(n\kappa\epsilon)-\frac{f'^2\kappa^2}{288}+\frac{P(r)}{11520r^2}\right] \\ &= \frac{1}{576\pi^3 f^2}\left(\frac{P(r)}{80r^2}-\frac{f'^2\kappa^2}{2}-\frac{\kappa^4}{5}\right)+\frac{\kappa}{24\pi^3 f^2}\sum_{n=1}^{\infty}\left[n^3\kappa^3-\frac{f'^2}{4}n\kappa\right]\cos(n\kappa\epsilon) \end{aligned} \tag{5.3.7}$$

and

$$G_{E,log} = \frac{-L(r)}{11520\pi^3 r^4}\left(\ln\left[\frac{f\mu^2}{2\kappa^2}\right]-2\sum_{n=1}^{\infty}\frac{\cos(n\kappa\epsilon)}{n}\right). \tag{5.3.8}$$

We can now add equations (5.3.7) and (5.3.8) to achieve a final form of the renormalisation terms,

$$\begin{aligned} G_{E,sing} =& \frac{1}{576\pi^3 f^2}\left(\frac{P(r)}{80r^2} - \frac{f'^2\kappa^2}{2} - \frac{\kappa^4}{5} - \frac{f^2 L(r)}{20r^4}\ln\left[\frac{f\mu^2}{2\kappa^2}\right]\right) \\ &+ \frac{\kappa}{24\pi^3 f^2}\sum_{n=1}^{\infty}\left(n^3\kappa^3 - \frac{f'^2}{2}n\kappa + \frac{f^2 L(r)}{240r^4}\frac{1}{n\kappa}\right)\cos(n\kappa\epsilon). \end{aligned} \tag{5.3.9}$$

5.4 Further Calculation

Besides what has already been stated in this chapter we have taken the calculation no further but can still discuss some aspects. Using equation (5.3.9) we could now write an expression for the vacuum polarisation however we again take inspiration from the work carried out on the brane and split the vacuum polarisation into numeric and analytic contributions,

$$\langle\phi^2\rangle_{\text{analytic}} = \frac{-1}{576\pi^3 f^2}\left(\frac{P(r)}{80r^2} - \frac{f'^2\kappa^2}{2} - \frac{\kappa^4}{5} - \frac{f^2 L(r)}{20r^4}\ln\left[\frac{f\mu^2}{2\kappa^2}\right]\right) \tag{5.4.1}$$

and

$$\begin{aligned} \langle\phi^2\rangle_{\text{numeric}} =& \frac{\kappa}{\pi}\sum_{n=1}^{\infty}\left[\sum_{l=0}^{\infty} N_l G_l C_{\omega l} p_{\omega l} q_{\omega l} - \frac{1}{24\pi^2 f^2}\left(n^3\kappa^3 - \frac{f'^2}{2}n\kappa + \frac{f^2 L(r)}{240r^4}\frac{1}{n\kappa}\right)\right] \\ &+ \frac{\kappa}{2\pi}\sum_{l=0}^{\infty} N_l G_l C_{0l} p_{0l} q_{0l}. \end{aligned} \tag{5.4.2}$$

It seems that it will be a simple extension to keep following the brane methodology from this point (e.g. point coincidence has been completed as almost a side note, we already have WKB terms and known transforms for series calculation). However there are three pertinent issues presented in these calculations that prevented any sort of rapid analysis. Firstly, $\langle\phi^2\rangle_{\text{analytic}}$ contains a logarithmic term that diverges at the horizon so

this object is not a simple as it was on the brane even though we have a massless field on a Ricci flat spacetime. The effect of this term is then strengthened by the overall factor of dividing by the square of the metric function leading every term in $\langle\phi^2\rangle_{\text{analytic}}$ to diverge at the horizon. Behaviour like this has been encountered previously (e.g. [75]) so this is not an insurmountable obstacle. Also as suggested in §4.14 this may be better handled by the introduction of Green-Liouville asymptotics [12].

The next issue is that we cannot be sure that we do have appropriate techniques to calculate the sums in (5.4.2). The summand in this expression is similar to, but more complicated than, that encountered on the brane (3.4.9), and for $d = 6$ has a leading order of $O(n^3)$. From the brane methodology we have the Watson-Sommerfeld formula (3.7.1) however this results in multiple integrals that require careful work if used within a double sum and required key terms to cancel, see §3.7. From the work in the $d = 5$ bulk we found the Abel-Plana formula, §4.10, to be extremely useful but its application was not simple. Both the Watson-Sommerfeld and Abel-Plana formulae produce integrals that could only be handled numerically for the brane and $d = 5$ bulk calculations. The introduction of more complicated integrands to these integrals will make numeric calculations more difficult. The Watson-Sommerfeld also has a second integral, (3.7.31), that was handled analytically on the brane but this may not be the case for more complicated integrands.

The third issue may be one that renders the first two points temporarily moot. If we return to look at equation (5.2.2) we have proceeded ignoring the fact that we began with a Green's function that was divergent even without full point coincidence, the issue we have referred to as an unphysical divergence, §3.3. We demonstrated in §4.11 and §4.12 that renormalisation without dealing with the unphysical divergences posed a serious problem. Even knowing this we showed in §4.12 that attempting to regularise the inner sum with a summand of large leading order is also not a guaranteed method to allow final renormalisation. In the $d = 6$ case the leading order is $O(l^4)$, continuing the increase of the order by two with every single step up in dimension.

We could remove from the mode sum (5.2.2) the five terms needed (there is no $O(l^{-1})$ term) to guarantee the inner sum to be regular. However this seems impractical as it introduces terms into the mode sum that we cannot predict how to handle when we wish to implement a technique, like the Watson-Sommerfeld formula, to proceed. However this has not been tested to the stage of including the renormalisation terms which, after using using the distributional identities (B.0.4), may be in form to help calculate the terms we introduced. If cutting off the leading orders approach is not feasible then the only known solution would be to turn to our final methodology for the $d = 5$ case. The introduction of terms from Minkowski spacetimes, §4.9, and a generalised approach, §4.13, could be used to take into account the removal of the unphysical divergence and the final renormalisation however this introduces its own application problems. Analysis will be required to investigate which point splitting scheme leads to a practical calculation. Also introducing fields in Minkowski spacetimes will be more complex than before and it will require determining which and how many Minkowski setups will be needed (considerations include how many fields will be enough, how many massless, how many massive and in which numbers of dimensions).

5.5 Summary

In this chapter we have laid out the initial steps for the calculation of $\langle\phi^2\rangle_{\rm ren}$ in the $d = 6$ bulk. We have derived the Green's function, and its components, for the mode sum expression of $\langle\phi^2\rangle_{\rm ren}$. We have numerically calculated all the modes required, that is over four hundred values at two hundred radial points, and derived their WKB approximation (in fact we have done this for all the cases $d = 6 \to 11$ but have no more to say on the additional cases). We have also produced the required renormalisation terms required to progress to final calculation.

Finally we have discussed how a complete calculation of $\langle\phi^2\rangle_{\rm ren}$ can be attempted.

We have reviewed multiple methods and also raised the difficulties attached to each. The methodology from the brane calculation and that which we introduced for the $d = 5$ bulk both could be used to progress towards results. However the brane calculation approach requires the removal of unphysical divergences which here would mean introducing four complicated terms into the calculation. Our new bulk approach will work in theory for this problem but derived the functions for a generalised approach, which Minkowski spacetimes to use and the radial matching all present serious challenges. Further using the bulk methodology will fall prey to the problem we encountered in our test results from Ch. 4 in that the WKB approximation cannot be assumed to hold near the horizon. However we have posited that the use of Green-Liouville asymptotics [12] will help with this issue.

Chapter 6

Conclusions and Future Work

For a complete description of what we have achieved we quickly restate the setup of our problem from Ch. 1 . We have taken a thermal quantum scalar field and placed it on a curved spacetime background assuming no backreaction. Our spacetime exists as a brane world in which we place a $d = 4$ tensionless brane within a higher dimensional bulk consisting of additional, periodic, space-like dimensions of small radius. The background is curved due to the presence of a black hole attached to the brane with a Schwarzschild-Tangherlini metric meaning it possesses hyperspherical symmetry (but no charge or spin). Further we assume that the black hole is small compared to the radius of the additional dimensions and hence we may treat them as flat. The eventual purpose of looking at this setup is to find the renormalised stress-energy tensor for the field. Without loss of generality we place the field in a Hartle-Hawking vacuum as this is the easiest to work with and the difference in expectation values between this and another quantum state is easier to calculate than a renormalised expectation value. The construction of the renormalised stress-energy tensor requires the object $\langle 0_H|\phi(x)\phi(x)|0_H\rangle$ (denoted $\langle\phi^2\rangle$) and its derivatives. This object is the auto-correlation of the field and is termed the vacuum polarisation. Our aim has been to investigate the vacuum polarisation.

In Ch. 2 we demonstrated the equations required to formulate our setup, methodology from previous successful calculations of the vacuum polarisation in $d = 4$ and the mathematical objects to be used later (Synge's world function, hyperspherical harmonics etc.). We provided a rough outline of the application of previous methodologies for these types of objects along with the derivations of the steps involved. Finally we derived the methodology to find the WKB terms that will approximate numeric modes in later chapters and discussed its implementation.

6.1 On the Brane

We have considered a massless field on the metric projected onto the bisection of the Schwarzschild-Tangherlini spacetime which we use as the brane. We have chosen the field to be conformally coupled to the background geometry which for $d = 4$ gives the coupling constant $\xi_c = \frac{1}{6}$. The Schwarzschild-Tangherlini metric projected on the brane is an extension of the Schwarzschild metric except with a metric function dependent on the number of bulk dimensions. The Schwarzschild-Tangherlini metric and the Schwarzschild metric are identical if $d = 4$. Our main result on the brane is that we have shown that the calculation of the vacuum polarisation can be extended to include a bulk through this function. Further we can plot results for the vacuum polarisation within $r = 1.005 \rightarrow 11r_h$ for a bulk with $d = 4 \rightarrow 11$.

This calculation can be done using a previously established methodology [3, 17, 75]. The method of introducing the renormalisation terms through distributional identities holds but summing over the results of these identities becomes trickier. Numerical modes calculated from the radial ODE must be kept to high accuracy (at least twenty eight digits) to avoid errors in the differential solver for higher numbers of dimensions. We have shown that with this level of numerical accuracy our analytic approximation (WKB) to our numerical modes allows for smooth plotting of the polarisation down to $r = 1.006$.

We have also compared the results near to the horizon to the on horizon results, provided by Cormac Breen, to show a match within the expected error of our approximation. A result from the original methodology with the normal Schwarzschild metric showed that the analytic components of the calculation are a good approximation to the final value. We have demonstrated that this is not generally true, for a bulk of $d = 5$ the approximation is weak and as d then increases such an approximation is not applicable as numeric contributions take over.

The work on the brane can be continued in several avenues. Firstly a bulk with $d > 11$ could be considered though we feel this would add little as we have established a clear pattern in behaviour as d increases. As the value of d is increased the difficulty of required numerical calculations also increases. Similar to work in $d = 4$ this calculation could now be attempted including a massive field, other couplings to the background or a modification to the metric through a brane with tension (cosmological constant $\Lambda \neq 0$), non-zero charge, non-zero spin etc. The most important extension to this work would be its application in calculating the renormalised stress-energy tensor for this system. This would allow us to see for the first time the effect of a higher dimensional bulk on the RSET on the brane for QFT in curved space. There has been much work done, some results are summarised here [49], to calculate Hawking fluxes in the same setup as ours, as well as including some of our suggested extensions. However Hawking fluxes are off diagonal components of the RSET that do not require renormalisation.

6.2 In the Bulk

In the bulk we have considered a massless field extending through all the dimensions of the brane and bulk. We have demonstrated that the value of the coupling to the background can be left unspecified for our calculations as the spacetime is Ricci flat. Our primary result in the bulk, and the main result of this research, is that we have found a methodology

that produces a regular value for the vacuum polarisation in the $d = 5$ bulk. No previous work has produced a methodology for calculation of a regular vacuum polarisation for the $d = 5$ bulk away from the horizon. We have produced plots of test calculations, in the region $r = 1.005 \rightarrow 11r_h$, using this methodology and numerical techniques such as from [68]. The application of this new methodology makes use of two free parameters and our test calculations have been performed for fifteen combinations of these parameters.

In the bulk (for unspecified d) we have shown the required Green's function that is equivalent to the point split vacuum polarisation. It has been previously established that the renormalisation terms differ between odd and even dimensions [23]. As mentioned above the $d = 5$ calculation (as a test of solving for odd d) had not previously been solved and the $d = 6$ calculation, which has similarities with the $d = 4$ calculation, was also unperformed outside the horizon (on the horizon performed by [69]). In our $d = 5$ work we investigated three main approaches to handling the renormalisation terms. The first applied a method of dimensional reduction to produce a simpler problem but this proved intractable. The second made use of directly matching the renormalisation singularities to identical singularities in the equivalent vacuum polarisation calculations for a massive quantum scalar field on Minkowski spacetimes that do not share the radial coordinate with the original curved spacetime. We demonstrated that this method did not contain enough freedom to cancel the divergent sums. Our final, and successful, approach introduces multiple Minkowski scalar fields each multiplied by a function, of all radial coordinates, and then summed together. Although we demonstrated analytically that this will produce a finite value for the vacuum polarisation our test calculations did not properly confirm this as a negative divergence remained at the horizon. The newly introduced functions are sensitive to two free parameters and their influence is difficult to account for. Also we know that the WKB approximation breaks down near the horizon but this effect was not apparent during the calculations on the brane, in the bulk it is clear that it does not capture and cancel all the divergent behaviour.

Above we mentioned methods one and two that failed in our work specifically because they were inspired by the cancellation of an unphysical divergence in [75] and the black hole spacetime threaded by a cosmic string [68]. Although unsuitable for our calculation here they should be considered as potential approaches calculations of the vacuum polarisation in other circumstances, particularly when d is even. This is true for the $d = 6$ bulk where we have given some preliminary discussion. Although the similarity to the $d = 4$ case suggests a common approach, this may become intractable or involve numerical too complex work so any of the three proposed methods for the $d = 5$ bulk may become appropriate. While working with $d > 4$ we attempted to keep our work general and we retained quantities, such as as field mass, in our calculations until simplification was needed to achieve results. We can see from the behaviour of these quantities in the early stages of calculation that they will not simplify calculations as d increases. In fact more new approaches may be needed. However we have demonstrated some behaviour in the final result that allows some speculation. it appears that for even dimensions there will always be a sizable finite amount produced by analytic contributions to the total that increases with d. A numeric contribution increases more rapidly with d modifying the result near the horizon. For odd d there is no such sizable, analytic contribution for the numeric contribution to modify (although there is a small one). Hence, although we expect the final results for odd and even dimensions are of similar order the odd results will likely remain smaller.

As for the brane this work can be extended in $d = 5$ by the removal of certain simplifications (e.g. $m \neq 0$, $\Lambda \neq 0$) these scenarios will likely contain new difficulties and are beyond discussion here. In our opinion the first step from the $d = 5$ work is a confirmation of the methodology through calculation. This will require an approximation for our numeric modes that encodes the behaviour of the modes near the horizon and at infinity much better. We have suggested Green-Liouville asymptotics [12] but this requires testing. The above mentioned $d = 6$ methodology requires completion and may only require an application of our successful $d = 5$ approach to be finished, algebraic and numeric

complications not withstanding. We select this method as an approach to investigate first as if it is proven to work for $d = 6$ then it is a methodology for any value of d, however again the numerics and approximations may render accurate results unreliable. Our final point is that, of course, the obvious extension of this work is to produce a methodology for calculating the RSET. We accept that actual calculation of the RSET will first require refinement of the numerical work on the vacuum polarisation. Once achieved this would provide the first look at a RSET in a higher dimensional bulk within QFT in curved space.

Appendices

Appendix A

A Note on Distributions

Here we briefly discuss some details concerning distributions (also known as generalised functions) relevant to this work. We shall do this using the Dirac delta function as an example.

As a distribution the delta function can be defined by its action on a continuous, compactly supported test function producing a finite result,

$$\int_{-\infty}^{\infty} \delta(x-a)f(x)dx = f(a). \tag{A.0.1}$$

Formally δ is a linear functional on the space of test functions to the finite values of those test functions. We may also state that

$$\delta(x-a) = 0 \tag{A.0.2}$$

but only for $x \neq a$ (other distributions may be finite but non-zero under a similar condition), in the limit $x \to a$ the delta function diverges.

The delta function can be represented as a series by way of Fourier theory,

$$\delta(x-a) = \frac{1}{2\pi}\sum_{n=-\infty}^{\infty} e^{in(x-a)} = \frac{1}{2\pi} + \frac{1}{2\pi}\sum_{n=1}^{\infty}\cos\left[n(x-a)\right], \tag{A.0.3}$$

which clearly only holds for $x \neq a$ and the series are not absolutely convergent. Series representations like those above are common in this work (see below for an example) and we term these series to be convergent in the sense that if used as an integral kernal with a test function the result would be finite, see (A.0.1) above.

Now we may look at a clear example in equation (2.5.3) which relates the unrenormalised vacuum polarisation, $\langle T(\phi(x)\phi(x'))\rangle$, and the Euclidean Green's function, $G_E(x,x')$. Such objects are understood to be well defined distributions (an operator valued distribution in the case of the vacuum polarisation) for $x \neq x'$ and the mode sum representation of $G_E(x,x')$, (2.7.1), is deemed convergent. We then allow for renormalisation techniques by accepting that it is possible to subtract terms from a series representation such that the series converges in the standard summation sense after taking the limit $x \to x'$.

A final note on the Green's function mode sum representation paraphrased from [68]; it is a sum over a complete set of mode functions and equations of the form (2.7.1) are understood in the sense of smearing with smooth functions of compact support in our manifold $\mathcal{M}$.

Appendix B

Distributional Identities

Here we state and justify some distributional identities used within this text. The status of series representations of distributions was discussed in Appendix A.

First, from the statement of the Fourier series of the Dirac delta function with constants λ and a

$$\delta(\lambda x - a) = \frac{1}{2\pi} + \frac{1}{\pi}\sum_{n=1}^{\infty}\cos[n(\lambda x - a)] \tag{B.0.1}$$

we can write

$$\sum_{n=1}^{\infty}\cos(n\kappa\epsilon) = -\frac{1}{2} \tag{B.0.2}$$

which holds for $\epsilon \neq 0$.

Now as presented by [41] we demonstrate a re-expression of a series divergent in the

limit $\epsilon \to 0$

$$\begin{aligned}
\sum_{n=1}^{\infty} \sin(n\kappa\epsilon) &= \frac{1}{2i} \sum_{n=1}^{\infty} \left(e^{in\kappa\epsilon} - e^{-in\kappa\epsilon} \right) \\
&= \frac{1}{2i} \left(-\frac{e^{i\kappa\epsilon}}{1 - e^{i\kappa\epsilon}} - \frac{1}{e^{i\kappa\epsilon} - 1} \right) \\
&= \frac{1}{2i} \left(\frac{e^{i\kappa\epsilon} + 1}{e^{-i\kappa\epsilon} - 1} \right) \\
&= \frac{1}{2} \cot \left(\frac{\kappa\epsilon}{2} \right) \\
&= \frac{1}{\kappa\epsilon} - \frac{\kappa\epsilon}{12} + O(\epsilon^3).
\end{aligned} \tag{B.0.3}$$

We may then take the result of (B.0.3), including its higher order terms, and through differentiation and integration produce the following identities which hold as ϵ tends to zero;

$$\begin{aligned}
\ln(\kappa\epsilon) &\sim -\sum_{n=1}^{\infty} \frac{1}{n} \cos(n\kappa\epsilon) \\
\frac{1}{\epsilon} &\sim \sum_{n=1}^{\infty} \kappa \sin(n\kappa\epsilon) \\
\frac{1}{\epsilon^2} &\sim -\sum_{n=1}^{\infty} \kappa^2 n \cos(n\kappa\epsilon) - \frac{\kappa^2}{12} \\
\frac{1}{\epsilon^3} &\sim -\frac{1}{2} \sum_{n=1}^{\infty} \kappa^3 n^2 \sin(n\kappa\epsilon) \\
\frac{1}{\epsilon^4} &\sim \frac{1}{6} \sum_{n=1}^{\infty} \kappa^4 n^3 \cos(n\kappa\epsilon) - \frac{\kappa^4}{720}
\end{aligned} \tag{B.0.4}$$

and so on.

Appendix C

WKB Terms on the Brane

The complete list of $\beta_{\omega l}(r)$ expressions referenced in §3.5 are given below. For conciseness we write $f \equiv f(r)$, $R \equiv R(r)$ and $\chi \equiv \chi_{\omega l}$.

Note that these functions were calculated using Mathematica and the typesetting was done by the $TeXForm$, $Collect$ and $Simplify$ commands, using the notation $g^{(k)}(x) = \frac{d^k g(x)}{dx^k}$, only alignment has been corrected.

For $\beta_{0\omega l}(r)$ there are no coefficients

$$\beta_{0\omega l} = \frac{1}{2\chi(r)} \tag{C.0.1}$$

For

$$\beta_{1\omega l} = A_1\chi(r)^{-3} + A_2\chi(r)^{-5} + A_3\chi(r)^{-7} \tag{C.0.2}$$

we have the coefficients below.

$$A_1 = \frac{r^2}{64}\left[-4r^2 f f'' + r^2 f'^2 - 12 r f f' \right. \tag{C.0.3}$$
$$\left. -16 m^2 r^2 f - 16\xi r^2 f R - 4f^2 + 4f\right]$$
$$A_2 = \frac{\omega^2 r^6}{32}\left[2r^2 f f'' - 3r^2 f'^2 + 8 r f f' - 8 f^2\right] \tag{C.0.4}$$
$$A_3 = \frac{\omega^4 r^{10}}{64}\left[5r^2 f'^2 - 20 r f f' + 20 f^2\right] \tag{C.0.5}$$

For

$$\beta_{2\omega l} = B_1 \chi(r)^{-5} + B_2 \chi(r)^{-7} + B_3 \chi(r)^{-9} + B_4 \chi(r)^{-11} + B_5 \chi(r)^{-13} \tag{C.0.6}$$

we have the coefficients below.

$$\begin{aligned} B_1 = \quad & \frac{27 f'^4 r^8}{4096} + \frac{3}{16} m^4 f^2 r^8 + \frac{3}{16}\xi^2 f^2 R^2 r^8 - \frac{3}{128} m^2 f f'^2 r^8 - \frac{3}{128}\xi f R f'^2 r^8 \\ & + \frac{5}{256} f^2 f''^2 r^8 + \frac{3}{8} m^2 \xi f^2 R r^8 - \frac{1}{32}\xi f^2 f' R' r^8 + \frac{3}{32} m^2 f^2 f'' r^8 \\ & - \frac{11}{512} f f'^2 f'' r^8 + \frac{3}{32}\xi f^2 R f'' r^8 - \frac{1}{16}\xi f^3 R'' r^8 - \frac{1}{64} f^3 f^{(4)} r^8 \\ & - \frac{17}{512} f f'^3 r^7 + \frac{7}{32} m^2 f^2 f' r^7 + \frac{7}{32}\xi f^2 R f' r^7 - \frac{5}{16}\xi f^3 R' r^7 \\ & + \frac{9}{128} f^2 f' f'' r^7 - \frac{1}{8} f^3 f^{(3)} r^7 - \frac{5}{32} m^2 f^3 r^6 - \frac{3}{32} m^2 f^2 r^6 \\ & + \frac{43}{512} f^2 f'^2 r^6 + \frac{3}{512} f f'^2 r^6 - \frac{5}{32}\xi f^3 R r^6 - \frac{3}{32}\xi f^2 R r^6 \\ & - \frac{25}{128} f^3 f'' r^6 - \frac{3}{128} f^2 f'' r^6 + \frac{1}{128} f^3 f' r^5 - \frac{9}{128} f^2 f' r^5 + \frac{3}{256} f^4 r^4 \\ & - \frac{3}{128} f^3 r^4 + \frac{3}{256} f^2 r^4 \end{aligned} \tag{C.0.7}$$

$$
\begin{aligned}
B_2 = \omega^2\Big[& -\frac{145 f'^4 r^{12}}{1024} + \frac{15}{64} m^2 f f'^2 r^{12} + \frac{15}{64}\xi f R f'^2 r^{12} - \frac{13}{128} f^2 f''^2 r^{12} \\
& - \frac{5}{32}\xi f^2 f' R' r^{12} - \frac{5}{32} m^2 f^2 f'' r^{12} + \frac{165}{512} f f'^2 f'' r^{12} \\
& - \frac{5}{32}\xi f^2 R f'' r^{12} - \frac{7}{64} f^2 f' f^{(3)} r^{12} + \frac{1}{64} f^3 f^{(4)} r^{12} \\
& + \frac{185}{256} f f'^3 r^{11} - \frac{15}{16} m^2 f^2 f' r^{11} - \frac{15}{16}\xi f^2 R f' r^{11} + \frac{5}{16}\xi f^3 R' r^{11} \\
& - \frac{153}{128} f^2 f' f'' r^{11} + \frac{9}{32} f^3 f^{(3)} r^{11} + \frac{5}{4} m^2 f^3 r^{10} - \frac{349}{256} f^2 f'^2 r^{10} \\
& - \frac{15}{256} f f'^2 r^{10} + \frac{5}{4}\xi f^3 R r^{10} + \frac{153}{128} f^3 f'' r^{10} + \frac{5}{128} f^2 f'' r^{10} \\
& + \frac{9}{8} f^3 f' r^9 + \frac{5}{32} f^2 f' r^9 - \frac{3}{32} f^4 r^8 - \frac{5}{32} f^3 r^8 \Big]
\end{aligned}
\tag{C.0.8}
$$

$$
\begin{aligned}
B_3 = \omega^4\Big[& \frac{1085 f'^4 r^{16}}{2048} - \frac{35}{128} m^2 f f'^2 r^{16} - \frac{35}{128}\xi f R f'^2 r^{16} + \frac{21}{256} f^2 f''^2 r^{16} \\
& - \frac{385}{512} f f'^2 f'' r^{16} + \frac{7}{64} f^2 f' f^{(3)} r^{16} - \frac{385}{128} f f'^3 r^{15} \\
& + \frac{35}{32} m^2 f^2 f' r^{15} + \frac{35}{32}\xi f^2 R f' r^{15} + \frac{343}{128} f^2 f' f'' r^{15} \\
& - \frac{7}{32} f^3 f^{(3)} r^{15} - \frac{35}{32} m^2 f^3 r^{14} + \frac{847}{128} f^2 f'^2 r^{14} + \frac{35}{512} f f'^2 r^{14} \\
& - \frac{35}{32}\xi f^3 R r^{14} - \frac{343}{128} f^3 f'' r^{14} - \frac{427}{64} f^3 f' r^{13} - \frac{35}{128} f^2 f' r^{13} \\
& + \frac{357}{128} f^4 r^{12} + \frac{35}{128} f^3 r^{12} \Big]
\end{aligned}
\tag{C.0.9}
$$

$$
\begin{aligned}
B_4 = \omega^6\Big[& -\frac{693 f'^4 r^{20}}{1024} + \frac{231}{512} f f'^2 f'' r^{20} + \frac{1155}{256} f f'^3 r^{19} \\
& - \frac{231}{128} f^2 f' f'' r^{19} - \frac{3003}{256} f^2 f'^2 r^{18} + \frac{231}{128} f^3 f'' r^{18} \\
& + \frac{231}{16} f^3 f' r^{17} - \frac{231}{32} f^4 r^{16} \Big]
\end{aligned}
\tag{C.0.10}
$$

$$
\begin{aligned}
B_5 = \omega^8\Big[& \frac{1155 f'^4 r^{24}}{4096} - \frac{1155}{512} f f'^3 r^{23} + \frac{3465}{512} f^2 f'^2 r^{22} - \frac{1155}{128} f^3 f' r^{21} \\
& + \frac{1155}{256} f^4 r^{20} \Big]
\end{aligned}
\tag{C.0.11}
$$

For

$$\beta_{3\omega l} = C_1\chi(r)^{-7} + C_2\chi(r)^{-9} + C_3\chi(r)^{-11} + C_4\chi(r)^{-13} + C_5\chi(r)^{-15} + C_6\chi(r)^{-17} + C_7\chi(r)^{-19} \tag{C.0.12}$$

we have the coefficients on the following pages.

$$
\begin{aligned}
C_1 = -\frac{r^6}{131072}\Big[&320f^6 + 64\Big(32\xi R^{(4)}r^6 + 8f^{(6)}r^6 + 448\xi R^{(3)}r^5 + 136f^{(5)}r^5 \\
&+ 1680\xi R''r^4 + 668f^{(4)}r^4 + 1680\xi R'r^3 + 1008f^{(3)}r^3 + 252m^2r^2 + 252\xi Rr^2 \\
&+ 279f''r^2 - 3f'r - 15\Big)f^5 - 16\Big(6720\xi^2R^2r^4 + 579f'^2r^2 + 32\xi R\Big(40\xi R''r^4 \\
&+ 10f^{(4)}r^4 + 280\xi R'r^3 + 96f^{(3)}r^3 + 420m^2r^2 + 221f''r^2 + 73f'r - 25\Big)r^2 \\
&- 8f'\Big(48\xi R^{(3)}r^5 + 10f^{(5)}r^5 + 344\xi R''r^4 + 94f^{(4)}r^4 + 300\xi R'r^3 + 140f^{(3)}r^3 \\
&- 292m^2r^2 - 183f''r^2 - 5\Big)r + 4\Big(160\xi^2R'^2r^6 + 18f^{(3)2}r^6 + 320m^2\xi R''r^6 \\
&+ 80m^2f^{(4)}r^6 + 768m^2f^{(3)}r^5 + 1680m^4r^4 + 441f''^2r^4 - 80\xi R''r^4 - 20f^{(4)}r^4 \\
&- 160f^{(3)}r^3 + 16\xi R'\Big(4f^{(3)}r^3 + 140m^2r^2 + 27f''r^2 - 25\Big)r^3 - 200m^2r^2 \\
&+ 2f''\Big(8\xi R''r^4 + 10f^{(4)}r^4 + 134f^{(3)}r^3 + 884m^2r^2 - 125\Big)r^2 - 15\Big)\Big)f^4 \\
&+ 32\Big(640\xi^3R^3r^6 + 160\xi^2R^2\Big(12m^2r^2 + 3f''r^2 + 5f'r - 3\Big)r^4 + 377f'^3r^3 \\
&- 4\xi R\Big(-231r^2f'^2 + 4r\Big(20\xi R'r^3 - 100m^2r^2 - 47f''r^2 + 35\Big)f' - 10\Big(5f''^2r^4 \\
&+ 6\Big(4m^2r^2 - 1\Big)f''r^2 + 3\Big(1 - 4m^2r^2\Big)^2\Big)\Big)r^2 + f'^2\Big(88\xi R''r^4 + 34f^{(4)}r^4 \\
&+ 296\xi R'r^3 + 356f^{(3)}r^3 + 924m^2r^2 + 1215f''r^2 - 215\Big)r^2 + 2f'\Big(309f''^2r^4 \\
&+ 8\xi R'\Big(-20m^2r^2 + f''r^2 + 5\Big)r^3 + 5\Big(80m^4r^4 - 56m^2r^2 + 9\Big) + f''\Big(54f^{(3)}r^5 \\
&+ 376m^2r^4 - 90r^2\Big)\Big)r + 2\Big(31f''^3r^6 + 25\Big(4m^2r^2 - 1\Big)f''^2r^4 \\
&+ 15\Big(1 - 4m^2r^2\Big)^2f''r^2 + 5\Big(4m^2r^2 - 1\Big)^3\Big)\Big)f^3 - 4r^2f'^2\Big(960\xi^2R^2r^4 + 3117f'^2r^2 \\
&+ 160\xi R\Big(12m^2r^2 + 11f''r^2 + 19f'r - 3\Big)r^2 + 8f'\Big(20\xi R'r^3 + 58f^{(3)}r^3 + 380m^2r^2 \\
&+ 681f''r^2 - 85\Big)r + 4\Big(387f''^2r^4 + 110\Big(4m^2r^2 - 1\Big)f''r^2 + 15\Big(1 - 4m^2r^2\Big)^2\Big)\Big)f^2 \\
&+ 540r^4f'^4\Big(4m^2r^2 + 4\xi Rr^2 + 9f''r^2 + 11f'r - 1\Big)f - 1125r^6f'^6\Big]
\end{aligned}
\tag{C.0.13}
$$

$$
\begin{aligned}
C_2 =& \frac{r^{10}\omega^2}{65536}\Big[-6528f^6 + 32\Big(8f^{(6)}r^6 + 448\xi R^{(3)}r^5 + 320f^{(5)}r^5 + 5376\xi R''r^4 \\
&+ 3436f^{(4)}r^4 + 16464\xi R'r^3 + 12912f^{(3)}r^3 + 12096m^2r^2 + 12096\xi Rr^2 \\
&+ 16095f''r^2 + 4308f'r - 168\Big)f^5 - 16\Big(13440\xi^2R^2r^4 + 24569f'^2r^2 \\
&+ 112\xi R\Big(2f^{(4)}r^4 + 40\xi R'r^3 + 44f^{(3)}r^3 + 240m^2r^2 + 253f''r^2 + 338f'r \\
&- 40\Big)r^2 + 4f'\Big(5404\xi R'r^3 + 15479f''r^2 + 2\Big(56\xi R^{(3)}r^5 + 22f^{(5)}r^5 + 672\xi R''r^4 \\
&+ 431f^{(4)}r^4 + 2900f^{(3)}r^3 + 4732m^2r^2 - 504\Big)\Big)r + 4\Big(5729f''^2r^4 + 56\xi R'\Big(2f^{(3)}r^3 \\
&+ 20m^2r^2 + 34f''r^2 - 5\Big)r^3 + f''\Big(168\xi R''r^4 + 124f^{(4)}r^4 + 2186f^{(3)}r^3 \\
&+ 7084m^2r^2 - 1071\Big)r^2 + 2\Big(39f^{(3)2}r^6 + 14\Big(44m^2r^2 - 9\Big)f^{(3)}r^3 + 7\Big(4m^2r^2 \\
&- 1\Big)\Big(f^{(4)}r^4 + 60m^2r^2 - 5\Big)\Big)\Big)\Big)f^4 + 16r\Big(34442r^2f'^3 + r\Big(336\xi R''r^4 + 502f^{(4)}r^4 \\
&+ 6552\xi R'r^3 + 10284f^{(3)}r^3 + 30632m^2r^2 + 30632\xi Rr^2 + 61177f''r^2 - 4886\Big)f'^2 \\
&+ 4\Big(392m^2f^{(3)}r^5 + 705f''f^{(3)}r^5 + 2240m^4r^4 + 2240\xi^2R^2r^4 + 4973f''^2r^4 \\
&+ 5180m^2f''r^4 + 28\xi R'\Big(20m^2r^2 + 16f''r^2 - 5\Big)r^3 - 98f^{(3)}r^3 - 840m^2r^2 \\
&- 1071f''r^2 + 28\xi R\Big(20\xi R'r^3 + 14f^{(3)}r^3 + 160m^2r^2 + 185f''r^2 - 30\Big)r^2 \\
&+ 70\Big)f' + 2rf''\Big(560\xi^2R^2r^4 + 461f''^2r^4 + 182\Big(4m^2r^2 - 1\Big)f''r^2 \\
&+ 56\xi R\Big(20m^2r^2 + 13f''r^2 - 5\Big)r^2 + 35\Big(1 - 4m^2r^2\Big)^2\Big)\Big)f^3 - 112r^2f'^2\Big(240\xi^2R^2r^4 \\
&+ 3678f'^2r^2 + 20\xi R\Big(24m^2r^2 + 33f''r^2 + 88f'r - 6\Big)r^2 + f'\Big(140\xi R'r^3 \\
&+ 286f^{(3)}r^3 + 1760m^2r^2 + 4277f''r^2 - 370\Big)r + 3\Big(264f''^2r^4 + 55\Big(4m^2r^2 - 1\Big)f''r^2 \\
&+ 5\Big(1 - 4m^2r^2\Big)^2\Big)\Big)f^2 + 70r^4f'^4\Big(464m^2r^2 + 464\xi Rr^2 + 1329f''r^2 + 2312f'r \\
&- 116\Big)f - 26285r^6f'^6\Big]
\end{aligned}
\tag{C.0.14}
$$

$$
\begin{aligned}
C_3 =& \frac{3r^{14}\omega^4}{131072}\Big[503360f^6 - 64\Big(23352\xi Rr^2 + 38323f'r + 2\Big(36f^{(5)}r^5 + 616\xi R''r^4 \\
&+ 990f^{(4)}r^4 + 5544\xi R'r^3 + 8032f^{(3)}r^3 + 11676m^2r^2 + 23111f''r^2 - 1071\Big)\Big)f^5 \\
&+ 16\Big(6720\xi^2R^2r^4 + 300467f'^2r^2 + 224\xi R\Big(12f^{(3)}r^3 + 60m^2r^2 + 191f''r^2 \\
&+ 696f'r - 15\Big)r^2 + 16f'\Big(9f^{(5)}r^5 + 308\xi R''r^4 + 405f^{(4)}r^4 + 3234\xi R'r^3 \\
&+ 5048f^{(3)}r^3 + 9744m^2r^2 + 23783f''r^2 - 1281\Big)r + 4\Big(46f^{(3)2}r^6 + 15984f''^2r^4 \\
&+ 168\Big(4m^2r^2 - 1\Big)f^{(3)}r^3 + 2f''\Big(38f^{(4)}r^4 + 616\xi R'r^3 + 1550f^{(3)}r^3 + 5348m^2r^2 \\
&- 1029\Big)r^2 + 105\Big(1 - 4m^2r^2\Big)^2\Big)\Big)f^4 - 32r\Big(2f''^2\Big(252m^2r^2 + 252\xi Rr^2 + 367f''r^2 \\
&- 63\Big)r^3 + 159825f'^3r^2 + 2f'^2\Big(308\xi R''r^4 + 353f^{(4)}r^4 + 5236\xi R'r^3 + 9718f^{(3)}r^3 \\
&+ 28952m^2r^2 + 28952\xi Rr^2 + 84617f''r^2 - 5082\Big)r + 2f'\Big(1680\xi^2R^2r^4 + 15620f''^2r^4 \\
&+ 56\xi R\Big(6f^{(3)}r^3 + 60m^2r^2 + 169f''r^2 - 15\Big)r^2 + 2f''\Big(308\xi R'r^3 + 699f^{(3)}r^3 \\
&+ 4732m^2r^2 - 1029\Big)r^2 + 21\Big(4m^2r^2 - 1\Big)\Big(4f^{(3)}r^3 + 20m^2r^2 - 5\Big)\Big)\Big)f^3 \\
&+ 28r^2f'^2\Big(960m^4r^4 + 960\xi^2R^2r^4 + 9688f''^2r^4 + 5280m^2f''r^4 - 480m^2r^2 \\
&+ 111657f'^2r^2 - 1320f''r^2 + 160\xi R\Big(12m^2r^2 + 33f''r^2 + 154f'r - 3\Big)r^2 \\
&+ 16f'\Big(110\xi R'r^3 + 249f^{(3)}r^3 + 1540m^2r^2 + 5233f''r^2 - 330\Big)r + 60\Big)f^2 \\
&- 420r^4f'^4\Big(248m^2r^2 + 248\xi Rr^2 + 962f''r^2 + 2467f'r - 62\Big)f + 145005r^6f'^6\Big]
\end{aligned}
\tag{C.0.15}
$$

$$
\begin{aligned}
C_4 =& -\frac{11r^{18}\omega^6}{32768}\Big[31773r^6f'^6 - 126r^4ff'^4\Big(519r^2f'' + 2076rf' + 88m^2r^2 + 88\xi r^2R \\
&- 22\Big) + 168r^3f^2f'^2\Big(rf''\Big(164r^2f'' + 44m^2r^2 + 44\xi r^2R - 11\Big) + 5457rf'^2 \\
&+ 2f'\Big(37r^3f^{(3)} + 1261r^2f'' + 240m^2r^2 + 10\xi r^3R' + 240\xi r^2R - 55\Big)\Big) \\
&- 96f^5\Big(50r^4f^{(4)} + 1064r^3f^{(3)} + 6709r^2f'' + 13196rf' + 1792m^2r^2 + 280\xi r^3R' \\
&+ 1792\xi r^2R - 308\Big) + 48rf^4\Big(41407rf'^2 + 2rf''\Big(86r^3f^{(3)} + 1087r^2f'' + 308m^2r^2 \\
&+ 308\xi r^2R - 77\Big) + 4f'\Big(25r^4f^{(4)} + 748r^3f^{(3)} + 6793r^2f'' + 1652m^2r^2 \\
&+ 210\xi r^3R' + 1652\xi r^2R - 308\Big)\Big) - 16r^2f^3\Big(61r^4f''^3 + 110266rf'^3 \\
&+ 6rf'f''\Big(43r^3f^{(3)} + 1087r^2f'' + 308m^2r^2 + 308\xi r^2R - 77\Big) + 3f'^2\Big(25r^4f^{(4)} \\
&+ 1482r^3f^{(3)} + 22497r^2f'' + 4844m^2r^2 + 420\xi r^3R' + 4844\xi r^2R - 1001\Big)\Big) \\
&+ 373888f^6\Big]
\end{aligned}
\tag{C.0.16}
$$

$$
\begin{aligned}
C_5 =& \frac{429r^{22}\omega^8}{131072}\Big(rf' - 2f\Big)^2\Big[4943r^4f'^4 - 4r^2ff'^2\Big(1671r^2f'' + 6684rf' + 140m^2r^2 \\
&+ 140\xi r^2R - 35\Big) - 16f^3\Big(80r^3f^{(3)} + 1339r^2f'' + 4006rf' + 140m^2r^2 + 140\xi r^2R \\
&- 35\Big) + 16rf^2\Big(83r^3f''^2 + 3709rf'^2 + f'\Big(40r^3f^{(3)} + 1339r^2f'' + 140m^2r^2 \\
&+ 140\xi r^2R - 35\Big)\Big) + 30928f^4\Big]
\end{aligned}
\tag{C.0.17}
$$

$$
C_6 = -\frac{255255r^{26}\omega^{10}}{65536}\Big(rf' - 2f\Big)^4\Big[3r^2f'^2 - 2rf\Big(rf'' + 4f'\Big) + 8f^2\Big] \tag{C.0.18}
$$

$$
C_7 = \frac{425425r^{30}\omega^{12}}{131072}\Big(rf' - 2f\Big)^6 \tag{C.0.19}
$$

Appendix D

Integral Results for $I_i(\omega, r)$

Here is the complete list of I_i expressions calculated in Mathematica from section 3.7 using $f \equiv f(r)$ and $R \equiv R(r)$.

We remind the reader that the objects I_i are arrive from the application of the Watson-Sommerfeld identity,

$$\sum_{l=0}^{\infty} \mathcal{F}(l) = \int_0^{\infty} \mathcal{F}\left(\lambda - \frac{1}{2}\right) d\lambda - Re\left[i \int_0^{\infty} \frac{2}{1+e^{2\pi\lambda}} \mathcal{F}\left(i\lambda - \frac{1}{2}\right) d\lambda\right], \tag{D.0.1}$$

to the inner summand of our mode sum. The I_i are then the terms that result from the left integral on the right hand side of the equation.

$$I_0(\omega, r) = -\frac{\omega}{f} \tag{D.0.2}$$

$$I_1(\omega, r) = -\frac{1}{2\omega}\left[m^2 + \left(\xi - \frac{1}{6}\right) R\right] - \frac{1}{24 r^2 \omega} \tag{D.0.3}$$

$$
\begin{aligned}
I_2(\omega, r) =& \frac{r^2 f}{1920 r^2 \omega^3}\Big[r^3\Big(160m^2 f' + 32(5\xi - 1)Rf' - 160\xi f R' + 32 f R'\Big) \\
&+ r^4\Big(- 160\xi f' R' + 24 f' R' - 80\xi f R'' + 8 f R'' + 240 m^4 + 480 m^2 \xi R \\
&+ 8\Big(30\xi^2 - 1\Big)R^2\Big) + r\Big(40 f' - 192 f f'\Big) + r^2\Big(160 m^2 f + 80(2\xi - 1) f R \\
&- 120 m^2 - 120\xi R + 32 R\Big) - 192 f^2 + 192 f - 17\Big]
\end{aligned}
\tag{D.0.4}
$$

$$
\begin{aligned}
I_3(\omega,r) = &- \frac{f}{107520r^6\omega^5}\Big[36480f^4 - 16\Big(- 42\xi R^{(4)}r^6 + 3R^{(4)}r^6 - 168\xi R^{(3)}r^5 + 24R^{(3)}r^5 \\
&+ 728\xi R''r^4 - 116R''r^4 - 896\xi R'r^3 + 220R'r^3 + 1568m^2r^2 + 112(14\xi+1)Rr^2 \\
&+ 6120f'r + 800\Big)f^3 + 8\Big(- 420\xi^2R'^2r^6 - 252\xi R'^2r^6 + 44R'^2r^6 \\
&- 840m^2\xi R''r^6 + 336m^2R'r^5 - 1680m^2\xi R'r^5 + 1680m^4r^4 \\
&+ 4\Big(420\xi^2 - 182\xi - 109\Big)R^2r^4 + 1386\xi R''r^4 - 160R''r^4 - 1792\xi R'r^3 + 78R'r^3 \\
&+ 2380m^2r^2 - 15660f'^2r^2 - 4R\Big(210\xi^2R''r^4 + 147\xi R''r^4 - 20R''r^4 \\
&+ 2\Big(210\xi^2 - 91\xi - 4\Big)R'r^3 + 182m^2r^2 - 840m^2\xi r^2 - 4(84\xi - 415)f'r \\
&- 595\xi - 543\Big)r^2 + 4f'\Big(168\xi R^{(3)}r^5 - 15R^{(3)}r^5 - 4(56\xi+1)R''r^4 \\
&+ (293 - 420\xi)R'r^3 + 336m^2r^2 + 4870\Big)r - 2841\Big)f^2 + \Big(6720m^6r^6 \\
&+ 16\Big(420\xi^3 + 210\xi^2 - 11\Big)R^3r^6 - 11760m^4r^4 + 16R^2\Big(3\Big(35\Big(12m^2r^2 - 7\Big)\xi^2 \\
&+ 35\Big(4m^2r^2 - 1\Big)\xi + 22\Big) + 4r\Big(210\xi^2 + 161\xi - 41\Big)f'\Big)r^4 + 13440f'^3r^3 \\
&+ 4620m^2r^2 + 2R\Big(48r^2(378\xi - 41)f'^2 - 16r\Big(\Big(630\xi^2 + 259\xi - 57\Big)R'r^3 \\
&- 14m^2(60\xi + 23)r^2 + 1169\xi - 346\Big)f' + 3\Big(560m^4(6\xi+1)r^4 \\
&- 280m^2(14\xi+1)r^2 + 770\xi - 317\Big)\Big)r^2 + 16f'^2\Big((574\xi - 67)R''r^4 \\
&- 4(441\xi - 59)R'r^3 + 2268m^2r^2 - 70\Big)r^2 - 16f'\Big(- 840m^4r^4 \\
&+ \Big(7\Big(180m^2r^2 - 193\Big)\xi + 228\Big)R'r^3 + 2338m^2r^2 + 518\Big)r + 883\Big)f \\
&- 14r^2f'^2\Big(240m^4r^4 + 8\Big(30\xi^2 - 1\Big)R^2r^4 - 120m^2r^2 + 8R\Big(60m^2\xi r^2 \\
&+ 4(5\xi - 1)f'r - 15\xi + 4\Big)r^2 - 8f'\Big(r^3(20\xi - 3)R' - 5\Big(4m^2r^2 + 1\Big)\Big)r - 17\Big)\Big]
\end{aligned}
\tag{D.0.5}
$$

Appendix E

Mode Sum Convergence Checks

The following three pages contain plots to check the order of convergence for n in the on brane mode sums of equation (3.7.53). Each page contains results for a single value of bulk d. For $\sum_n a_n$, where a_n is the result of the l sum over the modes minus the WKB terms, each plot shows on the horizontal $\ln(n)$ and on the vertical $\ln|a_n|$. From left to right the kth plot shows the values at $r = 0.7+0.4k$; this is purely due to space constraints on the page, plots were checked at all available values of r. The blue lines are that taken from our data while the purple lines show the log results for $O(n^{-7})$ (the expected order of convergence) shifted vertically to share a starting point with our data.

Results for $d = 4$.

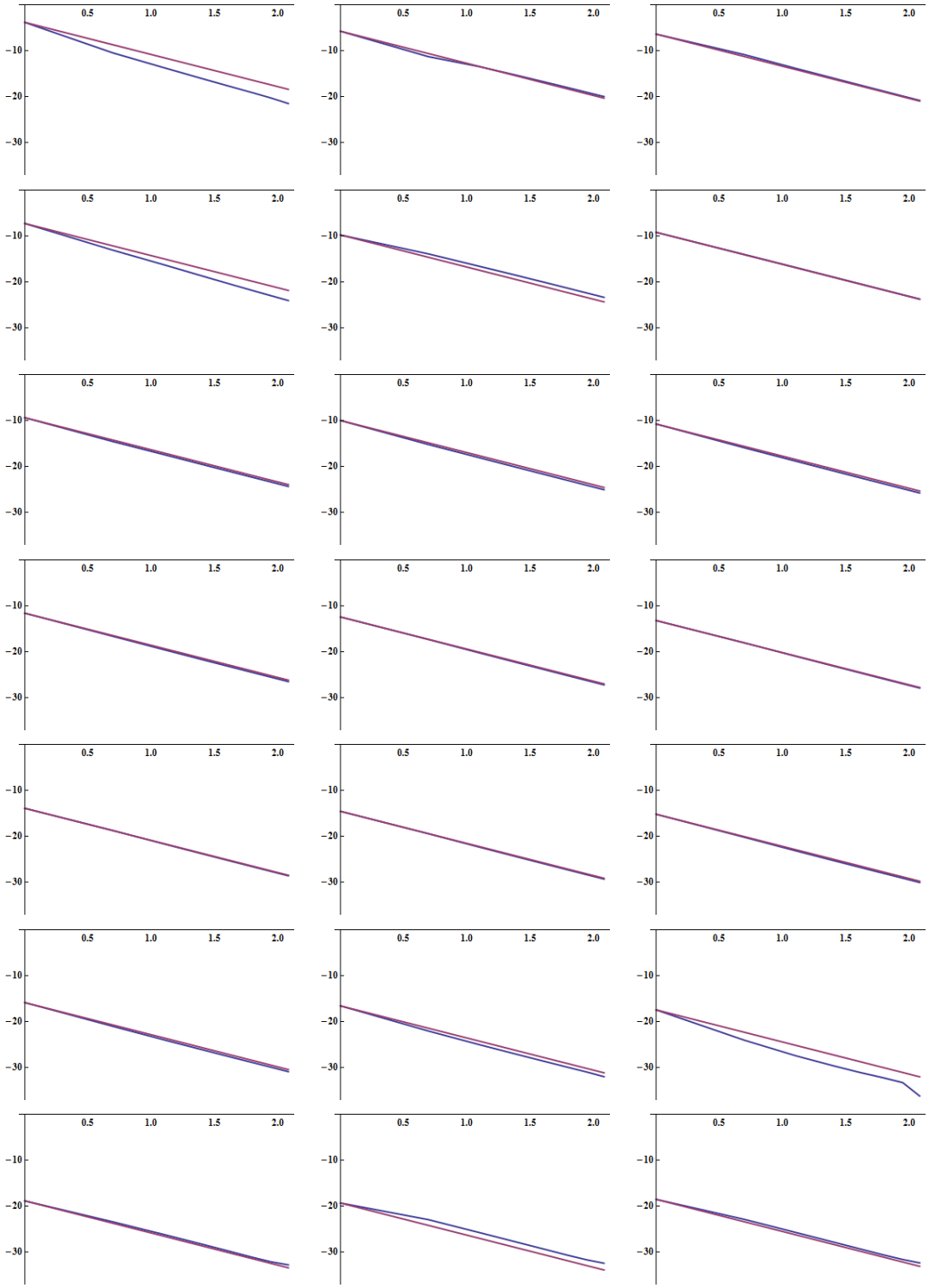

Results for $d = 6$.

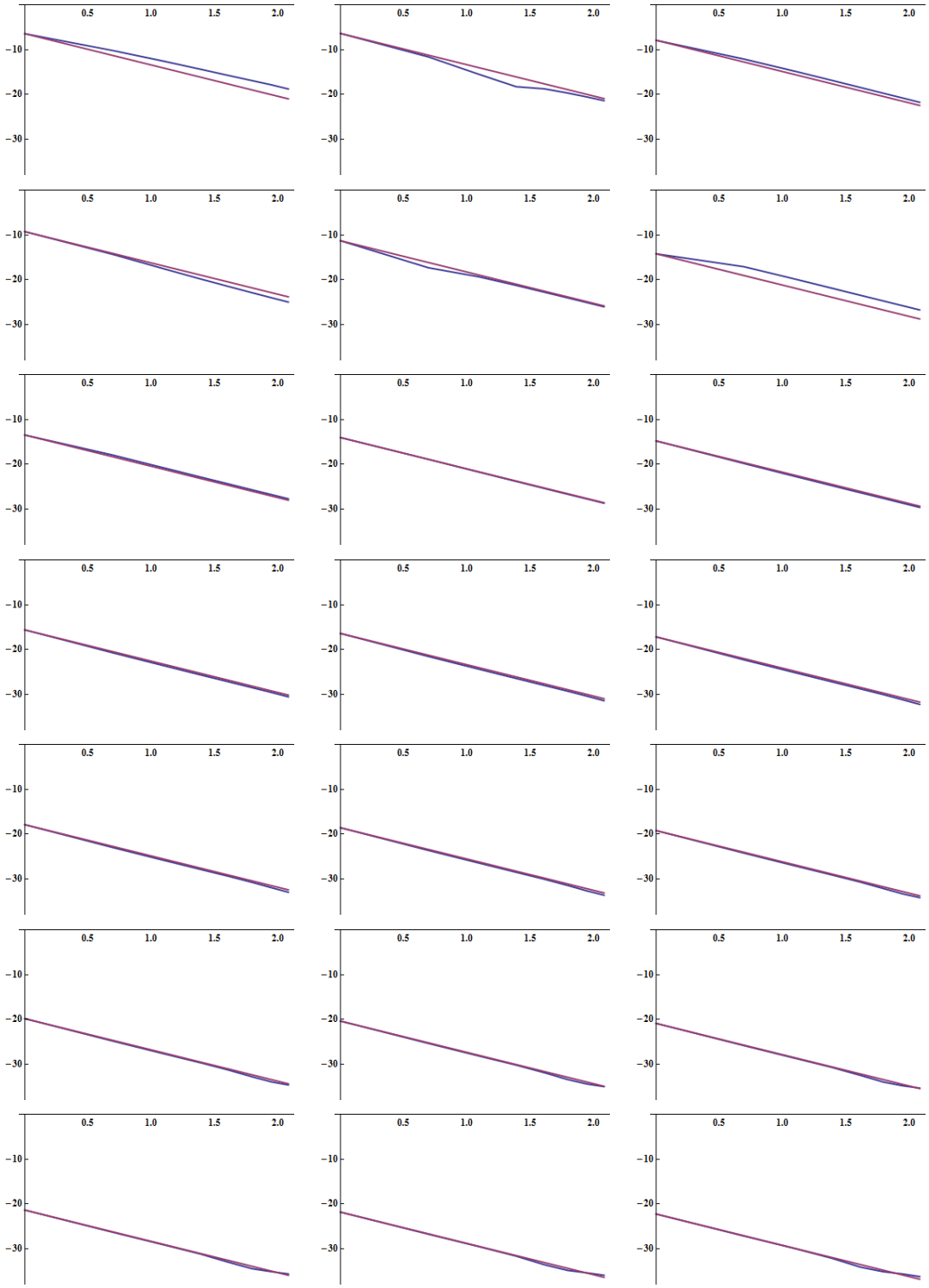

Results for $d = 11$.

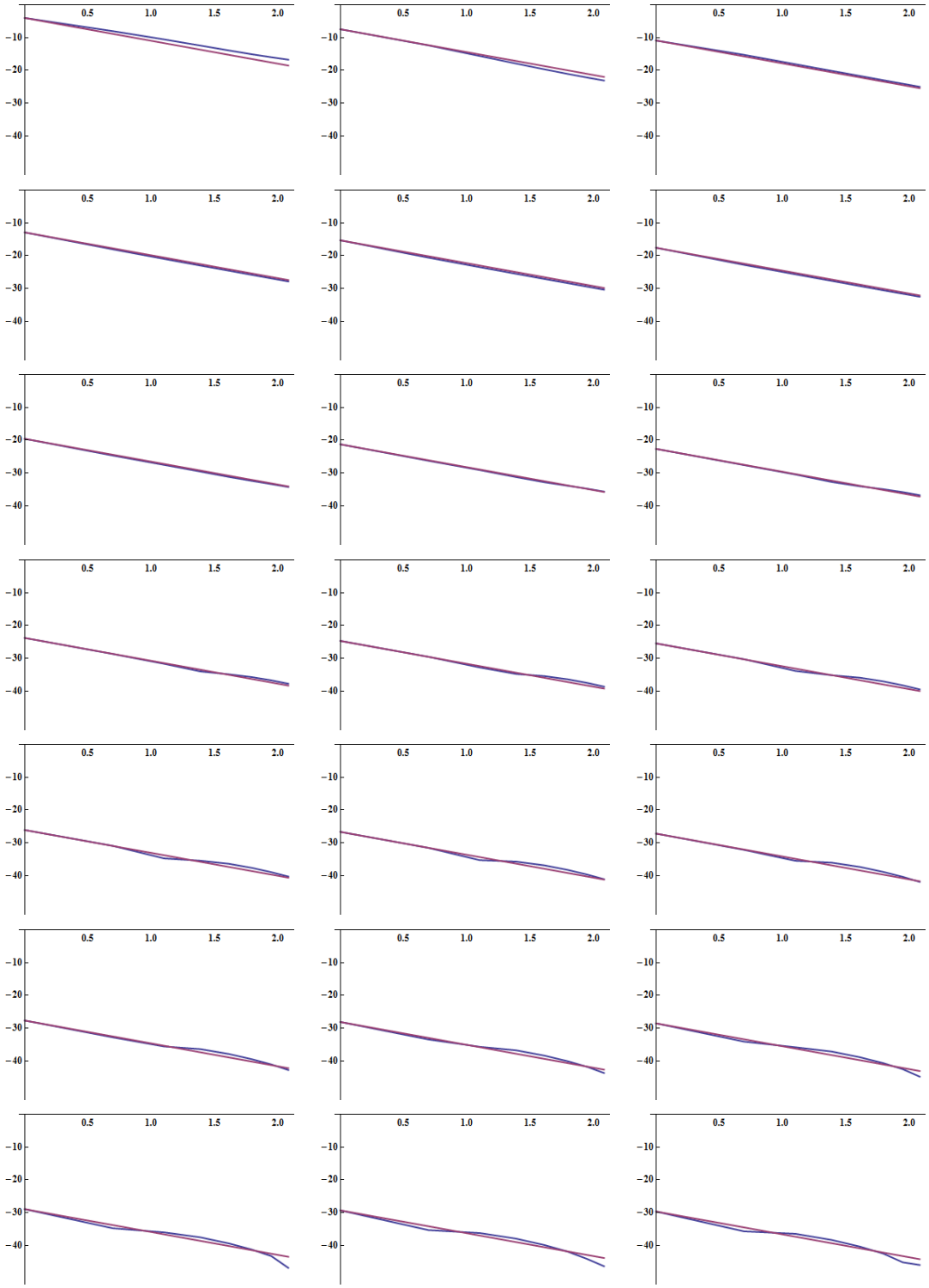

References

[1] A. C. Aitken. *On Bernoulli's numerical solution of algebraic equations.* Proceedings of the Royal Society of Edinburgh, Vol. XLVI, 1926.

[2] P. R. Anderson. A method to compute $\langle\phi^2\rangle$ in asymptotically flat, static, spherically symmetric spacetimes. *Phys. Rev. D*, 41:1152–1162, 1990.

[3] P. R. Anderson, W. A. Hiscock, and D. A. Samuel. Stress-energy tensor of quantized scalar fields in static spherically symmetric spacetimes. *Phys. Rev. D*, 51:4337–4358, 1995.

[4] N. Arkani-Hamed, S. Dimopoulos, and G. R. Dvali. The hierarchy problem and new dimensions at a millimeter. *Phys. Lett. B*, 429:263–272, 1998.

[5] N. Arkani-Hamed, S. Dimopoulos, and G. R. Dvali. Phenomenology, astrophysics and cosmology of theories with submillimeter dimensions and TeV scale quantum gravity. *Phys. Rev. D*, 59:086004, 1999.

[6] M. Bander and C. Itzykson. Group theory and the hydrogen atom. *Rev. Mod. Phys.*, 38:330–345, 1966.

[7] M. Bander and C. Itzykson. Group theory and the hydrogen atom. II. *Rev. Mod. Phys.*, 38:346–358, 1966.

[8] J. D. Bekenstein. Black holes and entropy. *Phys. Rev. D*, 7:2333–2346, 1973.

[9] N. D. Birrell and P. C. W. Davies. *Quantum fields in curved space.* Cambridge University Press, 1982.

[10] D. G. Boulware. Quantum field theory in Schwarzschild and Rindler spaces. *Phys. Rev. D*, 11:1404, 1975.

[11] C. Breen. Correspondence by email.

[12] C. Breen and A. C. Ottewill. Extended Green-Liouville asymptotics and vacuum polarization for lukewarm black holes. *Phys. Rev. D*, 82:084019, 2010.

[13] C. Breen and A. C. Ottewill. Hadamard renormalisation of the stress energy tensor on the horizons of a spherically symmetric black hole space-time. *Phys. Rev. D*, 85:064026, 2012.

[14] M. R. Brown and A. C. Ottewill. Exact and approximate renormalized stress tensors in curved space-time. *Paris 1986, Proceedings, string theory, quantum cosmology and quantum gravity: integrable and conformal invariant theories*, pages 424–435, 1986.

[15] P. Candelas. PhD thesis, University of Oxford, 1977.

[16] P. Candelas. Vacuum polarization in Schwarzschild spacetime. *Phys. Rev. D*, 21:2185–2202, 1980.

[17] P. Candelas and K. W. Howard. Vacuum $\langle\phi^2\rangle$ in Schwarzschild spacetime. *Phys. Rev. D*, 29:1618–1625, 1984.

[18] S. Chatrchyan et al. Search for microscopic black holes in pp collisions at $\sqrt{s} = 8$ TeV. *JHEP*, 1307:178, 2013.

[19] S. M. Christensen. Vacuum expectation value of the stress tensor in an arbitrary curved background: the covariant point separation method. *Phys. Rev. D*, 14:2490–2501, 1976.

[20] S. M. Christensen. Regularization, renormalization, and covariant geodesic point separation. *Phys. Rev. D*, 17:946–963, 1978.

[21] S. M. Christensen and S. A. Fulling. Trace anomalies and the Hawking effect. *Phys. Rev. D*, 15:2088–2104, 1977.

[22] Y. Décanini and A. Folacci. Off-diagonal coefficients of the DeWitt-Schwinger and Hadamard representations of the Feynman propagator. *Phys. Rev. D*, 73:044027, 2006.

[23] Y. Décanini and A. Folacci. Hadamard renormalization of the stress-energy tensor for a quantized scalar field in a general spacetime of arbitrary dimension. *Phys. Rev. D*, 78:044025, 2008.

[24] R. Decca, E. Fischbach, D. E. Krause, and D. Lopez. Testing Newtonian gravity at the nanometer distance scale using the iso-electronic effect. *Phys. Lett. A*, 318:165–171, 2003.

[25] B. S. DeWitt. Dynamical theory of groups and fields. *Conf. Proc. C*, 630701:585–820, 1965.

[26] NIST Digital Library of Mathematical Functions. http://dlmf.nist.gov/, Release 1.0.7 of 2014-03-21.

[27] A. Erdelyi. *Higher Transcendental Functions Volumes I-III.* McGraw-Hill Book Company, 1953.

[28] I. V. Fialkovski. Modification of Abel-Plana formula for functions with non-integrable branch-points. *Phys. Scripta*, 78:015012, 2008.

[29] A. Flachi and T. Tanaka. Vacuum polarization in asymptotically anti-de Sitter black hole geometries. *Phys. Rev. D*, 78:064011, 2008.

[30] P. Foka. Overview of results from ALICE at the CERN LHC. *J. Phys. Conf. Ser.*, 455:012004, 2013.

[31] V. P. Frolov. *Black hole physics: Basic concepts and new developments.* Springer, 1998.

[32] V. P. Frolov, F. D. Mazzitelli, and J. P. Paz. Quantum effects near multidimensional black holes. *Phys. Rev. D*, 40:948–954, 1989.

[33] C. R. Frye and C. J. Efthimiou. *Spherical harmonics in p dimensions.* World Scientific Publishing Company, Singapore, 2014.

[34] S. B. Giddings and S. D. Thomas. High-energy colliders as black hole factories: the end of short distance physics. *Phys. Rev. D*, 65:056010, 2002.

[35] R. Gregory. Braneworld black holes. *Lect. Notes Phys.*, 769:259–298, 2009.

[36] C. M. Harris and P. Kanti. Hawking radiation from a (4+n)-dimensional black hole: exact results for the Schwarzschild phase. *JHEP*, 0310:014, 2003.

[37] J. B. Hartle and S. W. Hawking. Path integral derivation of black hole radiance. *Phys. Rev. D*, 13:2188–2203, 1976.

[38] S. W. Hawking. Black hole explosions. *Nature*, 248:30–31, 1974.

[39] S. W. Hawking. Particle creation by black holes. *Commun. Math. Phys.*, 43:199–220, 1975.

[40] R. Herman. PhD thesis, Montana State University, 1996.

[41] K. W. Howard. Vacuum $T^{\mu}{}_{\nu}$ in Schwarzschild spacetime. *Phys. Rev. D*, 30:2532–2547, 1984.

[42] C. Itzykson and J.B. Zuber. *Quantum field theory.* Dover Publications Inc., 1980.

[43] B. P. Jensen, J. G. Mc Laughlin, and A. C. Ottewill. One-loop quantum gravity in Schwarzschild space-time. *Phys. Rev. D*, 51:5676–5697, 1995.

[44] B. P. Jensen and A. Ottewill. Renormalized electromagnetic stress tensor in Schwarzschild spacetime. *Phys. Rev. D*, 39:1130–1138, 1989.

[45] T. Kaluza. On the problem of unity in physics. *Sitzungsber. Preuss. Akad. Wiss. Berlin (Math. Phys.)*, 1921:966–972, 1921.

[46] P. Kanti. Black holes in theories with large extra dimensions: A Review. *Int. J. Mod. Phys. A*, 19:4899–4951, 2004.

[47] P. Kanti. Black holes at the LHC. *Lect. Notes Phys.*, 769:387–423, 2009.

[48] P. Kanti and J. March-Russell. Calculable corrections to brane black hole decay. 1. The scalar case. *Phys. Rev. D*, 66:024023, 2002.

[49] P. Kanti and E. Winstanley. Hawking radiation from higher-dimensional black holes. 2014.

[50] O. Klein. Quantum theory and five-dimensional theory of relativity. *Z. Phys.*, 37:895–906, 1926.

[51] J. D. Lambert. *Numerical methods for ordinary differential systems : the initial value problem*. Wiley, Chichester New York, 1991.

[52] P. D. Mannheim. *Brane-Localised Gravity*. World Scientific Publishing Company, 2005.

[53] P. Marquet. Charged particle in the extended formulation of general relativity. *Abraham Zelmanov Journal*, 2:171, 2009.

[54] C. W. Misner, K. S. Thorne, and J. A. Wheeler. *Gravitation*. W. H. Freeman, 1974.

[55] D. Morgan, S. Thom, E. Winstanley, and P. M. Young. Some general properties of the renormalized stress-energy tensor for static quantum states on (n+1)-dimensional spherically symmetric black holes. *Gen. Rel. Grav.*, 39:1719–1734, 2007.

[56] V. Mukhanov and S. Winitzki. *Introduction to quantum effects in gravity.* Cambridge University Press, 2007.

[57] C. Müller. *Spherical Harmonics (Lecture Notes in Mathematics).* Springer, 1966.

[58] E. Poisson. The motion of point particles in curved space-time. *Living Rev.Rel.*, 7:6, 2004.

[59] L. Randall and R. Sundrum. A large mass hierarchy from a small extra dimension. *Phys. Rev. Lett.*, 83:3370–3373, 1999.

[60] V. A. Rubakov. Large and infinite extra dimensions. *Phys. Usp.*, 44:871–893, 2001.

[61] M. O. P. Sampaio. Charge and mass effects on the evaporation of higher-dimensional rotating black holes. *JHEP*, 0910:008, 2009.

[62] M. Scandurra. The ground state energy of a massive scalar field in the background of a semitransparent spherical shell. *J. Phys. A*, 32:5679–5691, 1999.

[63] J. H. Schwarz. From superstrings to M theory. *Phys. Rept.*, 315:107–121, 1999.

[64] D. Shanks. *Non-linear transformations of divergent and slowly convergent sequences.* University of Maryland, College Park, 1954.

[65] J. L. Synge. *Relativity: The General Theory.* North-Holland, Amsterdam, 1960.

[66] G. Szego. *Orthogonal Polynomials.* American Mathematical Society; 4th edition, Providence, USA, 1975.

[67] F. R. Tangherlini. Schwarzschild field in n dimensions and the dimensionality of space problem. *Nuovo Cim.*, 27:636–651, 1963.

[68] P. Taylor. PhD thesis, University College Dublin, 2011.

[69] R. T. Thompson and J. P. S. Lemos. DeWitt-Schwinger renormalization and vacuum polarization in d dimensions. *Phys. Rev. D*, 80:064017, 2009.

[70] W. G. Unruh. Notes on black hole evaporation. *Phys. Rev. D*, 14:870, 1976.

[71] M. Visser. van Vleck determinants: Geodesic focusing and defocusing in Lorentzian space-times. *Phys. Rev. D*, 47:2395–2402, 1993.

[72] M. Wald. *Quantum field theory in curved spacetime and black hole thermodynamics.* University of Chicago Press, 1994.

[73] S. Weinburg. *The quantum theory of fields.* Cambridge University Press, 2005.

[74] E. Winstanley. Black holes, TeV-scale gravity and the LHC. 2013.

[75] E. Winstanley and P. M. Young. Vacuum polarization for lukewarm black holes. *Phys. Rev. D*, 77:024008, 2008.